Anaerobic fermentation merging the carboxylate and syngas platforms

Harnessing the potential of mixotrophic communities

Zur Erlangung des akademischen Grades eines

DOKTORS DER INGENIEURWISSENSCHAFTEN (DR.-ING.)

von der KIT-Fakultät für Chemieingenieurwesen und Verfahrenstechnik des

Karlsruher Instituts für Technologie (KIT)

genehmigte

DISSERTATION

von

B. Eng. Flávio C. F. Baleeiro

aus Goiânia, Brasilien

Acknowledgments

I am deeply indebted to Dr. Heike Sträuber. Heike believed in my potential since day zero and agreed to start to co-write my PhD proposal in 2017 despite not knowing me in person. Thank you, Heike, for sharing your wisdom and investing so much hard work, time, and patience into this project!

Heike and Dr. Sabine Kleinsteuber were always available and helped me conceptualize and realize this work from beginning to end. They thoroughly revised and contributed to every iteration of the manuscripts, presentations, reports, etc. and supported me by providing all the resources necessary. I am very fortunate to have had them as supervisors. Prof. Sergio B. de Oliveira and Dr. Athaydes Leite are also acknowledged here for introducing me to Heike and Sabine in the first place.

I must thank Dr. Anke Neumann and Prof. Christoph Syldatk for being my supervisors at the KIT and for supporting my work and my project, especially during my stay in Karlsruhe in 2020. In Karlsruhe, I was lucky to have met Alba, Albo, Aline, André, Beate, Carolin L., Christin, Daniela, Fei, Habibu, Marcus, Michaela, Nebyat, Olga, Pascal, Rebecca, Susanne, and the TeBi group at the KIT. They made moving to a new town during a pandemic a much more enjoyable experience.

I also express my gratitude to my colleagues from the Helmholtz Centre for Environmental Research (UFZ) in Leipzig. At the UFZ, I had fruitful discussions and received precious input on my work thanks to interdisciplinary activities organized under the lead of Prof. Hauke Harms, such as the department seminars and the PhD talks. I also profited from the courses and conferences organized by the HIGRADE team and from the cultural activities organized by the UFZ international office. I am particularly grateful to Ute, who helped me by sequencing thousands of samples and assisted me in my (not so successful) initiative to learn the Saxonian dialect.

Most of this work was realized in cooperation with the department Biochemical Conversion at the *Deutsches Biomasseforschungszentrum* (DBFZ). Thanks to the cooperation between DBFZ and UFZ, I had access to state-of-the-art infrastructure from both the worlds of engineering and microbiology.

I was lucky to be the co-supervisor of Carolin K., Felix, Magda, Lukas, Myra, and Jana R. during their bachelor's, master's, or internship works. Their energy, commitment, and creativity contributed generating quality data to this thesis.

My dear mother, my dear father, my amazing brothers, my wonderful niece, and my Freire and Baleeiro relatives: I deeply appreciate your love, your guidance, and your understanding during the years I have spent abroad. I know that a mere acknowledgement is no substitute for a present son, brother, uncle, cousin, or nephew. However, I hope you agree with me that this endeavor is

worth the sacrifice. The friends I have had the pleasure to make in the past years are also reminded here. Among them, Adi, Bruna, Jana M., Laura, Leandro, Malte, Manuel, Martin, Nico, Pallav, René, Swamini, Tobias, and Washington. Their friendship made Leipzig feel much closer to home.

Preamble

The chapters of this doctoral thesis are based on four published peer-reviewed articles and on two submitted manuscripts. They were written in the quest to improve feasibility and sustainability of anaerobic carboxylate production using syngas ($H_2/CO_2/CO$) as a co-substrate. Conceptualization, investigation, and drafting of the manuscripts were done during the doctoral period. To adapt the manuscripts into chapters, minor changes in the text, format, and figures were done.

Chapter 1 introduces the topics of carboxylate chain elongation and syngas fermentation culminating in the choice of a process rationale which is further adopted in the thesis. This chapter is based on the publication:

Syngas-aided anaerobic fermentation for medium-chain carboxylate and alcohol production: the case for microbial communities
Flávio C. F. Baleeiro, Sabine Kleinsteuber, Anke Neumann, Heike Sträuber (2019)
Applied Microbiology and Biotechnology 103, 8689-8709
DOI: 10.1007/s00253-019-10086-9

Chapter 2 presents the exploratory experiments in serum bottles enriching microbial communities with different histories under a H_2/CO_2 headspace to produce medium-chain carboxylates. This chapter is based on the publication:

Hydrogen as a co-electron donor for chain elongation with complex communities
Flávio C. F. Baleeiro, Sabine Kleinsteuber, Heike Sträuber (2021)
Frontiers in Bioengineering and Biotechnology 9, 650631
DOI: 10.3389/fbioe.2021.650631

In Chapter 3, the effects of different syngas mixtures with carbon monoxide on the fermentation of complex biomass were studied using serum bottles. This chapter is based on the submitted manuscript:

Formate-induced CO tolerance and innovative methanogenesis inhibition in co-fermentation of syngas and plant biomass for carboxylate production
Flávio C. F. Baleeiro, Lukas Varchmin, Sabine Kleinsteuber, Heike Sträuber, Anke Neumann (2022)
manuscript submitted for publication
DOI: 10.1101/2022.06.30.498223

Chapter 4 presents a reactor with H_2/CO_2 recirculation developed to simultaneously co-feed gaseous and organic substrates in an open system. This chapter is based on the publication:

Recirculation of H_2, CO_2, and ethylene improves carbon fixation and carboxylate yields in anaerobic fermentation

Flávio C. F. Baleeiro, Sabine Kleinsteuber, Heike Sträuber (2022)

ACS Sustainable Chemistry & Engineering 10(13), 4073-4081

DOI: 10.1021/acssuschemeng.1c05133

The gas recirculation reactor allowed to track molecular balances over long periods of time. This feature is explored in Chapter 5 to study the cumulative effects of air intrusion on the microbial community and the carboxylate production. This chapter is based on the publication:

Effect of oxygen contamination on propionate and caproate formation in anaerobic fermentation

Flávio C. F. Baleeiro, Magda S. Ardila, Sabine Kleinsteuber, Heike Sträuber (2021)

Frontiers in Bioengineering and Biotechnology 9, 725443

DOI: 10.3389/fbioe.2021.725443

Chapter 6 adds the last layer of complexity by co-feeding a syngas mixture with carbon monoxide and an organic substrate model in an open system. A stable mixotrophic community was enriched and it served as a model to understand how syngas co-feeding affects carboxylate production. This chapter is based on the submitted manuscript:

Mixotrophic chain elongation with syngas and lactate as electron donors

Flávio C. F. Baleeiro, Jana Raab, Sabine Kleinsteuber, Anke Neumann, Heike Sträuber (2022)

manuscript submitted for publication

List of publications

Peer-reviewed original publications on which this thesis is based

Syngas-aided anaerobic fermentation for medium-chain carboxylate and alcohol production: the case for microbial communities
Flávio C. F. Baleeiro, Sabine Kleinsteuber, Anke Neumann, Heike Sträuber (2019)
Applied Microbiology and Biotechnology 103, 8689-8709
DOI: 10.1007/s00253-019-10086-9

Hydrogen as a co-electron donor for chain elongation with complex communities
Flávio C. F. Baleeiro, Sabine Kleinsteuber, Heike Sträuber (2021)
Frontiers in Bioengineering and Biotechnology 9, 650631
DOI: 10.3389/fbioe.2021.650631

Effect of oxygen contamination on propionate and caproate formation in anaerobic fermentation
Flávio C. F. Baleeiro, Magda S. Ardila, Sabine Kleinsteuber, Heike Sträuber (2021)
Frontiers in Bioengineering and Biotechnology 9, 725443
DOI:10.3389/fbioe.2021.725443

Recirculation of H_2, CO_2, and ethylene improves carbon fixation and carboxylate yields in anaerobic fermentation
Flávio C. F. Baleeiro, Sabine Kleinsteuber, Heike Sträuber (2022)
ACS Sustainable Chemistry & Engineering 10(13), 4073-4081
DOI: 10.1021/acssuschemeng.1c05133

Original manuscripts submitted to peer-reviewed journals on which this thesis is based

Formate-induced CO tolerance and innovative methanogenesis inhibition in co-fermentation of syngas and plant biomass for carboxylate production
Flávio C. F. Baleeiro, Lukas Varchmin, Sabine Kleinsteuber, Heike Sträuber, Anke Neumann (2022)
manuscript submitted for publication
DOI: 10.1101/2022.06.30.498223

Mixotrophic chain elongation with syngas and lactate as electron donors
Flávio C. F. Baleeiro, Jana Raab, Sabine Kleinsteuber, Anke Neumann, Heike Sträuber (2022)
manuscript submitted for publication

Oral presentations in conferences

A thermodynamic model to predict carbon fixation potential in syngas-aided anaerobic fermentation

Flávio C. F. Baleeiro, Sabine Kleinsteuber, Ranjana Chowdhury, Heike Sträuber

International Workshop on Hybrid Technologies for Conversion of Lignocellulosic Biomass to Biofuel (2019), Kolkata, India

H_2/CO_2 gas recirculation to improve lactate-to-caproate selectivity

Flávio C. F. Baleeiro, Sabine Kleinsteuber, Anke Neumann, Heike Sträuber

1st International Chain Elongation Conference - ICEC (2020), Wageningen, The Netherlands

Community dynamics during mixotrophic anaerobic fermentation with H_2, CO_2, CO, and ethylene supplementation

Flávio C. F. Baleeiro, Sabine Kleinsteuber, Heike Sträuber

Annual Conference of the Association for General and Applied Microbiology – VAAM (2022), Düsseldorf, Germany

Anaerobic co-fermentation of syngas for sustainable biobased carboxylates

Flávio C. F. Baleeiro, Sabine Kleinsteuber, Heike Sträuber

18th International Conference on Renewable Resources & Biorefineries – RRB (2022), Bruges, Belgium

Poster presentations

Merging carboxylate and syngas platforms and microbiome to obtain value from lignocellulosic biomass

Flávio C. F. Baleeiro, Heike Sträuber

17th International Symposium on Microbial Ecology - ISME (2018), Leipzig, Germany

Methanogenic and acidogenic communities reveal a trade-off between *n*-caproate production and competing pathways in H_2/CO_2-based carboxylate chain elongation

Flávio C. F. Baleeiro, Sabine Kleinsteuber, Heike Sträuber

Annual Conference of the Association for General and Applied Microbiology – VAAM (2019), Mainz, Germany

H_2/CO_2-based carboxylate chain elongation: case study with an acidogenic and a methanogenic inoculum

Flávio C. F. Baleeiro, Heike Sträuber

16th IWC World Conference on Anaerobic Digestion (2019), Delft, The Netherlands

Abstract

Biorefineries based on waste biomass and synthesis gas (syngas, i.e. mixtures of H_2, CO_2, and CO) can support the transition to a new biobased, circular economy through the production of platform chemicals and fuels. Among the many candidate technologies, carboxylate chain elongation (CE) and syngas fermentation (SF) are two promising bioprocesses performed by anaerobic bacteria. Separately, CE and SF face their own challenges to become feasible processes. Waste biomass can be converted to high value medium-chain carboxylates (MCCs) via CE using microbial communities as biocatalysts. However, CE yields and product concentrations are strongly limited by electron donor (ED) bioavailability of the feedstock. Conveniently, H_2 and CO from syngas are sources of EDs thanks to the Wood-Ljungdahl pathway (WLP) present in certain bacteria. SF already has its first commercial plants operating with CO-rich waste gas from steel mills using pure cultures, but its product spectrum is limited to commodities such as acetate and ethanol.

This thesis aims to enhance the feasibility of the carboxylate and syngas platforms by merging CE and SF technologies via fermentation. To achieve this, a single-pot anaerobic process strategy using microbial communities was adopted, different operating conditions were investigated, and chemical balances of the bioreactors were monitored. The emerged community structures were analyzed to elucidate the microbial interactions that enable the co-fed syngas to influence carboxylate production.

The first exploratory studies were carried out in batch systems. They confirmed that H_2/CO_2 alone could only sustain minor MCC concentrations (up to 1.2 g L^{-1} n-caproate) and that co-feeding an organic ED (ethanol, lactate, or sugars from plant biomass) is necessary to achieve extractable MCC concentrations. Abundant H_2 had a beneficial – albeit subtle – impact on MCC production and favored the enrichment of bacteria related to the genera *Clostridium* sensu stricto 12, *Eubacterium*, *Megasphaera*, and *Caproiciproducens*. On the other hand, CO strongly shaped the community and had a mixed effect on the product pool by increasing overall carboxylate production but decreasing selectivity to the elongated carboxylates. Inoculation with a highly diverse inoculum was necessary to obtain a community that was able to use syngas to improve MCC production. As a consequence, these inocula also contained hydrogenotrophic methanogens such as *Methanobacterium* and *Methanobrevibacter* that had to be inhibited with 2-bromoethanosulfonate (2-BES), ethylene, or CO to avoid diversion of electrons to methane.

Considering the lessons learned in closed batch systems, a reactor with gas recirculation able to operate continuously was developed. The first pair of prototypes were stirred-tank reactors (STRs) operated with an organic feedstock model (lactate/acetate) and H_2/CO_2 recirculation for 84 days. The gas recirculation system could keep the availability of the gaseous substrates constantly high and became a toolbox for enriching mixotrophic communities. By using ethylene

as a scalable methanogenesis inhibitor in one of the reactors, electron selectivity to *n*-caproate (from 2.3% to 17%), carbon fixation (up to 0.20 g CO_2 L^{-1} d^{-1}), and abundances of acetogenic bacteria (*Clostridium* sensu stricto 12, *Eubacterium*, and *Colidextribacter*) were increased due to the higher H_2/CO_2 partial pressure.

The gas recirculation concept was adapted and operated further: a pair of STRs operated for additional 139 days and a pair of bubble column reactors (BCRs) operated for 116 days. Long-term operation revealed two major hindrances to mixotrophic MCC production, namely, air contamination and occurrence of ethylene-tolerant methanogens. In comparison to their anoxic counterparts, reactors that had air intrusion rates between 97 ± 28 and 474 ± 33 mL O_2 L^{-1} d^{-1} produced more propionate at the cost of *n*-caproate and showed higher abundances of Actinobacteria, which outgrew Clostridia. The activity of ethylene-tolerant *Methanobrevibacter* was about 33% lower than that of *Methanobrevibacter* enriched in absence of ethylene. Still, activity of the ethylene-tolerant methanogen was high enough to outcompete acetogens.

Finally, a pair of STRs operated with H_2, CO_2, CO, and ethylene recirculation for 292 days showed long-term effectiveness of methanogenesis inhibition by using CO and ethylene in conjunction. The reactor with syngas recirculation enriched a mixotrophic community acclimatized to CO that was able to source half of its substrates from inorganic EDs (i.e. H_2 and CO). The mixotrophic community presented a stable output of *n*-butyrate (up to 5 g L^{-1}) and *n*-caproate (up to 4.3 g L^{-1}) as its main products while fixing up to 1.4 g CO_2 eq. L^{-1} d^{-1} into carboxylates. In comparison to a purely heterotrophic community consuming acetate and lactate, the mixotrophic community produced 50% more carboxylates (in terms of electron equivalents) longer than acetate. The most abundant bacteria in these communities were identified and had putative functional roles assigned to them. Bacteria closely related to *Clostridium luticellarii* and *Eubacterium aggregans* were key players connected to mixotrophic CE metabolism.

Production of elongated carboxylates using mixotrophic communities can support the transition from our current fossil-based economy into the bioeconomy. For the carboxylate platform, the concept developed in this thesis can increase MCC yields from organic feedstocks while converting anaerobic fermentation into a net carbon-fixing process. For the syngas platform, production of MCCs means the valorization of H_2, CO_2, and CO into products more valuable than acetate and ethanol.

This thesis identifies key operational factors of the syngas-aided fermentation, quantifies the potential improvements in carboxylate production, demonstrates long-term operation stability, and elucidates the structure of the mixotrophic community behind the fermentation. Thus, it serves as foundation for future scale-up projects pursuing commercial implementation of syngas-aided anaerobic fermentation.

Zusammenfassung

Bioraffinerien zur Produktion von Plattformchemikalien und Kraftstoffen aus organischen Reststoffen oder Abfällen und Synthesegas (Syngas, d. h. Gemische aus H_2, CO_2 und CO) können den Übergang zu einer neuen biobasierten Kreislaufwirtschaft befördern. Unter den vielen infrage kommenden Technologien sind die mikrobielle Kettenverlängerung von Carboxylaten (*chain elongation*; CE) und die Synthesegasfermentation (SF) zwei vielversprechende Bioprozesse, bei denen anaerobe Bakterien zum Einsatz kommen. Sowohl bei der CE als auch bei der SF müssen jeweils eigene Herausforderungen bewältigt werden, um effiziente und wirtschaftliche Verfahren zu entwickeln. Organische Rest- und Abfallstoffe können durch CE in hochwertige mittelkettige Carboxylate (*medium-chain carboxylates*; MCCs) umgewandelt werden, wobei mikrobielle Gemeinschaften als Biokatalysatoren eingesetzt werden. Die Ausbeuten und Produktkonzentrationen sind dabei jedoch stark vom Vorhandensein und der Bioverfügbarkeit von Elektronendonoren (ED) im Rohstoff begrenzt. Dank des Wood-Ljungdahl-Wegs (*Wood-Ljungdahl pathway*; WLP), der in bestimmten Bakterien vorhanden ist, können aber auch H_2 und CO aus Synthesegas als Quellen für ED herangezogen werden. Für SF gibt es bereits erste kommerzielle Anlagen, die mit CO-reichem Abgas aus Stahlwerken unter Verwendung von Reinkulturen arbeiten, aber ihr Produktspektrum ist auf Grundstoffe wie Acetat und Ethanol beschränkt.

Diese Arbeit hat das Ziel, die CE- und SF-Technologien zusammenzuführen, Fermentationen der Carboxylat- und Synthesegasplattformen zu analysieren und deren Durchführbarkeit zu verbessern. Dafür wurde eine Ein-Topf-Prozessstrategie mit anaeroben mikrobiellen Gemeinschaften in den Fokus gestellt, verschiedene Betriebsbedingungen untersucht und chemische Bilanzierungen der Bioreaktoren vorgenommen. Parallel dazu wurde die Entwicklung der mikrobiellen Gemeinschaften analysiert, um mikrobielle Interaktionen, die eine simultane Verwertung von Syngas und organischen Substraten zur Carboxylatproduktion ermöglichen, aufzuklären.

Die ersten Sondierungsstudien wurden mit Batch-Systemen durchgeführt. Sie bestätigten, dass mit H_2/CO_2 allein nur geringe MCC-Konzentrationen erhalten werden können (bis zu 1,2 g L^{-1} *n*-Caproat) und dass die gleichzeitige Zufuhr eines organischen ED (Ethanol, Laktat oder Zucker aus pflanzlicher Biomasse) notwendig ist, um extrahierbare MCC-Konzentrationen zu erzielen. Die Zugabe von H_2 im Überschuss hatte einen positiven – wenn auch geringen – Einfluss auf die MCC-Produktion und begünstigte die Anreicherung von Bakterien der Gattungen *Clostridium* sensu stricto 12, *Eubacterium*, *Megasphaera* und *Caproiciproducens*. Demgegenüber beeinflusste CO die Entwicklung der Mischkultur stark und hatte eine differenzierte Wirkung auf die Produktbildung, indem es die Gesamtcarboxylatproduktion erhöhte, aber die Selektivität für die verlängerten Carboxylate verringerte. Eine Inokulation mit einer sehr diversen mikrobiellen Gemeinschaft war notwendig, um eine Mischkultur anzureichern, die in der Lage war, Syngas für

eine verbesserte MCC-Produktion zu nutzen. Jedoch enthielten solche Inokula auch hydrogenotrophe Methanbildner wie *Methanobacterium* und *Methanobrevibacter*, die mit 2-Bromethansulfonat (2-BES), Ethylen oder CO gehemmt werden mussten, um eine Umleitung von Elektronen aus dem Substrat in Richtung Methanbildung zu vermeiden.

Unter Berücksichtigung der Erfahrungen mit geschlossenen Batch-Systemen wurde ein Reaktor mit Gasrückführung entwickelt, der kontinuierlich betrieben werden kann. Bei den ersten beiden Prototypen handelte es sich um Rührkesselreaktoren (*stirred-tank reactors*; STRs), die für 84 Tage mit einem organischen Modellsubstrat (Laktat/Acetat) und H_2/CO_2-Rezirkulation betrieben wurden. Das Gasrezirkulationssystem sorgte für eine konstant hohe Verfügbarkeit der gasförmigen Substrate und wurde damit zu einem Schlüsselelement für die Anreicherung mixotropher Gemeinschaften. Durch die Verwendung von Ethylen als skalierbarem Methanogenese-Inhibitor wurden die Elektronenselektivität zu *n*-Caproat (von 2,3 % auf 17 %), die Kohlenstofffixierung (bis zu 0,20 g CO_2 L^{-1} d^{-1}) und die Abundanzen acetogener Bakterien (*Clostridium* sensu stricto 12, *Eubacterium* und *Colidextribacter*) aufgrund des höheren H_2/CO_2-Partialdrucks erhöht.

Das Gasrezirkulationskonzept wurde weiter angepasst und getestet: zwei STRs wurden für weitere 139 Tage und zwei Blasensäulenreaktoren (*bubble column reactors*; BCRs) für 116 Tage betrieben. Im Langzeitbetrieb zeigten sich zwei Haupthindernisse für die mixotrophe MCC-Produktion, nämlich die Kontamination mit Luft und das Auftreten von ethylentoleranten Methanogenen. Im Vergleich zu den anoxischen Reaktoren produzierten die Reaktoren mit Lufteintragsraten zwischen 97 ± 28 und 474 ± 33 ml O_2 L^{-1} d^{-1} mehr Propionat auf Kosten von *n*-Caproat und wiesen höhere Abundanzen von Actinobakterien auf, die die Clostridien überwuchsen. Die Aktivität von ethylentoleranten *Methanobrevibacter* war etwa 33 % kleiner als von *Methanobrevibacter*, die in Abwesenheit von Ethylen angereichert wurden. Dennoch war die Aktivität der ethylentoleranten Methanogenen hoch genug, um Acetogene zu verdrängen.

Schließlich wurde in zwei STRs, die 292 Tage lang mit einer Rezirkulation von H_2, CO_2, CO und Ethylen betrieben wurden, eine Langzeitwirksamkeit von CO und Ethylen bei deren gleichzeitiger Verwendung als Methanogenesehemmstoff nachgewiesen. Im Reaktor mit Syngasrezirkulation wurde eine an CO angepasste mixotrophe Gemeinschaft angereichert, die die Hälfte ihrer Substrate aus anorganischen ED (d. h. H_2 und CO) bezog. Die mixotrophe Gemeinschaft wies eine stabile Produktion von *n*-Butyrat (bis zu 5 g L^{-1}) und *n*-Caproat (bis zu 4,3 g L^{-1}) als Hauptprodukte auf, während sie bis zu 1,4 g CO_2-Äquivalente L^{-1} d^{-1} in Carboxylate umwandelte. Im Vergleich zu einer rein heterotrophen Gemeinschaft, die Acetat und Laktat verbraucht, produzierte die mixotrophe Gemeinschaft 50 % mehr Carboxylate mit größerer Kettenlänge als Acetat (in Bezug auf Elektronenäquivalente). Die in diesen Gemeinschaften am häufigsten vorkommenden Bakterien und deren wahrscheinliche Funktionen im Stoffwechsel wurden identifiziert. Bakterien, die eng mit *Clostridium luticellarii* und *Eubacterium aggregans*

verwandt sind, spielten eine Schlüsselrolle im Zusammenhang mit dem mixotrophen CE-Stoffwechsel.

Die Entwicklung von Prozessen zur Produktion mittelkettiger Carboxylate mit Hilfe von mixotrophen Gemeinschaften kann den Übergang von unserer derzeitigen auf fossilen Rohstoffen basierenden Wirtschaft zur Bioökonomie unterstützen. Für die Carboxylat-Plattform kann das in dieser Arbeit entwickelte Konzept die MCC-Ausbeuten aus organischen Rohstoffen erhöhen und gleichzeitig die anaerobe Fermentation in einen Prozess mit Netto-Kohlenstoff-fixierung umwandeln. Für die Synthesegas-Plattform bedeutet die Produktion von MCCs die Verwertung von H_2, CO_2 und CO zur Gewinnung von Substanzen, die hochwertiger sind als Acetat und Ethanol.

In dieser Arbeit werden die wichtigsten Betriebsparameter für syngasgestützte Fermentationen identifiziert, potenzielle Verbesserungsmöglichkeiten bei der Carboxylatproduktion quantifiziert, eine langfristige Prozessstabilität nachgewiesen und die Struktur der mixotrophen Gemeinschaft als Basis solcher Fermentationen aufgeklärt. Damit dient die Arbeit als Grundlage für künftige Scale-up-Projekte, die eine kommerzielle Umsetzung der syngasgestützten anaeroben Fermentation anstreben.

Table of contents

1. Theoretical background and research proposal

This chapter is based on the publication:

Author contributions

Flávio C. F. Baleeiro: conceptualization, data analysis and curation, visualization, first draft, and manuscript revision.

Sabine Kleinsteuber, Anke Neumann, and Heike Sträuber: conceptualization, project supervision, data analysis support, and manuscript revision.

Since 2008, when Steinbusch et al. (2008) purposely co-fed H_2 to a microbial community to improve the production of carboxylates and alcohols, many studies have been trying to merge the syngas and the carboxylate platforms as a way of complementing the limitations of one technology with the other's advantages. Recent reviews have covered these two platforms separately: Angenent et al. (2016); De Groof et al. (2019); and Holtzapple et al. (2022) covered anaerobic fermentation for carboxylate CE with microbial communities while Fernandez-Naveira et al. (2016); Liew et al. (2016); Molitor et al. (2017); and Bengelsdorf et al. (2018) reviewed the production of chemicals through the fermentation of syngas using pure and mixed cultures. This chapter introduces the theoretical background of these two platforms and considers the different uses of syngas with microbial communities (sometimes also referred to as consortia, reactor microbiota, mixed cultures or open cultures) to aid or to completely sustain production of MCCs.

1.1. General overview of chain elongation

Through a pathway known as reverse β-oxidation (RBO), linear short-chain monocarboxylates (SCCs, e.g. acetate, propionate, *n*-butyrate, *n*-valerate) are elongated by two carbons to MCCs (e.g. *n*-caproate, *n*-heptanoate, *n*-caprylate) with the help of an electron donor (ED) (Figure 1a). Once a broth is rich in MCCs and EDs are available, it is possible to trigger bacterial solventogenesis metabolism by changing reactor operating conditions to produce medium-chain alcohols (MCAs, e.g. *n*-hexanol, *n*-heptanol, and *n*-octanol) from their MCC counterpart, thereby expanding the product spectrum of CE (Ganigue et al., 2016).
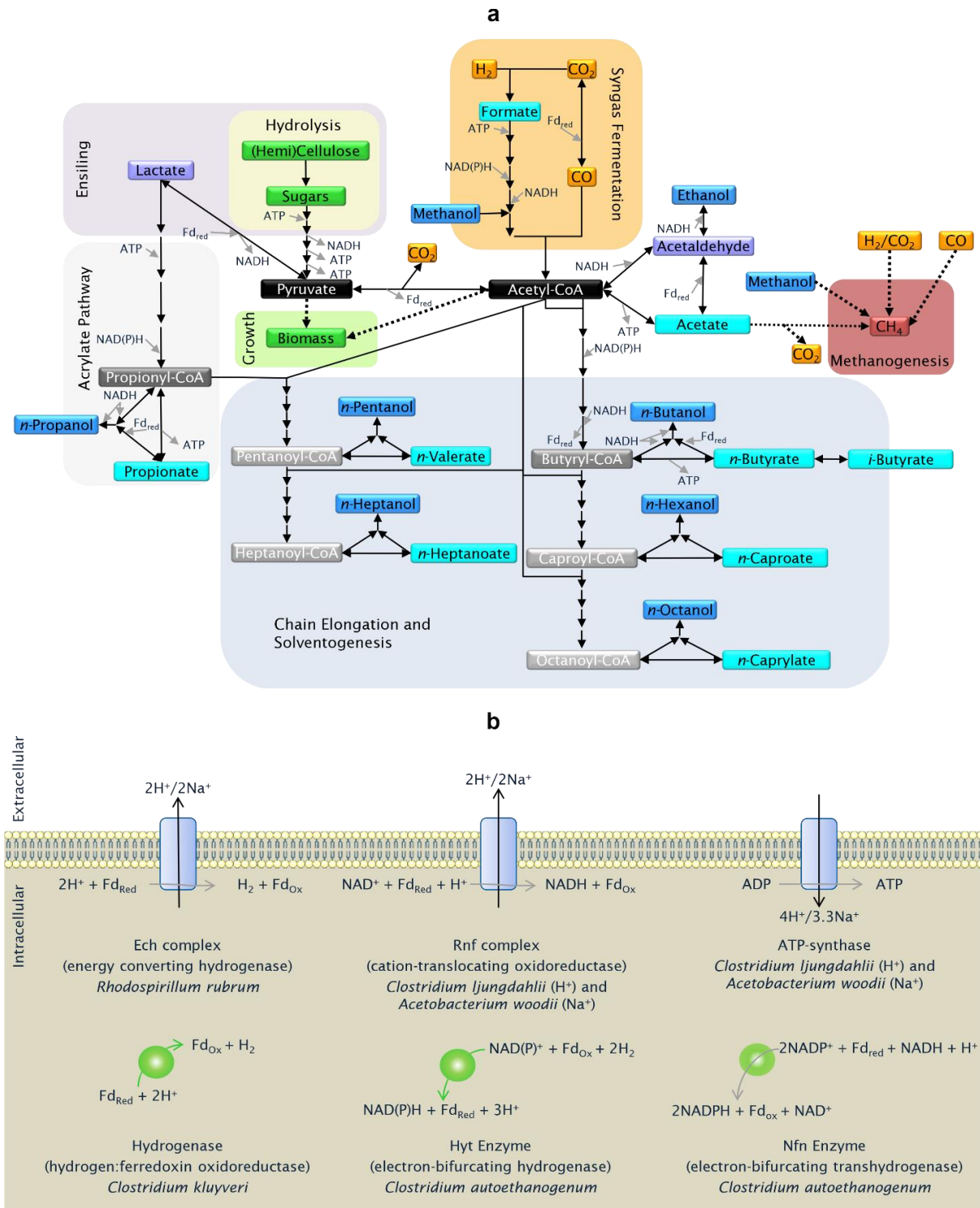
Figure 1. Most relevant metabolic arsenal of an anaerobic microbial community for syngas-aided chain elongation for MCC production. **a** Different metabolic routes can be realized by a single cell or by two or more species with extracellular transfer of intermediates. Each arrow represents one reactional step realized by an enzyme, phosphorylation steps are omitted for conciseness. The direction of the arrow suggests the most favorable direction of the reaction during MCC production. Dashed lines illustrate simplified pathways. **b** Both the WLP and RBO pathways are intimately connected to energy conservation, electron cycling and the ionic homeostasis of the cell. Some of the most relevant soluble and membrane-bound enzymes for CE and SF are shown with exemplary stoichiometry values. The arrow directions indicate the normal reaction direction during autotrophic growth or carboxylate production. These reactions are generally reversible under the physiological conditions of the cell.

1.2. Medium-chain carboxylates and alcohols of special interest

MCCs and MCAs are potential platform chemicals and biofuels that could meet many market needs that nowadays are met by fossil resources. Among MCCs, *n*-caproate (a C6 compound) and *n*-caprylate (a C8 compound) have received special attention in CE research. This is attributed, among other reasons, to higher C/O ratios, higher energy density, and low water solubility. Regarding alcohols, similar reasoning justifies research focus on MCAs such as *n*-hexanol (Fernández-Naveira et al., 2017). The highly reduced and almost water insoluble *n*-octanol would be also a desired product from acidogenic-solventogenic fermenters, but its production in anaerobic fermentations has been restricted to trace amounts up to now (Richter et al., 2016a).

Production of even-numbered MCCs depends on the presence of an ED that generates acetyl-CoA (i.e. ethanol or lactate) and even-numbered SCCs (e.g. acetate, *n*-butyrate), which are more commonly present in acidogenic reactors than their odd-numbered counterparts. Since *Clostridium kluyveri* produces *n*-valerate when fed by propanol and acetate (Kenealy and Waselefsky, 1985), one way to extend product selectivity to odd-numbered MCC is to use *n*-propanol as an ED. The reason for this is shown in the metabolic network in Figure 1a, in which propionyl-CoA (from *n*-propanol) condenses with acetyl-CoA during CE forming the odd-numbered *n*-valerate through pentanoyl-CoA (Kenealy and Waselefsky, 1985; Marounek et al., 1989). Since the RBO pathway can be intermediated by acetyl-CoA together with propionate (or propionyl-CoA), it is, in principle, also possible to produce odd-numbered MCC from lactate and acetate by a bacterium such as *Megasphaera elsdenii* that possesses both the RBO and the acrylate pathways (Weimer and Moen, 2013), the latter being a lactate-consuming pathway intermediated by propionyl-CoA (Figure 1a).

1.3. Limitation by electron donors

Despite its potential to convert waste biomass into higher-value MCCs, CE is strongly limited by the ED. Ethanol and - more recently - lactate have been often used as EDs (Zhu et al., 2015; Angenent et al., 2016; Cavalcante et al., 2017). As most industrial waste streams have lower ethanol or lactate concentrations than ideally needed to promote high yield CE, considerable amounts of these chemicals have to be procured to the fermenter feed.

Ethanol and lactate supplementation to improve MCC has consequences on the economics and sustainability of the process:

1) Large-scale streams of diluted ethanol and lactate, e.g. corn beer from bioethanol plants or acid whey from dairy production lines can be concentrated to the commodity-grade chemical by inexpensive, mature technologies (e.g. pressure swing adsorption for ethanol and evaporation/crystallization for lactate) (Kosaric et al., 2000; Chahal and Starr, 2006). This means that the feasibility of using ethanol or lactate for MCC production would be restricted to niche waste streams - streams that for certain reasons cannot be used for commodity ethanol or lactate

production. Some of these streams have been already studied, such as wine lees with diluted ethanol (Kucek et al., 2016c) or lactate from ensiled crop by-products (Scarborough et al., 2018b; Sträuber et al., 2018; Lambrecht et al., 2019).

2) Considering the environmental impact, ethanol use was identified as the biggest accountable factor for the environmental impact in terms of global warming potential, acidification potential and eutrophication potential during n-caproate production from waste biomass (Chen et al., 2017). The impact of supplemented lactate in the MCC production life cycle remains to be assessed. However, it can be anticipated that the environmental impact of procured lactate is not too different from that of ethanol since commercial lactate is also produced by sugar fermentation or by chemical synthesis from fossil derivatives (Chahal and Starr, 2006; Endres and Siebert-Raths, 2009).

In order to improve process feasibility, it is highly desirable to supplement the waste streams feed with more affordable EDs than ethanol and lactate. Novel strategies are studied to diversify ethanol and lactate usage in CE. Among them, the usage of strains that produce MCCs from sugars or methanol that could come from waste biomass (Chen et al., 2016; Jeon et al., 2016; Jankowska et al., 2018), bioelectrochemical systems (Jourdin et al., 2018; Vassilev et al., 2019), phototrophic organisms (Doud et al., 2017), and approaches using the reductive power of H_2 and CO (Steinbusch et al., 2008; Liew et al., 2016) have been investigated.

1.4. Syngas as an alternative source of electron donors

With the capacity to convert the lignin fraction, biomass gasification technologies may have an important place in the integrated biorefinery of the future. Gasification products are considered third-generation (3G) substrates, among them, syngas (i.e. H_2, CO_2, and CO) and water-gas shifted gas (i.e. H_2 and CO_2) can be an extra source of electrons and carbon for MCC production (Cueto-Rojas et al., 2015; Liew et al., 2016). Besides, H_2 from electrochemical processes could also be fed to the anaerobic fermenter as long as a carbon source is provided (Rabaey and Rozendal, 2010; Vassilev et al., 2018). In this chapter, water-shifted gas and H_2 gas are all referred as syngas for simplicity.

The gateway for incorporating syngas into the carboxylate pool is the WLP (Figure 1a). In the WLP of homoacetogens, H_2, CO_2, and CO are fixed into acetyl-CoA with consumption of ATP. Downstream, acetyl-CoA can either be converted to acetate, returning the ATP investment, or to ethanol, oxidizing NAD(P). As shown in Figure 1b, the pathway depends on the interconversion of these electron carriers through hydrogenases in the cytosol and cation export complexes such as the Rnf complex (e.g. in *Clostridium ljungdahlii* and *Acetobacterium woodii*) or the Ech complex (e.g. in *Moorella thermoacetica* and *Rhodospirillum rubrum*) (Schuchmann and Müller, 2014). Net ATP gain in autotrophically grown homoacetogens is still possible thanks to the ion-motive force maintained by these ion export complexes (i.e. Rnf or Ech) and ion import made by transmembrane ATP synthases (Figure 1b). There is in-depth literature covering current

knowledge of SF by anaerobic bacteria (Schuchmann and Müller, 2014; Diender et al., 2015; Liew et al., 2016; Bengelsdorf et al., 2018).

Other, less common products of syngas fermenting bacteria are formate, 2,3-butanediol, *n*-butyrate, *i*-butyrate, *n*-caproate, *n*-butanol, and *n*-hexanol (Bengelsdorf et al., 2018). Up to date, only a few strains are reported to be able to form *n*-caproate from syngas, and *Cl. carboxidivorans* is the only known species able to form *n*-hexanol from syngas (Phillips et al., 2015). When *Cl. carboxidivorans* was not found in syngas-fed microbiota, it was assumed that *n*-caproate/*n*-caprylate production occurred via a multi-species synergy with conventional CE intermediated by acetate (or *n*-butyrate) and ethanol from the WLP (Ding et al., 2010; Ganigue et al., 2015). Still, typical ethanol-based chain-elongating species, such as *Cl. kluyveri*, have frequently been absent in studies where *n*-caproate and *n*-caprylate was produced (Kucek et al., 2016b; Grimalt-Alemany et al., 2018; Nzeteu et al., 2018).

1.5. Microbial communities and pure cultures

Syngas can be swiftly consumed by pure strains producing a limited range of short-chain chemicals such as acetate and ethanol (Molitor et al., 2017). *Cl. carboxidivorans* P7 (Ramachandriya et al., 2013; Phillips et al., 2015) is a remarkable exception because, to date, no other pure culture has been confirmed to produce the C6 carboxylate and alcohol when fed only with syngas. Yet, even after media optimization for strain P7, concentrations of C6 produced from syngas remained one order of magnitude lower (i.e. ~1 g L^{-1}) than those produced in conventional CE reactors (i.e. ~10 g L^{-1} of *n*-caproate or about the solubility limit of *n*-caproate at the working pH) (Grootscholten et al., 2014; Ramio-Pujol et al., 2015; Reddy et al., 2018; Fernandez-Naveira et al., 2019). Even though there are other strains producing MCCs from syngas (e.g. the syngas-fermenting species *E. limosum* that can also produce C6 from methanol), their product titers will hardly increase by an order of magnitude. Thus, without considering the use of genetic engineering, some studies have adopted two-culture approaches with homoacetogenic and acidogenic strains (Diender et al., 2016; Richter et al., 2016a; Gildemyn et al., 2017).

Microbial communities share the low MCC titers of *Cl. carboxidivorans* when fed only by syngas (Molitor et al., 2017). However, mixed cultures of lactate- or ethanol-based acidogenic reactors can have productivities and concentrations of MCC comparable to pure cultures albeit in a broader range of pH (De Groof et al., 2019). Comparison of mixed cultures with *Cl. carboxidivorans* and co-cultures (e.g. *Cl. kluyveri/Cl. ljungdahlii*) is limited since microbial communities are the only option to directly convert complex biomass (e.g. lignocellulose) to MCCs. Therefore, a co-feeding strategy of syngas and degradable types of biomass can make mixed cultures feasible for syngas-fermenting reactors. In other words, open cultures may excel in syngas-aided – and not in syngas-based – CE.

The use of open mixed cultures can further add simplifications to the bioprocess of MCC production. It is known from anaerobic digestion research that microbial communities can

operate steadily in unsterile reactors (Werner et al., 2011; Agler et al., 2014), which can help lower process capital and operating costs in comparison to monoseptic conditions. Besides, it is expected that communities can better handle the inhibitors and contaminants typically found in syngas. Aromatics, tars, HCN, sulfur oxides, and many other compounds – besides H_2, CO_2, and CO – can be found in real syngas and some are known to negatively affect performance of the best syngas fermenters (Sikarwar et al., 2016; Oswald et al., 2018b). Open mixed cultures have shown robustness and resilience in hydrolysis and fermentative reactor operation and are used to degrade biomass of varying quality despite the presence of natural inhibitors in the substrate, such as alkaloids (Popp et al., 2016) and phenolic compounds (Chapleur et al., 2016). This characteristic resilience to substrate quality fluctuations has been decisive for the success of technologies in anaerobic digestion and wastewater treatment (Werner et al., 2011).

The biggest hurdles for the application of open mixed cultures may be instability of the community and lack of knowledge of the microbial interactions in these systems (Werner et al., 2011; Arslan et al., 2016). It is not trivial to establish a common ground for comparing kinetics between pure and mixed cultures. However, it can be observed that when operating with mixed cultures fed with syngas, longer fermentation times (in the order of dozens and hundreds of days) are generally needed to achieve steady production rates in comparison with pure cultures, the latter having more reproducible and definable kinetics. The study done by Ganigue et al. (2015) can be taken as an example, where batch trials with syngas-fed *Cl. carboxidivorans* and with an enriched carboxydotrophic mixed culture were realized for 4 and 20 days with a pure culture and a microbial consortium, respectively. Dynamics and fermentation time to achieve stable conversion rates can also be in the order of dozens of days for microbial communities degrading solid substrates as shown by Sträuber et al. (2016), where a 200-day pre-cultivated community was used to degrade corn silage in semi-continuous reactors. Fortunately, studies on acidogenic bacterial communities do not have to start from scratch because much of the knowledge developed with methanogenic communities in anaerobic digesters is useful for MCC-producing communities (Agler et al., 2012; Agler et al., 2014; Spirito et al., 2014). In the next years, the remaining knowledge gaps on acidogenic bacterial communities may be tackled with the advancement of high-throughput omics approaches and increasing accessibility of cell-level analytical techniques. Notwithstanding, deeper understanding in microbial ecology will offer applied insights on what happens and what does not within such fermentative communities.

1.6. Process rationales for merging the syngas and carboxylate platforms

The concept of merging SF and CE in order to take profit from its synergies has been a topic in several previous studies. Figure 2 summarizes the process strategies adopted in the studies that attempted to join CE and SF. Figures 2a and 2d are syngas-*based* strategies, in which syngas is the sole substrate, while Figures 2b, 2c, and 2e are syngas-*aided* strategies, in which syngas is a supplemental substrate.
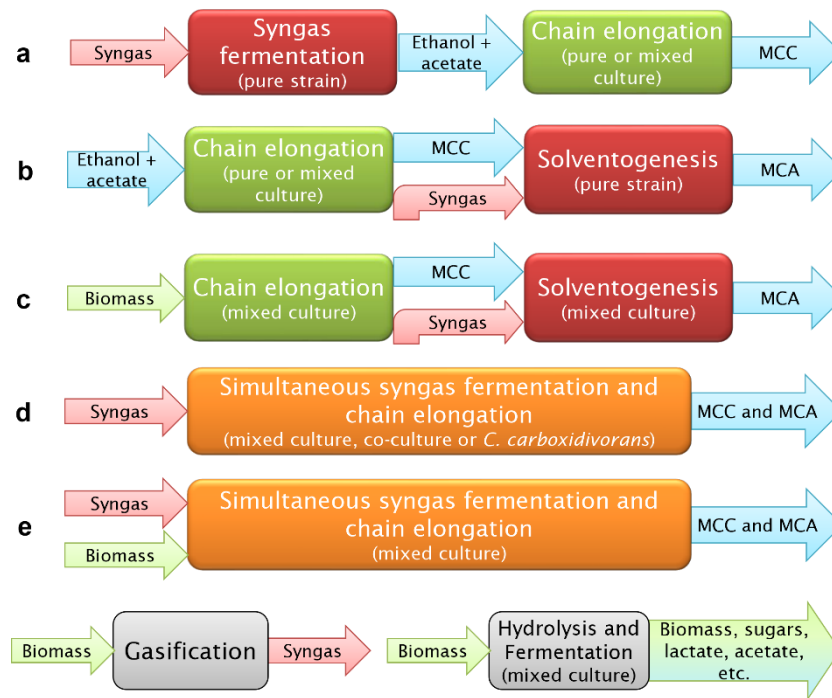
Figure 2. Strategies for merging syngas fermentation (SF) and chain elongation (CE). Ethanol can be substituted by lactate as electron donor (ED) for CE. Virtually all organic fractions of feedstock biomass can be incorporated to SF by gasification, although not all biomass types are feasible. Fractions of biomass can be incorporated to CE by microbial hydrolysis and fermentation. MCC: medium-chain carboxylates; MCA: medium-chain alcohols.

The scheme depicted in Figure 2a shows SF in the first process step and a CE reactor receives the effluent from the first reactor, preferably with a high ethanol:acetate ratio. The first reactor depends on solventogenic carboxydotrophic bacteria and the CE reactor needs, therefore, bacteria able to realize ethanol-based CE. Studies that adopted this strategy opted out for a pure strain for the SF step and for *Cl. kluyveri* or a mixed culture for the CE step (Vasudevan et al., 2014; Kucek et al., 2016b).

Figure 2b shows CE as first step and SF in series for reducing MCCs into MCAs. Richter et al. (2013) built the case for lowering medium costs by assuming prices for laboratory-grade, non-bulk nutrients. The authors acknowledged that laboratory-grade nutrient prices are higher than industrial-grade ones but sustained the point that the estimate is still valid to prove the need for lower nutrient costs. This nutrient cost overestimation is sometimes orders of magnitude higher than from industrial-grade ingredients, thus it is still not clear that medium costs are indeed such a big hindrance for viability of SF and CE as bioprocesses.

The strategy depicted in Figure 2c allows the incorporation of feedstock biomass to the substrate pool and can work with two differently acclimatized microbial communities. It is a possible answer to the incompatibilities of process conditions of CE, SF, and solventogenesis reported previously (Ganigue et al., 2016; Richter et al., 2016a). The first stage operates as a hydrolysis and CE reactor and the second stage converts carboxylates to alcohols through syngas-based solventogenesis. However, one serious caveat against this strategy is that

microbial communities have never excelled in alcohol production. Using a pure culture in the second step is likely unfeasible in large scale, since the intermediate MCC broth would have to be sterilized before being fed to a pure culture.

Figure 2d is a scheme for simultaneous SF and CE to produce MCCs and MCAs. A strain like *Cl. carboxidivorans* P7 can produce MCCs and MCAs from syngas in a single process step. Despite *Cl. carboxidivorans* being able to grow on cellulose, cellobiose and pectin (Liou et al., 2005), no reports about its mixotrophic growth on syngas and complex biomass feedstocks were found. Therefore, it is assumed here that *Cl. carboxidivorans* is not a viable culture for simultaneous degradation of biomass and SF. Without biomass hydrolysis, the only way to use waste biomass in this process configuration is by a preceding conversion to syngas. When using communities, MCCs titers from such configuration have remained low. Reactors that allow high mass transfer such as hollow-fiber membrane biofilm reactors have been used to successfully increase selectivity to MCCs. However, the maximum concentration of *n*-caproate or *n*-hexanol of around 1 g L^{-1} seems to be the limit for this strategy (Zhang et al., 2013; Ganigue et al., 2016; Shen et al., 2018).

It is possible to carry out anaerobic fermentation co-feeding syngas and biomass feedstocks and using microbial communities enriched for MCCs production (Figure 2e). Such "syngas-aided anaerobic fermentation" uses biomass that is preferably rich in EDs such as lactate, ethanol, or sugars. Similarly to conventional ensiling, lactic acid bacteria can convert fractions of the lignocellulose to lactate *in situ*, which in turn is consumed during CE by other bacteria. In parallel, the reductive power of H$_2$ and CO could alleviate ED scarcity, lowering process costs or increasing total conversion of feedstocks to MCCs. So far, a few studies applied this strategy in batch bottles (Steinbusch et al., 2011; Esquivel-Elizondo et al., 2018; Nzeteu et al., 2018). Interestingly, product concentrations of the strategy in Figure 2e are not limited as they are in Figure 2d and studies indicate that the added syngas can increase concentration and selectivity to the more reduced chemicals, i.e. the longer-chain carboxylates and alcohols. In one example, batch tests showed that a lactate-based CE community produced 130% more *n*-caproate (totaling 10.4 g L^{-1}) under a H$_2$-rich headspace (Nzeteu et al., 2018). A similar synergy was reported by Wu et al. (2019), where 44% more *n*-caproate (totaling 5.5 g L^{-1}) was obtained from lactate-based CE with H$_2$ co-feeding. This was also observed by Steinbusch et al. (2011) – though to a lesser extent of about 10% increase of *n*-caproate, to 8.2 g L^{-1} – when bubbling H$_2$ to a mixed culture that was performing ethanol-based CE.

1.7. Competing pathways in microbial communities

Despite the advantages offered by microbial communities, competing pathways to MCC production will likely be present in the bioreactor and have to be dealt with. Fortunately, these pathways have been studied and strategies to steer them towards the desired process have been proposed. Table 1 sums up these generally undesired pathways when producing MCCs by mixed

cultures with the help of syngas. The effect of each pathway is discussed and known strategies that are able to inhibit partially or completely these pathways are listed.

High partial pressures of H_2 from syngas help to thermodynamically inhibit certain competing pathways, such as excessive oxidation of ethanol and lactate alcohol and carboxylates (Table 1). On the other hand, the continuous presence of H_2 means that the sulfate reducing and methanogenic members of the community can also grow abundantly.

The same cannot be said about hydrogenotrophic methanogenesis (HM). Differently from acetoclastic methanogenesis (AM), HM has been found to be persistent at pH values as low as 5.2 (Savant et al., 2002) and the most common way to selectively inhibit it in laboratory studies – using relatively high concentrations of 2-bromoethanosulfonate (50 mM) – would be too expensive for a refinery-scale process. Additionally, no single proposed action in Table 1 is able to completely counter HM alone without also compromising MCC yields. Thus, new cost-effective and selective ways to hinder HM still need to be studied if syngas-based fermentation with microbial communities is to become a biorefinery process. Despite the fact that sulfate-reducing bacteria (SRB) are able to outcompete even methanogens for consumption of H_2 and acetate (Plugge et al., 2011), competition from SRB can be avoided simply by keeping sulfate concentrations sufficiently low and using reduced sulfur supplements as sulfur source (Table 1).

Table 1. Competing pathways in syngas-aided MCC production with microbial communities.

Pathway	Description	Effect	Can be countered by
Acetoclastic/ acetotrophic methanogenesis (AM)	$$CH_3COO^- + H^+ \rightarrow CH_4 + CO_2$$ Methanogenic archaea can produce methane from acetate.	Consumption of acetate into CH_4 and CO_2. Secondary effect: pH increase of the reactor broth.	• pH values lower than 7 (Arslan et al., 2016); • High concentration of undissociated carboxylates (Zhang et al., 2018); • High CO partial pressure (Esquivel-Elizondo et al., 2018); • Low hydraulic retention time (Grootscholten et al., 2013); • Heat-shock or pH treatment of the inoculum (Grimalt-Alemany et al., 2018); • Fluoromethane and fluoroacetate (only AM) (Liu et al., 2011); • Chemical inhibitor 2-bromoethanosulfonate (2-BES) (Zinder et al., 1984); • High ammonium concentrations (Koster and Koomen, 1988); • High salinity (De Vrieze et al., 2016); • High organic loading rates (Bjornsson et al., 2000); • Psychrophilic conditions (20°C) (Liu et al., 2018).
Hydrogenotrophic methanogenesis (HM)	$$4H_2 + CO_2 \rightarrow CH_4 + 2H_2O$$ With a higher affinity to H_2, this pathway can consume H_2 from syngas at faster rates than those of the WLP if a hydrogenotrophic archaea are well established in the mixed culture (Heimann et al., 2010). Possibly one of the most challenging pathways to inhibit in large scale operation of SF with open mixed cultures.	Shunt of electrons (in the form of H_2) into methane, instead of MCC and MCA. Secondary effect: broth dilution due to H_2O production.	

11

Excessive ethanol oxidation	$CH_3CH_2OH + H_2O \rightarrow CH_3COO^- + H^+ + 2H_2$ In conventional ethanol-based CE it is common that about 1/6 of the ethanol is oxidized to acetate for ATP production through substrate level phosphorylation. In open cultures, an excess of ethanol tends to be oxidized to acetate in syntrophy with HM.	Consumption of the ED uncoupled with MCC and MCA production. Secondary effect: pH decrease of the reactor broth.	• High H_2 partial pressure (Ding et al., 2010); • High hydraulic retention time (HRT) (Roghair et al., 2018b); • High acetate concentration (Grimalt-Alemany et al., 2018); • High CO partial pressure (tested with ethanol) (Esquivel-Elizondo et al., 2018); • Low CO_2 loading rate (tested with ethanol) (Roghair et al., 2018a); • Low reducing potential of medium (Weghoff et al., 2015).
Excessive lactate oxidation	$CH_3CHOHCOO^- + H_2O \rightarrow CH_3COO^- + 2H_2 + CO_2$ Analogously to excessive ethanol oxidation, lactate can be converted to acetate for net ATP generation.	Consumption of the ED uncoupled with MCC and MCA production.	
Anaerobic carboxylate oxidation	$CH_3COO^- + H^+ + 2H_2O \rightarrow 4H_2 + 2CO_2$ Acetate and MCC can be oxidized to CO_2 in syntrophy with HM.	Consumption of acetate and MCC. Secondary effect: pH increase of the reactor broth.	• High H_2 partial pressure (Steinbusch et al., 2011); • Low pH (Arslan et al., 2012).
Dissimilatory sulfate reduction	$4H_2 + SO_4^{-2} + H^+ \rightarrow HS^- + 4H_2O$ H_2, acetate, ethanol and lactate can be used as EDs for sulfate reduction in highly exergonic reactions realized by sulfate reducing bacteria.	Shunt of carbon and electrons outside the carboxylate platform. Secondary effects: pH increase, broth dilution and buildup of potentially toxic sulfide concentrations.	• Use of reduced sulfur sources such as bisulfide (HS-) and cysteine instead of sulfate (Hu et al., 2015).

1.8. Thermodynamics in anaerobic fermentation

A myriad of metabolic pathways can be realized by anaerobic communities in the ranges of pH and temperature in which CE and SF perform best. When the community is not limited by the lack of a gene, its expression, or by kinetic phenomena, it is ultimately limited by thermodynamics. It has been shown that such thermodynamic limitation holds true for many metabolic routes in anaerobes (Kleerebezem and Stams, 2000; Heimann et al., 2010; Richter et al., 2016b). Catabolic reactions most relevant to SF and CE are shown in Table 2 with their Gibbs free energy calculated for biochemical standard conditions (T=298 K; pH 7.0; 1 M or 100 kPa of each reactant and product) as well as for conditions closer to those of an anaerobic fermenter co-fed with syngas (pH=5.5, T=310 K, 100 mM acetate, P_{H2}=P_{CO2}=P_{CO}=30 kPa, 10 mM or 1 kPa for other reactants and products). As shown in Table 2, some strategies are conceivable to selectively favor MCC formation. According to reactions No. 6 - 10, high concentrations of SCCs thermodynamically favor CE reactions. This is, indeed, seen in practice in experiments with acidogenic reactors (Arslan et al., 2016) besides giving selective advantage to acidogenic bacteria over methanogenic archaea at a defined pH (Zhang et al., 2018). As a trade-off, SCC concentrations higher than 50 mM generally increase the lag-phase of anaerobic cultures (Jaros et al., 2012).

Ethanol, which is a common electron donor for CE, can be formed by acetate reduction assisted with H_2 consumption in the near-equilibrium reaction No. 3 or with CO consumption in the more exergonic reaction No. 4 (Table 2). Biologically, however, not every homoacetogen is able to couple ethanol formation with net ATP gain (Molitor et al., 2017) and autotrophic ethanol production from H_2/CO_2 or CO is less frequently observed than homoacetogenesis in microbial communities. As an example, ethanol formation from H_2/CO_2 by *Acetobacterium woodii* would lead to net ATP loss. On the other hand, *Cl. autoethanogenum* is able to sustainably produce ethanol from H_2/CO_2 or CO (Mock et al., 2015).

Table 2. Reactions in syngas-aided CE performed by an open mixed culture and their thermodynamic feasibility. For conciseness, the most essential reactions are shown and reactions that occur in practice can be derived from them. For instance, in certain conditions of substrate concentration conventional CE with *Cl. kluyveri* occurs through five times reaction No. 8 or No. 9 coupled with the reverse reaction of No. 5.

	No.	Reaction (reverse reaction)	$\Delta G_r'^0$ kJ	$\Delta G_r'^{310K}$ kJ	$\Delta G_r^{Reactor}$ kJ
Syngas Fermentation	1	Hydrogenotrophic acetogenesis (acetate oxidation) $4H_2 + 2CO_2 \rightarrow CH_3COO^- + H^+ + 2H_2O$	-95.1	-88.0	-66.4
	2	Carboxydotrophic acetogenesis $4CO + 2H_2O \rightarrow CH_3COO^- + H^+ + 2CO_2$	-175	-172	-162
	3	Acetate reduction to ethanol (excessive ethanol oxidation) $CH_3COO^- + H^+ + 2H_2 \rightarrow CH_3CH_2OH + H_2O$	-9.64	-6.48	-15.1
	4	Acetate reduction to ethanol with CO $CH_3COO^- + H^+ + 2CO + H_2O \rightarrow CH_3CH_2OH + 2CO_2$	-49.6	-48.0	-62.8
	5	Carboxydotrophic hydrogenogenesis $CO + H_2O \rightarrow H_2 + CO_2$	-20.0	-20.9	-24.1
Chain Elongation	6	Ethanol-acetate elongation to *n*-butyrate $C_2H_5OH + CH_3COO^- \rightarrow CH_3(CH_2)_2COO^- + H_2O$	-38.6	-38.3	-32.3
	7	Ethanol-butyrate elongation to *n*-caproate $C_2H_5OH + CH_3(CH_2)_2COO^- \rightarrow CH_3(CH_2)_4COO^- + H_2O$	-38.8	-38.5	-26.6
	8	Ethanol-propionate elongation to *n*-valerate $C_2H_5OH + CH_3CH_2COO^- \rightarrow CH_3(CH_2)_3COO^- + H_2O$	-38.6	-38.3	-26.4
	9	Lactate-acetate elongation to *n*-butyrate $CH_3CHOHCOO^- + CH_3COO^- + H^+ \rightarrow CH_3(CH_2)_2COO^- + H_2O + CO_2$	-57.7	-58.4	-64.4
	10	Lactate-butyrate elongation to *n*-caproate $CH_3CHOHCOO^- + CH_3(CH_2)_2COO^- + H^+ \rightarrow CH_3(CH_2)_4COO^- + H_2O + CO_2$	-57.9	-58.6	-49.8
Biomass conversion	11	Anaerobic hexose oxidation to acetate $C_6H_{12}O_6 + 2H_2O \rightarrow 2CH_3COO^- + 2H^+ + 4H_2 + 2CO_2$	-213	-225	-226
	12	Anaerobic hexose oxidation to *n*-butyrate $C_6H_{12}O_6 \rightarrow CH_3(CH_2)_2COO^- + H^+ + 2H_2 + 2CO_2$	-261	-270	-273
	13	Hexose to propionate $C_6H_{12}O_6 + 2H_2 \rightarrow 2\,CH_3CH_2COO^- + 2H^+ + 2H_2O$	-357	-358	-345
	14	Lactate fermentation from hexose $C_6H_{12}O_6 \rightarrow 2\,CH_3CHOHCOO^- + 2H^+$	-194	-198	-192
	15	Cellulose hydrolysis $C_6H_{10}O_5 + H_2O \rightarrow C_6H_{12}O_6$	-6.27	-6.60	-6.60
Competing	16	Hydrogenotrophic methanogenesis $4H_2 + CO_2 \rightarrow CH_4 + 2H_2O$	-131	-126	-122
	17	Acetotrophic methanogenesis $CH_3COO^- + H^+ \rightarrow CH_4 + CO_2$	-35.7	-37.9	-55.8
	18	Lactate oxidation to acetate $CH_3CHOHCOO^- + H_2O \rightarrow CH_3COO^- + 2H_2 + CO_2$	-9.46	-13.6	-17.0

$\Delta G_r'^0$ is the Gibbs free energy of reaction for biochemical standard conditions, i.e. T=298.15 K, activities equal to 1 and pH=7.

$\Delta G_r'^{310K}$ is the Gibbs free energy of reaction for standard conditions, except T=310.15 K.

$\Delta G_r^{Reactor}$ is the Gibbs free energy for conditions assumed for a simultaneous SF/CE reactor: pH=5.5, T=310.15 K, 100 mM acetate, $P_{H2}=P_{CO2}=P_{CO}=30$ kPa, 10 mM (or 1 kPa) for other reactants and products. Calculation of Gibbs free energy, correction for temperature and chemicals activity were done according to Kleerebezem and Van Loosdrecht (2010).

At pH 7.0 reactions can be more accurately described with bicarbonate instead of $CO_{2\ (g)}$. In that case, consider the reaction:

$$CO_2 + H_2O \rightarrow HCO_3^- + H^+ \qquad\qquad \Delta G_r'^0 = 4.7\ kJ \qquad \Delta G_r'^{310K} = 5.4\ kJ$$

CO is an important inorganic substrate because it removes kinetic hindrances of solventogenesis and the WLP. This is because CO can be used to reduce ferredoxin which is a key electron carrier for reductive metabolism (Figure 1a). Thermodynamically, acetogenesis and solventogenesis with CO (reactions No. 2 and 4, respectively, Table 2) are more favorable than the hydrogenotrophic reactions (reactions No. 1 and 3). Nevertheless, the role of CO in a community can be seen as a double-edged sword. CO is a substrate that can increase autotrophic activity, promote cell biomass formation and sustain solventogenesis, but it has nonselective inhibitory and toxic effects on microorganisms. Further, resistance to CO varies among different microbial species and although it is possible for a community to become acclimatized to it, high CO partial pressures limit microbial diversity (Guiot et al., 2011; Esquivel-Elizondo et al., 2017b). The main toxicity mechanisms of CO in microorganisms are due to irreversible inhibition of metalloenzymes such as the ferredoxin-dependent hydrogenases (Ragsdale, 2004; Yasin et al., 2015). Since hydrogenases and other enzymes involved in the electron transport are metalloenzymes, this mechanism can explain the observed hindrance of H_2 and CO_2 consumption by autotrophs in the presence of CO (Diender et al., 2015). Whatever the consequences of CO on biomass degradation, SF, or CE are, further studies aiming to understand these trade-offs could add much to the topic of integrating syngas to the carboxylate platform.

H_2 is formed during ethanol-based CE (e.g. 4 times reaction No. 6 coupled with a reversed reaction No. 3, Table 2) and anaerobic fermentation of sugars (reactions No. 11 and 12) (Arslan et al., 2012; Angenent et al., 2016). These exergonic reactions are often limited by kinetics rather than by thermodynamic equilibrium and high partial pressures of H_2 are not enough to completely halt them (Gonzalez-Cabaleiro et al., 2015). However, supplying exogenous H_2 to an anaerobic community can help to select mixotrophic bacteria that grow on both organic and inorganic (H_2/CO_2) substrates. Mixotrophic acetogens are able to improve conversion efficiency of electrons and carbon by realizing homoacetogenic fermentation, via which 1 mol of a hexose is converted to 3 mols of acetate (reaction No. 11 coupled with reaction No. 1, Table 2) (Schuchmann and Muller, 2016). Also the production of carboxylates with chains longer than acetate can be improved by H_2 addition. A study done by Arslan et al. (2012) found that a microbial community fed by higher H_2 partial pressures had improved conversion of carbohydrate-rich waste and yielded more acetate, *n*-butyrate, and *n*-caproate. Production of longer-chain carboxylates from H_2 and CO_2 is believed to not occur with H_2 as a direct ED and it is thought to be intermediated by ethanol and acetate instead (Ding et al., 2010; Gonzalez-Cabaleiro et al., 2015).

There is still no clear model for how H_2 is able to improve MCCs yields in lactate-based fermentation with mixed cultures athough it has been observed consistently (Andersen et al.,

15

2015; Scarborough et al., 2018a; Wu et al., 2019). Small amounts of lactate are produced by homoacetogens such as *Cl. ljungdahlii* growing on syngas (Hermann et al., 2020). Since lactate-base CE has very favorable thermodynamics (Reactions No. 9 and 10, Table 2), low concentrations of lactate produced by homoacetogens could, in principle, be enough to enable lactate-based CE by other fermentative bacteria in the community. Analogously to ethanol-based CE realized by *Cl. kluyveri*, the lactate-based chain elongator *Ruminococcaceae* bacterium CPB6 also oxidizes part of the lactate into SCC for ATP generation, producing H_2 as consequence (reaction No. 19) (Zhu et al., 2017; Wang et al., 2018). Similar metabolism is seen in mixed cultures (Zhu et al. 2015) where consumption of 3 mols of lactate produces 2 moles of H_2, 3 moles of CO_2 and 1 mol of *n*-caproate. If autotrophs are active in the community, the produced H_2/CO_2 can be reincorporated to the carboxylate pool via the WLP.

The predictive power of such thermodynamic analysis in MCC production is limited to the when product and substrate inhibition is negligible. The longer the chain of the carboxylate or alcohol the higher is its inhibiting effect on a mass basis. Moreover, inhibition by MCCs is especially strong in acidic media, where more carboxylates are found in their undissociated form. Undissociated carboxylic acids can jeopardize the pH homeostasis of cells by passively crossing the cellular membrane or even by dissolving it. Accordingly, inhibition by MCAs occurs due to their hydrophobic nature.

The effects of temperature on the thermodynamics also need to be taken into consideration. Besides the clear effect of temperature on microbial kinetics, temperature changes the solubility of gases in water and the Gibbs free energy of reactions realized by the microbial community. Figure 3 depicts the effects of temperature on gas solubility and reactions energetics in the range from 25°C to 55°C. Figure 3a shows particular strong effects of temperature on the solubility of CO_2 and CO, while solubility of H_2 barely changes. Even when CO_2 and CO are not the limiting substrates, lowering the temperature to increase their solubility can be worth considering, since experience has shown that increasing the availability of these substrates significantly impacts the process performance (Roghair et al., 2018a). On the other hand, diffusion coefficients increase with temperature, thus, lowering temperature to increase gas solubility should be applicable to systems that are not limited by gas-liquid mass-transfer (Diender et al., 2015).

a

b
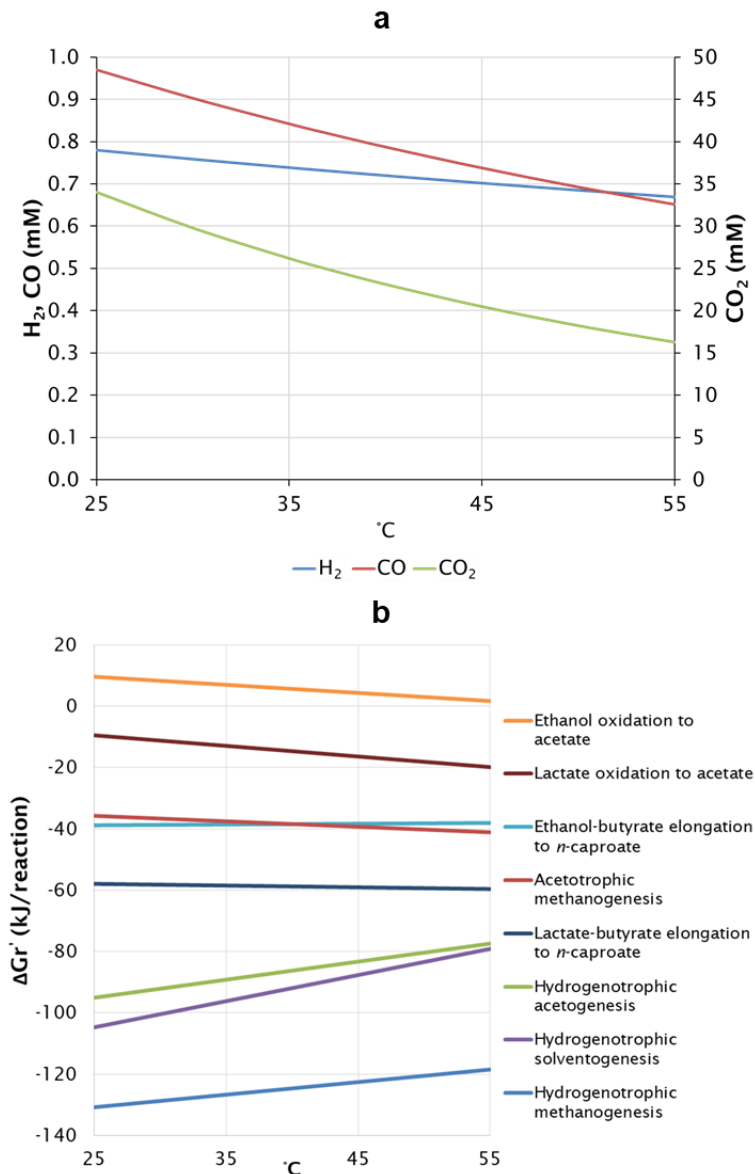
Figure 3. Lower temperatures increase the solubility of gaseous substrates in water (**a**), thermodynamically favor gas-consuming reactions and have little effect on CE reactions (**b**). Gas solubility values calculated for unbuffered water using Henry's law with temperature correction according to the Van't Hoff equation. $\Delta G_r'^0$ is the Gibbs free energy of reaction with activity of chemical species equal to 1, at 25°C and pH=7.0.

In general, lower temperatures make gas-consuming reactions more favorable with a particular strong effect on hydrogenotrophic solventogenesis (Figure 3b). This could explain better yields of *n*-caproate and *n*-hexanol obtained by Ramio-Pujol et al. (2015) when growing *Cl. carboxidivorans* on syngas at 25°C in comparison to cultivations at 37°C. Reactions able to generate ATP through substrate level phosphorylation, i.e. ethanol and lactate oxidation, are less favorable at lower temperatures (Figure 3b). Even though bacteria partly rely on such reactions during CE, low temperatures might not have a prohibiting to CE since most of energy of the pathway is harvested from the membrane ion-motive force via ATP synthase (Angenent et al., 2016) (Figure 1b). The effect of temperature on thermodynamics of ethanol- and lactate-based

CE reactions is nearly negligible in the range of 25°C and 45°C ([Figure 3b](#)). In the practice, however, most CE studies are carried out between 30°C and 40°C and, for unclear reasons, MCC production is very limited at temperatures higher than 40°C (Holtzapple et al., 2022; Wang and Yin, 2022).

With 122 kJ reaction^{-1} available for energy conservation, hydrogenotrophic methanogens rely on the very exergonic HM (Reaction No. 17, [Table 2](#)) which are often inhibited by kinetics rather than thermodynamics. Hence, temperatures lower than 25°C have been proposed as a tool to decrease HM activity in acidogenic reactors (Liu et al., 2018), despite the improved thermodynamics of HM at lower temperatures ([Figure 3b](#)). However, the fact that some industrial scale biogas reactor can operate at temperatures around 25°C (Liebetrau et al., 2019) suggests that low temperature operation alone might not be sufficient to outcompete methanogens.

1.9. Hydrogen, carbon dioxide, and carbon monoxide availability to microorganisms

H_2 and CO are poorly soluble in water ([Figure 3a](#)) and improving gas-liquid mass transfer is a center topic in SF. Be it in bubble column, gas-lift, or stirred-tank reactors, SF depends on high bubbling flow rates to overcome mass transfer limitations. Even when not consumed, excess H_2 and CO in the broth reduces oxidation-reduction potential (ORP) and ratios of reduced electron carriers in the cell (Valgepea et al., 2018) affecting metabolic pathways, steering product pools, and selecting for auto- and mixotrophic microorganisms in a community. Moreover, intensive bubbling in stirred reactors also offers the secondary advantage of lowering the power input of stirring (Takors et al., 2018). At first thought, high gas flow rate seems to be incompatible with the typically low consumption rates of syngas by mixed cultures (Molitor et al., 2017). Gassing out unconverted syngas for dozens of days as a microbial community shapes itself might be unfeaseble even at lab-scale reactors. Moreover, syngas might be consumed at even slower rates when co-fed with organic feedstocks. Therefore, recirculating gas – in contraposition to a one-pass strategy – might be more adequate to mixed cultures and syngas co-feeding ([Figure 4](#)).
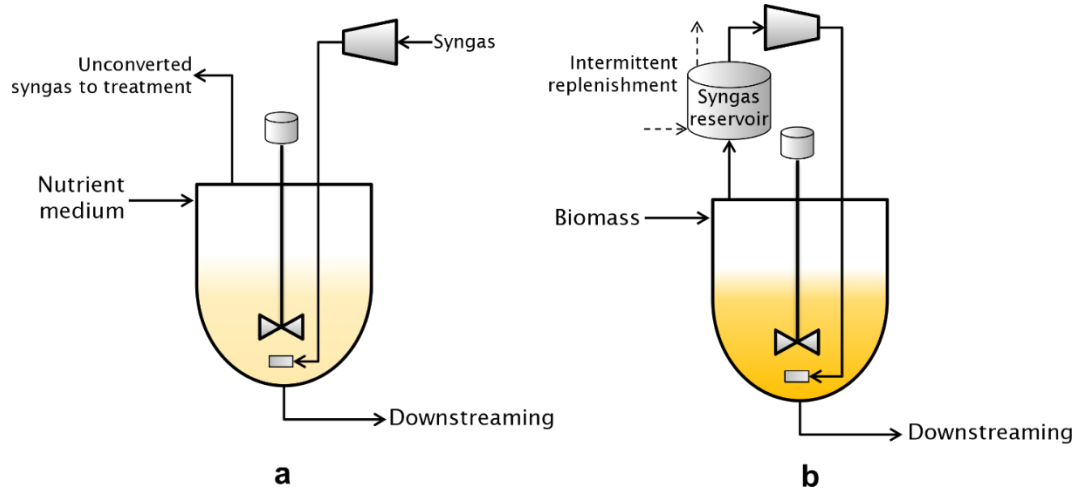
Figure 4. Strategies for continuous syngas supply to bioreactors. **a** Bioreactor with conventional single-pass gas strategy commonly used in SF studies and pure cultures. **b** Bioreactor with gas recirculation, possibly a more fitting strategy for microbial communities and syngas co-feeding with organic feedstocks (biomass).

Gas recirculation has not been a common strategy for bioreactors fed with syngas. This is partly due to the fact that SF reactor systems have been usually developed for pure cultures, as seen in the reactor schemes described by Asimakopoulos et al. (2018). With a gas recirculation strategy (Figure 4b), the syngas flow rate can be kept high regardless of the community's gas consumption rate. This way, higher H_2 and CO conversion can be achieved without harming gas-liquid transfer. Gas recirculation also means that gas composition inevitably changes with time and the depletion of H_2 and CO together with the accumulation of other gases (inhibitors, inert gases, and methane) needs intermittent feeding and purging cycles to be carried out.

One reason to avoid operating at too low H_2 partial pressures during gas recirculation is that it can selectively favor HM considering that hydrogenotrophic methanogens are known to have higher affinity to H_2 than homoacetogens (Heimann et al., 2010). Besides, the amount of gaseous substrate in the aqueous phase in the equilibrium, C_g^*, depends on the partial pressure of gas, p_g, according to Henry's law (Equation 1). In the kinetic regime, the actual available gaseous substrate to microorganisms, C_g, also depends on C_g^* according to Equation 2, described for a 1st order one-dimensional diffusion. Consequently, a low p_g of the gaseous substrate also lowers mass transfer rates. Such transient characteristic of gas recirculation and its effect on the community metabolism would also have to be considered.

$$C_g^* = H \, p_g \tag{1}$$

$$\frac{dC_g}{dt} = k_l a \, (C_g^* - C_g) \tag{2}$$

For Equations 1 and 2: C_g^* is the equilibrium concentration of gas in the liquid, in M; H is the Henry coefficient for the gas, in M/atm; p_g is the partial pressure of the gas, in atm; $k_l a$ is the coefficient of gas-liquid transfer per area times the interfacial gas-liquid area per volume, in h^{-1};

and C_g is the concentration of gas in the liquid, in M. $k_l a$ depends on the gas flowrate, on the strategy for liquid-gas contact in the reactor, and on the gas diffusivities.

CO_2 is not commonly the limiting gaseous substrate, nevertheless, concentration of this gas can become limiting in some cases in acidogenic systems (Vasudevan et al., 2014). CO_2 differs itself from H_2 and CO as solubility of CO_2 is controlled by – besides temperature (Figure 3a) – chemical equilibria of the carbonate system (Figure 5). As a consequence, CO_2 solubility is highly dependent on the pH for values between 5.0 and 8.0, a range within which most acidogenic bioreactors work. At pH values lower than 5.0, CO_2 solubility is lowest, though water still harbors a significant fraction of CO_2 (roughly 45%) in form of aqueous CO_2.
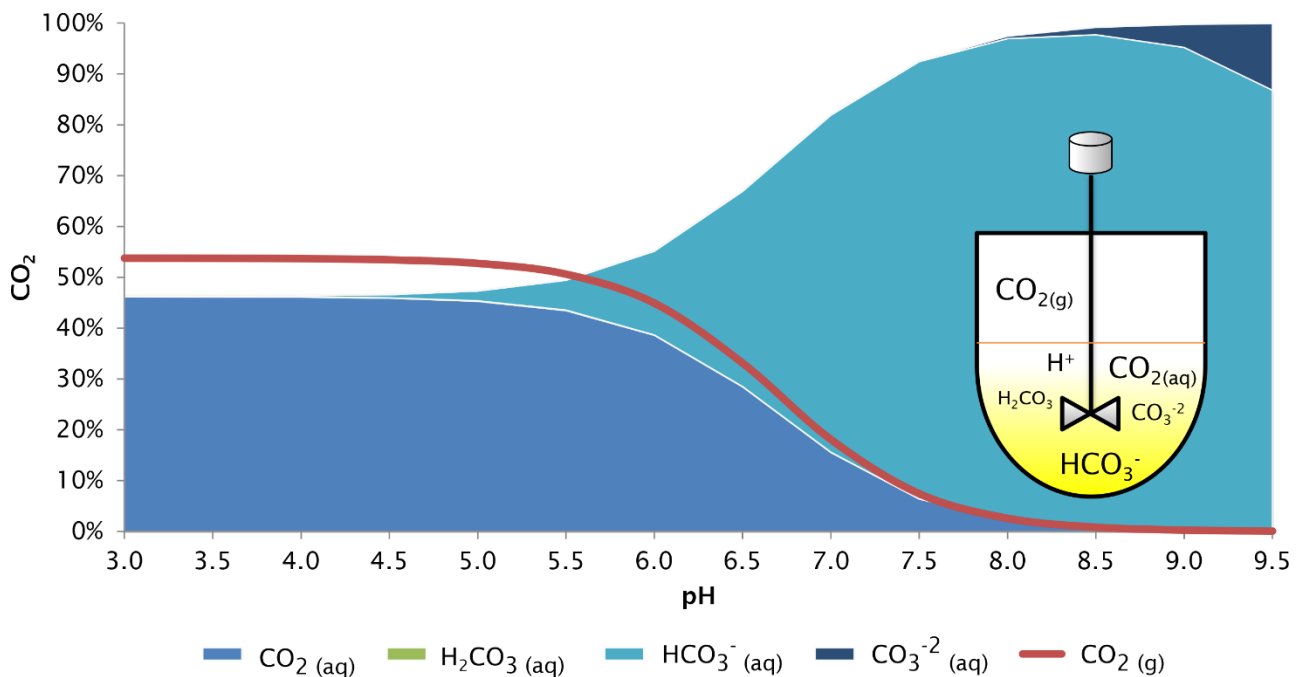
Figure 5. Percentages of CO_2 species in the gas and in the aqueous phase as function of pH at 25°C for a closed system with 50% headspace and a diluted aqueous phase. For CO_2 partial pressures that are not too high (<1000 kPa), this pattern is independent of the total amount of CO_2 in the system (Diamond and Akinfiev, 2003). The carbonic acid species is present in very small amounts and it is, therefore, not visible in the graph. Calculations were done similarly to Seinfeld and Pandis (2016). Henry's law and dissociation constants were obtained from Sander (2015) and Greenwood and Earnshaw (2012), respectively.

1.10. Product downstream processing

Traditionally, anaerobic fermentation research has taken profit from lessons learned in anaerobic digestion research (Agler et al., 2014). Nevertheless, one specific challenge of anaerobic fermentations is product downstream processing (DSP). Unlike methane, the desired product in anaerobic digestion, linear MCCs and MCAs are liquids under ambient conditions and form aqueous solutions. Distillation, the DSP technology classically adopted in the ethanol and acetate industries, could be considered as an alternative for purification of their longer-chain counterparts. However, high operational costs could incur on distillation of MCC and MCA because their concentrations in the broth are generally lower than 2% w/v (i.e. 20 g/L) (Arslan

et al., 2016), in comparison to the typical concentrations in ethanol fermentation of at least 6% w/v (Dias et al., 2015).

Solubility of MCCs and MCAs in water decreases the longer their carbon chain is. As a consequence, in industrial scale, *n*-caproate and *n*-caprylate could have lower DSP costs due to their lower solubility, in comparison to *n*-butyrate, which is miscible in water. Besides, carboxylates tend to be less soluble in water at lower pH values, when they are found in their non-ionized forms. These features were explored in previous studies that used liquid-liquid extraction with apolar solvents and pH shifts to extract MCCs (Agler et al., 2014; Ge et al., 2015; Braune et al., 2021). Differently from organic acids, solubility of alcohols cannot be altered by changing pH so their DSP options a more restricted, essentially, to the techniques of traditional solvent-water extraction, such as 'salting out'. DSP might be a decisive criterion to favor the production of MCCs over MCAs, especially considering that further conversion of MCCs to MCAs or alkanes can adopt mature chemical conversion routes (Pham et al., 2010; Holtzapple et al., 2022). Further processing of MCCs is a promising option for alkane production and can be achieved through, for instance, Kolbe electrolysis (Urban et al., 2017).

1.11. Stoichiometry and economic feasibility of the process

The most fundamental limitation of feedstock biomass conversion is imposed by the overall stoichiometry of the process. The stoichiometry of the process depends on the substrate, the final product, and on the pathways used to reach it. Neglecting the inorganic fraction of dry lignocellulosic biomass and assuming the chemical formula of cellulose ($C_6H_{10}O_5$), <u>Figure 6</u> compares the maximum stoichiometric yields for some carboxylates, alcohols, and biomethane. Without considering the intricacies of the conversion of recalcitrant fractions, both major processes for making biomass bioavailable (i.e. hydrolysis and biomass gasification) present equivalent theoretical stoichiometric yields. Big differences in the maximum stoichiometric conversion appear depending on the ability of the biocatalyst to grow mixotrophically or not, as seen for acetate in <u>Figure 6</u>. Cultures that grow only heterotrophically do not reincorporate H_2 and CO_2 produced in the fermentation of biomass-derived sugar and have, therefore, lower maximum conversion to carboxylates. For methane production, stoichiometric conversion from biomass (cellulose) is inherently low regardless if it is produced through HM, AM, or methylotrophic methanogenesis.
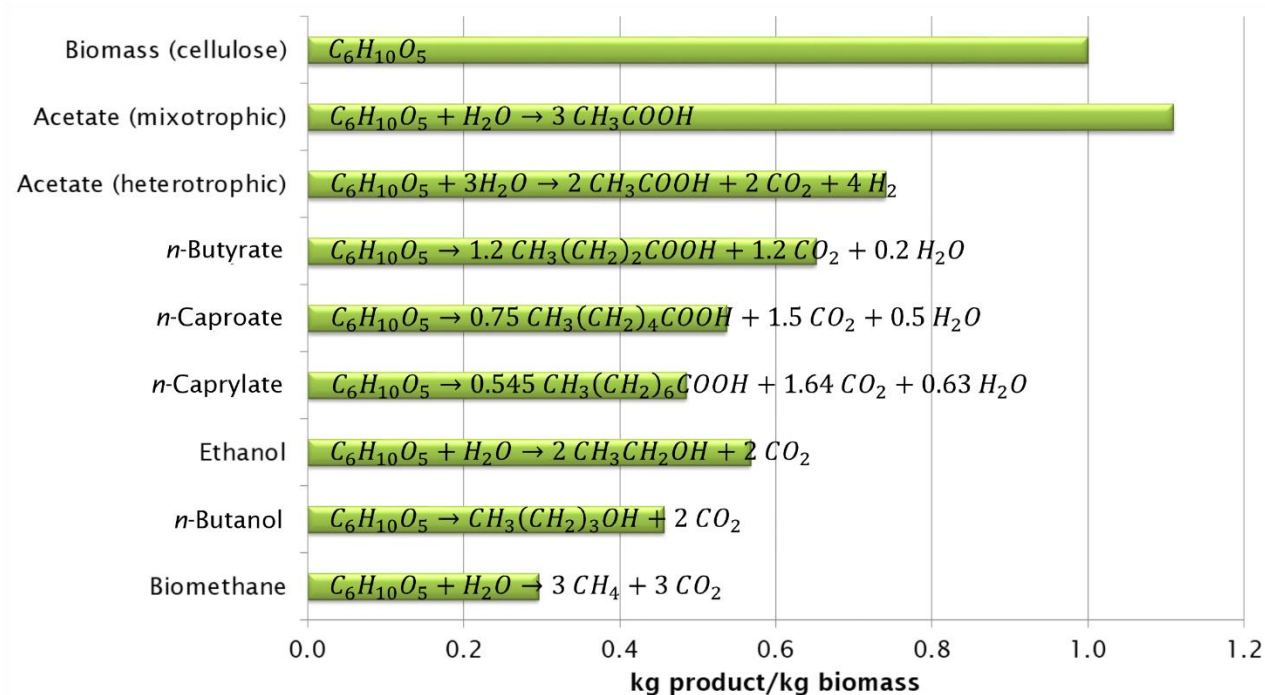
Figure 6. Stoichiometric yield limits of biomass derivatives. The chemical formula of cellulose is assumed for the biomass substrate. 1 mol of cellulose consumes 1 mol of water through hydrolysis or through gasification, the latter producing syngas (H_2/CO_2/CO). The reactions for *n*-butyrate, *n*-caproate, and *n*-caprylate are for bioprocesses in which the H_2 and CO_2 produced during fermentation can be reincorporated into the carboxylate pool via SF.

Producing longer-chain carboxylates and alcohols increases the potential for carbon emissions and decreases the maximum stoichiometric conversion ([Figure 6]). In an integrated biorefinery process this should not be a problem because SF allows reincorporation of CO_2 into the carboxylate pool as long as enough sustainably-sourced H_2 is supplied. Thus, production of chemicals beyond acetate and ethanol from syngas is a promising concept as a bioprocess and its success as an industrial process depends basically on ensuring a sufficient conversion of syngas and biomass to chemicals in the bioreactor with low-cost process.

Considering dry biomass as the raw material (with the cellulose chemical formula) and the maximum stoichiometric conversion, [Figure 7] presents the cost gaps for each product of different bioprocess concepts, in comparison to other more mature process.
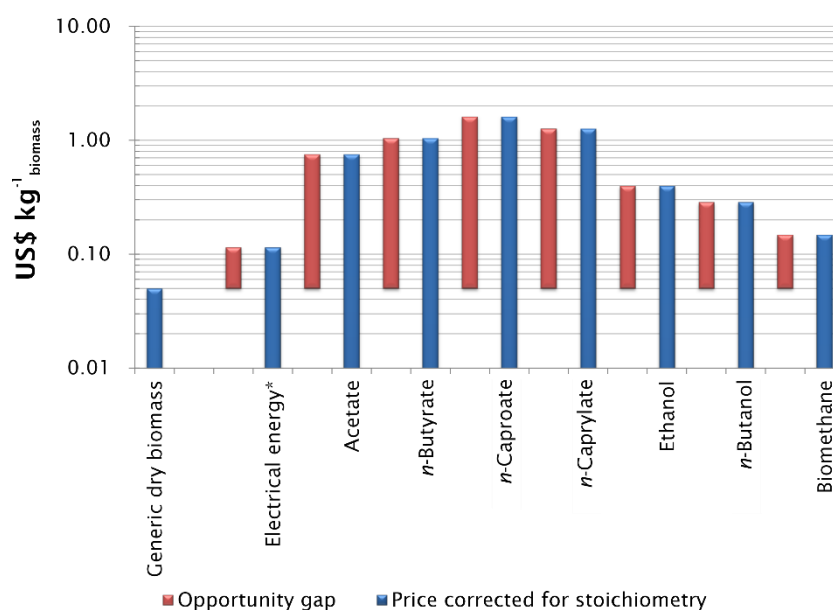
Figure 7. Different alternative uses of feedstock biomass in US$ (2016) on a basis of 1 kg of dry biomass. The chart considers maximum stoichiometric conversions together with market prices on a single basis of kg of biomass (cellulose). A generic cost of 0.05 $ per kg of dry biomass is assumed. *Considering 1 kWh per kg of dry biomass and 0.12 $ kWh^{-1}. Elaborated based on information from Kleerebezem and van Loosdrecht (2007); Granda (2015); Biddy et al. (2016); DOE (2016); de Medeiros et al. (2017).

Each kilogram of dry biomass, once converted to syngas, has the highest margin if used to produce n-caproate, 1.61 $ $kg_{biomass}^{-1}$ (before considering conversion losses and process costs), in comparison to 0.40 $ $kg_{biomass}^{-1}$ when used to produce ethanol. This is due to the actual high market price of n-caproate of around 3.00 $ kg^{-1} in high-value markets such as food/feed additives, cosmetics, and food-grade sanitizers (Granda, 2015). However, prices per kilogram for commodity-grade chemicals like ethanol are generally much lower than specialty chemicals like n-caproate. Despite many possible applications, the n-caproate market is still small in comparison to acetate, ethanol, and n-butanol. If MCCs become a chemical platform for alcohol, ketone, and hydrocarbon commodities, their prices (and production costs) will have to be low enough to compete with the existing fossil-based chemical platforms.

1.12. Open questions and research proposal

Among the different process rationales for merging the carboxylate and syngas platforms, those relying on mixed cultures offer the most promise as they enable high MCC titers and the conversion of all types of biomass. Yet, our knowledge about these processes is the most limited.

The extent to which syngas can help enhance MCC production with mixed cultures is not known. Depending on the study, the improvement of n-caproate production by addition of H_2 is in the range of 10% to 130% and no such estimates exist for exogenous CO. Besides, most of these studies have been carried out in batch systems and idealized environments. Operation of mixed culture fermentation in open systems is necessary to identify which competing pathways need to be considered and to discover yet unknown challenges and synergies of combining the syngas and carboxylate platforms. The lack of experiments using continuous reactors may be

due to the difficulty of reconciling two types of substrate with different kinetics in anaerobic communities (i.e. H_2, CO_2, and CO as opposed to lignocellulose, lactate, and ethanol) using conventional chemostats.

The mechanisms via which syngas can enhance MCC production are also poorly understood. Interspecies ethanol transfer remains the main assumption for the observed synergy between SF and CE, even though it has never been tested. Uncultured bacteria, which are abundant in open cultures, could harbor new pathways for the production of C6 and C8 compounds from syngas. Thus, studying the structure of different communities with advanced molecular techniques during cultivation on syngas and biomass will help clarify these issues.

In this chapter, we have identified a one-pot process with microbial communities (<u>Figure 2e</u>) as the most promising strategy. Therefore, this work focuses on the use of microbial communities co-fed with syngas mixtures and organic substrates.

Firstly, 50-mL batch systems were used in which no cell washout nor microbial immigration occur. In these closed systems, different syngas mixtures were co-fed with organic model feedstocks under different operating conditions. Next, the co-feeding of syngas and organic substrates was adapted to open systems with 1-L bioreactors. Since syngas is a less favored substrate than high ATP-yielding organic substrates, a reactor with continuous gas recirculation (<u>Figure 4b</u>) was assembled and used as a toolbox to shape the microbial community in favor of mixotrophy. The resulting microbial communities were analyzed together with carbon and electron balances to support decision making in future scale-up projects.

2. Enriching communities in closed systems under hydrogen/carbon dioxide headspaces

This chapter is based on the publication:

Author contributions
Flávio C. F. Baleeiro: conceptualization, methodology, investigation, data analysis, visualization, first draft, and manuscript revision.
Sabine Kleinsteuber and Heike Sträuber: conceptualization, methodology, project supervision, data analysis support, and manuscript revision.

2.1. Introduction

This chapter investigates the effects of H_2 feeding on MCC production in serum bottles by: *i*) enriching three microbial communities from different inocula towards *n*-butyrate and MCC formation with H_2 as the main ED; *ii*) comparing the dynamics of the three microbial communities along the enrichment; *iii*) identifying adequate fermentation parameters; and *iv*) co-feeding conventional EDs (lactate and ethanol) and H_2 in the last enrichment step.

2.2. Materials and methods

2.2.1. Experimental design of batch cultures

The experiments carried out along with the community enrichment are schematized in Figure 8. The duration of each experiment varied from 21 to 92 days, depending on the time to reach stable *n*-caproate concentration or complete acetate consumption (Table A1). All conditions were tested in duplicates and included controls for the presence of H_2 (using N_2 instead) and abiotic controls (receiving 10% v/v of deionized, sterile water instead of inoculum). The batch experiments were done in 250 mL serum bottles filled with 50 mL culture liquid and capped with butyl rubber stoppers.
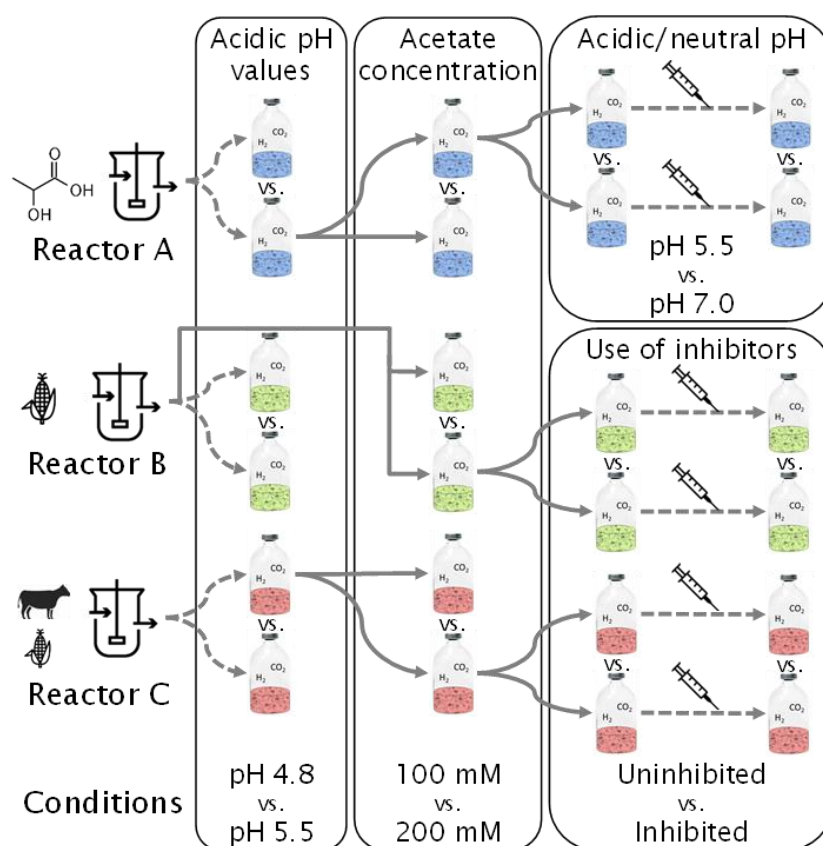
Figure 8. Enrichment scheme and overview of experiments. Reactor A was fed with lactate and xylan, reactor B with corn silage, and reactor C with corn silage and cow manure. The syringe icon symbolizes addition of organic EDs (lactate and ethanol). One bottle with H_2/CO_2 is depicted for each condition and experiment. Duplicates, H_2-free, and abiotic controls are not shown. Full arrows mean transfer from selected bottles with 10% inoculation. Dashed arrows mean new experiments without dilution of the inoculum.

The microbial communities originated from three different types of anaerobic, mesophilic reactors operating at near neutral or slightly acidic pH. Community A stemmed from a continuous bench-scale acidogenic reactor operated for MCC production, fed with xylan and lactate, operating at pH 5.5, 38°C, and an HRT of 8 d (Liu et al., 2020a). Community B stemmed from a continuous lab-scale acidogenic reactor operated for MCC production, fed with unsterile corn silage and inoculated from the reactor described by Lambrecht et al. (2019) (pH of 6.25, 38°C, and HRT of 4 d). Community C stemmed from a full-scale anaerobic digester operated for biogas production, fed with cow manure and corn silage, operating at 37°C, neutral pH, and with an HRT of 42 d. The reactors from which communities A and B originated produced mainly acetate, n-butyrate, and n-caproate, whereas the reactor from which community C originated produced biogas (CH_4 and CO_2). Inocula from reactors B and C were sieved under N_2 flow with a 0.355 mm mesh size to remove excessive amounts of solids.

Culture bottles were pressurized to approx. 2.0 bar_a of H_2/CO_2 mix (or N_2/CO_2 mix for H_2-free controls) with 80 vol.% H_2 (or N_2) and 20 vol.% CO_2 and incubated at 37°C in a rotatory shaker at 200 rpm. Headspaces were flushed and repressurized in the beginning of each experiment and whenever pressure was detected to be lower than 1.2 bar_a. Before inoculation and (re)pressurization, the headspace of each bottle was flushed with 250 mL min^{-1} of gas mixture for 10 minutes to purge the previous headspace and to ensure anoxic conditions.

In the first batch experiment, communities were tested at pH values of 4.8 and 5.5 in their original reactor broths (Figure 8). Acetate (100 mM) was added to act as a buffer and to thermodynamically favor CE over the more common acetate formation from H_2 and CO_2. The conditions resulting in highest MCC production for the majority of the communities in each batch experiment were applied as baseline conditions in the next experiment. Thus, for testing the effect of acetate concentration (second batch experiment) and for the inhibition experiment (third batch experiment), an initial pH of 5.5 was set in all bottles. For the third experiment (effect of pH in community A and effect of methanogenesis inhibition in communities B and C), the initial acetate concentration was 200 mM. As part of the enrichment scheme, the best-performing carboxylate-producing pair of duplicates was selected to inoculate the succeeding batch culture.

The inhibition experiment aimed to investigate the competition between methanogenesis and MCC production through the use of chemical methanogenesis inhibitors. Since community A showed no methanogenic activity, the effects of pH values of 5.5 and 7.0 were compared instead of using methanogenesis inhibitors. The fourth experiment consisted in the addition of 60 mM lactate and 30 mM ethanol to the bottles of the third experiment (Figure 8), aiming to investigate the effect of H_2 during lactate- and ethanol-based CE.

Starting from the second experiment, batch cultures were set up in a defined medium and inoculated with 10% reactor broth or broth from the first experiment. The basal growth medium was adapted from Liu et al. (2020a) differing in the absence of Na_2CO_3 and in the presence of

6.62 g L^{-1} sodium acetate and 1.16 g L^{-1} acetic acid (bottles with 100 mM acetate) or 13.24 g L^{-1} sodium acetate and 2.31 g L^{-1} acetic acid (bottles with 200 mM acetate). For the methanogenesis inhibition experiment, 10.5 g L^{-1} of sodium 2-BES was used for community C and 9 mL (ca. 4.5 kPa) of ethylene was added in the bottle headspace for community B. For 2-BES, the concentration used was based on Zinder et al. (1984). For ethylene, an amount just below the value tested on *Acetobacterium woodii* by Schink (1985b) was used. For the addition of organic EDs, 10 mL of pre-dissolved DL-lactic acid/ethanol in basal medium was added to each bottle to reach final concentrations of 5.4 g L^{-1} lactate (60 mM) and 1.4 g L^{-1} ethanol (30 mM) in order to start the experiment with 50 mL broth. During sampling procedures, the pH value was adjusted to 4.8, 5.5, or 7.0 with 4 M KOH or 4 M HCl if necessary. The main buffers in this study were acetate and other monocarboxylates (pK$_a$~4.8), the phosphate system (pK$_{a2}$~7.2), the carbonate system (apparent pK$_a$~6.1), and lactate (pK$_a$~3.8). Media were made anoxic by stirring in an anaerobic glovebox for at least three hours. Media were sterilized by autoclaving at 121°C for 20 minutes, except for vitamins and cysteine concentrates, which were sterilized by filtration with 0.2 μm cellulose acetate syringe filters (Labsolute, Germany).

2.2.2. Analytical methods

The serum bottles were monitored periodically for gas production and consumption, chemical composition of the gas and liquid phases, optical density at 600 nm (OD$_{600}$), and community composition with sampling procedures adapted from Logroño et al. (2020). Carboxylates and alcohols in the liquid phase were measured with high performance liquid chromatography (HPLC) coupled with a refractive index detector (RID) as described by Apelt (2020) using a modified method with a column temperature of 55°C and a flow rate of 0.7 mL min^{-1}. Determination of gas composition was analyzed with gas chromatography (GC) with a thermal conductivity detector (TCD) as described by Logroño et al. (2020). Monitoring of pressure and gas sampling in the headspace was done always before and after repressurization of bottles to determine the components balances in the gas phase.

2.2.3. Microbial community and correlation analyses

Amplicon sequencing of the 16S rRNA gene with Illumina MiSeq was done on cell pellets collected at the end of each batch. For community C in the first two experiments, genomic DNA was extracted from frozen cell pellets using the NucleoSpin Soil Kit (Macherey-Nagel, Germany) according to the manufacturer's manual. For all other cell pellets, NucleoSpin Microbial DNA Kit (Macherey-Nagel, Germany) was used. Quality assessment, quantification, and storage of the extracted DNA as well as polymerase chain reaction (PCR) and library preparation were done according to the protocols for 16S rRNA genes described by Logroño et al. (2020). Raw sequence data for this study was deposited at the European Nucleotide Archive (ENA) under the study accession code PRJEB40259 (http://www.ebi.ac.uk/ena/data/view/PRJEB40259). The primers used are described by Klindworth et al. (2013) and target the V3 and V4 regions of the 16S rRNA gene. Primer sequences were removed from adapter-clipped reads using Cutadapt (Martin,

2011) and further sequence data analysis was done through the DADA2 workflow, using the amplicon sequence variant (ASV) approach as described by Callahan et al. (2016). According to read quality profiles, forward and reverse reads were truncated at the length of 278 and the other parameters of the workflow were used in their default values. Taxonomic assignments were done using the SILVA 138 reference database (Yilmaz et al., 2014; McLaren, 2020). Diversity analysis, filtering, agglomeration, normalization, and subsetting of the microbiome census data were realized with the phyloseq package for R (McMurdie and Holmes, 2013). All samples were rarified to an equal depth of 40,000 counts (lowest read number was 43,381). For the predominating ASVs, MegaBLAST (Morgulis et al., 2008) was used to find the most similar cultured species within the NCBI standard nucleotide collection and the 16S ribosomal RNA sequences database (NCBI, 2018). A Spearman correlation matrix was used with $p<0.01$ for correlation analyses between ASV abundances and abiotic data considering the non-control culture bottles.

2.2.4. Assumptions for electron balances, rates, and selectivity

To quantify the chemical fluxes in the cultures, electron balances were calculated. Electron balancing overcomes the errors that unmonitored H_2O formation and consumption cause in mass and mole balances and gives a uniform basis to calculate the consumption and production of chemical compounds in terms of mol e⁻. To calculate biomass weight from biomass concentration (OD_{600}), a factor of 0.456 $g_{dry\ mass}$ L^{-1} per OD_{600} unit was used, which is an average value for *Escherichia coli* cultures (Myers et al., 2013) and was confirmed in our laboratory to be a realistic in-between value for anaerobic cultures grown autotrophically (Logroño et al., 2020) and heterotrophically (Liu et al., 2020a) in similar media.

Table A2 lists the components and their conversion factors considered in the balances. The relative standard deviations of the electron balances were typically between 2% and 20%, suggesting that the monitored compounds represented the bulk of the pool of electrons that were channeled during the fermentation. Error sources of the electron balances were most likely the decrease of broth volume due to sampling (typically 10% by the end of each batch), limited accuracy of the chemical analytics, and unmonitored compounds. As a convention, consumption of compounds is shown as negative values.

Production rates for the chemicals in the liquid and in the gaseous phase were calculated with Equations 3 and 4, respectively.

$$Production\ rate\ [mg\ L^{-1}d^{-1}] = \frac{C_f - C_i\ [mg\ L^{-1}]}{duration\ of\ experiment\ [d]} \tag{3}$$

where C_f and C_i are the concentrations of the chemical at the end and beginning of the experiment, respectively,

$$Gas\ production\ rate\ [mg\ L^{-1}d^{-1}] = \frac{m\ [mg]}{V_{broth}\ [L] \times duration\ of\ experiment\ [d]} \tag{4}$$

where V_{broth} is the average volume of broth along the experiment and m is the accumulated gas mass produced in the period.

Selectivity of organic EDs to caproate was calculated on the basis of electron equivalents according to Equation 5.

$$Selectivity\ [mol\ e^- caproate\ (mol\ e^- ED)^{-1}] = \frac{\Delta n_{caproate}\ [mol\ e^-]}{\Delta n_{ethanol} + \Delta n_{lactate} + n_{YE}\ [mol\ e^-]} \tag{5}$$

where $\Delta n_{ethanol}$ and $\Delta n_{lactate}$ are the consumed ethanol and lactate, respectively, n_{YE} is the amount of yeast extract initially present in the medium, in this study 4.3 mmol e$^-$ (500 mg L^{-1} in medium), and $\Delta n_{caproate}$ is the produced caproate. For the first experiment, which was done with the undiluted broth of reactors, an amount of yeast extract of 4.3 mmol e$^-$ was assumed to account for the unmonitored substrates present in the broth.

2.3. Results

Three different enrichment cultures A, B, and C were established and along the enrichment, the effects of different pH values, acetate concentrations, and methanogenesis inhibition measures on their production performances and community developments were studied in three consecutive batch experiments as shown in Figure 8. An overview of the *n*-butyrate and *n*-caproate production rates of the three communities at all conditions tested in this study is shown in Table A3.

2.3.1. Effect of different acidic pH values and acetate concentration.

First, the effect of H$_2$ addition on the communities in their original broth at pH values of 5.5 and 4.8 was investigated and the cultures were compared with H$_2$-free controls. Small H$_2$ consumption and no methanogenic activity was detected in community A (Figure 9a). At pH 5.5, H$_2$ addition resulted in the accumulation of on average 3712 mg L^{-1} (62 mM) more acetate (not shown) and 610 mg L^{-1} (6.9 mM) more *n*-butyrate in comparison to H$_2$-free controls. Initially, broth from reactor A still contained substantial amounts of carboxylates as well as unconsumed xylan and lactate as substrates, which contributed to some *n*-caproate production regardless of pH or H$_2$ addition. H$_2$ addition caused no significant difference in *n*-caproate production rates in community A at pH 4.8 and pH 5.5. However, the community showed higher H$_2$ consumption rates at pH 5.5 (Figure 9a).
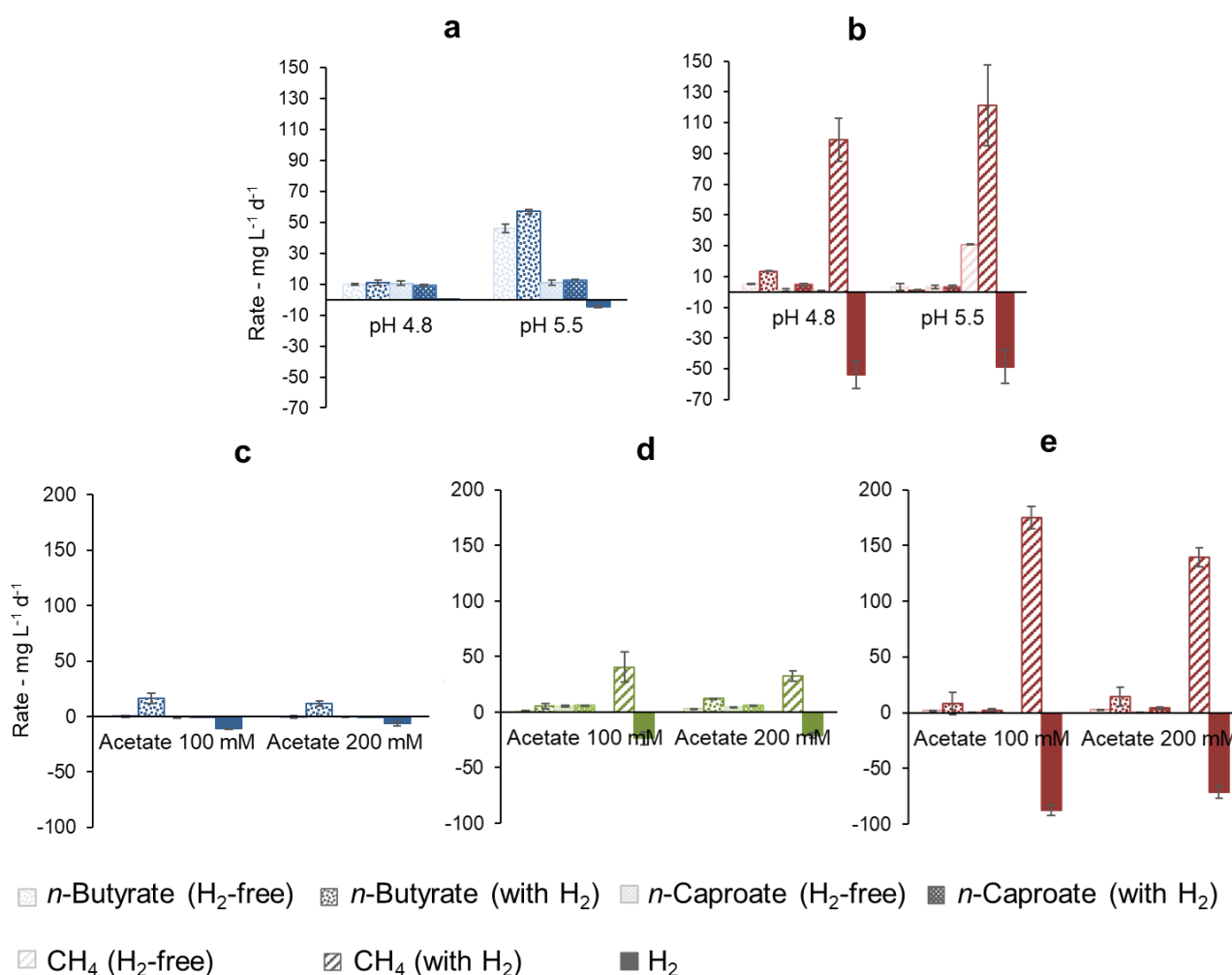
Figure 9. Effect of pH and acetate concentration on the production rates (positive values) and consumption rates (negative values) of n-butyrate, n-caproate, CH_4, and H_2. Communities A (**a** and **c**), B (**d**) and C (**b** and **e**) are shown. The pH experiment was carried out with 100 mM acetate in the original community broths. The acetate experiment adopted a pH of 5.5. Results for the pH experiment are not shown for community B as it showed no activity after acidification to the desired pH values. Error bars represent standard errors.

By monitoring of pressure and composition of gas and liquid chemicals, no microbial activity was detected in the broth from reactor B after acidification to pH 5.5 or 4.8. Broth of reactor B originally contained the highest concentration of carboxylates among the three broths used in this study (data not shown).

In comparison to community A, community C consumed more H_2 (Figure 9b). CH_4 was the main product, even at initial pH values as low as 4.8 and 5.5. At pH 5.5, acetate (100 mM) was depleted relatively fast at rates of 474 ± 2 mg L^{-1} d^{-1} (without H_2) and 278 ± 50 mg L^{-1} d^{-1} (with H_2). Acetate consumption caused the loss of buffering capacity and consequently a tendency for pH increase towards neutral conditions. At pH 4.8 with H_2, slow acetate consumption occurred at a rate of 35 ± 3 mg L^{-1} d^{-1}, but no acetate consumption was observed in H_2-free controls (-0.9 ± 1.8 mg L^{-1} d^{-1}). In this experiment with community C, accumulation of MCC was outperformed by methanogenic activity (Figure 9b). Still, at pH 4.8, a higher caproate concentration of $360 \pm$

31

28 mg L^{-1} (H_2-free: 50 ± 38 mg L^{-1}) was detected in the presence of H_2, whereas at pH 5.5 no such difference was seen (131 ± 13 mg L^{-1} and 124 ± 3 mg L^{-1} in H_2-containing and H_2-free bottles, respectively).

Since higher concentrations of acetate are known to selectively favor acidogens and CE over methanogens (Zhang et al., 2018; Cavalcante et al., 2020), the performances of cultures at acetate concentrations of 200 mM and 100 mM were compared in the following enrichment step.

Figures 9c, 9d, and 9e show production and consumption rates for n-caproate, CH_4, and H_2. For a deeper analysis including acetate and i-butyrate, Figure A1 presents balances in terms of electron equivalents. In Figure 9c, it can be seen that community A, free of methanogenic activity, could not produce n-caproate and its H_2 consumption (10.56 ± 0.01 mg L^{-1} d^{-1} and 6.5 ± 1.9 mg L^{-1} d^{-1} at 100 mM and 200 mM acetate, respectively) coincided with an accumulation of n-butyrate (between 12 ± 2 mg L^{-1} d^{-1} and 16 ± 5 mg L^{-1} d^{-1} at 200 mM and 100 mM, respectively). Higher acetate concentration was detrimental to H_2 consumption and n-butyrate production of this community, indicating that the microbiota may have been affected by acid inhibition.

Acetate concentration did not have a strong influence on carboxylate production by community B, whereas H_2 presence increased butyrate production slightly (Figure 9d). Communities B and C showed hydrogenotrophic methanogenic activity, which was partially suppressed by a higher acetate concentration (Figures 9d and 9e). There were no signs of methane production associated with acetate consumption in any of the cases. Accumulation of n-caproate, n-butyrate, and i-butyrate by community C was more favorable at higher acetate concentrations and in H_2-containing bottles (3.1 ± 0.7 mmol e⁻, 9.1 ± 2.7 mmol e⁻, and 3.1 ± 1.9 mmol e⁻, respectively), even though such effect was dwarfed by 209 ± 12 mmol e⁻ CH_4 produced by methanogenic activity (Figure 9d and Figure A1c).

As methanogenesis impeded enrichment of acidogenic microorganisms in communities B and C even with 200 mM acetate, the effect of methanogenesis inhibition was tested on these communities.

2.3.2. Effect of acidic/neutral pH (community A)

In the following enrichment step, pH values of 5.5 and 7.0 were tested on community A (Figure 8). Neither production of caproate nor consumption of H_2 in significant amounts were observed at this step (Figure A2a). Community A produced only n-butyrate (19 ± 9 mg L^{-1} d^{-1}) in the presence of H_2 and at pH 5.5. Subsequently, effects of pH values of 5.5 and 7.0 (and presence of H_2) were further compared after the addition of lactate (5400 mg L^{-1}) and ethanol (1380 mg L^{-1}) to the bottles with community A (Figure 8). Regardless of the pH value or H_2 presence, community A stopped consuming ethanol at a concentration of 185 ± 28 mg L^{-1} ethanol within the first five days, whereas lactate consumption halted at a concentration of 448 ± 181 mg L^{-1} lactate after nine to 19 days. Lactate and ethanol addition allowed higher n-butyrate production rates of 317 ± 107 mg L^{-1} d^{-1} (pH 5.5, with H_2) and 172.9 ± 0.7 mg L^{-1} d^{-1} (pH 7.0, with H_2) in

comparison to previous batches ([Figure A2b](#)). Some H_2 consumption could be maintained at pH 5.5 (14 ± 10 mg L^{-1} d^{-1}) and was more likely connected to *n*-butyrate production ([Figure A3a](#)). Nearly no *n*-caproate production could be maintained by community A at any of the pH values. At pH 7.0 in the absence of H_2, probably some lactate was converted to propionate.

2.3.3. Effect of methanogenesis inhibition (communities B and C)

For communities B and C, methanogenic activity was suppressed by the use of chemical inhibitors ([Figure 10](#)). H_2 consumption of 14.1 ± 5.6 mg L^{-1} d^{-1} (community B) and 4.4 ± 1.6 mg L^{-1} d^{-1} (community C) was observed in the cultures with inhibitor, but it was smaller than in the cultures without inhibitor. In this enrichment step, community B proved to be a better H_2 consumer than community C when methanogenesis was inhibited. Moreover, *n*-butyrate and *n*-caproate production rates of community B were clearly higher when H_2 was present. *n*-Caproate concentrations peaked at 1.9 g L^{-1} after 39 days under uninhibited conditions but averaged to 1.23 ± 0.03 g L^{-1} at the end of the experiment (48 days), suggesting that some caproate may have been consumed. Caprylate, which can be formed by CE coupled to *n*-caproate consumption, was not detected. Significant accumulation of *i*-butyrate was also observed in both communities in bottles with H_2. At the end of the experiment with community B, *i*-butyrate concentrations were 1.5 ± 0.1 g L^{-1} and 1.75 ± 0.06 g L^{-1} under uninhibited and inhibited conditions, respectively.
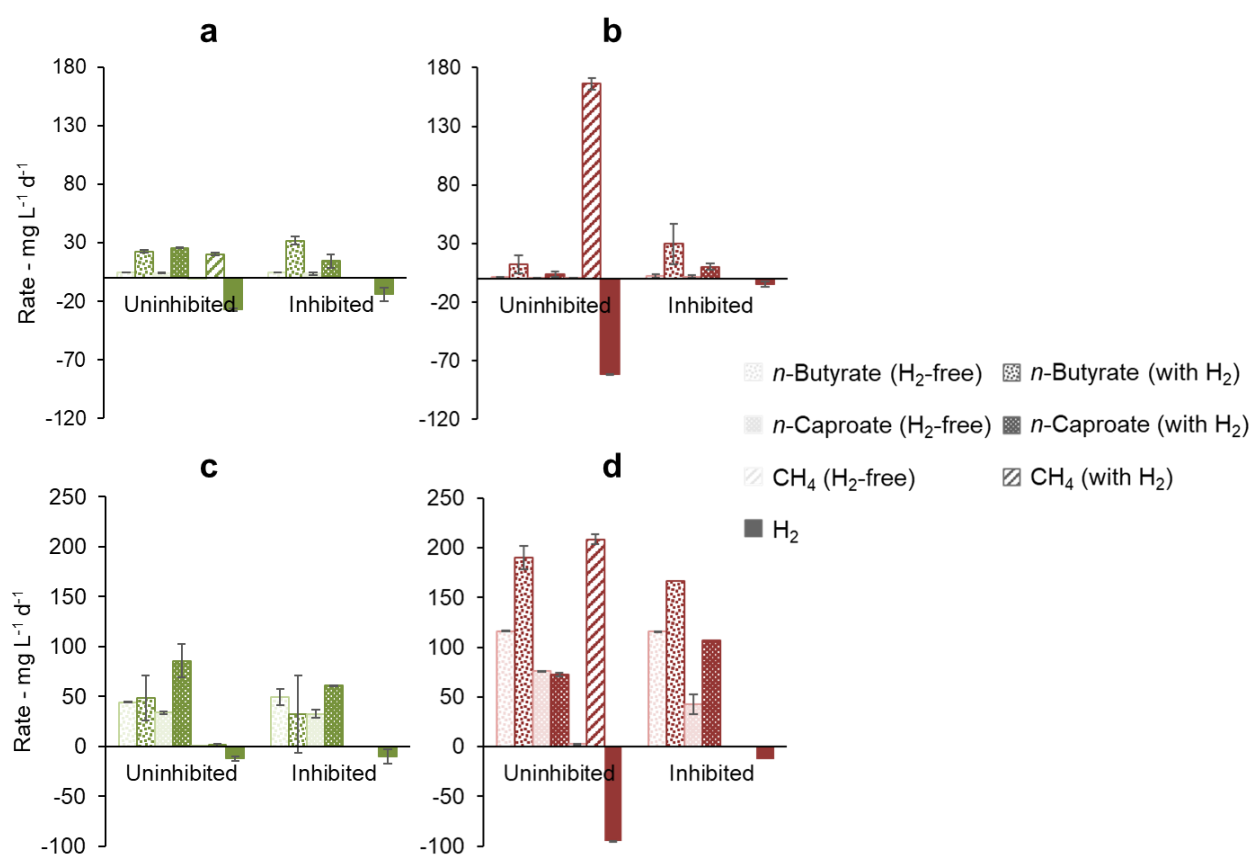
Figure 10. Effect of methanogenesis inhibition on production and consumption rates of *n*-butyrate, *n*-caproate, CH_4, and H_2 before (**a** and **b**) and after (**c** and **d**) addition of lactate and ethanol. Communities B (**a** and **c**) and C (**b** and **c**) are shown.

Regarding community C, the highest *n*-butyrate and *n*-caproate production rates were observed when H_2 and the methanogenesis inhibitor were present (Figure 10b). In this case, the inhibitor was decisive to prevent routing of H_2 to methane and thus to facilitate carboxylate production. Figure A4 illustrates how the methanogenesis inhibitor could avoid the periodical H_2 depletion in community C cultures.

To test communities B and C for the effects of H_2 addition and methanogenesis inhibition in the presence of lactate and ethanol, 5400 mg L^{-1} lactate and 1380 mg L^{-1} ethanol were added to the culture bottles (Figure 8).

Cultures of community B consumed lactate completely within the first 12 days whereas ethanol was completely consumed within 19 to 26 days. Most of the H_2 consumption occurred in the same period as lactate and ethanol consumption (Figure A5). Lactate and ethanol addition allowed much higher production rates of carboxylates in comparison to the previous experiments, up to 86 ± 17 mg L^{-1} d^{-1} *n*-caproate in community B (Figure 10c) and 190 ± 12 mg L^{-1} d^{-1} *n*-butyrate in community C (Figure 10d). Methanogenesis nearly stopped in community B without the use of an inhibitor (1 ± 2 mg L^{-1} d^{-1} CH_4) whereas it remained active in community C when an inhibitor was not present (209 ± 39 mg L^{-1} d^{-1} CH_4). In the presence of the organic EDs, non-methanogenic H_2 consumption was up to 12 ± 2 mg L^{-1} d^{-1} in community B (uninhibited conditions) and 13 mg L^{-1} d^{-1} in the bottle with inhibitor in community C (no standard error available).

Community B channeled between 79% and 143% more electrons into caproate when H_2 was present, as shown in the electron balance in Figure A3b. Among the bottles with H_2, bottles with inhibitor accumulated somewhat less *n*-caproate, but more *i*-butyrate. The positive effect of H_2 on the caproate production by community C was more distinct in the presence of the methanogenesis inhibitor, which guaranteed H_2 availability along the whole fermentation, similarly to what was observed before lactate and ethanol addition. The main end-products in terms of electron equivalents were (in descending concentrations) *n*-caproate, *i*-butyrate, and *n*-butyrate in community B (Figure A3b) and *n*-butyrate, *n*-caproate, and *i*-butyrate in community C (Figure A3c).

2.3.4. Development of caproate production and selectivity along the enrichment experiments

To show the impact of H_2 presence and of each condition on the efficiency of *n*-caproate production, Figure 11 depicts the selectivity to *n*-caproate and the performance of each community in terms of highest *n*-caproate concentration achieved for the tested condition.
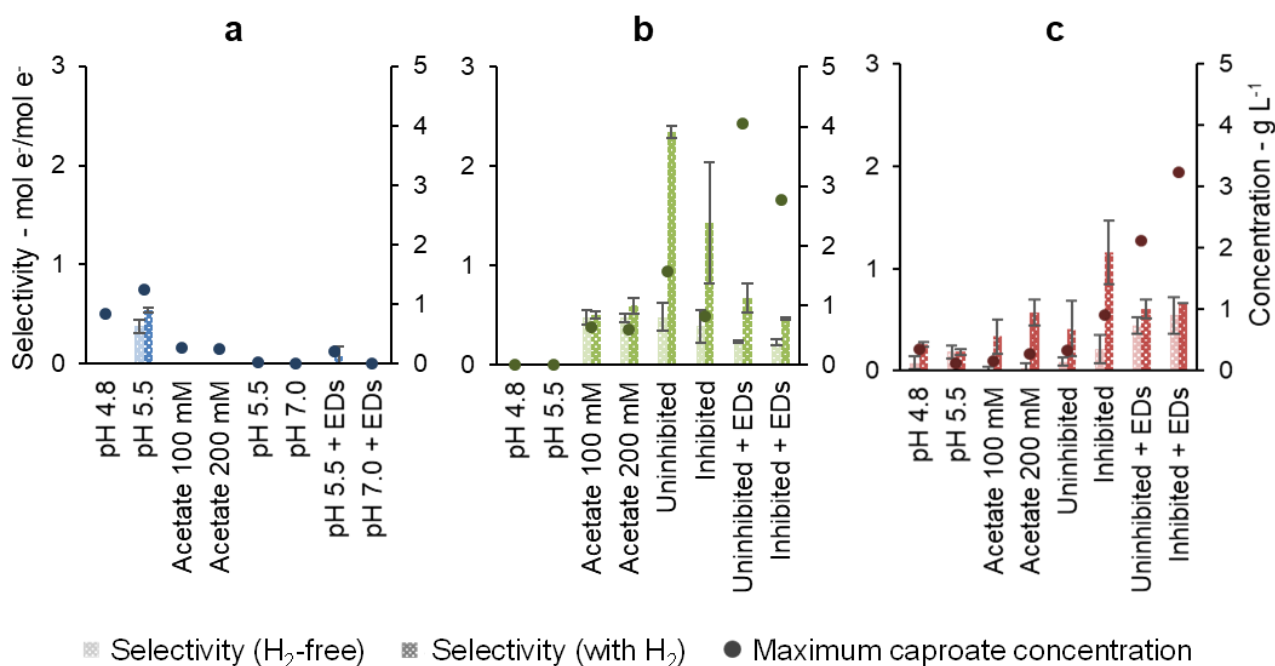
Figure 11. Selectivity of organic EDs (lactate, ethanol, and yeast extract) to *n*-caproate and maximum caproate concentration achieved by communities A (**a**), B (**b**), and C (**c**).

During the enrichment, maximum *n*-caproate concentrations increased with communities B and C, whereas community A lost the ability to produce *n*-caproate during the enrichment (Figure 11). All maxima of *n*-caproate concentration were achieved under the presence of H_2. Communities B and C both achieved peak concentrations after lactate and ethanol were added but methanogenesis inhibition had different effects on them. Community B peaked at 4.0 g L^{-1} in the absence of the inhibitor, while community C peaked at 3.2 g L^{-1} in the presence of the inhibitor. Community A achieved a maximum concentration of 1.2 g L^{-1} in the first experiment at pH 5.5, probably due to residual substrates in the original reactor broth. Nevertheless, H_2 presence favored production of *n*-butyrate by this community in the latest experiment at both pH values of 5.5 and 7.0 (Figure A3a).

Selectivities of organic EDs, i.e. lactate, ethanol, and yeast extract, to caproate in the presence of H_2 were at least as high as under H_2-free conditions (Figure 11). In the latter steps of the enrichment, selectivities of communities B and C were more clearly enhanced by the presence of H_2. The highest selectivity achieved by community B was 2.34 ± 0.06 mol e$^-$/mol e$^-$ under uninhibited conditions, while community C achieved 1.2 ± 0.3 mol e$^-$/mol e$^-$ when methanogenesis was inhibited. Before the addition of lactate/ethanol, the organic EDs available were yeast extract (500 mg L^{-1}, 86 mmol e$^-$ L^{-1}) and residual substrates from the original reactor broth. Therefore, a decrease in selectivity was observed when lactate (60 mM, 720 mmol e$^-$ L^{-1}) and ethanol (30 mM, 360 mmol e$^-$ L^{-1}) were added in higher concentrations.

Overall, no ethanol accumulation was observed and only trace amounts of *n*-valerate, *i*-valerate, *i*-caproate, and *n*-caprylate were detected along the study. Abiotic controls showed no

activity, except for one control bottle for community A at pH 7.0. This abiotic control bottle was contaminated during the experimental procedure for the addition of lactate and ethanol and therefore not considered further.

2.3.5. Community structure

Amplicon sequencing revealed different degrees of diversity and community composition of the original inocula for enrichment of the communities A, B, and C. As shown in terms of richness in Figure 12, inoculum diversity of community C was the highest, followed by the inocula of communities B and A, respectively. Shannon and Simpson indices are also presented in Figure 12 to help visualize the decrease in structural complexity of each community along the enrichment. At the end of the enrichment, communities B and C presented Shannon and Simpson indices of the same order of magnitude, whereas the diversity of community A was characterized by lower values.
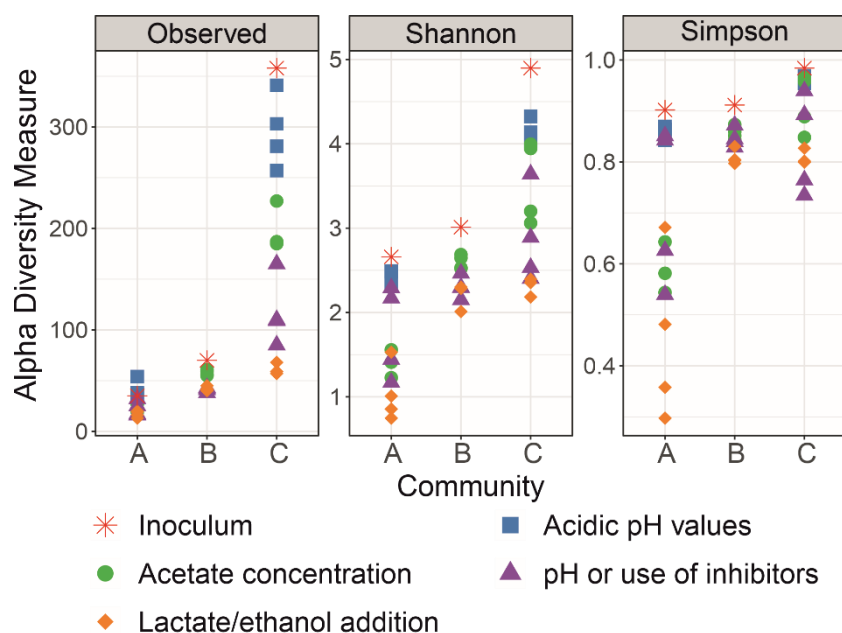
Figure 12. Diversity of communities A, B, and C throughout the enrichment in terms of richness (observed ASVs), Shannon index, and Simpson index.

By following the community development from the inoculum until the end of the lactate/ethanol addition experiment, Figure 13 shows the community compositions of the cultures with H_2. Additionally, community compositions of all cultures including H_2-free controls can be found in Figure A6. Despite the fact that all communities comprised the genera *Caproiciproducens* and *Clostridium* sensu stricto 12 at the end of the enrichment, there were fundamental differences at the ASV level within these genera (Figure 13). Table A4 provides the taxonomic affiliation for the most abundant ASVs found in this study.
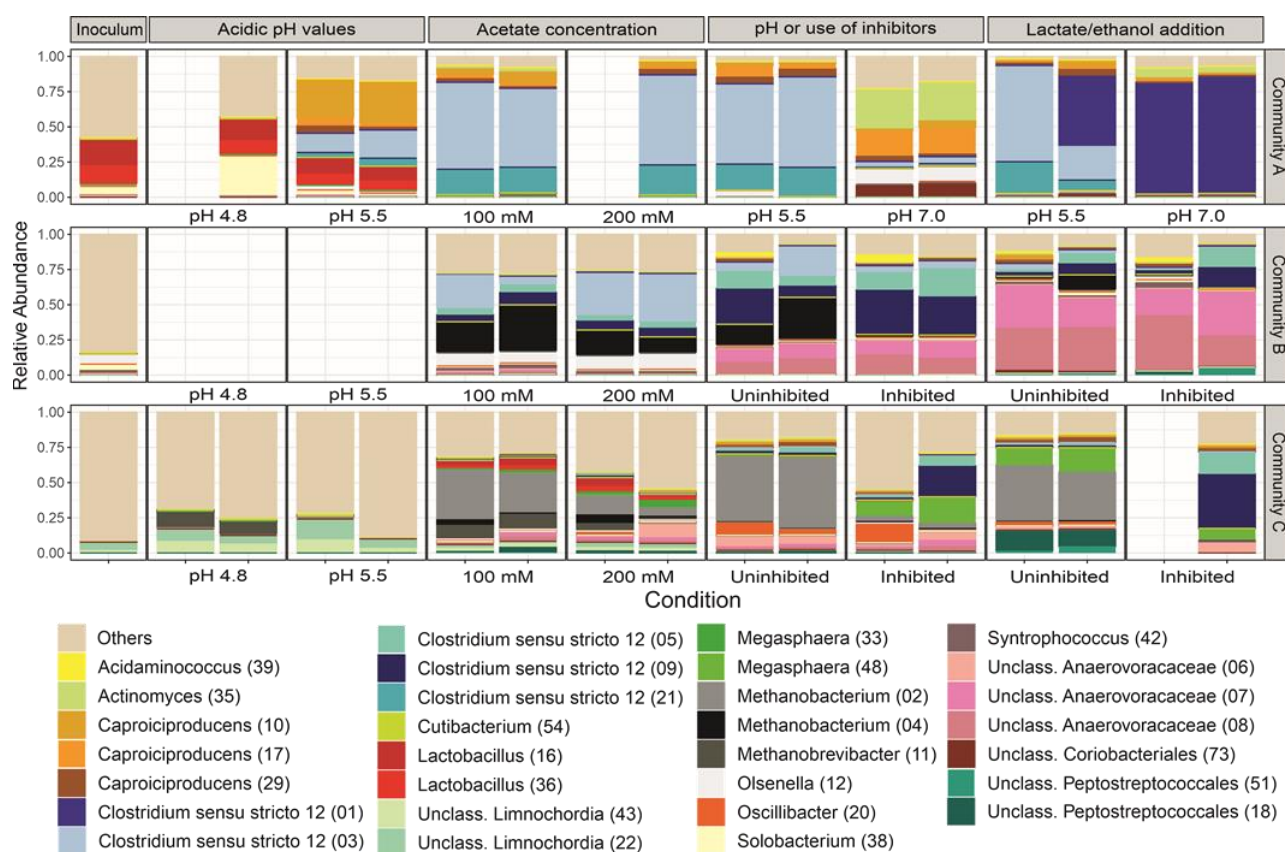
Figure 13. Community profiles resolved to the ASV level (ASV numbers in parentheses) at each condition tested with H_2/CO_2. The 30 most abundant ASVs in the dataset are shown. Duplicates are shown. Slots left blank represent samples that could not be sequenced.

Community A, initially dominated by *Caproiciproducens* ASV 10 at pH 5.5, shifted to the dominance of three ASVs assigned to *Clostridium* sensu stricto 12 (ASVs 1, 3, and 21) and of *Caproiciproducens* ASV 17 (Figure 13). Community B developed to a more diverse consortium composed mainly of two ASVs assigned to the family *Anaerovoracaceae* (ASVs 7 and 8), two ASVs assigned to *Clostridium* sensu stricto 12 (ASVs 5 and 9), *Caproiciproducens* ASV 29, and *Methanobacterium* ASV 4, which persisted in one of the uninhibited duplicates (Figure 13). Community C was finally composed of *Clostridium* sensu stricto 12 ASVs 5 and 9, *Anaerovoracaceae* ASV 6, *Megasphaera* ASV 48, and *Caproiciproducens* ASVs 10 and 29 in the culture with H_2 and inhibitor. The presence of the methanogenesis inhibitor shaped community C more strongly than community B. In the absence of the inhibitor, *Methanobacterium* ASV 2 was dominant in community C. Besides *Megasphaera* ASV 48, *Peptostreptococcales-Tissierellales* ASV 18 was the most enriched bacterial taxon in the absence of the inhibitor (Figure 13).

The most enriched *Clostridium* spp. could be divided into two groups: ASV 1 with 100% BLAST identity to *Clostridium tyrobutyricum* and ASVs 3, 5, 9, and 21 with high BLAST similarity (>97%) to *Clostridium luticellarii* (Table A4). *Clostridium* sensu stricto 12 (ASVs 3, 5, 9, and 21) were the most enriched *Clostridium* spp. and two of them (ASVs 3 and 21) were positively correlated to hydrogen consumption in community A (correlation coefficients of 0.77 and 0.84, respectively) (Figure A7). The *Cl. luticellarii*-related ASVs 5 and 9 also correlated positively to some indicators

of caproate formation in communities B and C. ASV 9 correlated to selectivity to caproate in community B (coefficient of 0.73, Figure A8) and ASVs 5 and 9 to maximum caproate concentration in community C (0.70 and 0.67, respectively, Figure A9).

The most abundant ASV of the genus *Caproiciproducens*, ASV 17, found in the latest enrichment phase of community A, had 100% BLAST identity with strain BL-6 (Liu et al., 2020b), a strain isolated from the same bioreactor that community A stemmed from. *Caproiciproducens* ASV 17 was different from the *Caproiciproducens* ASVs originally present in community A and from those present in communities B and C (ASVs 10 and 29). *Caproiciproducens* ASV 10 correlated to maximum caproate concentration in community A (0.55, Figure A8) and community C (0.67), while *Caproiciproducens* ASV 29 correlated to *n*-caproate formation rate in community C (0.41, Figure A9). ASVs 10 and 29 were distantly related to *Caproicibacter fermentans* (95% similarity, Table A4).

Among the *Anaerovoracaceae*, ASVs 7 and 8 were enriched in community B and correlated to the *n*-butyrate production rate (0.85 and 0.83, respectively). ASV 8 correlated to the *n*-caproate production rate (0.91) and selectivity (0.80, Figure A8). *Anaerovoracaceae* ASV 6 was present in community C, however, no significant correlation could be found (Figure A9).

Megasphaera ASV 48 enriched in community C only correlated to caproate selectivity and caproate maximum concentration at a higher significance level of $p<0.05$ (data not shown) but not at $p<0.01$ (Figure A9). *Megasphaera* ASV 48 had a BLAST similarity of 99.8% to *M. elsdenii* (Table A4), a well-known caproate producer.

Methanobacterium ASVs 2 and 4 were responsible for methane formation in communities B (ASV 4 with correlation factor of 0.92, Figure A8) and C (ASV 2 with correlation factor of 0.60, Figure A9) under uninhibited conditions (Figure 13).

2.4. Discussion

The enrichment experiments allow discussion from three perspectives: *i)* strategies in dealing with methanogenesis, which revealed to be the main competitive pathway; *ii)* the potential to improve *n*-caproate production with added H_2; and *iii)* identification of the key microbial players that emerged during the enrichment.

2.4.1. The methanogenesis factor

Coincidently, the communities that could produce *n*-caproate in the presence of H_2 were the same as those that presented hydrogenotrophic methanogenesis. In community C, a pH value of 4.8 was enough to inhibit acetoclastic methanogenesis. On the other hand, hydrogenotrophic methanogenesis was still observed at pH 4.8 (with 100 mM acetate) with an activity slightly lower than at pH 5.5 (Figure 9b), suggesting a relevant, yet surmountable acid inhibition of methanogens. Considering the fact that methanogenic activity has been rarely reported at such low pH (Savant et al., 2002; Horn et al., 2003), the methane formation observed in the first experiment with community C could be due to the high solids content of the biogas reactor broth,

which can shelter microorganisms through mass transfer gradients (Abbassi-Guendouz et al., 2012). Surprisingly, community C continued to present a robust methanogenic activity, which channeled most of the H_2 to CH_4 even at strongly inhibiting pH (5.5) and acetate concentration (200 mM) conditions (Zhang et al., 2018) in the following enrichment step ([Figure 9e](#)). When not actively suppressed by a chemical inhibitor, hydrogenotrophic methanogenesis was recurrent in community C throughout all the experiments, while methanogens faded out from community B along the enrichment without the need for an inhibitor ([Figure 9](#) and [Figure 10](#)). Differently, acetoclastic methanogenesis played only a minor role at pH 5.5 and 200 mM acetate, as suggested by the small consumption of acetate in the electron balances for community C ([Figure A1c](#) and [Figure A3c](#)), where CH_4 production was only slightly higher than H_2 consumption.

While the use of a methanogenesis inhibitor on community C (2-BES) increased production rates ([Figure 10b](#)) and selectivity ([Figure 11c](#)) to *n*-caproate, the inhibitor used on community B (ethylene) had an opposite effect ([Figure 10a](#) and [Figure 11b](#)). The inhibition mechanism of ethylene on methanogens has not been clearly elucidated, however, it is expected to be different from that of 2-BES (Schink, 1985b; Liu et al., 2011). To the best of our knowledge, no negative effects of ethylene on acetogens have been reported so far. In the absence of inhibitors, methanogenic activity was much stronger in community C than in community B to a point where H_2 became limiting in community C but not in community B. If 2-BES had detrimental effects on community C, these would have been shadowed by the effects of higher H_2 availability ([Figure A4](#)). Another possibility is that ethylene does not inhibit *i*-butyrate production whereas 2-BES is reported to do so (Huang et al., 2020). In fact, just as much electrons were channeled to *i*-butyrate (12 ± 4 mmol e⁻) as to *n*-caproate (12.2 ± 0.2 mmol e⁻) when ethylene was used ([Figure A3b](#)), whereas less electrons were channeled to *i*-butyrate (26 mmol e⁻) than to caproate (36 mmol e⁻) when 2-BES was used ([Figure A3c](#)). Although *i*-butyrate can theoretically be isomerized back to *n*-butyrate (Tholozan et al., 1988), *i*-butyrate production may compete with *n*-caproate formation when *n*-butyrate is the electron acceptor. The inhibition of 2-BES on *i*-butyrate formation was previously reported, but its mechanism is still not clear (Angelidaki and Ahring, 1995; Huang et al., 2020). According to the results found here, inhibition of *i*-butyrate formation by 2-BES may also inflate MCC yields. Thus, for more conservative estimates of MCC formation in systems with high potential to produce branched-chain carboxylates, suggest the use of ethylene as methanogenesis inhibitor instead of 2-BES is recommended.

High salinity may also have inhibited methanogens, in particular in the later stages of the enrichment when acetate concentration was doubled and 2-BES was used. In this study, medium salinity started at around 14 g L⁻¹ (NaCl equivalents, in experiments with 100 mM acetate), increased to 17 g L⁻¹ in cultures with 200 mM acetate, and finally increased up to 22 g L⁻¹ when 2-BES was added in cultures of community C. Notably, De Vrieze et al. (2016) reported a shift from methanogenesis to carboxylate production in upflow anaerobic sludge blanket reactors at salinity values higher than 19 g L⁻¹ (calculated from conductivity value according to McDougall and Barker (2011)). Considering that no controls for salinity were used, the extent to which

salinity inhibited methanogens in this study is unclear. Methanogens remained active in inhibitor-free cultures of community C at 200 mM acetate and about 17 g L^{-1} NaCl equivalents (Figures 10b and 10d). At the highest salinity values (22 g L^{-1}), 2-BES was present and, as expected (Zinder et al., 1984), completely inhibited methanogens.

2.4.2. Enhancing *n*-caproate production

Although the production of *n*-caproate with H$_2$ as main ED could be increased in most communities, the maximum *n*-caproate concentrations of 1.5 g L^{-1} still fell short of the values around 10 g L^{-1} reached by the best-performing anaerobic fermenters fed with organic EDs (De Groof et al., 2019). Besides, when only H$_2$ (besides 500 mg L^{-1} yeast extract) was the available ED, small *n*-caproate production rates up to 25.7 ± 0.7 mg L^{-1} d^{-1} were observed (Figure 10a), which is in the same order of magnitude as observed by Zhang et al. (2013). Hence, to benefit from the effects of H$_2$ on MCC production, two organic EDs (lactate and ethanol) were co-fed with H$_2$, thereby increasing production rates and concentrations of caproate in communities B and C. In the presence of lactate and ethanol, *n*-caproate formation rates increased to 107 mg L^{-1} d^{-1} (Figure 10d). We expect the maximum *n*-caproate concentration (4.0 g L^{-1}) and production rate (107 mg L^{-1} d^{-1}) to have plenty of room for improvement as many important parameters (e.g. substrate ratios, pH, and temperature) have not been optimized in this study. For instance, assuming an ED to electron acceptor ratio of 1:1, the concentrations of ethanol and lactate used in this study could sustain up to 6.5 g L^{-1} *n*-caproate. In comparison to the anaerobic fermentation of lactate in the absence of H$_2$, the observed benefits of H$_2$ addition were higher concentrations, selectivities, and production rates of both *n*-caproate and *n*-butyrate. Regarding the preferred fermentation strategies for the concept, those that can maintain a high concentration of acetate in the bioreactor (e.g. in-line extraction of MCCs, operation at lower pH values, inhibition of methanogenesis) can be useful to improve MCC production despite the known inhibiting effects of acetate on microbial communities (Agler et al., 2014; Zhang et al., 2018). It is assumed that an acetate concentration of 200 mM, such as in this study, is an attainable condition in anaerobic fermenters fed with lignocellulosic biomass, especially when coupled with in-line extraction for MCC, such as liquid-liquid extraction (Agler et al., 2014; Kaur et al., 2020). As a next step, the concept of H$_2$ and organic EDs co-feeding can be adapted to continuous reactors to test its feasibility under conditions closer to an industrial-scale fermenter. During the upscaling process, lessons learned from syngas fermentation research can be useful to tackle the challenges of feeding H$_2$ as a substrate, such as micro-sparging to overcome low gas-mass transfer rates and using bubble-column reactors to keep power input low (Takors et al., 2018). Moreover, at industrial scale, renewable H$_2$ is ideally sourced from water hydrolysis fueled by renewable energy or from lignocellulose gasification.

Under conditions tested here, H$_2$ addition could not sustain production of neither short-chain nor medium-chain alcohols. Even though the slightly acidic pH values used in most of the experiments are known to favor production of solvents such as *n*-butanol and *n*-hexanol

(González-Cabaleiro et al., 2013; Ganigue et al., 2016), none of these alcohols was detected in this study. Based on the current knowledge on homoacetogenic pure cultures, when solvents are the desired products, co-feeding with CO-containing gases, such as syngas, is suggested (Diender et al., 2019; Infantes-López, 2020).

2.4.3. Key players in hydrogen-aided chain elongation

Community A, in contrast to the more diverse communities B and C, did not show the ability to produce caproate when only H_2 and yeast extract were the available EDs. One reason could be a missing link in the H_2-to-caproate metabolic chain, i.e. the WLP, solventogenesis, interspecies ED transfer, or the RBO pathway. Considering that only a handful of cultured bacterial species possessing more than one of these capabilities are known (Angenent et al., 2016; Bengelsdorf et al., 2018), a high diversity inoculum improves the chances to obtain an acidogenic community that can profit from H_2 as a co-ED. Nevertheless, after the community is enriched for H_2-aided CE, high microbial diversity may not be a requirement for the bioreactor to work optimally.

Based on the correlations with *n*-caproate production and selectivity (Figure A7, Figure A8, and Figure A9), four taxonomic groups that might be involved in the *n*-caproate metabolism were identified: members of the genus *Clostridium* sensu stricto 12 (ASVs 3, 5, 9, and 21) related to *Cl. luticellarii*, members of the family *Anaerovoracaceae* (ASVs 6, 7, and 8) (formerly *Clostridiales* family XIII (Parks et al., 2018)), and members of the genus *Caproiciproducens* (ASVs 10 and 29) related to *Caproicibacter fermentans* (Table A4). Although the mechanism through which *n*-caproate was produced in the presence of H_2 remains unknown, correlation analysis may provide some hints.

In communities B and C, no bacterial taxon correlated to H_2 consumption rates could be found. This was likely due to the more intense consumption of H_2 for methanogenesis in inhibitor-free cultures of these communities. Considering that no culture in this study showed net H_2 formation, negative correlations to H_2 consumption rate to certain bacterial taxa (as found in Figure A8 and Figure A9) may simply mean that bacteria were slower H_2 consumers than archaea. Still, abundances of ASVs assigned to *Clostridium* sensu stricto 12 correlated positively to H_2 consumption in community A (Figure A7), whereas other ASVs affiliated to *Clostridium* sensu stricto 12 were linked to *n*-caproate formation (Figure A8 and Figure A9). With relatively high abundances in all communities, the genus *Clostridium* sensu stricto 12 thrived particularly in communities A and C after lactate and ethanol addition (Figure 13). So far, hydrogenotrophy and *n*-caproate production have not been reported as functions of *Cl. luticellarii* (Wang et al., 2015). However, its genome harbors typical genes of the WLP (Poehlein et al., 2018) and *Cl. luticellarii* was the main candidate to elongate propionate to *n*-valerate and to produce *i*-butyrate in a recent study (de Smit et al., 2019). Moreover, a *n*-caproate producer recently isolated in our laboratory, Clostridiales bacterium isolate BL-3, is also closely related to *Cl. luticellarii* (Liu et al., 2020b; Liu et al., 2020c). *Cl. luticellarii* is closely related to *Cl. ljungdahlii* (a solventogen and syngas fermenter) and *Cl. kluyveri* (a chain elongator) (Wang et al., 2015; de

Smit et al., 2019). Moreover, it is important to highlight that the fact that no ethanol accumulated in our experiments should not exclude the possibility of this ED being the one intermediating the H_2-to-caproate through interspecies transfer. With ethanol having faster consumption kinetics than those of H_2 in acidogenic cultures (González-Cabaleiro et al., 2013; Weimer et al., 2015), intermediate ethanol may be present in concentrations below the detection limit or its production-consumption cycles could have been overlooked with the sampling frequency of this study. In fact, sporadic occurrence of small ethanol concentrations (12 - 130 mg L^{-1}, data not shown) were observed. However, with the experimental design and methodology adopted here, no conclusions could be drawn from this observation.

Judging by their notable abundances in different experiments, ASVs assigned to the *Anaerovoracaceae* fared well under a broad range of conditions and substrates ([Figure 13]), including H_2, lactate, and ethanol, besides being one of the suspects to produce *n*-caproate in community B. Such versatility is seen in only few *n*-caproate producers, being *E. limosum* one of the few examples, albeit it does not grow with ethanol (Wade, 2015). For reference, the distantly related *Eubacterium pyruvativorans* ([Table A4]) is a *n*-caproate producer that does not use ethanol, grows slowly on lactate and needs SCC to realize a CE metabolism that is uninhibited by high H_2 partial pressure (Wallace et al., 2004).

The ASVs related to *Caproiciproducens* (in all communities) and *Megasphaera* (in community C) had minor but consistent abundances along the enrichment ([Figure 13]). ASVs of these two genera had established presence before lactate addition, hence their growth could have relied on the presence of yeast extract, interspecies metabolite transfer, or H_2 consumption. Their closest related species (*Caproicibacter fermentans* and *M. elsdenii*) are best known for their abilities to produce caproate from sugars or lactate (*M. elsdenii*) (Rosenberg et al., 2014; Flaiz et al., 2019; Lee et al., 2020), but neither for hydrogenotrophy nor ethanol consumption. Interestingly, in one of the first reports on *M. elsdenii* (Elsden and Lewis, 1953), the species was shown to consume H_2 together with pyruvate while realizing CE metabolism when SCCs were available. For instance, *Caproiciproducens galactitolivorans*, a chain elongator closely related to *Caproicibacter fermentans,* has not been observed to utilize ethanol but was reported to have its growth enhanced in co-culture with other ethanol-, acetate- and *n*-butyrate-producing bacteria (Kim et al., 2015).

2.5. Conclusion

Overall, the simultaneous occurrence of phylogenetically distinct families within the *Firmicutes* (i.e. *Clostridiaceae*, *Veillonellaceae*, *Ruminococcaceae*, and *Anaerovoracaceae*) hints to a broad taxonomic range of suspected *n*-caproate producers that thrive in the presence of H_2. The results of this chapter suggest a widespread synergy between H_2, lactate, and ethanol on *n*-caproate production by complex communities and add up to the growing body of evidence that abundant H_2 availability can improve efficiency of MCC-producing microbiota ultimately acting as a co-ED. Still, plenty remains to be understood regarding the underlying mechanisms through

which this synergy occurs. For that, it is necessary to design studies that better resolve the metabolic network in such complex microbiota with the help of, for instance, meta-omics approaches.

The different conditions tested in batch cultures can serve as a starting point to better devise strategies that alleviate ED scarcity on continuous CE reactors with the help of H_2. Instead of depending exclusively on an organic ED or on H_2, it is advised to develop a CE process in which both types of EDs are co-fed in order to improve MCC production rates, concentrations, and selectivities. For kick-starting the bioreactor, the more diverse inoculum should be favored over the more specialized one. When methanogenesis misroutes electrons from H_2, ethylene should be favored over 2-BES as an inhibitor in order to not collaterally inhibit i-butyrate formation.

3. Fermentation of syngas and plant biomass in closed systems

Author contributions
Flávio C. F. Baleeiro: conceptualization, methodology, investigation, data analysis, visualization, first draft, and manuscript revision.
Lukas Varchmin: conceptualization, methodology, investigation, and data analysis.
Sabine Kleinsteuber, Anke Neumann and Heike Sträuber: conceptualization, project supervision, data analysis support, and manuscript revision.

3.1. Introduction

Several studies have explored the use of microbial communities to produce carboxylates from syngas components in a one-pot process. They approached the topic by *i*) innovative ways of supplying H_2 (Calvo et al., 2021; Ntagia et al., 2021), *ii*) enrichment of microbial communities in mineral media with syngas (Esquivel-Elizondo et al., 2017a; Esquivel-Elizondo et al., 2017b; He et al., 2021), *iii*) co-fermentation of H_2/CO_2 (or $H_2/CO_2/CO$) with synthetic organic substrates (Wu et al., 2019; Liu et al., 2020d), and *iv*) co-fermentation of H_2/CO_2 with organic waste streams (González-Tenorio et al., 2020). In general, the presence of H_2 and CO helped increasing carboxylate yields and selectivity to medium-chain carboxylates. Yet, we found no studies with complete syngas mixtures ($H_2/CO_2/CO$) and plant biomass.

Carbon monoxide is expected to have a major impact on the plant biomass fermentation. Despite being a key substrate for acetogenic bacteria, CO is a strong inhibitor of hydrogenases (Ragsdale, 2004) and hence disrupts the electron transport chains of bacteria that rely on these enzymes. This is aggravated in fermentative bacteria, which often rely on [Fe-Fe] hydrogenases that are particularly sensitive to CO (Diender et al., 2015). Yet, there are ways to overcome CO inhibition of fermentative bacteria. For instance, *Cl. kluyveri* was less prone to CO inhibition when grown in co-culture with acetogens (e.g., *Cl. autoethanogenum*) in bottles without shaking (Diender et al., 2016). Besides, the presence of formate, a common extracellular metabolite in anaerobic microbial communities, allowed *Acetobacterium woodii* to tolerate up to 25 kPa CO (Bertsch and Müller, 2015), and low concentrations of formate (<100 mg L^{-1}) improved the growth of *Cl. ljungdahlii* and *Cl. carboxidivorans* on syngas (Ramio-Pujol et al., 2014).

This chapter aims to understand the main effects of syngas on the carboxylate production during the anaerobic fermentation of plant biomass by using corn silage as a model feedstock. Focus was given to the syngas composition taking in consideration the double-edged role of CO in carboxylate production.

3.2. Material and methods

3.2.1. Batch cultivation

In an anaerobic chamber, 50 mL of anoxic mineral medium (preparation and composition are described in Appendix B.1 and Table B1, respectively) were added to 250-mL-serum bottles containing 5.5 g of fresh matter of corn silage each, resulting in a volatile solids (VS) concentration of 30 g$_{VS}$ L^{-1}. All bottles contained at least the autochthonous microbial community of the corn silage as inoculum. Bottles additionally inoculated with a community adapted to syngas received cells from an enrichment reactor (see below Section 3.2.3, Source of the adapted community). To harvest the cells from the enrichment reactor, the fermentation broth was centrifuged at 4,816 × g and 4°C for 10 minutes. The supernatant was discarded and the cells were washed and resuspended in the equal volume of anoxic mineral medium. Alternatively, the untreated broth from the enrichment reactor, which was rich in carboxylates, was either used

instead of mineral medium or 10% of the medium was substituted with it (inoculation with 100% or 10% reactor broth). The serum bottles were closed with butyl rubber stoppers and sealed with aluminum crimps. All batch cultures were prepared in duplicates.

The bottles were initially pressurized with 150 kPa (1.5 bar$_a$). Different partial pressures of H_2 and CO were applied (Figure 14), resulting in a combined partial pressure of 98 kPa. This ensured a fixed amount of electron donors in the headspace. The only exceptions were the condition "CO_2", which contained neither CO nor H_2, and the condition "$CO+CO_2$", which contained 49 kPa CO but no H_2. All cultivation bottles initially contained 24 kPa CO_2. N_2 was used as a filling gas to reach the final pressure. In two pairs of bottles, 3 mL ethylene was additionally added to the pressurized bottles to achieve 1.5 kPa ethylene at 0 kPa CO (98 kPa H_2) and 5 kPa CO (93 kPa H_2) (Figure 14). In one pair of bottles, 0.2 mL of formic acid was added at 9 kPa CO (89 kPa H_2) to reach a concentration of 5 g L^{-1} formate (Figure 14). The pH was corrected with 4 M KOH immediately after formic acid addition. For abiotic controls, the sealed and pressurized bottles with corn silage and mineral medium were autoclaved for 20 minutes at 121°C.

Figure 14. Summary of all conditions tested in batch cultures. Yellow bottles contained at least corn silage, mineral medium, and CO_2. Additionally, CO and H_2 were added as indicated. As special conditions, formate or ethylene was additionally added, or untreated reactor broth was used as source of the adapted community instead of washed cells.

The batch cultures were incubated on a rotary shaker at 32°C and 200 rpm. Fermentations were carried out at a pH value of 5.9 ± 0.5. Sampling of the liquid phase and pH correction with 4 M NaOH were done weekly. The pressure was monitored twice per week. When a pressure lower than 100 kPa was detected, the bottle was re-pressurized to 150 kPa. Before every pressurization, the headspace of the bottle was purged with 2.5 L of the corresponding gas mixture. By monitoring the chemicals in the gas and aqueous phase, little to no activity was detected in the abiotic controls (Figure B1), and the amount of DNA extracted from cell pellets was too low for microbial community analysis. For practical reasons, the experiments were divided in three different batches lasting from 31 to 38 d. For information on how the experiments were divided in different batches and the exact duration of each batch see Appendix B.2.

3.2.2. Corn silage

Corn silage from a farm in Neichen (Saxony, Germany) was transported and stored in vacuum-sealed polyester bags at room temperature until its use. Soluble chemicals in the silage were quantified (0.41 ± 0.04 g L^{-1} acetate, 0.21 ± 0.06 g L^{-1} ethanol, and 3.2 ± 0.1 g L^{-1} lactate). The content of VS on a fresh matter basis for the substrate was 27.1 ± 0.1%.

3.2.3. Source of the adapted community

The syngas-adapted community used as inoculum for the batch cultures originated from two 1.0-L STRs that were being operated near atmospheric pressure (102 kPa) with continuous syngas recirculation (32% H_2, 32% CO, 16% CO_2, 2% ethylene, 2% He, and rest N_2 at 40 mL min^{-1}) at an HRT of 14 d, pH 6.0, and 32°C. Once a day, fermentation broth was harvested and mineral medium (Table B1) containing additionally 12 g L^{-1} acetate and 12 g L^{-1} lactate was fed. At the time the inoculum was collected, the enrichment reactors had been operated for 83 days and had an average carboxylate composition of 11 g L^{-1} acetate, 3.4 g L^{-1} n-butyrate, 2.6 g L^{-1} n-caproate, and 1.1 g L^{-1} i-butyrate. Methanogenesis rates were very low (about 2.2 mL CH_4 L^{-1} d^{-1}) and syngas consumption rates were relatively high (150 mL H_2 L^{-1} d^{-1} and 237 mL CO L^{-1} d^{-1} on average). The original microbial community composition of the adapted community is shown in Figure B2.

3.2.4. Analytical methods

The VS content of corn silage was determined according to Strach (2020). To estimate the corn silage degradation during fermentation, a procedure based on total solids (TS) measurement was applied. At the end of the fermentation, the whole content of each bottle was separated by sieving (0.84 mm mesh size). The retained solids were washed with 50 mL phosphate buffer saline solution (PBS; pH 7.4, 11.8 mM phosphates) for 30 minutes at room temperature in a rotary shaker at 150 rpm. Afterwards, the resulting mixture was sieved again and the TS content of the solid fraction was determined by drying it at 105°C until a constant weight was obtained

(24 to 48 h). The difference between the TS content (in %) of the abiotic control and the TS content (in %) of the test bottle was defined as the solids degradation, in percentage points (p.p.).

For measuring pH and concentrations of chemicals in the bottles, 0.3 mL of liquid was collected once a week from each bottle. Liquid samples were centrifuged at 9,000 × g for 10 minutes and a defined amount of the resulting supernatant was diluted five times with PBS to reach a neutral pH value before being analyzed. For analyzing the concentration of chemicals in corn silage, an elution of 25 g substrate with 250 mL PBS was carried out for 24 h at room temperature (Apelt, 2020). The resulting liquid samples were filtered with 0.22 µL nylon syringe filters before being analyzed via HPLC. Concentrations of linear monocarboxylates from formate to n-caprylate, linear alcohols from ethanol to n-hexanol as well as lactate, i-butyrate, i-valerate, and i-caproate were measured using a 1100 series HPLC-RID/UV system (Agilent Technologies, Germany) equipped with pre-column and column Rezex ROA-Organic Acid H+ (8%) (Phenomenex, Germany). For compounds with UV absorption at 280 nm, concentration values obtained via UV were averaged with the values obtained via a RID. The mobile phase of HPLC was 5 mM H_2SO_4 at 0.6 mL min^{-1}. A sample injection volume of 20 µL was used and the temperatures of the column oven and RID were kept at 55°C and 50°C, respectively. Concentrations of n-propanol, n-butanol, n-pentanol, n-hexanol, n-heptanoate, n-caprylate, i-valerate, and i-caproate in this chapter generally remained below 100 mg L^{-1} and are not shown.

The bottle headspace pressure was analyzed using a manometer GDH 14 AN (Greisinger electronic, Germany). Afterwards, 2 mL of gas sample was collected twice a week for gas composition analysis via GC-TCD. The GC-TCD system measured the fractions of H_2, CO_2, CO, ethylene, N_2, O_2, and CH_4 and was described previously by Mohr et al. (2018).

Rates in this chapter are average rates specific to the volume of broth (50 mL). Average rates in terms of electron equivalents were used to compare production and consumption of chemicals under different cultivation conditions. The conversion factors shown in Table A2 were used for converting mass values into moles, electron equivalents, and carbon equivalents when necessary.

3.2.5. Microbial community analysis

For microbial community analysis, 16S rRNA amplicon sequencing was performed using the Illumina MiSeq platform. Cell pellets were collected from the culture bottles at the end of the experiments. Before being stored at -20°C, cell pellets were washed once with an equal volume of PBS (ca. 1.8 mL). DNA was extracted from the cell pellets using the ZymoBIOMICS DNA Miniprep kit (Zymo Research, Germany) with cell disruption within 20 min, following the manufacturer's instructions for non-soil samples. DNA quantification and quality assessment, PCR and library preparation were done as described by Logroño et al. (2020) for 16S rRNA. For PCR, primers for the V3 and V4 regions (Klindworth et al., 2013) were used. Filtering, denoising, and taxonomical assignment of the amplicon data were done as described in Section 2.2.3. Sequence counts of all samples were rarefied to the read number of the sample with the lowest

coverage in the dataset (56,674 counts). Raw sequence data for this study was deposited at the ENA under the study accession PRJEB49567 (http://www.ebi.ac.uk/ena/data/view/PRJEB49567).

3.3. Results and discussion

3.3.1. Comparing different starting conditions

To assess the impact of using a microbial community previously adapted to syngas and lactate (besides the autochthonous corn silage community), we compared inoculated cultures with cultures containing only the corn silage community. Figure B3 presents the product profiles of the fermentations with syngas (49 kPa CO, 49 kPa H_2, 24 kPa CO_2) depending on the way the adapted community was inoculated. As long as the inoculum did not contain high amounts of carboxylates from the enrichment reactor, i.e. when the inoculation was done with washed cells or with 10 vol % reactor broth, using the adapted community proved to be particularly important for accelerating the consumption of H_2 and CO. Yet, the maximum n-butyrate concentration was 1.2 ± 0.1 g L^{-1} and the adapted community contributed little to produce carboxylates longer than propionate. Since the addition of reactor broth at the beginning of the fermentations was not beneficial to produce medium-chain carboxylates, only washed cells were used in further tests with the adapted community. The results of this preliminary experiment (Figure B3) are summarized in Appendix B.3.

3.3.2. Effects of carbon monoxide, hydrogen, and syngas

Inoculating a community adapted to syngas was not enough to allow medium-chain carboxylate production from syngas and corn silage. Therefore, we tested the effects of the main syngas components (H_2 and CO) separately on the fermentation with both the autochthonous and the adapted communities.

Figure 15 shows the production and consumption rates of chemicals (in electron equivalents) together with the community composition under each condition. In cultures with CO, regardless of the community type, propionate was a main electron sink, whereas cultures without CO mostly routed more electrons to n-butyrate (Figure 15a). The presence of CO (49 kPa) inhibited the production of carboxylates with chains longer than propionate by both communities.

a

b

c
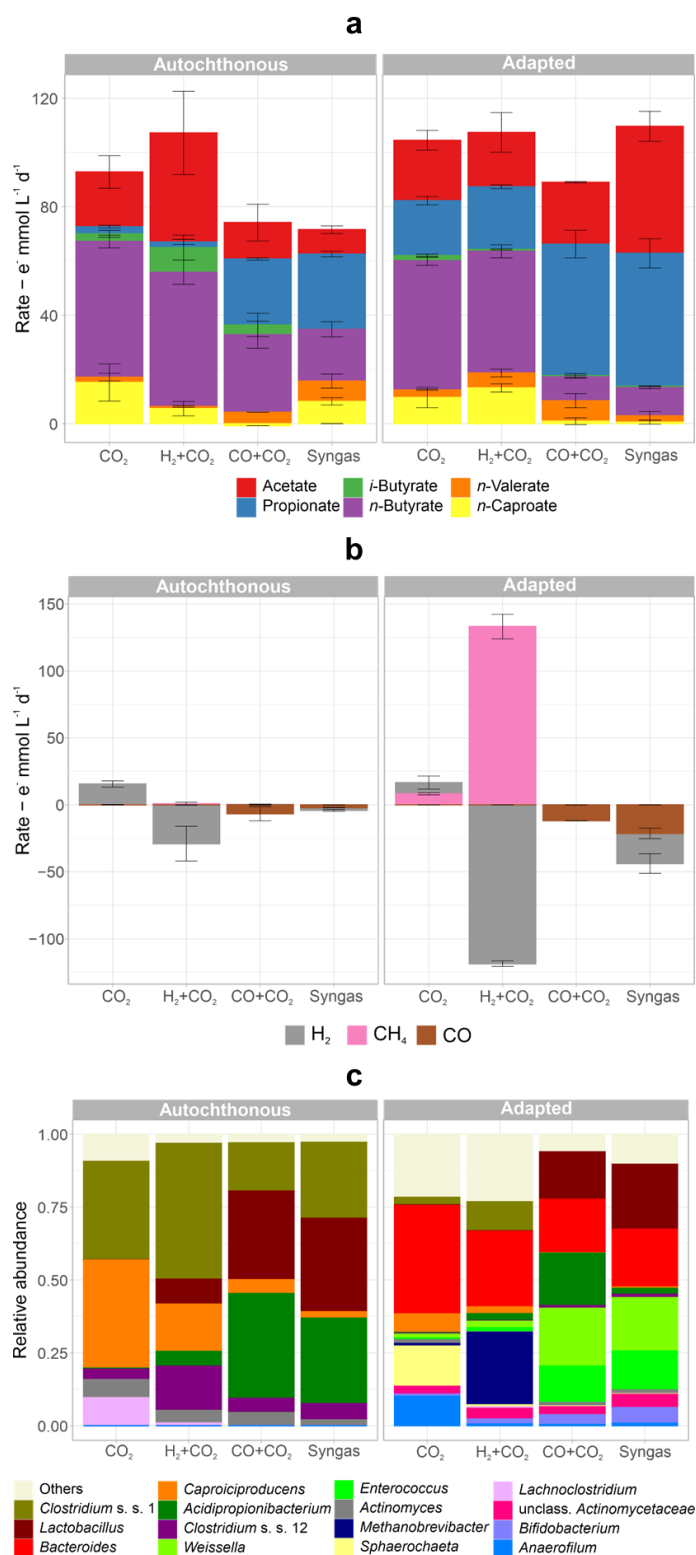
Figure 15. Production and consumption rates for liquid (**a**) and gaseous (**b**) chemicals and microbial community composition (**c**) in fermentations of corn silage with different syngas constituents. The 15 most abundant genera in the set are shown. Mean values of duplicate bottles are shown. Error bars indicate standard errors. Rates are in terms of electron equivalents. S.s.: sensu stricto.

Methane formation occurred only in the culture with the adapted community and was stronger when H_2 was present and CO was absent (H_2+CO_2, Figure 15b). In this case, routing of electrons

to CH_4 occurred to a similar extent as H_2 consumption (133 ± 9 e⁻ mmol CH_4 L⁻¹ d⁻¹ and 119 ± 2 e⁻ mmol H_2 L⁻¹ d⁻¹), indicating the activity of hydrogenotrophic methanogens in the adapted community. This was confirmed by the high relative abundance of *Methanobrevibacter* under this condition (H_2+CO_2 with the adapted community, Figure 15c).

The autochthonous community alone consumed some exogenous H_2 and produced extra acetate when CO was absent (H_2+CO_2, Figure 15b). Still, the adapted community achieved the highest CO consumption (21 ± 4 e⁻ mmol CO L⁻¹ d⁻¹), which occurred when both H_2 and CO were present (Syngas, Figure 15b). Under this condition, the adapted community presented a net carbon fixation rate of 3.8 ± 0.7 C mmol L⁻¹ d⁻¹ (equivalent to 167 ± 31 mg CO_2 L⁻¹ d⁻¹) (Figure B4).

H_2 and CO were likely converted to acetate by autotrophic acetogens such as *Clostridium* sensu stricto 12, a genus that was present (Figure 15c) and comprises acetogenic species. However, cultures with the adapted community with the highest H_2 and CO consumptions (excluding methanogenesis) had low relative abundances of *Clostridium* sensu stricto 12. The highest relative abundances were recorded for bacteria likely growing heterotrophically on sugars and lactate from the plant biomass: lactic acid bacteria (LAB; *Lactobacillus*, *Weissella*, *Enterococcus*, and *Bifidobacterium*), *Bacteroides*, *Acidipropionibacterium*, *Actinomyces*, and some clostridia (*Clostridium* sensu stricto 1, *Caproiciproducens*, and *Anaerofilum*).

The presence of H_2 or CO disadvantaged *Lachnoclostridium* (autochthonous community) and *Sphaerochaeta* and *Anaerofilum* (adapted community) (Figure 15c), genera commonly associated with improved lignocellulose degradation (Dröge et al., 2006; Yutin and Galperin, 2013; Azman et al., 2015; Yang and Wang, 2018). Other major shifts in microbial composition were due to the presence of CO. Cultures with CO (49 kPa CO) had greater relative abundances of LAB and *Acidipropionibacterium* at the cost of *Caproiciproducens*, *Methanobrevibacter*, and *Clostridium* sensu stricto 1. Swaps of relative abundances of lactate- and *n*-butyrate-producing bacteria also occur in other anaerobic systems and depend on pH and organic substrate type (Detman et al., 2021). Cultures without inoculation with syngas-adapted cells showed higher relative abundances of *Caproiciproducens, Clostridium* sensu stricto 1 and 12, *Actinomyces*, and *Acidipropionibacterium,* whereas cultures inoculated with the adapted community tended to have higher shares of *Bacteroides*, *Enterococcus*, *Weissella*, and *Bifidobacterium*. *Weissella*, *Bifidobacterium*, and *Enterococcus* were not detected in the adapted community inoculum, indicating that they originated from the corn silage community. *Bacteroides* was present in low abundances in the adapted community inoculum (Figure B2).

Propionate production by the autochthonous community in the fermentations with CO (Figure 15a) can be explained by high abundances of *Acidipropionibacterium* (Figure 15c), which compete with clostridia for lactate (Kim et al., 2022). Yet, the adapted community produced even more propionate under the same conditions (Figure 15a), despite low abundances of *Acidipropionibacterium*. So far, no isolated carboxydotroph is known to convert CO to

propionate, but co-cultures of carboxydotrophs and propionate producers can (Moreira et al., 2021). Thus, indirect conversion of CO to propionate intermediated by ethanol is possible. However, high abundances of heterofermentative LAB (i.e. *Weissella* and *Lactobacillus*, which can produce propionate from sugars and lactate (Gänzle, 2015; Zheng et al., 2020)) strongly indicates that electrons in propionate originated from the plant biomass and not from CO.

Interestingly, the relatively high H_2 and CO consumption by the adapted community in the fermentations with syngas (45 e⁻ mmol L^{-1} d^{-1} of gases consumed and 109 e⁻ mmol L^{-1} d^{-1} of carboxylates produced) did not result in much higher carboxylate production than that when only CO_2 was in the headspace (carboxylate production of 105 e⁻ mmol L^{-1} d^{-1}) ([Figure 15a]). This observation suggests that less plant biomass was consumed when H_2 or CO were present, which was confirmed by the analysis of the degradation degree ([Figure B5]). The presence of H_2 alone also slowed down biomass degradation, especially by the communities without methanogenic activity (autochthonous community, [Figure B5]). Headspaces rich in H_2 and H_2+CO_2 have been reported to slow down the degradation of organic waste streams. Arslan et al. (2012) noted a lower hydrolysis rate under a H_2-rich headspace, but not a change in the final hydrolysis degree of the solid fraction, implying a retarded utilization of the available organic feedstock. There, H_2 and H_2+CO_2 increased the overall carboxylate production by 47% and 150%, respectively, in comparison to a fermentation with a N_2 headspace.

Within the same community type (i.e. adapted or autochthonous), community compositions of cultures fed with CO (conditions "Syngas" and "CO+CO_2") were very similar. This fact pointed to the importance of CO among all other factors. To get a more detailed view on the effect of CO on the fermentation, further tests with partial pressures lower than 49 kPa CO were carried out.

3.3.3. Effect of different carbon monoxide concentrations

Production rates for chemicals and community compositions at partial pressures between 0 and 49 kPa CO for cultures with the adapted community are shown in [Figure 16]. During this experiment, partial pressures of H_2 were varied between 98 kPa H_2 (at 0 kPa CO) and 49 kPa H_2 (at 49 kPa CO) to maintain a constant availability of electron donors (98 kPa H_2+CO) under all conditions ([Figure 14]). [Figure B6] shows time profiles of the electron balances under these conditions.

As low as 5 kPa CO was enough to inhibit the electron flow to *n*-caproate and *n*-butyrate by 44% ([Figure 16a]). On the other hand, production of acetate and propionate increased by 126% and 151%, respectively, when CO partial pressure increased from 0 to 49 kPa.
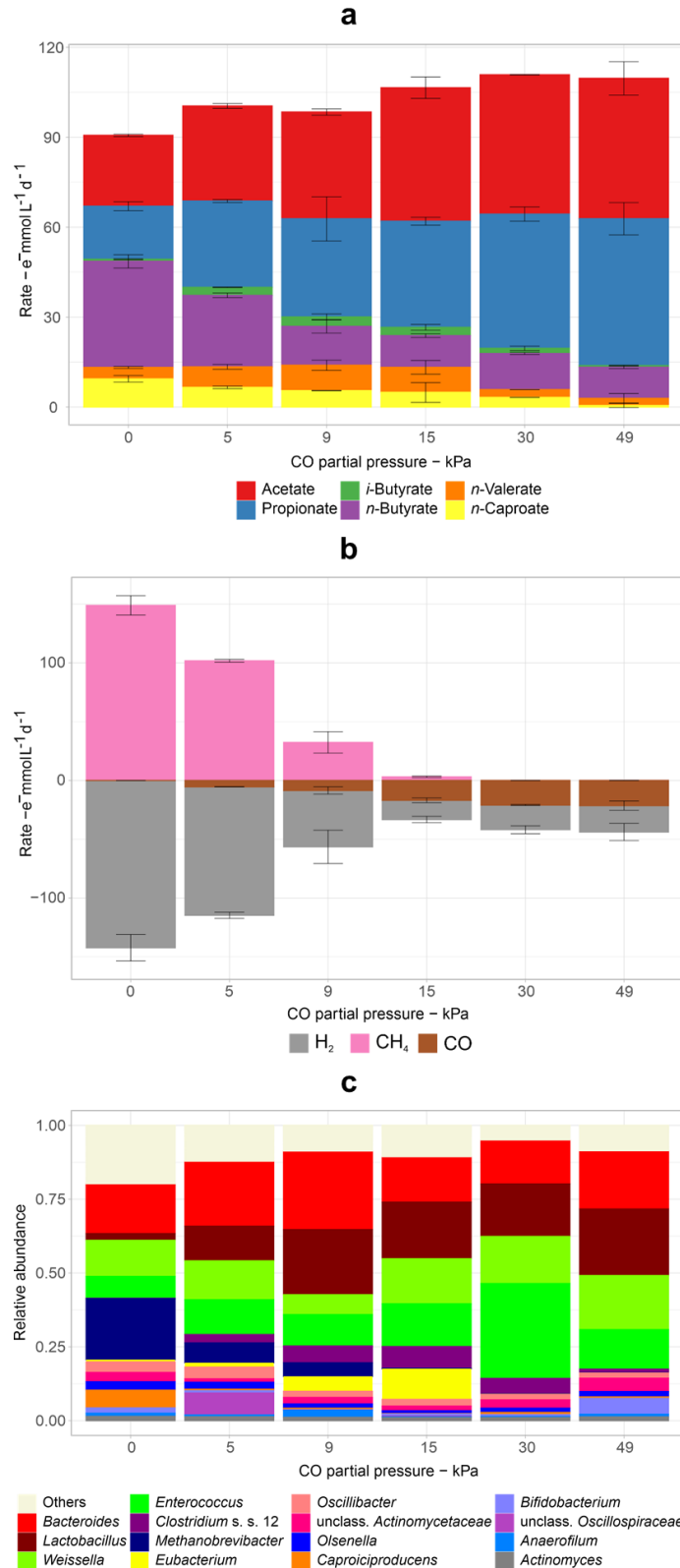
Figure 16. Effect of different partial pressures of CO on the carboxylate spectrum (**a**), gas production and consumption rates (**b**), and on the microbial community at the genus level (**c**). These tests were carried out with bottles inoculated with the adapted community. The 15 most abundant genera in the set are shown. Mean values of duplicate bottles are shown. Error bars indicate standard errors. Rates are in terms of electron equivalents. S.s.: sensu stricto.

CO partial pressures above 9 kPa did not affect *n*-butyrate production but inhibited *n*-caproate formation, which dropped to almost zero at 49 kPa CO ([Figure 16a](#)). *n*-Valerate production was only inhibited by more than 15 kPa CO. However, considering that *n*-valerate is produced from propionate (de Smit et al., 2019), this apparent CO tolerance could just be the effect of increased propionate production.

Higher CO partial pressures favored the incorporation of H_2 and CO into the carboxylate pool, although this effect became weaker with increasing CO pressure ([Figures 16a and b](#)). At 5 and 9 kPa CO, the carboxylate pool increased likely due to partial inhibition of methanogenesis ([Figure 16b](#)) and consequently higher H_2/CO_2 availability for acetogens. Nearly complete inhibition of methanogenesis by *Methanobrevibacter* was achieved at about 15 kPa CO, when CH_4 accounted for less than 3% (3.1 ± 0.6 e$^-$ mmol L^{-1} d^{-1}) of the total electron sink (111 e$^-$ mmol L^{-1} d^{-1}) ([Figures 16b and c](#)), similar to the study of Esquivel-Elizondo et al. (2018), in which 18 kPa CO completely inhibited methanogens in a mixed culture. An increase from 15 to 30 kPa CO improved H_2 and CO consumption further from 16 ± 3 to 21 ± 3 e$^-$ mmol H_2 L^{-1} d^{-1} and from 17 ± 2 to 20.9 ± 0.4 e$^-$ mmol CO L^{-1} d^{-1}, whereas H_2/CO consumptions were similar at 30 and 49 kPa CO ([Figure 16b](#)).

Overall, increasing CO partial pressures ([Figure 16c](#)) shaped the community consistently to what was observed previously when 49 kPa CO or 49 kPa H_2 + 49 kPa CO were used ("Adapted community", [Figure 15c](#)). LAB, Actinobacteria (e.g., *Acidipropionibacterium* and *Actinomyces*), and *Bacteroides* were either unaffected or profited from increasing CO partial pressures, whereas *Caproiciproducens* was sensitive to CO ([Figure 16c](#)). *Oscillibacter*, which generally had a comparably low abundance, was not inhibited by high CO partial pressures. This is relevant as *Oscillibacter* has previously been associated with *n*-valerate, *n*-caproate, and *n*-caprylate production as well as syngas consumption (Godwin et al., 2014; Contreras-Dávila et al., 2021; Joshi et al., 2021) and may be responsible for the formation of carboxylates with longer chains ($C \geq 4$) even at high CO pressures. A higher abundance of *Bifidobacterium* (a genus of lactate-producing actinobacteria) was observed at 49 kPa CO. Bacteria from this genus are selectively favored by high propionate concentrations (Kaneko et al., 1994), therefore, their higher relative abundance at high CO pressure could be a consequence of high propionate production rates ([Figure 16a](#)) rather than of CO itself.

At high CO partial pressures, the rates of electrons routed to acetate (up to 47 ± 6 e$^-$ mmol L^{-1} d^{-1} at 49 kPa CO) were close to the consumption rates of H_2 and CO (44 e$^-$ mmol L^{-1} d^{-1} H_2+CO at 49 kPa CO) indicating predominant acetogenic activity. However, genera known to harbor acetogens (*Clostridium* sensu stricto 12 and *Eubacterium*) had higher relative abundances at intermediate CO partial pressures between 5 and 30 kPa ([Figure 16c](#)).

3.3.4. Combined methanogenesis inhibition by ethylene and carbon monoxide

Ethylene is a minor component of syngas (Benevenuti et al., 2021) and, as seen in the previous chapter, an effective methanogenesis inhibitor at concentrations found in real syngas mixtures

(in the order of 1%). Therefore, we studied its effect during co-fermentation of plant biomass when methanogenic activity was at its peak (at 0 and 5 kPa CO).

Overall, cultures with ethylene produced more carboxylates than cultures without ethylene (Figure 17a). At 0 kPa CO (98 kPa H_2) and at 5 kPa CO (93 kPa H_2), ethylene addition increased the carboxylate production by 20% each. Ethylene showed no clear effect on the elongation of carboxylates and such increase was mainly due to the increased formation of acetate.
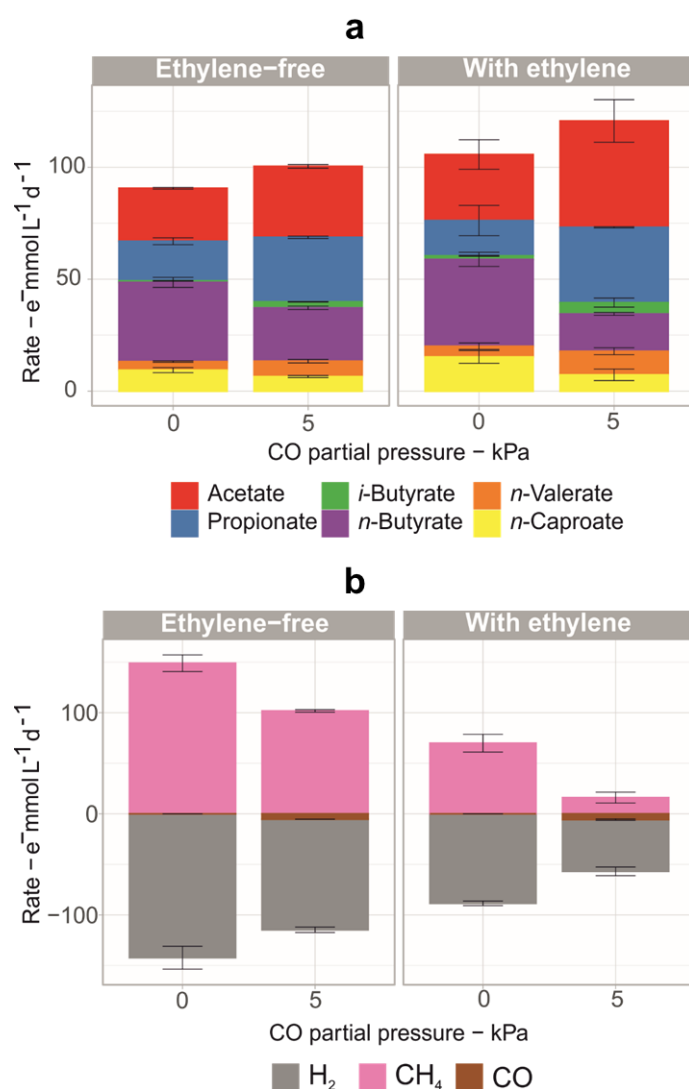
Figure 17. Effect of 1.5 kPa ethylene on the fermentation of corn silage with 0 kPa CO (98 kPa H_2) and 5 kPa CO (93 kPa H_2). Production or consumption rates of carboxylates (**a**) and gases (**b**) are shown in terms of electron equivalents. Error bars are standard errors. These tests were carried out with bottles inoculated with the adapted community.

Ethylene alone reduced methane production rates by about half (from 149 ± 8 to 69.9 ± 9 e⁻ mmol CH_4 L^{-1} d^{-1}), while 5 kPa CO alone reduced methane production rates by about one third (to 102 ± 1 e⁻ mmol CH_4 L^{-1} d^{-1}) (Figure 17b). When CO and ethylene were applied together, CH_4 production decreased 9-fold (to 16 ± 5 e⁻ mmol CH_4 L^{-1} d^{-1}). Ethylene had no effect on CO consumption but increased H_2 consumption (excluding methanogenesis). No consumption of

ethylene was observed. Increase of H_2 consumption by the bacterial share of the community due to the use of methanogenesis inhibitors was observed previously and was attributed to the increased H_2 availability after inhibiting methanogens (Figure 10 and Figure A4).

Figure 18 shows two benchmarks of the fermentation, i.e. carboxylate yields from the plant biomass and carbon fixation rates, at different CO partial pressures. The bottles with ethylene in combination with 5 kPa CO showed with 0.36 ± 0.07 g g_{VS}^{-1} the highest carboxylate yield of this study (Figure 18a). This yield is comparable to one of the highest yields achieved so far in continuous anaerobic fermenters fed with solid feedstock (without syngas and ethylene), namely 0.38 g g_{VS}^{-1} (Strazzera et al., 2021). The yield obtained with ethylene + 5 kPa CO was 44% higher than the yield achieved without syngas and 9% higher than the highest yield achieved with syngas containing 30 kPa CO.
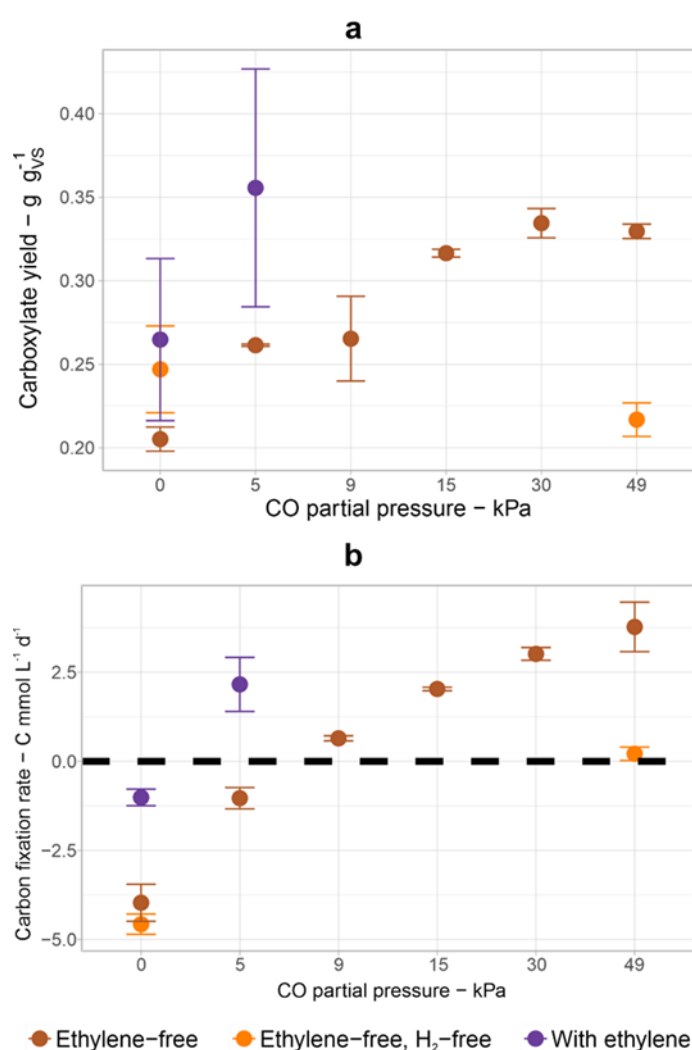
Figure 18. Carboxylate yields from biomass (**a**) and carbon fixation rates (**b**) of fermentations with different gas compositions with CO partial pressures between 0 and 49 kPa. Only results with the adapted community are shown.

The carbon fixation rates followed roughly the same trend as the carboxylate yields. Higher CO partial pressures allowed net carbon fixation up to a maximum of 3.0 ± 0.2 C mmol L^{-1} d^{-1}

(equivalent to 132 ± 9 mg CO_2 L^{-1} d^{-1}) ([Figure 18b](#)). This was achieved by inhibiting methanogenesis and by enhancing acetogenic activity, which in turn led to higher carboxylate production ([Figure 16](#)). Cessation of carbon emissions was achieved when at least 9 kPa CO (without ethylene) or 5 kPa CO (with ethylene) was supplied. Fermentation with 5 kPa CO and ethylene was able to fix carbon at a rate of 2.2 ± 0.8 C mmol L^{-1} d^{-1}, which was comparable to the carbon fixation rate of 2.03 ± 0.05 C mmol L^{-1} d^{-1} at 15 kPa CO ([Figure 18b](#)).

When used separately, CO and ethylene are imperfect methanogenesis inhibitors. CO is not a selective inhibitor and although ethylene is (see [Section 2.4.1](#), "The methanogenesis factor"), its inhibitory effect on archaeal hydrogenases can be bypassed by the expression of Fe-only hydrogenases (Baleeiro et al., 2021a). When used together, small amounts of CO and ethylene had a synergistic effect in inhibiting hydrogenotrophic methanogens. Without methanogens that can misroute electrons from exogenous H_2, anaerobic fermentation can be turned into a net carbon fixation process.

3.3.5. The role of formate in carbon monoxide tolerance

Under most conditions, transient concentrations of up to 1 g L^{-1} formate were observed. In one pair of bottles with the autochthonous community in presence of syngas (49 kPa CO), formate accumulated in the first 10 days and then remained stable at about 2.14 ± 0.06 g L^{-1} (high formate, [Figure B7](#)). In this case, *n*-butyrate and *n*-caproate concentrations were clearly higher (1.7 ± 0.2 and 0.66 ± 0.09 g L^{-1}, respectively) in comparison to a pair of bottles with low formate concentrations under the same conditions (0.5 ± 0.6 and 0.3 ± 0.1 g L^{-1}, respectively) (low formate, [Figure B7](#)). From this observation, we suspected a relationship between formate and fermentative bacteria overcoming CO inhibition, similar to what has been observed in pure cultures of *Acetobacterium woodii* (Bertsch and Müller, 2015). We tested this hypothesis by adding 5 g L^{-1} formate at the beginning of the fermentation at 9 kPa CO. With 5 g L^{-1} formate, the production of *n*-butyrate and *n*-caproate at 9 kPa CO (3.3 ± 0.8 g L^{-1} and 0.9 ± 0.2 g L^{-1}, respectively) was similar to that of the fermentations uninhibited by CO (3.1 ± 0.2 and 0.68 ± 0.08 g L^{-1}, respectively) ([Figure 19](#)).
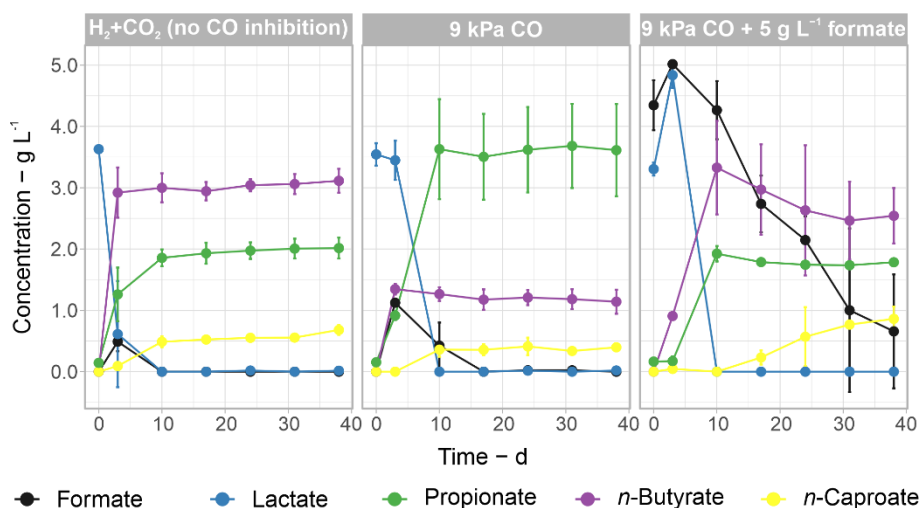
Figure 19. Fermentation profiles of the adapted community under a H_2+CO_2 headspace (uninhibited reference) and at 9 kPa CO with and without added formate. Mean values of duplicate bottles are shown, error bars are standard errors.

Based on the observations in Figure 19 and Figure B7, we propose a theoretical model to explain how formate could help n-butyrate- and n-caproate-producing bacteria to overcome inhibition by CO (Figure 20). These bacteria depend on hydrogenases to re-oxidize Fd_{red} (coupling it with H_2 formation) or to regenerate their NAD(P)H pools. NAD(P)H is required for the elongation cycles with the acyl-CoA and 3-hydroxy-acyl-CoA dehydrogenases (ACAD and 3-HACAD, respectively). On the other hand, formate dehydrogenases (Fdh) can be found in many acidogenic bacteria and these enzymes are assumed to be less sensitive to CO than hydrogenases (Wang et al., 2013). Thus, n-butyrate and n-caproate producers that have an Fdh can couple formate oxidation with NAD^+ reduction and bridge the gap left by hydrogenases inhibited by CO.
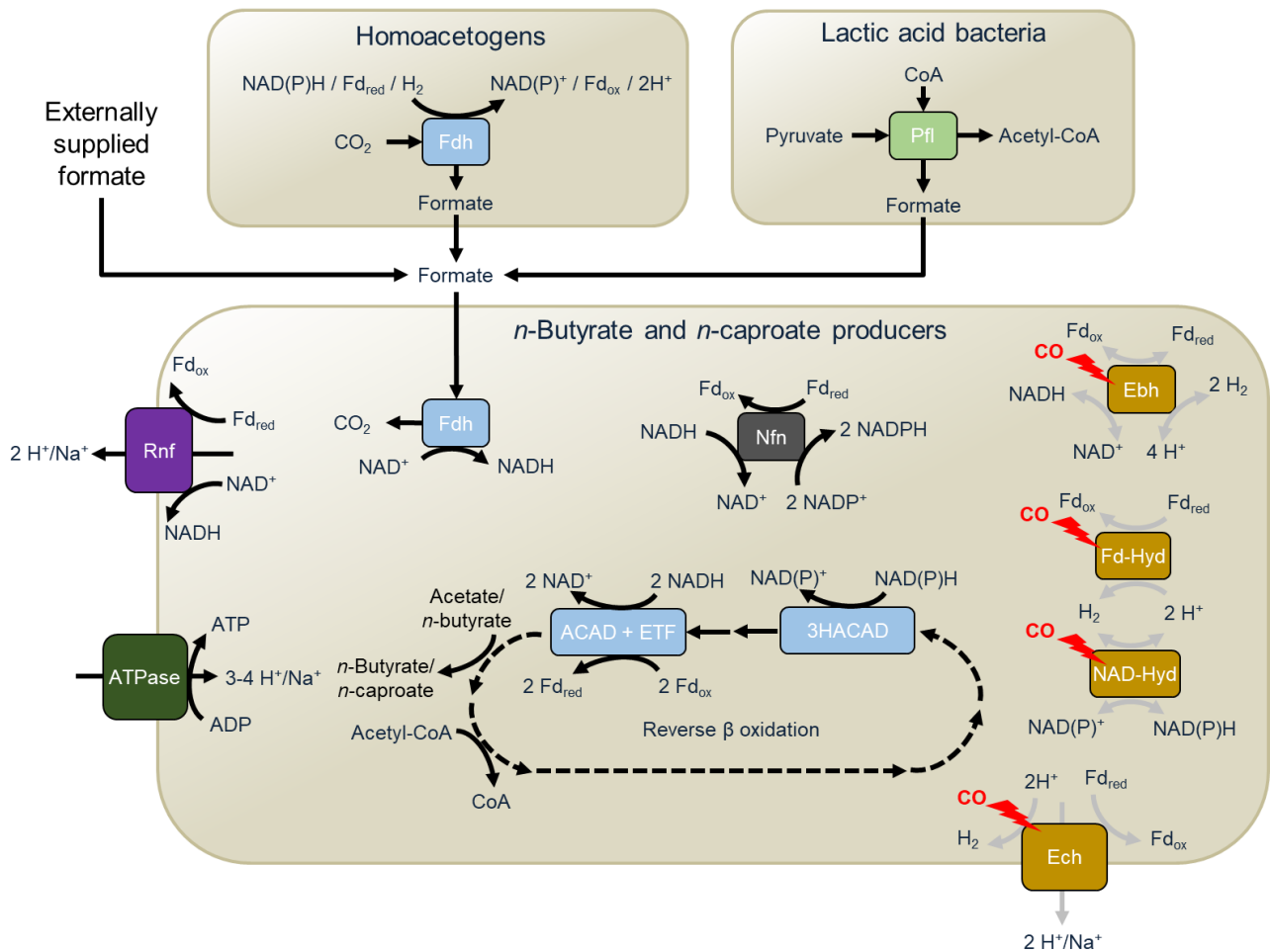
Figure 20. Theoretical model of formate-induced CO tolerance in *n*-butyrate and *n*-caproate producers performing reverse β-oxidation. The CO-inhibited enzymes in the lower box are typically involved in energy conservation in anaerobic acidogenic bacteria that lack cytochromes. Chain-elongating bacteria can compensate for this inhibition by oxidizing formate, thereby providing reduction equivalents needed for reverse β-oxidation. Dashed arrows represent sequential metabolic steps and grey arrows represent CO-inhibited processes. Abbreviations: 3-HACAD, 3-hydroxy-acyl-CoA dehydrogenase; ACAD, acyl-CoA dehydrogenase; Ebh, electron bifurcation hydrogenase; Ech, energy-conserving hydrogenase; ETF, electron-transferring flavoproteins A and B; Fdh, formate dehydrogenase; Fd-Hyd, Fd-dependent hydrogenase; NAD-Hyd, NAD-dependent hydrogenase; Nfn, NAD(P)$^+$ transhydrogenase; Pfl, pyruvate formate lyase.

Formate is an extracellular electron carrier between anaerobic microorganisms such as methanogens, acetogens, and sulfate-reducing bacteria (Schink, 1997; Stams et al., 2006). Under the conditions used here, we expect endogenous formate production to occur mainly in two different ways (Figure 20): *i*) during the conversion of pyruvate to acetyl-CoA via pyruvate formate lyase (Pfl) often found in LAB (Gänzle, 2015) and *ii*) as an intermediate in the metabolism of acetogens after the fixation of one CO_2 molecule with an electron pair (in the form of H_2, NADH, or Fd^{-2}) via Fdh in the methyl branch of the WLP (Bengelsdorf et al., 2018; Oswald et al., 2018a). According to the UniProt database (UniProt-Consortium, 2021), Fdh is predicted from the genomes of *Cl. butyricum* (*Clostridium* sensu stricto 1), *M. elsdenii*, *E. limosum*, and *Cl. luticellarii* (*Clostridium* sensu stricto 12). However, some other well-known acidogens such as

Cl. kluyveri and *Cl. tyrobutyricum* (both belonging to *Clostridium* sensu stricto 12) do not have annotated genes for Fdh.

Figure B8 presents the community compositions at the genus level for the cultures with inhibition or tolerance to CO. Higher relative abundances of *Clostridium* sensu stricto 1 were observed in the fermentation with the autochthonous community under the conditions CO+formate and H_2+CO_2 (no CO inhibition). In the adapted community, the presence of formate caused the absence of *Bacteroides,* which in contrast accounted for about 25% of the bacteria in the bottles without formate, and increased the share of less abundant genera (grouped in "others"), in similarity to uninhibited bottles. 16S rRNA amplicon sequencing does not provide direct information on the presence or absence of the Fdh gene in bacteria. Thus, we were not able to investigate links between Fdh-containing bacteria and formate-induced CO tolerance. Therefore, the proposed metabolic mechanism in Figure 20 should be further tested experimentally. Preferably, this should be done in less complex systems such as co-cultures or single cultures, while monitoring the expression of the respective genes.

Besides, there are other conceivable explanations for how formate restores the production of *n*-butyrate and *n*-caproate in CO-inhibited cultures. It is possible that formate favors *n*-butyrate and *n*-caproate producers by selectively inhibiting propionate producers that compete for lactate and sugars. Direct conversion of formate to *n*-butyrate could be another explanation. However, this conversion is energetically unfavorable (Jeong et al., 2015). To the best of our knowledge, pure cultures of acetogenic bacteria produce at best trace amounts of *n*-butyrate (and *n*-caproate) from formate. For instance, *E. limosum* can grow on formate but without *n*-butyrate production (Litty and Müller, 2021).

3.4. Conclusion

CO toxicity and inhibition of methanogens were the most important factors influencing the carboxylate production. Increasing CO partial pressures completely reshaped the microbial community and shifted the product spectrum from C≥4 carboxylates and methane to acetate and propionate. H_2 in the headspace had limited effects. When H_2 was present, it favored the growth of hydrogenotrophic methanogens, inhibited some bacterial genera commonly associated with lignocellulose degradation, and slowed biomass decomposition. From a sustainability perspective, a syngas composition with low partial pressures of CO and ethylene and high partial pressure of H_2 was particularly interesting since it showed a synergistic effect in inhibiting hydrogenotrophic methanogens and achieving net carbon fixation via acetogenesis. This syngas mixture yielded 44% more carboxylates than a conventional fermentation (with a N_2/CO_2 headspace) despite slower biomass degradation rates, hence reducing the dependence of anaerobic fermentation on biomass availability. From a process engineering perspective, costs could be saved by not having to remove ethylene from real syngas mixtures. Nevertheless, to achieve high yields of longer-chain carboxylates (C≥4), we recommend testing the concept by

operating the fermentation as a continuous process. In this way, chain-elongating bacteria that cope well with both CO and complex feedstocks could be selected.

Under most conditions, as little as 5 kPa CO was sufficient to hinder n-caproate and n-butyrate production. However, this inhibition was not observed in cultures with CO in which formate concentration remained above 2 g L^{-1}. To the best of our knowledge, formate-induced tolerance to CO has not yet been reported for mixed cultures nor for n-butyrate- and n-caproate-producing pure cultures. We postulate that formate could help fermentative bacteria maintain their NAD(P)H pool via formate dehydrogenase, thus bridging the gap left by hydrogenases inhibited by CO. Further experiments are needed to test this hypothesis. If true, this feature could be exploited in designing bioelectrochemical systems with CO or in fermentation technologies based on C1 substrates.

4. The gas recirculation reactor

This chapter is based on the publication:

Author contributions
Flávio C. F. Baleeiro: conceptualization, methodology, investigation, data analysis, visualization, first draft, and manuscript revision.
Sabine Kleinsteuber and Heike Sträuber: conceptualization, project supervision, data analysis support, and manuscript revision.

4.1. Introduction

In this chapter, a semi-continuous reactor with gas recirculation was developed with the aims of enriching a mixotrophic community and enhancing MCC production with exogenous H_2/CO_2 without increasing the supply of the organic ED (lactate). To deal with the resilient methanogenic activity, the use of a syngas contaminant, ethylene, as a methanogenesis inhibitor was tested in culture bottles and scaled up to the H_2/CO_2 recirculation reactor. Finally, the economics of using ethylene as a methanogenesis inhibitor in a large scale was compared to the use of the most popular methanogenesis inhibitor (2-BES).

4.2. Material and methods

4.2.1. Batch experiments in culture bottles

Two different culture bottle experiments were realized with duplicates to test the use of ethylene as methanogenesis inhibitor. The first batch lasted 48 days with H_2 (160 kPa) as ED and under conditions with and without ethylene. The second batch with addition of H_2 (160 kPa) and ethanol (1.7 g L^{-1}) lasted 63 days, and conditions with ethylene, with 2-BES, and without methanogenesis inhibitor were tested. Table C1 summarizes the tested conditions and the types of controls used in each batch experiment.

The inoculum for the batch experiments originated from "community C" from the study in Chapter 2 (Section 2.2.1), in which microbial communities were enriched on organic substrates and H_2/CO_2. Prior to their use, the inoculum sources were stored in serum bottles initially with 200 kPa H_2/CO_2 (80/20) in the dark and at room temperature. The basal medium used for batch experiments contained 0.5 g L^{-1} yeast extract and 200 mM acetate and is described in detail in Appendix C (Section C.1) The cultures were set up with 10 vol.% inoculum, whereas the abiotic control bottles received 10 vol.% sterile anoxic water instead. Preparation procedures for the fermentation and gas purging/pressurization cycles were done as described in Chapter 2. When applicable, 4.5 kPa ethylene was added to the pressurized culture bottles. For comparison of ethylene and 2-BES, every bottle received 1.7 g L^{-1} (37 mM) of ethanol in the beginning of the fermentation. 50 mM of 2-BES (sodium salt) was used in one set of duplicates, whereas all bottles without 2-BES received additionally 50 mM NaCl to achieve a similar salinity level. The culture bottles were incubated in a rotary shaker at 37°C and 200 rpm. The pH value was adjusted manually to 5.5 with 4 M KOH or 4 M HCl.

The headspace of the bottles was sampled once or twice per week (depending on methanogenic activity) for monitoring of pressure, gas composition, and gas production. Culture bottles were refilled when their pressure was 130 kPa or lower. The liquid phase was sampled weekly for analysis of organic acids and alcohols. Cell pellets were collected at the end of each batch for microbial community analysis.

4.2.2. Gas recirculation reactors

Two identical gas recirculation reactor systems were assembled for this study. Each system (Figure 21) consisted of a bioreactor Biostat A plus (Sartorius AG, Göttingen, Germany) with 1.0 L working volume, an 11 L (maximum volume) gas reservoir made of gas-tight, flexible multilayered aluminum-plastic composite material, a condenser, and Hei-Flow Precision peristaltic pumps (Heidolph Instruments GmbH, Germany). The whole system was connected with PVC tubes Tygon R-3603 or LMT-55 and checked regularly for gas leakages with a gas leak detector GLD-100 (Coy Laboratory Products, Grass Lake, USA). A peristaltic pump ensured a continuous gas flow of ca. 20 mL min^{-1} with injection in the liquid phase through a microsparger. The reactor was operated at 32°C with stirring speed of 300 rpm and 7 kPa overpressure on average. Temperature and pH were monitored and controlled, and ORP was monitored.
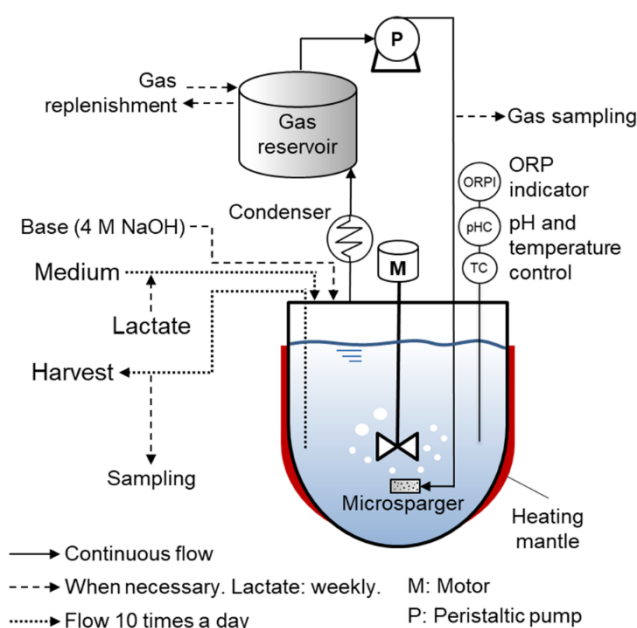
Figure 21. Scheme of the gas recirculation reactor.

The basal medium used in the reactor was similar to the medium used in the culture bottles experiment (Section C.1) with the following modifications: it contained 1.61 g L^{-1} NH$_4$Cl, did not contain yeast extract nor ethanol, and was prepared with acetic acid instead of a sodium acetate/acetic acid mixture. The basal medium was made anoxic and was sterilized and then stored at room temperature at pH 4.5. The inoculum for the reactor experiment, derived from a biogas reactor, was the same as the one used for "community C" from Chapter 2 (Section 2.2.1) and it was stored under anoxic conditions at room temperature in the dark before its use. For startup, each reactor received 14 vol.% of inoculum plus 86 vol.% of basal medium with pH adjusted to 6.0. Anoxic, concentrated cysteine and vitamin solution were added to the basal medium immediately before its addition to the vessel or its connection to the feed pump. 4 M NaOH was used to maintain the pH value between 5.9 and 6.0 and as sodium source. Depending on the amount of NaOH added, salinity of the broth was estimated to be in the range of 16 to 28

g L^{-1} NaCl equivalents. Feeding and harvesting were done with peristaltic pumps programmed to operate 10 times per day in pulses lasting 90 s each. Flows were set to an HRT of 14 days. On day 9 of operation, DL-lactic acid (90% purity) started to be fed with a syringe once a week in order to reach a lactate concentration of 6.0 g L^{-1} (67 mM) after each injection.

Before startup, the gas reservoirs of the assembled dry reactor systems were vacuumed and filled several times with 10 L N_2 to remove all O_2. A defined amount of helium was injected in the system and recirculated to estimate the rigid volume of the system (volume of the system without the gas reservoir). After inoculation and for every gas purging/replenishment cycle, the gas reservoir was emptied with a vacuum pump Laboport® N810FT (KNF Neuberger GmbH, Germany) and refilled with 10 L of H_2/CO_2 (80/20). Furthermore, 120 mL helium was injected with a syringe to act as an inert tracer gas to quantify volume variations due to microbial activity. Concentration of N_2 was monitored to identify and quantify possible air contamination in the system. For inhibition of methanogenesis, ethylene was added after gas replenishment to one of the reactors ensuring a minimum ethylene share of 1.3% in the recirculating gas. Once methanogenic activity was established, gas reservoirs were refilled once a week or when the H_2 share was below 60%, whichever came first. Gas purging and replenishment cycles were always preceded and succeeded by gas sampling in order to keep track of the volume of the system.

The reactor broth was sampled three times per week and before and after each lactate addition. The sampled broth was used for collection of cell pellets for microbial community analysis and for biomass concentration and chemical composition analysis.

Assumptions and calculation steps for the gas recirculation experiment are described in Appendix C (Section C.2). Conversion factors used for the electron and carbon balances are shown in Table A.2.

4.2.3. Analytical methods

Biomass concentration was determined by measuring the optical density at 600 nm (spectrophotometer Genesys 10 S, Thermo Scientific Inc., USA) as described in Section 2.2.4. Concentration of linear monocarboxylates C1-C8, normal alcohols C2-C6, *i*-butyrate, *i*-valerate, *i*-caproate, and lactate was measured by HPLC-RID (HPLC Prominence-i RID, Shimadzu Europa GmbH, Duisburg, Germany). H_2, CO_2, CH_4, He, N_2, and ethylene in the gas phase were analyzed by GC-TCD (Light Gas Analyzer ARNL4159 model 4016, PerkinElmer Inc., USA). Details of the chromatographic techniques were described in the Chapter 2 (Section 2.2.2).

4.2.4. Microbial community analysis

Cell pellets collected from serum bottles and from the gas recirculation reactors were washed with PBS solution (12 mM PO_4^{-3}) and stored at -20℃ until their use for amplicon sequencing of the 16S rRNA gene. Detailed description of DNA extraction, PCR, Illumina library preparation, and sequencing on the MiSeq platform can be found in the study of Logroño et al. (2020). Information on the primers and the bioinformatics workflow used for sample inference from

amplicon data can be found in Chapter 2 (Section 2.2.3). All samples were rarefied to an equal sequencing depth of 44,017 counts. Raw sequence data for this study was deposited at the ENA under the study accession number PRJEB41050 (http://www.ebi.ac.uk/ena/data/view/PRJEB41050).

4.2.5. Assumptions for economic analysis of gas recirculation

Assumptions adopted for the economic analysis of recirculating H_2, CO_2, and ethylene and using 2-BES are described in detail in Appendix C (Section C.3).

4.3. Results and discussion

This study was divided in two main experiments, namely batch tests in culture bottles and the operation of gas recirculation semi-continuous reactors. First, two batch tests were performed in serum bottles to understand the effectiveness of ethylene as an inhibitor, its stability, its effect on the carboxylate production, and to compare it with 2-BES. Afterwards, a pair of gas recirculation reactors was assembled and operated for 84 days.

To consider chemicals in the gaseous and aqueous phases simultaneously, results are presented in terms of electron equivalents. When relevant, reference is made to results in terms of chemicals concentrations in Appendix C.

4.3.1. Inhibition of methanogenesis in batch cultures

The electron balances for the first test are shown in Figure C1. Partial pressure of gases and concentration of chemicals are shown for the conditions with H_2 in Figure C2. Regardless of ethylene presence, more acetate was consumed when H_2 was present. The presence of H_2 with ethylene allowed a 3.7-fold higher *n*-butyrate and a 4.1-fold higher *i*-butyrate production, as well as a 56% higher *n*-caproate production in comparison to cultures with the presence of H_2 alone (Figure C1a). 243 ± 2 mmol e⁻ H_2 was consumed and 249 ± 3 mmol e⁻ CH_4 was produced when ethylene was not present (Figure C1b). The presence of ethylene inhibited virtually all methane production (0.1 ± 0.1 mmol e⁻ CH_4 produced), nevertheless 22 ± 4 mmol e⁻ H_2 was consumed. *n*-Caproate production in this batch experiment was low. Cultures with H_2 produced slightly more caproate on average (uninhibited: 2.0 ± 2.4 mmol e, with ethylene: 3.2 ± 2.3 mmol e⁻) than H_2-free controls (uninhibited: 1.4 ± 1.7 mmol e⁻, with ethylene: 1.2 ± 0.9 mmol e⁻) (Figure C1a). Abiotic controls showed no changes in chemical concentration (data not shown). CH_4 was not produced in cultures that did not receive exogenous H_2, indicating that acetoclastic methanogenesis did not play a role.

To compare the effects of ethylene and 2-BES on CE, a second batch of experiments was carried out with H_2, CO_2, and added ethanol to stimulate MCC production (assuming ethanol as the metabolite intermediating chain elongation from H_2/CO_2) (Figure C3 and Figure C4). When H_2 was present but no inhibitor was used, CH_4 was the most common product. Both 2-BES and ethylene completely inhibited methanogenesis (Figure C3b). The use of inhibitors did not

strongly affect *n*-butyrate or *n*-caproate formation ([Figure C3a](#)), however, 2-BES inhibited *i*-butyrate production almost completely ([Figure C4](#)).

To account for the possibility of ethylene consumption by the community, the amount of ethylene in the headspace of the bottles was monitored throughout the two batch experiments ([Figure C5](#)). No sign of ethylene consumption was found during the periods of the batch experiments. The observed stability of ethylene in the anaerobic cultures is in agreement with a previous study(Schink, 1985b), in which ethylene was not consumed over the whole period of the study (more than 3 months).

A comparison of the microbial community compositions of the inoculum and the inhibited cultures showed that *Methanobacterium* and *Methanobrevibacter* were the methanogens inhibited by ethylene and 2-BES ([Figure C6](#)). Being a closed batch system, a complete disappearance of methanogens could not be observed. In the presence of H_2, CO_2, and ethylene, the relative abundance of *Clostridium* sensu stricto 12 increased ([Figure C6a](#)). When ethanol was also available, an *Anaerovoracaceae* bacterium had the biggest increase in relative abundance ([Figure C6b](#)). Similar observations were found in Chapter 2, where *Clostridium* sensu stricto 12 grew most when H_2 was the only ED, but *Anaerovoracaceae* bacteria were most abundant when ethanol and lactate were co-fed. The patterns of the community inhibited by 2-BES or ethylene were similar ([Figure C6b](#)). A detailed discussion of the batch experiment results can be found in Appendix C ([Section C.4](#)).

4.3.2. Component balances in the gas recirculation reactors

The operation of the two H_2/CO_2 recirculation reactors was divided in two phases lasting 42 days each. The first phase was used for reactor startup and process stabilization. By the end of the start-up phase, hydrogenotrophic methanogenesis was well established in both reactors and ethylene was added to one of the reactors, starting the inhibition phase.

[Figure 22](#) summarizes the results of the two reactor experiments with the profiles of the accumulated compounds during the 84 days of fermentation. [Figure C7](#) presents the concentration profiles of compounds in the aqueous phase. Both reactors were fed with the same amount of lactate, however, the control reactor started lactate consumption later and some lactate was washed out in the beginning ([Figure 22](#)).

Butyrate was the main carboxylate produced. Weekly spikes of the substrates were reflected by the curves of lactate, *n*-butyrate ([Figure 22](#) and [Figure C7](#)), and acetate ([Figure C7](#)) suggesting that *n*-butyrate production was directly coupled with simultaneous consumption of lactate and acetate. Moreover, net consumption of acetate occurred regardless of whether methanogenesis was inhibited or not.
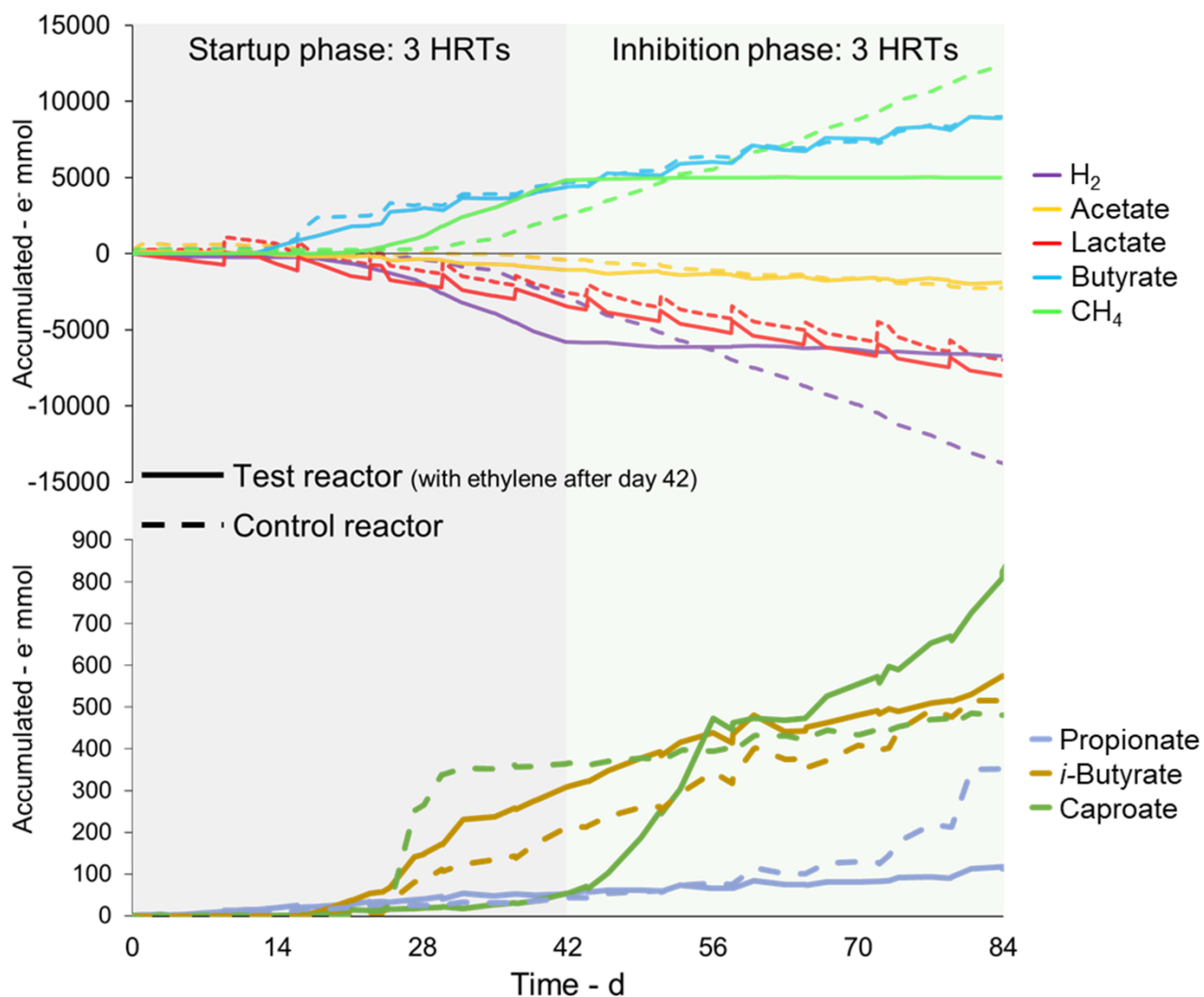
Figure 22. Accumulated substrate consumption and formation of compounds in the reactor with ethylene (Test reactor) and in the reactor without ethylene (Control reactor) shown in electron equivalents. Negative values mean consumption of the compound.

n-Butyrate production started earlier (day 14) than methanogenesis (between days 21 and 28). CH_4 formation rates were 216 and 262 mmol e^- L^{-1} d^{-1} in the control and in the test reactor, respectively, in the last seven days of the startup phase. CH_4 production stopped immediately after ethylene addition in the test reactor and H_2 consumption slowed down from 269 to 23 mmol e^- L^{-1} d^{-1}. Regarding H_2 availability, the partial pressure of H_2 in the control reactor often reached zero and fluctuated strongly in the range of 0 - 80 kPa (Figure C8). In the test reactor, partial pressures of H_2 and ethylene were within the range of 68 - 80 kPa and 1.3 - 4.8 kPa, respectively. The partial pressure of H_2 has a big influence on the thermodynamic feasibility of various microbial pathways. At very low H_2 partial pressures (in the order of 1 Pa), oxidation of carboxylates becomes feasible, while relatively high pressures (in the order of 10 kPa H_2) avoid excessive ethanol oxidation (Ge et al., 2015; Roghair et al., 2018a). Although the feasibility threshold of homoacetogenesis lies in the order of 1 kPa H_2 (Heimann et al., 2010), higher H_2 pressures (> 5 kPa) are typically preferred for kinetic reasons when growing homoacetogens

(Skidmore et al., 2013). H_2 partial pressure has mixed effects on CE. For instance, high H_2 partial pressures inhibit (although not completely) growth of pure cultures of *Cl. kluyveri* on ethanol, but in microbial communities H_2 abundance can boost chain elongation via interspecies ethanol transfer.

n-Caproate and propionate production was not clearly related to lactate consumption ([Figure 22](#) and [Figure C7](#)). An onset of propionate production, peaking at about 1 g L^{-1}, was observed in a late stage in the control reactor despite unchanged operating conditions. *i*-Butyrate production was not inhibited by the use of ethylene and its accumulation remained steady in both the control and the test reactor ([Figure 22](#)). In the control reactor, variations of *i*-butyrate concentration followed variations of *n*-butyrate concentration ([Figure C7a](#)) while this relation was less clear in the test reactor ([Figure C7b](#)). A discussion on the possible role of metabolic intermediates can be found in Appendix C ([Section C.5](#)).

The reactor with ethylene showed 55.7% less net consumption of acetate and higher accumulation of electrons in the *n*-butyrate and *n*-caproate pools ([Figure C9a](#)). Electron selectivity in the test reactor was 101% lactate-to-butyrate (88.2% in the control reactor), 16.9% lactate-to-caproate (2.3% in the control reactor), and 1.4% lactate-to-propionate (6.3% in the control reactor). Channeling of H_2 to CH_4 was mainly responsible for the consumption of 10.9 moles e^- H_2 in the control reactor and less than 10% of this consumption (0.93 mol e^- H_2) was observed in the reactor that received ethylene ([Figure C9b](#)). Despite being a small amount of electrons in comparison to the methanogenic process, the H_2 consumption in the reactor with ethylene accounted for 17% of the total ED consumption. In contrast, the non-methanogenic H_2 consumption accounted for 6.6% of the total EDs consumed in the control reactor for carboxylate production.

4.3.3. Net carbon fixation

Both reactors started with net carbon fixation, but there was a trend in the long run for loss of carbon fixation capacity ([Figure C10](#)). The test reactor became a net carbon emitter by the 3rd HRT period, whereas the control reactor became a net carbon emitter in the 5th HRT. The use of ethylene, injected for the first time in the beginning of the 4th HRT, reverted the trend for the test reactor ([Figure C10](#)). A maximum carbon fixation rate of 62.2 mmol C per 14-days period was observed, which was equivalent to 0.20 g CO_2 L^{-1} d^{-1}. CO_2 dissolution in the broth had only a small impact in the carbon fixation estimation.

4.3.4. Microbial community development

The development of the microbial communities in the gas recirculation reactors is shown in [Figure 23](#). By the end of the startup phase (day 42), the acidogenic genera *Clostridium, Caproiciproducens, Eubacterium,* and *Oscillibacter*, together with the methanogenic genus *Methanobacterium*, were the main settlers in both reactors. *Bacteroides* settled in both reactors from the middle until the end phase of the experiment. *Rummeliibacillus, Sutterella, Defluviitoga,*

Fastidiosipila, and unclassified *Actinomycetaceae* were only transiently detected during the startup phase.
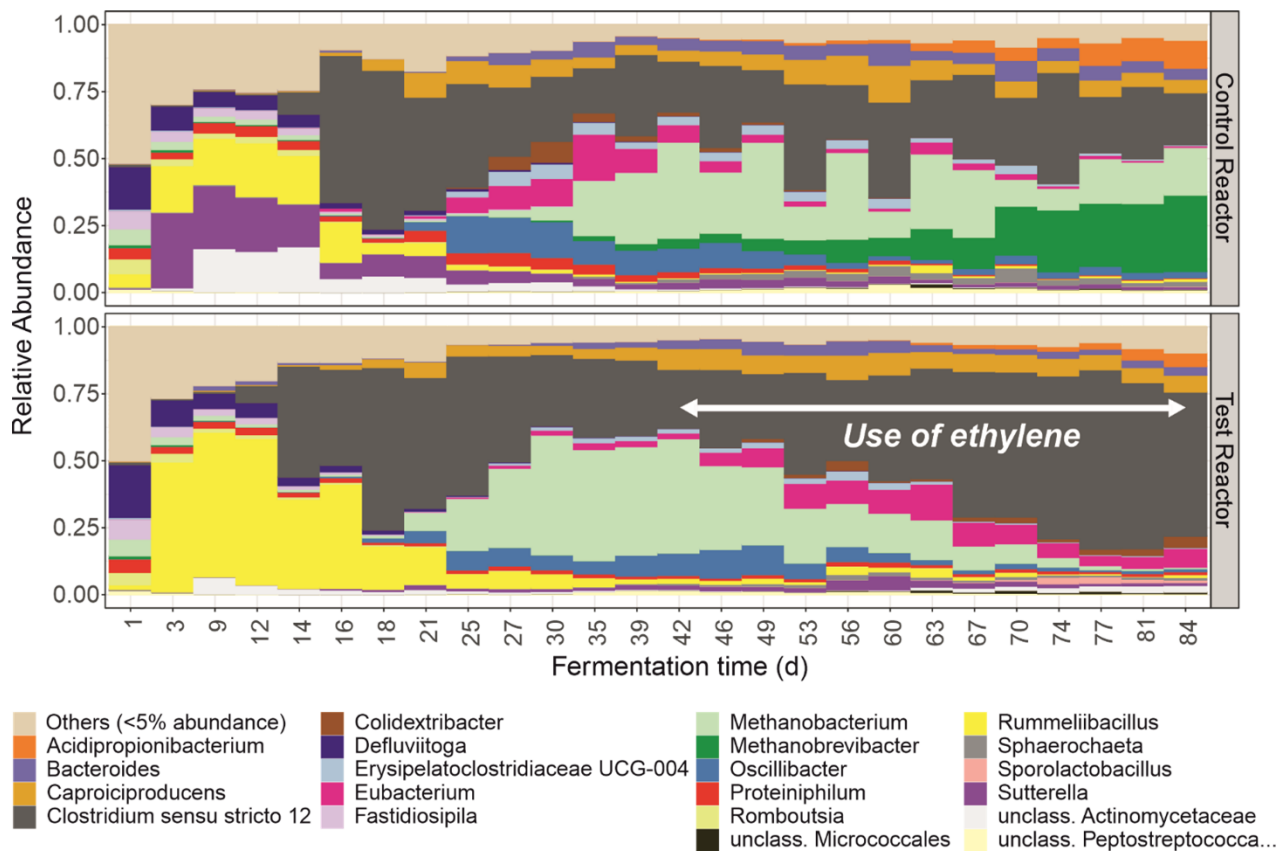
Figure 23. Microbial community profiles for the control and the test reactors. The latter received ethylene after day 42. Hydrogenotrophic methanogens of the genus *Methanobacterium* were washed out during the period in which ethylene was used.

In the control reactor, an additional methanogenic genus, *Methanobrevibacter*, ascended in the later experimental phase while *Eubacterium* and other less abundant genera were washed out from the reactor. With the use of ethylene in the test reactor, the washout of *Methanobacterium* gave room for higher relative abundances of *Clostridium*, *Eubacterium*, and *Colidextribacter*, genera that harbor acetogenic and acidogenic species. A slow but steady increase of *Acidipropionibacterium* was observed in the late fermentation stages in particular in the control reactor (Figure 23), which temporally corresponds to the profile of propionate concentration in the same period (Figure C7a).

n-Butyrate formation was positively correlated with the relative abundances of *Clostridium* sensu stricto 12 while caproate correlated positively with abundances of *Eubacterium*, *Oscillibacter*, *Caproiciproducens*, *Erysipelatoclostridiaceae* UCG-004, and *Colidextribacter* ($p < 0.01$, Figure C9). Production of CH_4 correlated positively with relative abundances of *Methanobacterium* and *Methanobrevibacter* (Figure C11), known as hydrogenotrophic methanogens. *i*-Butyrate production correlated with abundances of *Oscillibacter*, *Caproiciproducens*, *Bacteroides*, and *Erysipelatoclostridiaceae* UCG-004 (Figure C11). Presence of

ethylene correlated with higher relative abundances of *Clostridium* sensu stricto 12, *Eubacterium*, *Caproiciproducens*, *Colidextribacter*. It is worth notice that the analysis shows no distinctions between direct and indirect correlations. This is exemplified in the cases that are clearly indirect: correlations between abundances of some bacterial genera and CH_4 formation and between methanogens and formation of propionate and *i*-butyrate. Some of the ASVs within the acidogenic and acetogenic genera which had high similarities with isolates are presented in Appendix C (Section C.6).

Although the planktonic methanogens were observed to be almost completely washed out with the use of ethylene in the test reactor, biofilms attached to the vessel walls and other inner reactor surfaces still contained methanogens at the end of the experiment (Figure C12).

4.3.5. Ethylene as a scalable inhibitor

While 2-BES can be considered a specialty chemical (41 US$ kg^{-1}), ethylene is a commodity with a relatively low price (1 US$ kg^{-1}) and widely available on the chemical market. Moreover, ethylene (as well as acetylene) is a common constituent of syngas from biomass gasification in the concentrations used in this study (Abdoulmoumine et al., 2014; Karthikeyan et al., 2016). With gas recirculation, ethylene could be used as a recyclable methanogenesis inhibitor, which is not the case for 2-BES, as the latter is soluble in water and would be washed out from the aqueous phase. On the other hand, recirculation of gas increases the auxiliary power requirement of the process. Figure 24 presents an order of magnitude estimate of the operating cost of gas recirculation (depending on the compression pressure) and of using 2-BES (depending on its concentration) per m^3 of broth. As a reference for economic feasibility, the potential value that can be obtained by selling the carboxylates present in the fermenter broth is estimated to be between 8 US$ m^{-3} and 40 US$ m^{-3} (Figure 24). This value depends on the extractable carboxylate composition and the selling price of the carboxylates. Assumptions adopted for the economic analysis are described in detail in Appendix C (Section C.3). Four alternatives were compared: *i)* H_2/CO_2/ethylene recirculation at the flow used in this study (1.2 L h^{-1} L^{-1}); *ii)* H_2/CO_2/ethylene recirculation at a flow at optimized conditions with ten times the microbial gas consumption observed in the test reactor with ethylene (0.14 L h^{-1} L^{-1}); *iii)* recirculation of ethylene only (0.018 L h^{-1} L^{-1}); and *iv)* use of 2-BES for methanogenesis inhibition at concentrations up to 50 mM (10.5 g L^{-1} sodium 2-BES). The gas recirculation alternatives *i)-iii)* cost between 0.02 US$ m^{-3} and 2 US$ m^{-3}, which is well below the value range of the carboxylate broth. The use of 2-BES for inhibiting methanogenesis (option *iv)*) costs at least 43 US$ m^{-3} and is thus not economically feasible even at concentrations below those required for inhibition of hydrogenotrophic methanogens. Other operating costs of the process, such as reactor power input, consumption of chemicals, and downstream processing are not considered here. As a reference, an encompassing economic analysis considering downstream processing and capital costs (but excluding gas recirculation and methanogenesis inhibition costs) was done previously by Scarborough et al. (2018b) for an integrated lignocellulosic biorefinery producing

MCCs, ethanol, and electricity. For a more detailed economic analysis of the gas recirculating, the cost of supplying of H_2 and CO_2 as well as the pay-offs of gas recirculation (in terms of increased selectivity to MCCs, higher carboxylate production, and net carbon fixation) would have to be considered.
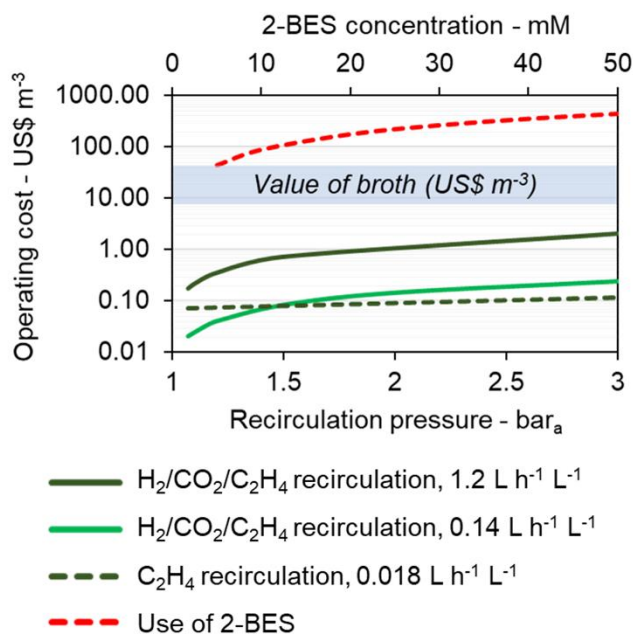
Figure 24. Estimated operating costs of 2-BES addition or H_2, CO_2, and ethylene (C_2H_4) recirculation depending on the pressure. The value of the carboxylate-containing broth is estimated to be between 8 US$ m^{-3} and 40 US$ m^{-3}.

Another difference between ethylene and 2-BES found in the batch experiments was that 2-BES showed inhibitory effects on *i*-butyrate formation, whereas ethylene did not. This fact could prove useful if the production of branched carboxylates is desired, in particular considering that *i*-butyrate and *i*-caproate have been recognized as potential bio-product platforms (de Leeuw et al., 2019; de Leeuw et al., 2020).

As a cautionary tale, it was shown that the biofilm formed in inner reactor parts contained methanogens from previous reactor operation phases (Figure C12). Since ethylene is a reversible inhibitor (Schink, 1985b), the planktonic community may be easily re-inoculated with methanogens from the biofilm or unsterile substrate if the use of ethylene ceases.

4.3.6. Mechanism of ethylene inhibition

Research on the mechanism of ethylene inhibition of methanogens and its effects on acidogenic bacteria has been not as encompassing as research with acetylene. Arguably, the mechanism of inhibition by ethylene may be comparable to that of acetylene, since ethylene also has a π C-C bond (Hyman and Arp, 1988). The specific inhibition by ethylene may be explained by its effect on some types of hydrogenases, specifically those which methanogens most depend on. Acetylene was shown to strongly inhibit [NiFe] hydrogenases of a methanogen (*Methanosarcina* sp. MST-AI DSM 2905) and of a sulfate-reducing bacterium (*Desulfovibrio*

gigas) while presenting no effect on the nickel-free hydrogenase of another sulfate-reducing bacterium (*Desulfovibrio vulgaris*) (He et al., 1989). Methanogenic archaea depend on [NiFe] hydrogenases for fast H_2 oxidation (Thauer et al., 2010) whereas fermentative bacteria (in particular *Firmicutes*) have a vast diversity of [FeFe] hydrogenases (Peters et al., 2015). Whether ethylene has a differential effect on these two types of hydrogenases needs to be tested in future studies, in particular because alternative inhibition mechanisms have been proposed (Sprott et al., 1982; Menon and Lyng, 2021). It is worth noticing that the effects of acetylene and ethylene on anaerobic cultures are not identical. Acetylene is a less selective inhibitor than ethylene since acetylene inhibits sulfate-reducing and nitrogen-fixing bacteria whereas ethylene does not (Brouzes and Knowles, 1971; Schink, 1985b). Ethylene also seems to be more stable in anaerobic systems than acetylene, since a rare metabolic pathway has been found that degrades acetylene in the absence of strong electron acceptors (e.g. sulfate) (Schink, 1985a; Sutton et al., 2017) while to the best of our knowledge no similar pathway is known for ethylene degradation.

4.3.7. Possibilities for process optimization

Developing, controlling, and optimizing a mixotrophic acidogenic community is not trivial because homoacetogens typically prefer higher ATP-yielding substrates (e.g. carbohydrates, ethanol, lactate) before switching to autotrophic metabolism, as seen in the case of *Cl. ljungdahlii* in the presence of fructose (Infantes-López, 2020). Under lactate starvation, homoacetogens are forced to put their substrate flexibility into use (Schuchmann and Muller, 2016). Here, the reactor system was operated in such a way that H_2 and CO_2 were always available, basal medium (with acetate) was fed ten times per day, and lactate was fed once a week. It is possible that this feeding strategy, which had a longer intermittency for lactate, may have helped favor autotrophy over heterotrophy. Another possible consequence of longer intervals of substrate feeding is the maintenance of high diversity in the community (Bonk et al., 2018). High community diversity is a factor that can help couple non-methanogenic H_2 consumption with MCC formation. Inhibition due to MCC toxicity was unlikely a concern in the system. The low MCC concentrations in this study (up to 0.7 mM undissociated *n*-caproic acid at pH 6.0) were well below MCC toxicity limits reported previously (7.5 mM undissociated *n*-caproic acid in ethanol-based CE (Ge et al., 2015) and 10.7 - 17.2 mM undissociated *n*-caproic acid in lactate-based CE) (Duber et al., 2018; Zhu et al., 2021).

There are reasons to argue for a two-step fermentative process that separates homoacetogenesis and chain elongation (Figure 2). For instance, homoacetogens can compete with chain elongating bacteria for lactate and other organic EDs. In this study, this competition did not seem to be a concern. Besides achieving net carbon fixation, homoacetogens also helped to replenish acetate as it was consumed by *n*-butyrate and *n*-caproate fermenters (55.7% less net acetate consumption when H_2 was kept abundant). Therefore, higher non-methanogenic gas consumption rates are generally desirable. In this direction, operation with CO or syngas

mixtures may help improve gas consumption, chain elongation, solventogenesis, and volumetric rates. Besides, CO helps inhibit methanogens.

4.4. Conclusion

Acetate and lactate were used as a simplified model of an organic feedstock with continuous H_2/CO_2 recirculation. This setup was a useful toolbox to *i*) enrich a mixotrophic microbial community, *ii*) simultaneously monitor component balances in the aqueous and liquid phases, and *iii*) economically apply a methanogenesis inhibitor. This toolbox can now be used to test the effects of process disturbances and operating conditions. One important next step is to use the gas recirculation system with real syngas mixtures containing CO. Besides, future studies should also aim to increase *n*-caproate concentration, since in this study the maximum *n*-caproate concentration achieved (up to 1.2 g L^{-1}, <u>Figure C7</u>) fell short in comparison to state-of-the-art CE processes. Depending on the desired products (SCCs, MCCs, alcohols, *i*-butyrate, etc.), the operation of the system may be optimized by adjusting gas-liquid feeding strategies, together with other operational parameters such as pH and temperature.

5. The effect of oxygen contamination on propionate and caproate formation

This chapter is based on the publication:

Author contributions
Flávio C. F. Baleeiro: conceptualization, methodology, investigation, data analysis, visualization, first draft, and manuscript revision.
Magda S. Ardila: investigation, data analysis, visualization, first draft, and manuscript revision.
Sabine Kleinsteuber: project supervision, data analysis support, and manuscript revision.
Heike Sträuber: conceptualization, project supervision, data analysis support, and manuscript revision.

5.1. Introduction

Oxygen from the air can easily enter anaerobic reactors by diffusion due to incomplete tightness or oxic feedstocks, and is considered a disturbance of the anaerobic processes. At first thought, MCC-producing mixed cultures should be protected from O_2 at all costs. So far, almost all isolated MCC producers are strict anaerobes to which O_2 causes damage via direct and indirect ways. O_2 gives rise to reactive oxygen species (ROS), such as O_2^- and H_2O_2, which are intermediates produced during O_2 reduction that severely damage cells if not promptly neutralized (Johnson and Hug, 2019). On the other hand, small amounts of oxygen may be desired in anaerobic processes. Micro-aeration, the controlled dosing of small amounts of air or oxygen (loosely defined from 5 to 5000 mL O_2 L^{-1} d^{-1}), has been mainly used to create different oxidative-reductive regions in digesters to favor biological desulfurization (Krayzelova et al., 2015; Nguyen and Khanal, 2018). Presence of O_2 can also be advantageous in fermentations with acetogens. During batch cultivation of *Cl. ljungdahlii* on H_2, CO, CO_2, and fructose, 8% O_2 in the headspace has been found to increase the production of ethanol (Whitham et al., 2015), which is an important ED for CE.

Although the possibilities with O_2 are being explored in many types of anaerobic technologies, no literature can be found about the effects of O_2 contamination rates on CE. Designing experiments to understand the effects of small oxygen contamination in mixed microbial communities is not trivial and monitoring of O_2 is challenging at the low concentrations found in micro-aerated systems (Nguyen and Khanal, 2018).

The anaerobic reactor system with continuous gas recirculation presented in the previous chapter allows to track cumulative component balances in the gas phase and could be used as a novel way to closely monitor air intrusion. This chapter investigates the effects of small air contamination on the dynamics of the microbial community and MCC production. For this purpose, two stirred-tank reactors (STRs) and two bubble column reactors (BCRs) with continuous H_2/CO_2 recirculation were operated with mixed cultures co-fed with lactate and acetate. One of the reactors of each type had periods with air contamination, while the other two were kept anoxic.

5.2. Materials and methods

5.2.1. Experimental design and reactor systems

Two pairs of reactors with continuous gas recirculation were assembled for this study. One pair consisted of STRs (STR-control and STR-test) and the other of BCRs (BCR-control and BCR-test). Assembly and configuration of the STRs were described in detail in Chapter 4 (Section 4.2.2). The BCRs were assembled and operated with the following differences in relation to the STRs: *i)* the BCR vessels consisted of bubble columns made of glass with a working volume of 1.2 L each; *ii)* the systems had no ORP monitoring; *iii)* pH monitoring and correction was done manually three times a week; *iv)* temperature regulation was carried out via the water jacket of

the vessels and a thermal bath; *v)* gas recirculation was carried out with micro-diaphragm gas pumps NMP 830 (KNF Neuberger GmbH, Germany) at a flow of ca. 1.5 L min^{-1}; and *vi)* an internal vertical hollow glass with holes of 1-2 mm was used to bubble the gas into the broth. In all other aspects, the BCRs were operated similarly to the STRs. The reactors were operated at 32°C, at pH values of 6.0 ± 0.1 (STRs) and 6.1 ± 0.3 (BCRs), and with an HRT of 14 d. The basal medium contained 133 mM lactate (12 g L^{-1}) and 200 mM acetate (12 g L^{-1}) as organic carbon sources and the gas reservoirs were periodically refilled with 10 L H_2/CO_2 (80/20), 240 mL ethylene (methanogenesis inhibitor), and 120 mL He (tracer gas). Basal medium composition, reactor start-up, and reactor operation were identical for STRs and BCRs and were done as described in Chapter 4 (Section 4.2.2), except that lactate was fed ten times per day along with the basal medium.
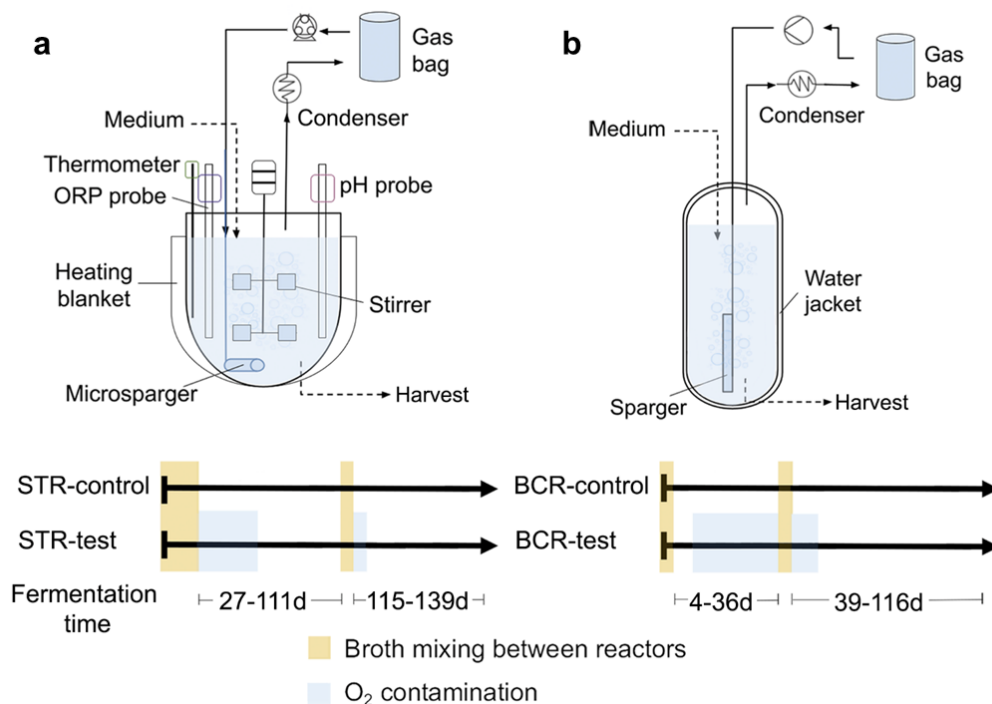
Figure 25. Gas recirculation reactors used in the study. Stirred tank reactors (STRs) (**a**) and bubble column reactors (BCRs) (**b**) with their respective timelines of events.

Figure 25 shows the two reactor types used in the study and the timelines with the oxygen contamination events. The four reactors were inoculated with the broth harvested from the test reactor operated with H_2/CO_2/ethylene recirculation described in Chapter 4 (Section 4.3.2). For STRs, the broths of the two reactors were mixed before the start of the experiment and before the second comparison period to ensure that both reactors started with identical microbial and chemical compositions for each comparison period. The same was done with the broths of the BCRs. Startup and broth mixing of STR-test and STR-control occurred on operation days 0-27 and the second broth mixture occurred on days 111-115 (Figure 25a). Startup and acclimatization of the community to a BCR occurred during the 86 days preceding the start of this study. Mixing of the BCR-control and BCR-test broths occurred on days 0-4 and 36-39

(Figure 25b). The broths were mixed without opening the reactors using Hei-Flow Precision peristaltic pumps (Heidolph Instruments GmbH, Germany), PVC tubes Tygon LMT-55, and three-way valves. The major air contamination events were detected in STR-test on days 27-59 and 115-119 and in BCR-test on days 11-36 and 39-50 (Figure 25).

The reactors that remained air-tight all the time were used as control reactors. Reactors STR-test and BCR-test presented detectable air intrusion at certain periods due to imperfect air-tight conditions. With the help of a H_2 leak detector (GLD-100, Coy Laboratory Products, USA), tightness problems that caused gas to leak out of the reactor systems were located and promptly solved. The same was not true for tightness problems that only allowed air to leak into the system and that were solved by trial and error interventions.

5.2.2. Analytical methods

HPLC-RID (HPLC Prominence-i RID, Shimadzu Europa GmbH, Germany) was operated under the conditions described in Chapter 2 (Section 2.2.2) for monitoring of the following chemicals in the aqueous phase: formate, acetate, ethanol, lactate, propionate, *n*-propanol, *n*-butyrate, *i*-butyrate, *n*-butanol, *n*-valerate, *i*-valerate, *n*-pentanol, *n*-caproate, *i*-caproate, *n*-hexanol, *n*-heptanoate, and *n*-caprylate. Biomass concentration was determined by measuring optical density at 600 nm (spectrophotometer Genesys 10 S, Thermo Scientific Inc., USA). Conversion factors for optical density 600 nm and biomass is described in Chapter 2 (Section 2.2.4). In the gas phase, H_2, CO_2, CH_4, He, O_2, N_2, and ethylene were monitored by GC-TCD as described by Logroño et al. (2020).

5.2.3. Microbial community analysis

Microbial communities were analyzed by 16S rRNA gene amplicon sequencing with taxonomic assignments done with the SILVA 138 reference database (Yilmaz et al., 2014). DNA extraction, PCR, and library preparation for Illumina MiSeq sequencing were described in Chapter 2 (Section 2.2.3). Trimming, filtering, and denoising of amplicon data as well as visualization of microbiome census data and Spearman correlations were done as described in Chapter 2 (Section 2.2.3). All samples were rarified to an equal depth according to the sample with the lowest read number in the dataset (4,977 counts). Raw sequence data for this study was deposited at the ENA under the study accession number PRJEB44209 (http://www.ebi.ac.uk/ena/data/view/PRJEB44209).

5.2.4. Component balance and estimation of oxygen contamination

Assumptions and calculation steps used for the component balances in the gas recirculation reactors are described in Appendix C.2. Direct measurements of O_2 concentration (such as by using dissolved oxygen probes) are not adequate to monitor micro-aerobic environments (Krayzelova et al., 2015). Therefore, O_2 contamination was determined indirectly via the N_2 concentration in the recirculating gas, using the N_2:O_2 ratio in air of 3.73 according to the Equation 6.

$$O_2 \text{ contamination rate [mL d}^{-1}\text{]} = \left. \frac{(Y_2 V_{gas\,2} - Y_1 V_{gas\,1})}{} \middle/ [3.73\,(t_2 - t_1)] \right. \tag{6}$$

For sampling points 1 and 2 in Equation 6: Y is the volumetric fraction of N_2 in the gas phase; V_{gas} is the gas volume of the system in mL; and t is the sampling time in days. Equation 6 holds true if no N_2 is formed or consumed in the reactor, if O_2 is below the detection limit, and if the increase in the system's gas volume due to air leaking in can be neglected. Calculations of contamination rates in the control reactors (STR-control and BCR-control) were used to determine standard errors for the O_2 contamination rate (Figure D1). ORP measurements did not show a clear relation with O_2 contamination rates (Figure D2) and were, hence, not used to quantify rates.

5.3. Results

The experiments were divided into two periods, each with one air contamination event. STR-test and BCR-test had O_2 intrusion from air for certain periods, while STR-control and BCR-control remained virtually anoxic throughout the study (calculated average contamination rates of 7 ± 33 and 3 ± 28 mL O_2 L^{-1} d^{-1}, respectively) and were adopted as controls for anoxic reactor operation. Before the start of each period, the broths of each reactor pair were mixed so that each pair started with a similar microbial community and broth composition. The broths from the STRs were not mixed with the broths from the BCRs, resulting in communities developing independently for each reactor type.

5.3.1. General performance of the gas recirculation reactors

The main carboxylates produced were propionate, n-butyrate, i-butyrate, n-valerate, n-caproate, and n-caprylate, with maximum concentrations presented in Table 3. The STRs reached higher n-caproate maxima and were the only ones in which n-caprylate was detected, whereas the BCRs reached higher propionate, n-valerate, and i-butyrate maxima. These differences can also be seen in terms of specific production and consumption rates given in mmol L^{-1} d^{-1} in Table D1. For all reactors, most of the lactate fed was consumed and differences in its consumption rates were due to washout of unconsumed substrate (Table D1). Except for the period when O_2 was present in detectable amounts, net consumption of acetate occurred in all reactors, ranging from 1.4 to 4.4 mmol L^{-1} d^{-1}, which corresponded to a fraction of the total acetate fed (14.3 mmol L^{-1} d^{-1}). With the exception of STR-control, where very little i-butyrate was produced, i-butyrate production rates ranged from 0.23 to 1.08 mmol L^{-1} d^{-1} and showed no clear relation to O_2 contamination (Table D1).

Table 3. Maximum concentration of carboxylates achieved in the experiments.

Reactor	Maximum concentration (g L^{-1})					
	propionate	*n*-butyrate	*i*-butyrate	*n*-valerate	*n*-caproate	*n*-caprylate
STR-control	1.3	3.4	0.5	0.3	4.6	1.1
STR-test	1.7	5.7	0.6	0.4	3.5	1.0
BCR-control	2.7	4.1	2.2	1.0	3.0	-
BCR-test	3.1	4.7	1.6	0.6	3.5	-

According to previous experience with the H_2/CO_2 recirculation reactors (Chapter 4), ethylene was used to inhibit CH_4 production. Even though the partial pressure of ethylene was higher than 1 kPa at all times, methanogens gradually acclimatized to the inhibitor. Methanogenesis was observed first in the reactors that remained anoxic throughout the experimental time: in BCR-control from day 0 and in STR-control from day 31. Later on, methanogenesis was also observed in STR-test from day 48 and in BCR-test from day 60. Methane production rates were similar in the control reactors STR-control and BCR-control (16.5 and 15.9 mmol L^{-1} d^{-1}, respectively) and the highest rate observed over a sustained period was 19.5 mmol L^{-1} d^{-1} during an anoxic operation period between days 59 and 111 of STR-test (Table D1).

With 200 mM acetate (12 g L^{-1}) originally present in the growth medium, no net acetate formation was observed and no clear signs of homoacetogenic activity were found. After discounting the H_2 used for CH_4 formation (assuming 1 mol CH_4 produced from 4 mol H_2), almost no additional H_2 consumption was seen in the control reactors STR-control and BCR-control. STR-control had a net H_2 formation of 3.73 mmol L^{-1} d^{-1}, whereas BCR-control showed a net H_2 consumption of 0.50 mmol L^{-1} d^{-1} (Table D1). In the periods with O_2 contamination, H_2 consumption rates remained relatively high, despite low methanogenic activity. STR-test showed additional H_2 consumption of 26.3 mmol L^{-1} d^{-1} between days 27 and 59 and of 64.7 mmol L^{-1} d^{-1} between days 115 and 119 (Table D1). This consumption of H_2 corresponded from 3.0 to 3.4 times the molar consumption of O_2 in the same period. In aerated periods in BCR-test, H_2 consumption after discounting methane production ranged from 1.1 to 3.6 times the oxygen consumption.

Electron balances encompassing the whole period of fermentation had errors of -0.63% (i.e. 0.63% of the monitored pool of electron equivalents had unexplained consumption) for STR-test, -0.73% for STR-control, -0.93% for BCR-control, and -1.61% for BCR-test.

5.3.2. Effect of oxygen on the fermentation in the stirred-tank reactor

Figure 26 shows the profiles of the cumulated amounts of carboxylates and O_2 as well as the microbial community composition at class level for the STRs. Between days 27 and 59, O_2 concentration in the gas phase remained below the detection limit in STR-test (Figure D3),

although a contamination rate of 220 ± 33 mL O_2 L^{-1} d^{-1} was detected. Between days 59 and 111, STR-test had an anoxic operation period although small O_2 contaminations occurred between days 104 – 111 (Figure 26a) and were the reason why the reactor could not reach perfectly anoxic conditions (21 ± 33 mL O_2 L^{-1} d^{-1}).

Even though *n*-butyrate and *n*-caproate were the main carboxylates produced in both reactors, *n*-caproate production in STR-test was, with 0.56 mmol L^{-1} d^{-1}, 72% lower than in STR-control (2.12 mmol L^{-1} d^{-1}) during the contamination period (days 27 – 59, Figure 26a). Under O_2 stress, STR-test produced more propionate (0.76 mmol L^{-1} d^{-1}, 6.4 times that of the control) but *n*-butyrate production was similar in both reactors. Moreover, O_2 contamination in STR-test caused 63% less methane production (6.05 of 16.5 mmol L^{-1} d^{-1}) and 38% less acetate consumption (1.80 of 2.91 mmol L^{-1} d^{-1}, Table D1). After anoxic conditions in STR-test had been restored (days 59 – 111), methane production was 18% higher than in the control reactor (19.5 of 16.5 mmol L^{-1} d^{-1}) and propionate production decreased slightly to 0.67 mmol L^{-1} d^{-1}. Under anoxic conditions in STR-test, propionate production slowed down from day 66 on, coinciding with an acceleration of *n*-caproate production (Figure 26a), which was still 16% lower than in the control (1.78 of 2.12 mmol L^{-1} d^{-1}).
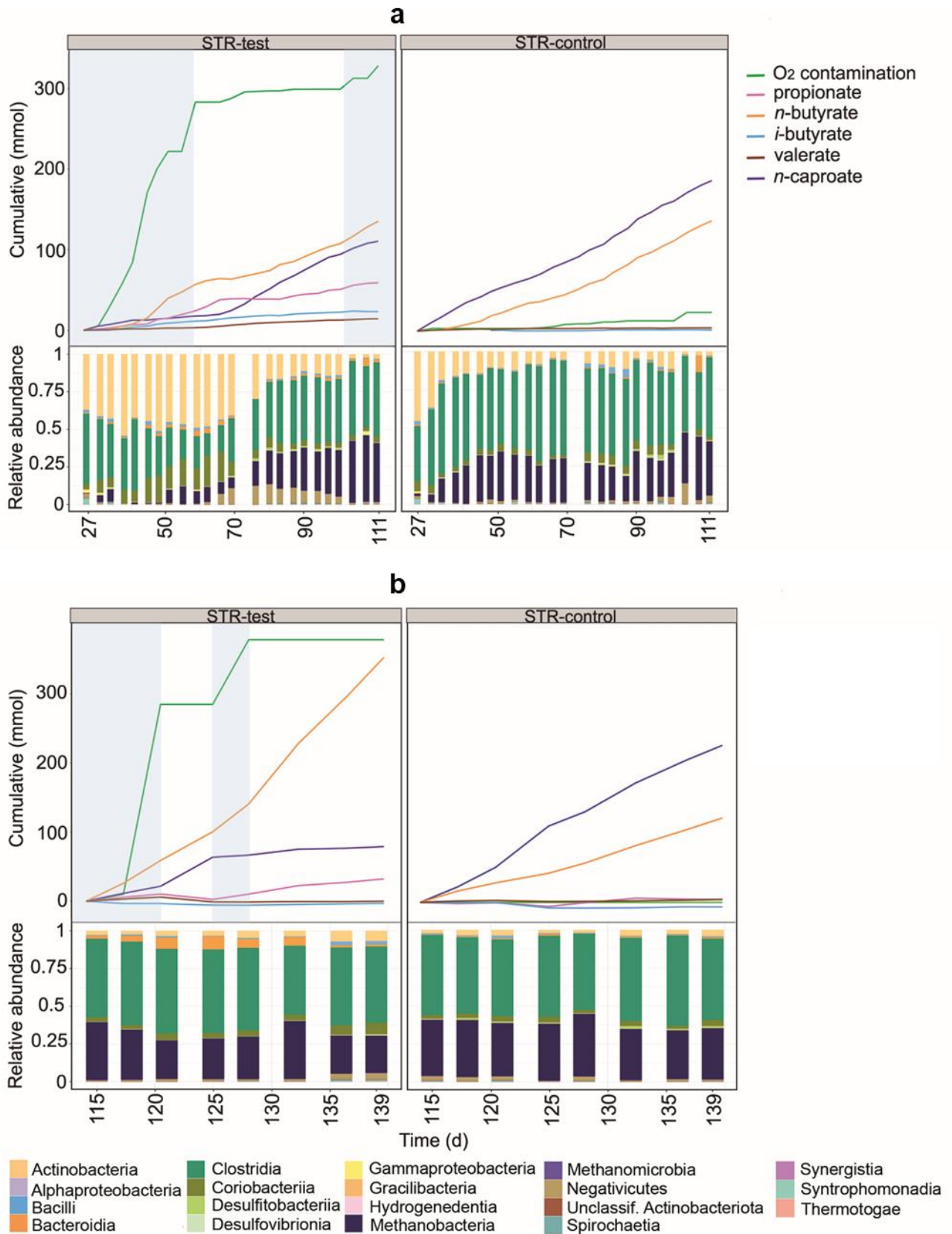
Figure 26. Profiles of the cumulated amounts of carboxylates and O₂, as well as community composition at class level between **a** days 27 and 111 and **b** days 115 and 139 for the STRs. Blue shading indicates the O₂ contamination period.

O2 contamination caused differences in microbial community composition that were visible up to the class level (Figure 26a). Clostridia and Methanobacteria predominated in the reactor that remained completely anoxic. In the other reactor, Actinobacteria and Coriobacteriia were the main classes found in periods when O2 contamination occurred. The community of STR-test converged to a composition similar to that of the control reactor after anoxic conditions had been restored.

For the same reactors, community composition with resolution to the genus level and concentrations of the main carboxylates are shown in Figure D4. Clostridia were mainly represented by the genera *Caproiciproducens*, *Clostridium* sensu stricto 12, and *Oscillibacter,* while the Actinobacteria belonged to the genera *Acidipropionibacterium* and *Actinomyces*. Methanogens were from the genus *Methanobrevibacter* and the Coriobacteriia were from the family *Eggerthellaceae*.

A second O2 contamination event occurred in STR-test between days 115 and 119 (Figure 26b), this time for a shorter period but at double rate (471 ± 33 mL O_2 L^{-1} d^{-1}) (Table D1). With the new contamination event in STR-test, CH_4 and *n*-caproate production rates fell to 32% (5.33 of 16.5 mmol L^{-1} d^{-1}) and 50% (1.06 of 2.12 mmol L^{-1} d^{-1}) of those of the control reactor, respectively (Table D1). This time, the O2 contamination coincided with an increase in *n*-butyrate formation rate from 1.51 to 2.76 mmol L^{-1} d^{-1}, and instead of increasing propionate production, *n*-valerate production reached four times that of the control reactor (0.29 in relation to 0.07 mmol L^{-1} d^{-1}). The short period of intense O2 contamination had a smaller impact on the microbial community composition and coincided with an increase in relative abundance of *Prevotella* belonging to the Bacteroidia (Figure D4b). In the last 20 days of operation of STR-test, O2 contamination was reduced but not completely stopped (39 ± 33 mL O_2 L^{-1} d^{-1}, Table D1) as shown between days 125 and 128 (Figure 26b). In this period, propionate production decreased to its lowest value in STR-test and *n*-butyrate production increased once more to 4.77 mmol L^{-1} d^{-1}. Although CH_4 formation increased again to the level observed during anoxic operation, *n*-caproate production could not be restored (Figure 26b).

5.3.3. Effect of oxygen on the fermentation in the bubble column reactor

Community composition and chemical production of the BCRs are shown in Figure 27 and in Figure D5. For this comparison period, the mixing of broths was not enough to ensure equal community compositions in BCR-test and BCR-control. The O2 contamination period between days 11 and 36 in BCR-test differed from the other contamination events since O2 concentrations up to 18% were detected in the gas phase between days 11 and 28 (Figure D3). Considering that the assumptions for balance calculations in the reactors do not account for high O2 concentrations, the O2 contamination rate determined for this period (97 ± 28 mL O_2 L^{-1} d^{-1}) might be inaccurate. When O2 was detected in the system, the microbial community in the BCR-test showed a strong dominance of *Rummeliibacillus* (Figure D5a) accompanied by Actinobacteria and Gammaproteobacteria (Figure 27a).
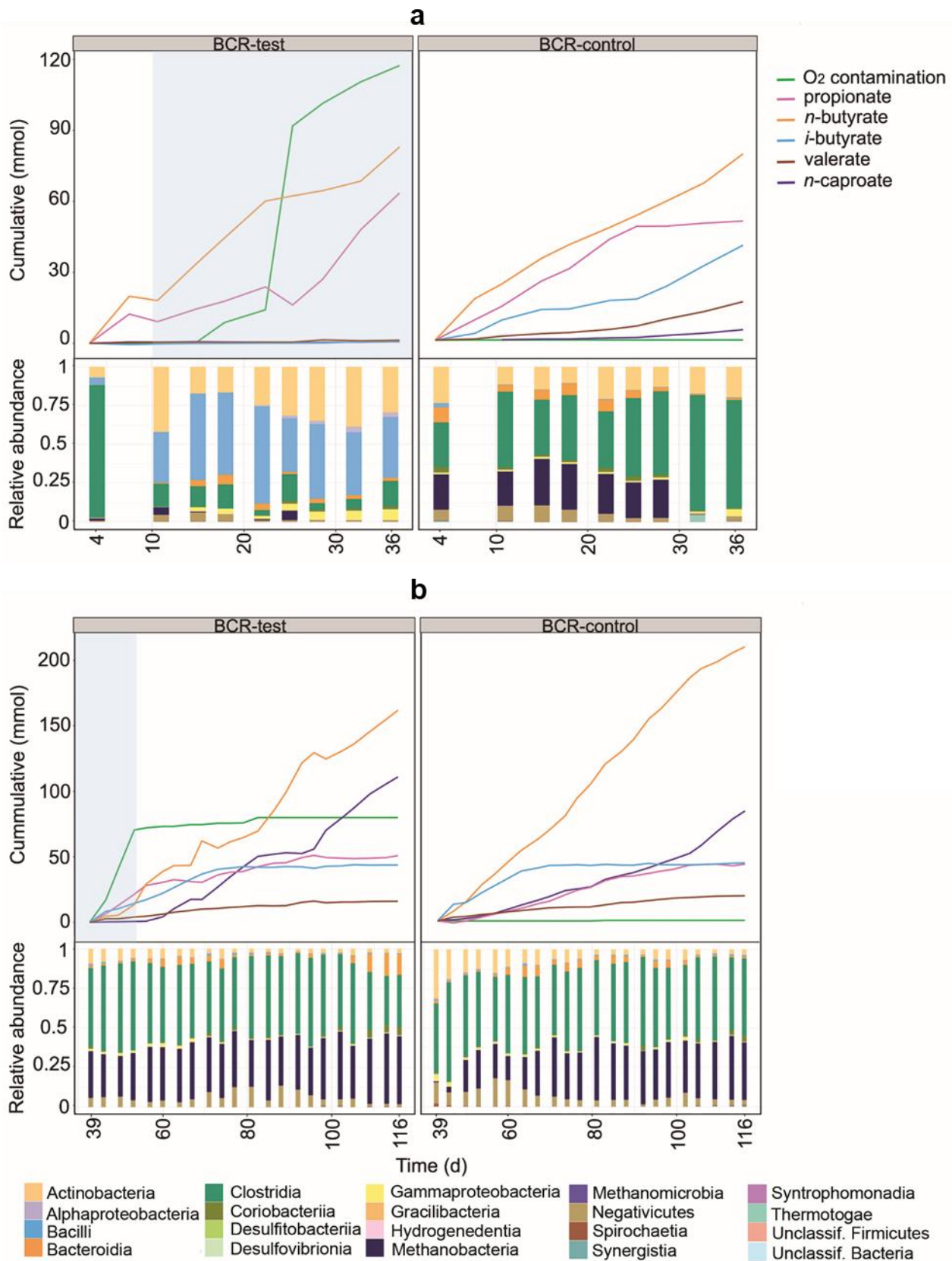
Figure 27. Profiles of the cumulated amounts of carboxylates and O_2, as well as community composition at class level between **a** days 4 and 36 and **b** days 39 and 116 for the BCRs. Blue shading indicates the O_2 contamination period. Between days 11 and 28, O_2 concentrations in the gas phase were detected up to 18% in BCR-test, hence, determination of O_2 consumption in this time period might not be accurate.

After mixing the broths of the bubble columns to start a new comparison period, BCR-test received 129 ± 28 mL O_2 L^{-1} d^{-1} between days 39 and 50 whereas BCR-control remained completely anoxic (Figure 27b). During the contamination period, BCR-test produced virtually no n-caproate (0.03 mmol L^{-1} d^{-1} in comparison to 0.92 mmol L^{-1} d^{-1} in control) and propionate was produced instead (1.78 mmol L^{-1} d^{-1}, 2.8 times that of the control). With O_2 contamination, BCR-test produced 46% less n-butyrate (1.22 of 2.25 mmol L^{-1} d^{-1}) and 91% less methane (1.41 of 15.9 mmol L^{-1} d^{-1}) than the control (Table D1). After O_2 contamination stopped in BCR-test (from day 50 on), n-caproate production recovered with a rate of 1.40 mmol L^{-1} d^{-1} while propionate formation decreased to 0.34 mmol L^{-1} d^{-1}. n-Butyrate and methane production recovered partially and remained 18% (1.84 of 2.25 mmol L^{-1} d^{-1}) and 25% (11.9 of 15.9 mmol L^{-1} d^{-1}) lower than that of the control, respectively.

Similarly to what was seen in the STRs, Actinobacteria increased their relative abundances at the cost of Clostridia and Methanobacteria during the O_2 contamination period in BCR-test (Figure 27b). In addition, Gammaproteobacteria also became more abundant during the contamination. Visualization of the community development at genus level in Figure D5b reveals that the main genera of Actinobacteria were the same as those found in the STRs (i.e. *Acidipropionibacterium* and *Actinomyces*). Besides the Clostridia genera that dominated in the STRs, a transient presence of *Eubacterium* was also observed in the BCRs. Gammaproteobacteria were represented by *Sutterella* and *Burkholderia* (Figure D5b).

5.3.4. Correlations between community members and abiotic parameters

Figure 28 shows Spearman correlations between the most abundant genera, O_2 contamination, and the formation or consumption rates of the main chemicals. In Table D2, the correlation coefficients and their p-values are listed. Positive correlations of n-caproate formation and relative abundances of *Caproiciproducens*, unclassified *Peptostreptococcales*, and *Methanobrevibacter* were found, whereas *Clostridium* sensu stricto 12, unclassified *Micrococcales, Acidipropionibacterium*, *Burkholderia*, *Rummeliibacillus, Dialister,* and *Sutterella* correlated negatively. Propionate production correlated positively to abundances of *Acidipropionibacterium, Burkholderia*, and *Proteiniphilum*. O_2 contamination correlated negatively with *Methanobrevibacter,* whereas positive correlations were found with abundances of unclassified *Eggerthellaceae*, unclassified *Actinomycetaceae*, *Actinomyces*, and *Proteiniphilum*. Abundances of *Clostridium* sensu stricto 12, *Acidipropionibacterium, Acidaminococcus,* and *Dialister* correlated positively with i-butyrate and n-valerate production. H_2 consumption after discounting methane production (i.e. non-CH_4 H_2 consumption) correlated positively with *Acidipropionibacterium, Actinomyces*, and unclassified *Micrococcales*. i-Butyrate production correlated negatively with relative abundances of *Methanobrevibacter*, *Caproiciproducens*, and unclassified *Peptostreptococcales*.
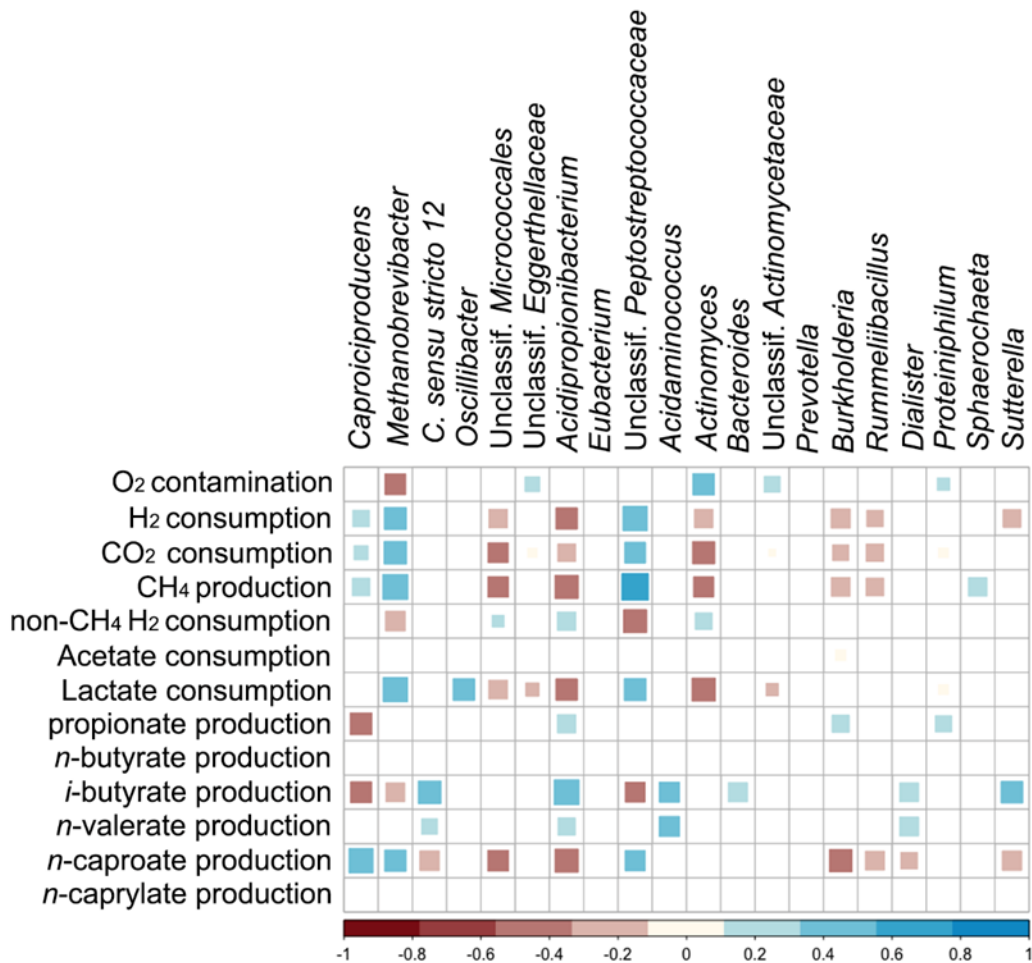
Figure 28. Spearman correlation matrix between the most abundant genera, O_2 contamination rate, and production/consumption rates of chemicals ($p < 0.01$). "non-CH_4 H_2 consumption" stands for H_2 consumption after discounting methane formation.

Among the most abundant ASVs, *Clostridium* sensu stricto 12 and *Acidipropionibacterium* had ASVs that were identical to isolated species in the Silva 138 database. Within the genus *Clostridium* sensu stricto 12, ASVs were assigned to *Cl. luticellarii*, *Cl. tyrobutyricum*, or *Cl. ljungdahlii* (the latter was also ambiguously assigned to *Cl. autoethanogenum, Cl. ragsdalei*, and *Cl. coskatii*). ASVs within *Acidipropionibacterium* were assigned to *A. acidipropionici*.

5.4. Discussion

Regardless of O_2 contamination, the BCRs had higher concentrations of propionate, *i*-butyrate, and *n*-valerate, whereas the stirred tank design facilitated higher concentrations of *n*-butyrate, *n*-caproate, and *n*-caprylate (Table D1). The production of *n*-valerate and *i*-butyrate was not clearly related to O_2 contamination (Figure 26, Figure 27, and Table D1), but its connection to *Clostridium* sensu stricto 12 (Figure 28), specifically *Cl. luticellarii*, was observed previously (de Smit et al., 2019; de Leeuw et al., 2020; Huang et al., 2020). *Cl. luticellarii* was shown to be important for *n*-valerate production from propionate (de Smit et al., 2019) and could therefore play an important role in the production of odd-chain MCC in chain elongation reactors. *n*-

Valerate and *i*-butyrate production also correlated with other genera that are not commonly known for the production of these compounds ([Figure 28](#)). Higher relative abundances of *Caproiciproducens* not only correlated significantly with caproate production ([Figure 28](#)) but were visually related to higher concentrations of *n*-caproate ([Figure D4](#) and [Figure D5](#)). The correlation of *n*-caproate production with the abundance of *Caproiciproducens* is not surprising, since this genus has been commonly found in other MCC-producing communities (Duber et al., 2020; Joshi et al., 2021).

Micro-aerobic conditions favored the classes Actinobacteria, Gammaproteobacteria, Bacilli, and Coriobacteriia over Clostridia and Methanobacteria. Notably, a similar pattern is known for gut microbiota, where Actinobacteria and Alpha- or Gammaproteobacteria have been observed to dominate over Clostridia in regions of the gut more exposed to O_2 (Friedman et al., 2018). One explanation is that the evolutionary younger taxa of aerotolerant Actinobacteria (e.g. propionibacteria) and Proteobacteria (Martin and Sousa, 2015) are generally better equipped with enzymes that mitigate the toxicity of ROS (e.g. catalases, H_2O_2 reductases, and superoxide dismutases) than typical strict anaerobes such as Clostridia (Kato et al., 1997; Johnson and Hug, 2019).

5.4.1. Partial acclimatization of methanogens to ethylene

Hydrogenotrophic methanogenesis was likely the main pathway for CH_4 production. This is supported by the results of previous experiments where *Methanobrevibacter* was one of the predominating community members under similar conditions with H_2/CO_2 in Chapter 4 ([Section 4.3.4](#)). Notably, methanogens partially overcame the inhibition by ethylene. The acclimatization occurred after 42 days of successful inhibition reported in the previous chapter ([Section 4.3.2](#)). To the best of our knowledge, such acclimatization has not been reported before. With ethylene, CH_4 production was relatively strong (up to 19.5 mmol L^{-1} d^{-1}) but still about one third lower than the rates observed in the absence of the inhibitor in the control reactor of Chapter 4 (up to 32.8 mmol L^{-1} d^{-1}) ([Figure C9](#)). We hypothesize that *Methanobrevibacter*, the main methanogenic genus found in our reactors, may have acclimatized to ethylene by expressing [Fe]-hydrogenases. For hydrogenotrophic methanogens, [Fe]-hydrogenases have less favorable kinetics than [NiFe]-hydrogenases. Still, some methanogens, including Methanobacteria, can express [Fe]-hydrogenases to grow under nickel-limiting conditions (Thauer et al., 2010). As postulated in the previous chapter ([Section 4.3.6](#)), ethylene might not exert an inhibitory effect on nickel-free hydrogenases as it does on [NiFe]-hydrogenases of methanogens. Considering that [Fe]-hydrogenases are not inhibited by O_2 (Thauer et al., 2010; Stiebritz and Reiher, 2012), micro-aerobic conditions and broth mixing between reactors could have caused further selection of methanogens expressing [Fe]-hydrogenases even if nickel was not limiting. Further studies using transcriptome or proteome analyses of pure methanogenic cultures are needed to test this hypothesis.

5.4.2. Steering the fermentation with small oxygen contamination

When the O_2 concentration in the gas phase increased up to 18% between days 11 and 28, the aerobic genus *Rummeliibacillus* (Vaishampayan et al., 2009; Her and Kim, 2013) flourished in the BCR and the concentrations of *n*-butyrate and propionate decreased (Figure D5a). With an O_2 concentration below the detection limit by day 28 (Figure D3), Actinobacteria abundance increased and propionate production reached its highest rates (Table D1).

Methanogenesis and *n*-caproate production were strongly inhibited by O_2 intrusion. After the contamination stopped, CH_4 production recovered on every occasion but *n*-caproate production did not (Table D1), indicating that the O_2 contamination had particularly strong detrimental effects on C4-to-C6 CE. In the period between days 119 and 139 in STR-test, *n*-caproate production did not increase after O_2 contamination rate changed from 474 ± 33 mL O_2 L^{-1} d^{-1} to 39 ± 33 mL O_2 L^{-1} d^{-1}, instead, the highest rates of *n*-butyrate production and acetate consumption were achieved. This was observed even with high relative abundances of *Caproiciproducens* in the community (Figure D4).

Relatively low O_2 contamination rates were found to favor propionate formation in lactate-based fermentation. However, the relationship between O_2 and propionate accumulation was not as straightforward as the inhibitory effect of O_2 on CE and methanogenesis. One possible reason is that propionate is not only a product of lactate fermentation, but also a substrate for *n*-valerate production by chain-elongating bacteria (Angenent et al., 2016). This could explain what was observed in the micro-aerobic period between days 115 to 119 in the STR-test, when propionate production did not increase but *n*-valerate production was relatively high (Table D1).

5.4.3. Key players that can profit from oxygen intrusion

Among the microorganisms enriched in the O_2 contamination periods, *Acidipropionibacterium* correlated to propionate production ($p<0.01$). Other Actinobacteria enriched during O_2 contamination did not correlate with propionate production and may have diverted electrons from lactate to products other than propionate, which could be another reason why STR-test showed lower propionate production rates (Table D1). *Actinomyces,* a facultative anaerobe (Rao et al., 2012), was particularly enriched in STR-test during an O_2 contamination period (Figure D4a). *Actinomyces* can grow anaerobically or aerobically on lactate and produces acetate, formate, and CO_2 during fermentative growth (Takahashi et al., 1994; Takahashi and Yamada, 1999; Rao et al., 2012). In agreement with the reported aerobic growth of *Actinomyces naeslundii* on lactate (Takahashi and Yamada, 1999), *Actinomyces* was likely not responsible for propionate production in the STR. The Coriobacteriia (*Eggerthellaceae*) observed in O_2 contamination periods belong to a family of strict anaerobes that are not reported to produce propionate (Gupta et al., 2013). *Proteiniphilum* (as well as *Dialister*) are genera with microaerophilic species that produce propionate, although it is not clear if from lactate (Tomazetto et al., 2018; Sakamoto et al., 2020). In this study, the abundance of *Proteiniphilum* correlated to O_2 contamination and to

propionate formation whereas no significant correlation was found between *Dialister*, propionate, and O_2 contamination (Figure 28).

Fermentation of lactate by propionate-producing bacteria commonly leads to a 2:1:1 stoichiometry of propionate to acetate to CO_2 (Equation 7). Gammaproteobacteria and Actinobacteria species that produce propionate are known to use methylmalonyl-CoA pathways rather than the acrylate pathway (Seeliger et al., 2002; Gonzalez-Garcia et al., 2017). In particular, *Acidipropionibacterium* spp. are among the most efficient propionate producers thanks to the highest energy efficiency of their methylmalonyl-CoA pathway (also known as Wood-Werkman cycle, a succinate pathway involving methylmalonyl-CoA:pyruvate transcarboxylase) (Scholz and Kilian, 2016; Gonzalez-Garcia et al., 2017).

$$3\ CH_3CHOHCOO^- \rightarrow 2\ CH_3CH_2COO^- + CH_3COO^- + CO_2 + H_2O \tag{7}$$

Even though it can express O_2-sensitive enzymes for fermentative growth similar to those in *Clostridium*, *Acidipropionibacterium* also has aerotolerant enzymes with similar functions (Piwowarek et al., 2018; McCubbin et al., 2020). Members of this genus are not only more tolerant to O_2 than clostridia, they have also been found to increase propionate and energy yields when exposed to O_2 (McCubbin et al., 2020).

It should be taken into account that propionibacteria, unlike many clostridia, do not form endospores (Gonzalez-Garcia et al., 2017). Hence, if exploration of propionate production is desired, shock treatments of the inoculum (e.g. with pH or heat), common techniques for starting non-methanogenic anaerobic bioprocesses (Table 1), should be avoided.

The phenomenon that lactate is diverted to propionate in chain elongation reactors under micro-aerobic conditions may have been overlooked in former studies. In one notable case, Kucek et al. (2016a) observed the competitive production of propionate in a lactate-based CE reactor. Although the possibility of O_2 contamination was not discussed, the study detected high abundances of *Acinetobacter*, strictly aerobic Gammaproteobacteria (Smet et al., 2014) commonly found in micro-aerated reactors (Krayzelova et al., 2015). To explain the propionate production observed in certain time periods, Kucek et al. (2016a) suggested the residual concentration of lactate in the reactor to be a determining factor. Although not discussed in the study, O_2 presence could have played a role in propionate production.

5.4.4. Possible roles of hydrogen during oxygen contamination

A common way for the reduction of O_2 in the presence of H_2 is shown in Equation 8 and is realized even by obligate anaerobes such as methanogens (Thauer et al., 2010), Negativicutes (Boga et al., 2007), and sulfate reducers (Dannenberg et al., 1992; Chen et al., 1993).

$$2H_2 + O_2 \rightarrow 2H_2O \tag{8}$$

H_2 consumption that was not attributed to methane formation was particularly high during O_2 contamination periods. In STR-test, it ranged from 3.0- to 3.4-fold molar O_2 consumption, while

in BCR-test it ranged from 1.1- to 3.6-fold. Considering the 2:1 ratio of H_2 to O_2 during H_2 oxidation (Equation 8), H_2 consumption not linked to methane formation in this study may have been related to other reactions during O_2 intrusion. Interestingly, similar consumption ratios of H_2 to O_2 (between 3.2 and 3.4) have been observed in communities dominated by hydrogen-oxidizing bacteria during autotrophic growth (Matassa et al., 2016). Nevertheless, we did not observe the presence of *Sulfuricurvum* (the genus enriched by Matassa et al. (2016)) and *Burkholderia*, a possible aerobic autotroph (Takors et al., 2018) found in our study, did not correlate positively with H_2 consumption nor with O_2 contamination. Besides, if aerobic hydrogen-oxidizing bacteria played a major role in the micro-aerobic reactors in our study, signs of biomass formation and carbon source (e.g. CO_2) consumption should have accompanied H_2 oxidation with O_2. However, no clear relation between O_2 contamination, biomass formation, and CO_2 consumption rates was found.

Communities enriched with propionate-producing bacteria in anaerobic reactors, such as *Acidipropionibacterium* spp., often correlate with high H_2 consumption or low H_2 production (Cabrol et al., 2017). In the presence of exogenous H_2, some propionate producers such as *Propionispira arboris* are able to perform homopropionate fermentation of lactate (Equation 9) producing neither CO_2 nor acetate (Thompson et al., 1984).

$$CH_3CHOHCOO^- + H_2 \rightarrow CH_3CH_2COO^- + H_2O \tag{9}$$

We did not observe *Propionispira* spp. in our reactors and its closest relative found in our system (*Dialister*) is only related at the order level (Veillonellales-Selenomonadales). Besides, Equation 9 alone cannot explain the high H_2 consumption during most of the micro-aerobic periods in this study. H_2 consumption not linked to methane was much higher than propionate formation. In fact, the period between days 39 and 50 of BCR-test had the lowest H_2 to O_2 consumption ratio and was the period with the highest propionate productivity (Table D1). Lastly, it is not clear if the correlation found between abundance of *Acidipropionibacterium* and H_2 consumption not linked to methane (Figure 28) is a direct one. H_2 consumption by isolated members of *Propionibacterium* is not observed during fermentative growth (Seeliger et al., 2002).

Homoacetogens consume H_2 and CO_2 (Reaction No. 1, Table 2) and, among them, at least *Cl. ljungdahlii* was shown to have some resistance against O_2 exposure (Whitham et al., 2015). Here, similar clostridia were detected in the reactors and *Clostridium* sensu stricto 12 was still present during some O_2 contamination events (Figure D4a and Figure D5b). Therefore, homoacetogenic activity could be considered to explain H_2 consumption during O_2 contamination. Nevertheless, no further evidence for this hypothesis was found. H_2 consumption was not accompanied by net CO_2 consumption and the net acetate production was unfavorable because acetate was fed in excess with the growth medium (12 g L^{-1} acetate) to favor chain elongation as an acetate-consuming reaction.

Another way that H_2 presence might have influenced the micro-aerated community is by amplifying the effects of O_2 contamination. The activation of O_2 into ROS by hydrogenases and reduced electron carriers might be accentuated by H_2 recirculation (Misra and Fridovich, 1971; Krab et al., 1982). Since we did not have a control reactor for the presence of H_2, we could not test this hypothesis.

5.5. Conclusion

Even small O_2 contaminations were detrimental to *n*-caproate and methane formation, but favored propionate formation. The relation of O_2 contamination and propionate formation was not straightforward: reactors with micro-aerobic conditions produced more propionate overall, but propionate production cycles were not always synchronous to O_2 contamination. Besides, the negative effects of O_2 on methane formation could be reversed in all cases whereas chain elongation could not always be resumed when O_2 contamination stopped. These patterns were observed in both STRs and BCRs, with the bubble column process being more sensitive to O_2 contamination. It is unclear whether the effects of O_2 reported in this study could be reproduced without the recirculation of H_2. It is possible that the H_2 recirculation amplified the effects of O_2 toxicity, since presence of H_2 can favor ROS formation by hydrogenases. Considering that H_2 consumption was particularly high during micro-aeration, H_2 may have acted as an important energy source for aerotolerant and aerobic microorganisms. Controlled O_2 contamination studies with co-cultures or mixed communities of lower complexity can shed light on how impactful H_2 recirculation during micro-aeration is.

Aerotolerant fermenting bacteria such as *Acidipropionibacterium* spp. are efficient propionate producers that could be regarded as welcomed guests rather than competitors. Here, they were the main candidates responsible for propionate production although their correlation with O_2 contamination was unclear. Instead, *Actinomyces* spp. (Actinobacteria that did not produce propionate) profited most from the micro-aerobic environment. Future experiments could help clarify if stable propionate-producing communities can be selected by micro-aeration. If micro-aeration facilitates propionate accumulation, a sequential anaerobic step can be used for chain elongation with high selectivity to odd-numbered MCCs. Studies with defined cultures aiming to understand what is behind the recovery of CE activity after micro-aerobic periods are also recommended.

A partial acclimatization of methanogens to ethylene was observed in this chapter. This led to low homoacetogenic activity and misrouting of most of the electrons from H_2 to CH_4, adding weight to the importance of co-feeding CO together with H_2/CO_2 to stimulate autotrophic activity. Considering the findings in Chapter 3 (<u>Section 3.3.4</u>), in which CO and ethylene had a synergistic effect when inhibiting methanogens in serum bottles, the next step was to operate the gas recirculation reactors with H_2, CO_2, CO, and ethylene in order to advance the attempts of merging the carboxylate and syngas platforms.

6. The microbial community behind efficient mixotrophic chain elongation

This chapter is based on the submitted manuscript:

Mixotrophic chain elongation with syngas and lactate as electron donors

Flávio C. F. Baleeiro, Jana Raab, Sabine Kleinsteuber, Anke Neumann, Heike Sträuber (2022)

manuscript submitted for publication

Author contributions

Flávio C. F. Baleeiro: conceptualization, methodology, investigation, data analysis, visualization, first draft, and manuscript revision.

Jana Raab: investigation and data analysis.

Sabine Kleinsteuber, Anke Neumann, and Heike Sträuber: conceptualization, project supervision, data analysis support, and manuscript revision.

6.1. Introduction

In this chapter, CO is used during the enrichment of a microbial community in an open system for the first time. The gas recirculation system was used to develop a mixotrophic CE process with a microbial community growing on syngas (H_2, CO_2, and CO) and organic substrates (lactate and acetate). This way, we aimed to understand the dynamics of the mixotrophic community and to identify its key players during its adaptation and stable phases in long term operation with a more realistic syngas mixture.

6.2. Experimental procedures

6.2.1. Bioreactor operation

Two identical Minifors reactors (INFORS AG, Switzerland) with a working volume of 1.0 L each and equipped with gas recirculation systems were operated inside a fume cupboard. Each reactor had a peristaltic pump (model 323, Watson Marlow Ltd, UK) operating continuously to recirculate a syngas mixture (32% H_2, 32% CO, 16% CO_2, and 20% N_2) from its gas reservoir to the broth via microspargers at a rate of 40 mL min^{-1}. Reactor 1 and Reactor 2 were operated at 32ºC and a pH value of 6.0 ± 0.1. Details of the system, the materials, the gas reservoir replenishment, the measures to inhibit methanogens, and how carbon fixation was determined can be found in the Supporting Information. An illustrative scheme and balance calculations were provided previously (Figure 21 and Appendix C.2).

The growth medium was formulated to be a feedstock model for chain elongation. It contained 133 mM lactate (12 g L^{-1}) as organic electron donor and 200 mM acetate (12 g L^{-1}) as organic electron acceptor. The complete composition of the growth medium is shown in Table E1. A description of the preparation, handling, and storage of the medium is available in Appendix E.2.

At start-up, each reactor was inoculated with a different microbial community. Reactor 1 received 50 vol% sludge from a mesophilic biogas reactor and 50 vol% lactate-free growth medium with 400 mM acetate. Before being used, the sludge was stored overnight for sedimentation to reduce the amount of solids added with the inoculum. Reactor 2 received 100 vol% broth of an enrichment culture able to produce ca. 4 g L^{-1} *n*-caproate from H_2/CO_2, lactate, and acetate under similar conditions (see STR-control, Section 5.3.1). Additional details on the origin and conditions of the inocula are available in Appendix E.3.

In total, the two reactors were operated for 292 days with the first 61 days being used to compare the two different communities. On day 61, the enriched community of Reactor 2 was discarded and the diverse community from Reactor 1 was distributed to both reactors to continue the experiments comparing three operational parameters in succession (Figure E1). From day 110 to 148, different feeding intervals (1 *vs.* 4 d) were compared, from day 181 to 261, the effect of acetate in the feed was investigated (200 mM acetate *vs.* acetate-free medium), and from day 272 to 292, different HRT values were compared (14 *vs.* 10 d). Each comparison phase was preceded by a stabilization period for both reactors, which was sufficient to reach a similar

state in terms of carboxylate concentration. Average production or consumption rates were calculated for the comparison phases only and are specific to the useful reactor volume (1.0 L).

6.2.2. Chemical analyses

To analyze the carboxylates and alcohols in each reactor, about 1.5 mL of broth was collected three times a week before feeding. Exceptionally, Reactor 1 was sampled on day 42 every 2-3 hours over one feeding cycle. HPLC-RID was used to quantify the concentrations of carboxylates and alcohols, while carboxylates were redundantly quantified via HPLC-UV at a wavelength of 280 nm. Gas samples were collected with every liquid sampling and always before and after the replenishment of the gas reservoir. GC-TCD was used to monitor the composition of gases. Details of the sample preparation procedures and configuration of the HPLC and GC systems have been described in Chapter 3 (Section 3.2.4). Biomass concentration was monitored via OD600 assuming 0.456 $g_{dry\ mass}$ L^{-1} per OD600 unit (Section 2.2.4). Conversion factors used for carbon and electron balances are presented in Table A2.

6.2.3. Microbial community analysis

About 6.0 mL of broth was collected from each reactor twice per week, always before feeding the reactors, to monitor the microbial community composition. Amplicons of the V3-V4 region of the 16S rRNA gene were sequenced using the Illumina MiSeq platform. Details of the wet-lab protocols such as DNA extraction, primers, and PCR conditions were described by Logroño et al. (2020). Information on the library preparation was described in Chapter 2 (Section 2.2.3). All samples were rarified to an equal depth of 31,892 read counts, which corresponded to the number of reads in the sample with the lowest read number. The raw, adapter-free sequence data for this study was deposited at the ENA under the study accession PRJEB52337 (http://www.ebi.ac.uk/ena/data/view/PRJEB52337). Details on the clustering technique used in this study are given in Appendix E.4.

6.3. Results and discussion

6.3.1. Start-up with different microbial communities

For the start-up, the two reactors were operated with an HRT of 14 d and fed with a mineral medium containing 200 mM acetate and 133 mM lactate once a day. Reactor 1 received an inoculum with a diverse community (richness of 392 ASVs), while Reactor 2 received an inoculum with an enriched community (26 ASVs). The composition of the inocula is shown in Figure E2.
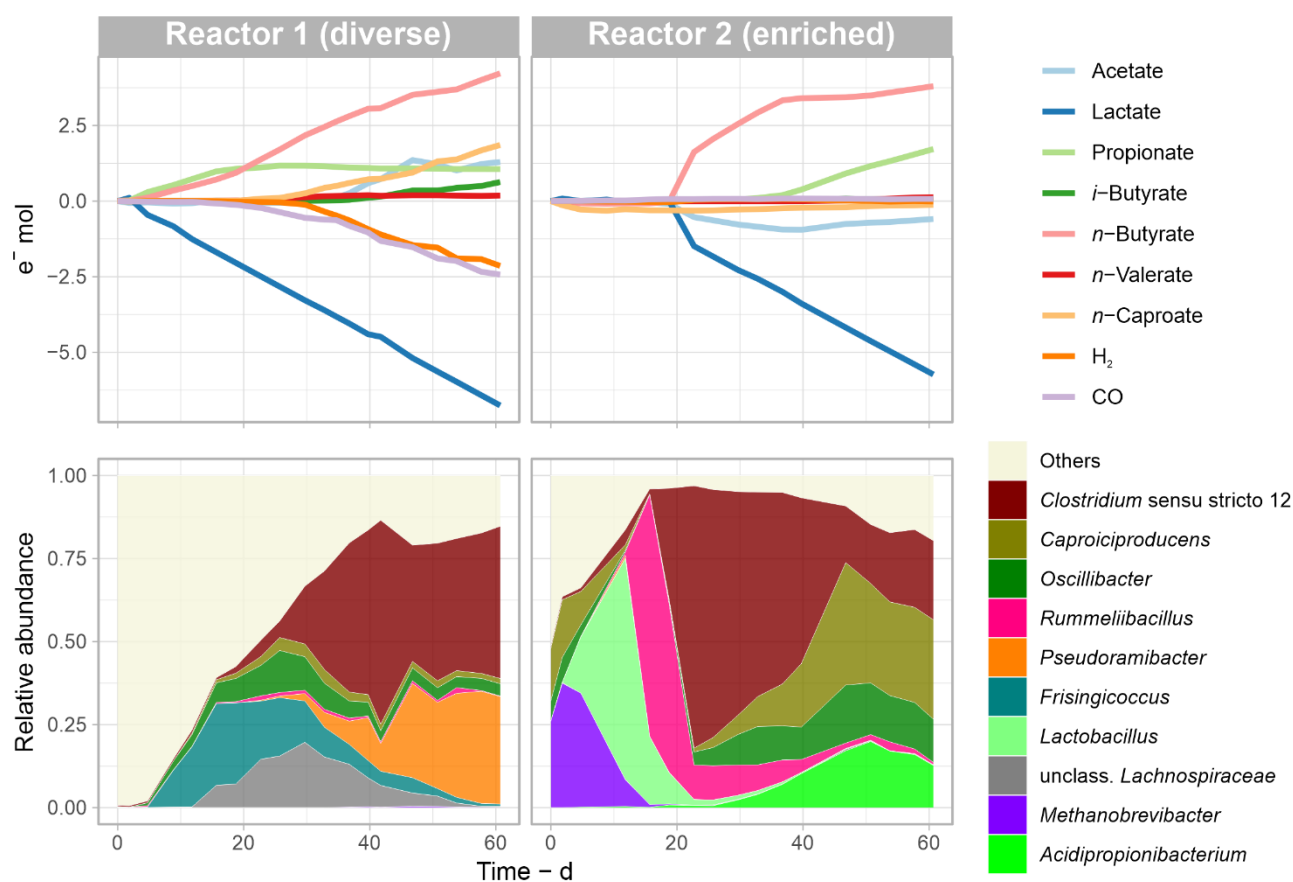
Figure 29. Cumulative electron profiles of chemicals and community composition at the genus level during the first 61 days of fermentation. A diverse community (Reactor 1) and an enriched community (Reactor 2) were compared. The ten most abundant genera during the period are shown.

The diverse community in Reactor 1 had a short lag phase of two days, after which lactate consumption started concomitantly with production of propionate and *n*-butyrate, as shown in Figure 29. Propionate production halted on day 16, enabling more *n*-butyrate to be formed. Gas consumption started on day 19, initially due to CO consumption, and accelerated after day 30 with simultaneous consumption of H_2 and CO. Also on day 30, *n*-caproate production started, coinciding with increasing relative abundances of *Clostridium* sensu stricto 12 and *Pseudoramibacter*. On day 33, in addition to the 12 g L^{-1} acetate already present in the feed, more acetate was produced concurrently with the consumption of H_2 and CO. Kinetic sampling over a feeding cycle of Reactor 1 revealed that all lactate was consumed within the first 8 h while H_2 and CO continued to be consumed during the whole 24-h cycle (Figure E3). Accumulation of acetate stopped suddenly on day 47, after reaching a peak of 19 g L^{-1} (Figure E4).

In Reactor 2, 19 days passed before the enriched community adapted to CO and started producing carboxylates (Figure 29). During the first days, the lack of microbial activity left the system in a relatively oxidized state (ORP of -112 mV), giving the broth the characteristic pink color of oxidized resazurin. Consequently, the period between days 2 and 19 presented very low biomass concentrations (OD600 of 0.07) and high relative abundances of facultative anaerobes *Lactobacillus* and *Rummeliibacillus* (Figure 29). On day 19, consumption of lactate and acetate

and concomitant formation of *n*-butyrate started. On day 37, *n*-butyrate production slowed down and was replaced by propionate formation, most probably by *Acidipropionibacterium*, resulting in a propionate-to-acetate ratio of 2:1.

Despite the high relative abundance of *Caproiciproducens* in the enriched community, *n*-caproate was not produced during the first 61 days operation of Reactor 2. Further, no consumption of CO or H_2 was observed despite the high relative abundance of *Clostridium* sensu stricto 12, a genus that harbors many homoacetogens. These observations are discussed below in Section 6.3.5 (Clostridial community dynamics).

6.3.2. Effect of changing operating conditions on process performance

The better performing diverse community was transferred to both reactors on day 61. In the following days (61 – 148 d), the community was given time to stabilize and the feeding interval was increased from 1 to 4 d in Reactor 1 (Figure E1). Increasing the feed interval had minimal impact on carboxylate production and community composition (see Appendix E.5 and Figure E5). In fact, the observed community dynamics emerged due to the routine reactor operation rather than the change in feeding regime. Remarkably, cyclic dynamics of *Clostridium* and *Eubacterium* were observed for the first time and persisted until the end of reactor operation. These dynamics are examined in more detail below.

Ceasing the acetate supply of Reactor 2 (181 – 261 d) and afterwards decreasing its HRT (272 – 292 d) had substantial effects on the production of carboxylates but not on the community structure at genus level (Figure E6). H_2+CO consumption and carbon fixation rates were 2.5- and 3.7-fold higher, respectively, once acetate supply ceased in Reactor 2 in comparison to Reactor 1, which remained being fed with 200 mM acetate (Figure E7a). On the other hand, production of elongated carboxylates (C≥4) was 25% lower when no acetate was fed. A decrease in HRT from 14 to 10 d caused an equivalent increase in production rates of carboxylates, when comparing Reactors 1 and 2 (Figure E7). Disregarding the operation with the enriched community, average carbon fixation rate was between 2.0 and 31.0 C mmol L^{-1} d^{-1} (0.088 and 1.4 g CO_2 equivalents L^{-1} d^{-1}, respectively), with the most favorable period seen in Reactor 1 while operating at an HRT of 14 d without acetate supply (Figure E7b). For perspective, these volumetric carbon fixation rates are comparable to rates of state-of-the-art microalgal reactors (Yahya et al., 2020). However, the carbon fixation reported here was due to CO consumption (Figure E7b).

6.3.3. Cyclic dynamics of community members

Although both reactors achieved a stable community composition and chemical output by day 148 d, relative abundances of *Clostridium* sensu stricto 12 and *Eubacterium* kept cycling oppositely (Figure E6). We observed that at higher CO partial pressures, relative abundances of *Clostridium* sensu stricto 12 increased, whereas *Eubacterium*, *Oscillibacter*, and *Colidextribacter* were more abundant during lower CO partial pressures (Figure 30). Moreover, *n*-caproate and

i-butyrate varied similarly, but *n*-butyrate varied in the opposite direction. Peaks of *n*-caproate did not always coincide with lower or higher partial pressures of CO, hence potential CO inhibition on chain elongation did not seem to be a major concern. Drops in *n*-butyrate concentration (and simultaneous increases in *n*-caproate concentration) frequently coincided with increasing relative abundances of *Clostridium* sensu stricto 12, although exceptions were also found.
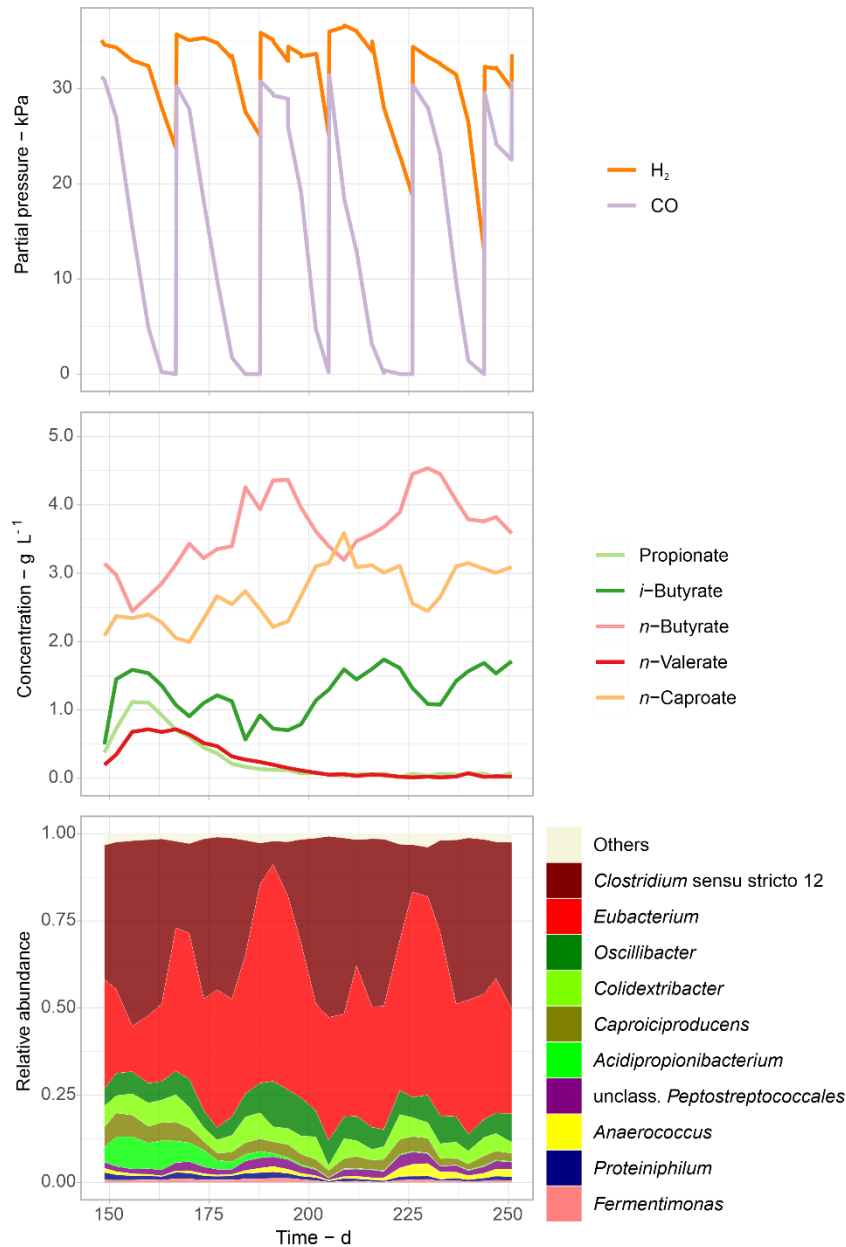
Figure 30. Cyclic dynamics of gas partial pressures, concentrations of carboxylates, and community composition over the longest period with constant operating conditions (Reactor 1, 148 – 250 d). The ten most abundant genera are shown.

6.3.4. Functional role of community members
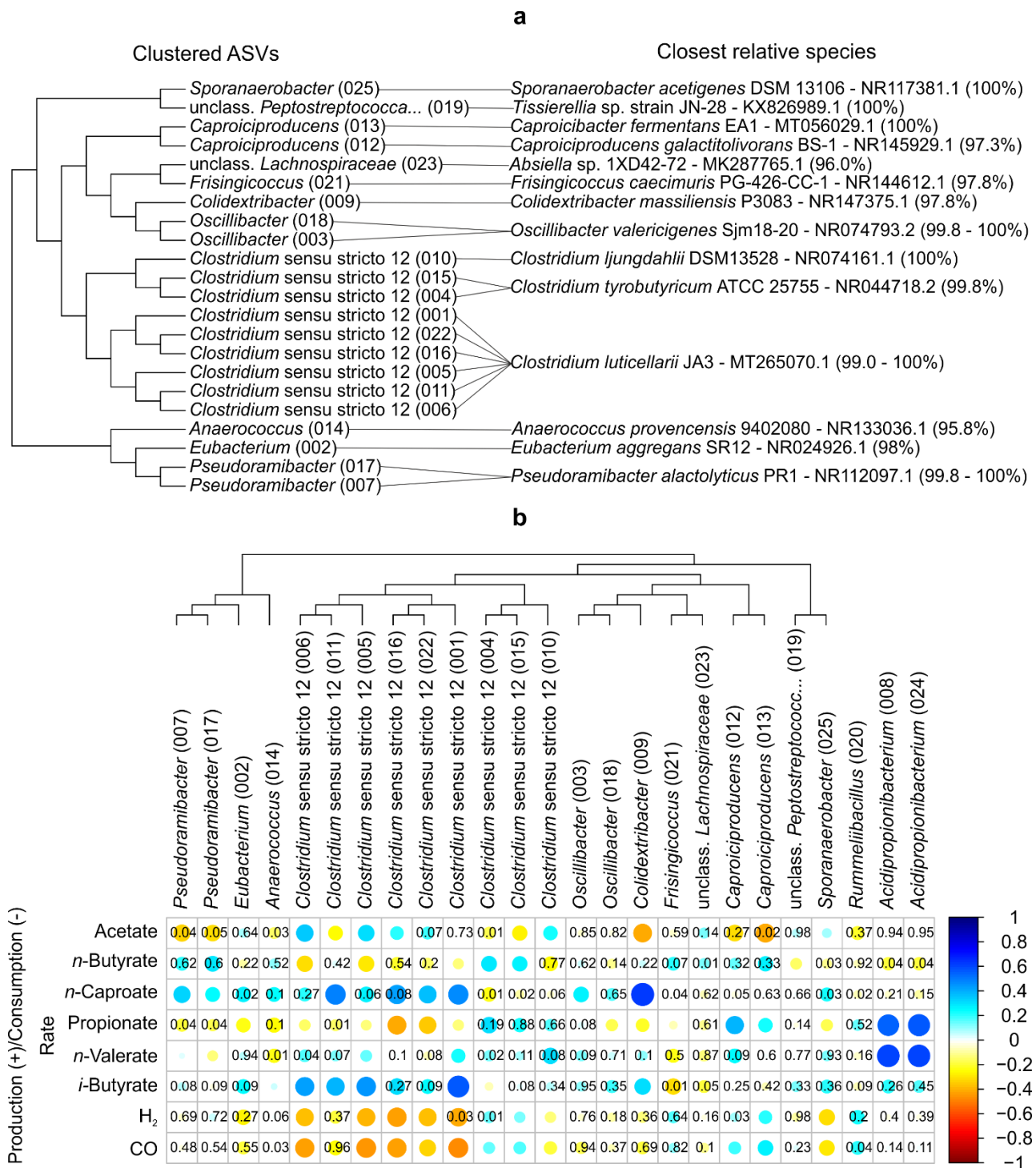
Figure 31. Clustering of the most abundant clostridial ASVs with the ASV number in parentheses (left) and their closest cultured relatives with BLAST identities in parenthesis (right) (**a**) and Spearman correlations between the 25 most abundant ASVs in the study and the production (+) or consumption (-) rates of chemicals (**b**). The p-values are omitted for significant correlations (p<0.01) and shown for correlations with p≥0.01.

Analyzing the community at the genus level limits the opportunities to deduce potential metabolic functions of community members. In this aspect, the genera *Eubacterium* and

Clostridium sensu stricto 12 are problematic since they harbor species with very distinct metabolic traits (Kalia et al., 2011; Wade, 2015). To improve the resolution of our community analysis, we performed a cluster analysis of the clostridial ASVs among the 25 most abundant ASVs and did a blastn search of these sequences in the NCBI database of 16S ribosomal RNA sequences to find the closest relative cultured species of each. The results are shown in Figure 31a. Additionally, Spearman correlations between relative abundance of the top 25 ASVs and production or consumption rates of the main carboxylates and gases are shown in Figure 31b.

Clostridium sensu stricto 12 contained nine abundant ASVs that had at least 99% similarity to *Cl. tyrobutyricum*, *Cl. ljungdahlii*, or *Cl. luticellarii* (Figure 31a). ASVs 004 and 015 were related to *Cl. tyrobutyricum*, which is a known heterotroph that can consume sugars, lactate, and acetate producing butyrate and H_2 at pH 6.0 (Zhu and Yang, 2004; Fu et al., 2021). Here, these two ASVs correlated with *n*-butyrate and H_2 production (Figure 31b). ASV 010 was a close relative of *Cl. ljungdahlii* (and consequently of its relatives: *Cl. ragsdalei*, *Cl. coskatii*, and *Cl. autoethanogenum*) (Figure 31a), which is mainly known for its autotrophic metabolism able to convert H_2, CO_2, and CO into acetate and ethanol (Bengelsdorf et al., 2018). This ASV correlated significantly (p<0.01) to homoacetogenic features, i.e. H_2 and CO consumption and acetate formation (Figure 31b).

The remaining six *Clostridium* sensu stricto 12 ASVs (ASVs 001, 005, 006, 011, 016, and 022) were related to *Cl. luticellarii* JA3. The type strain *Cl. luticellarii* FW431 has been reported to grow on methanol, H_2/CO_2, or lactate while producing a mixture of carboxylates ranging from acetate to *n*-caproate (Petrognani et al., 2020). Strain JA3 was recently isolated using a *Clostridium* growth medium with glucose and H_2/CO_2 (Xu et al., 2020). It has a relatively low 16S rRNA (whole gene) similarity of 97.05% to the type strain and has been designated as a possible new species (Xu et al., 2020). In our dataset, all *Cl. luticellarii* ASVs presented similar correlations (Figure 31b). Most of them showed significant (p<0.01) correlations with H_2 and CO consumption and with *i*-butyrate and *n*-caproate production indicating that these relatives of *Cl. luticellarii* acted as mixotrophic chain elongators in our reactor microbiome, in contrast to the common assumption of interspecies ethanol transfer during gas-to-*n*-caproate formation (Angenent et al., 2016). No information could be found in the literature on a possible carboxydotrophic metabolism (i.e. growth on CO) of *Cl. luticellarii*. Yet, *Cl. luticellarii* has all genes required for the Wood-Ljungdahl pathway (Poehlein et al., 2018), so carboxydotrophic metabolism is conceivable as suggested by the correlations with CO consumption found here.

Eubacterium was represented by a single ASV (ASV 002) with 98% similarity to *E. aggregans* and to *E. barkeri,* which have identical V3-V4 16S rRNA regions. *E. aggregans* and *E. barkeri* are *Eubacterium* sensu stricto that produce acetate and *n*-butyrate from lactate (Stadtman et al., 1972; Wade, 2015). *E. aggregans* has previously been exploited for its ability to grow on H_2/CO_2 producing acetate and *n*-butyrate, similar to *E. limosum* (Groher and Weuster-Botz, 2016). The *E. aggregans* strain isolated by Mechichi et al. (1998) does not grow on CO and no autotrophic metabolism was reported for *E. barkeri* (Stadtman et al., 1972). When it comes to CO

consumption, acetogenic *Clostridium* sensu stricto 12 species have higher growth rates than acetogenic *Eubacterium* species (Kang et al., 2020). Therefore, we assume that *Eubacterium* ASV 002 was specialized in H_2 and lactate consumption in our reactors and could only outcompete *Cl. luticellarii* relatives during periods of low CO partial pressure ([Figure 30](#)). Even though increasing relative abundances of ASV 002 coincided with decreasing H_2 partial pressure ([Figure 30](#)), this ASV did not correlate significantly with gas consumption. However, it did correlate with *n*-caproate formation (p=0.02) ([Figure 31b](#)). Hence, the lack of significant correlation of ASV 002 to gas consumption could be due to faster gas consumption rates of *Cl. luticellarii* relatives overshadowing activities of *Eubacterium*, similarly to what we observed previously between *Methanobacterium* and *Clostridium* ([Section 2.4.3](#)).

ASVs 007, 012, 013, and 017 were related to known heterotrophic chain elongators ([Figure 31a](#)): *Caproicibacter fermentans* (similar to ASV 013) produces *n*-caproate from lactate (Esquivel-Elizondo et al., 2020), while *Pseudoramibacter alactolyticus* (ASVs 007 and 017) and *Caproiciproducens galactitolivorans* (ASV 012) use sugars as electron donors for *n*-caproate production (Kim et al., 2015; Willems and Collins, 2015). Since lactate was the only organic electron donor in our study, the two ASVs related to *P. alactolyticus* and ASV 012 (related to *Ca. galactitolivorans*) might belong to yet uncultured species. In recent studies, *Pseudoramibacter* was among the main suspects of lactate-based chain elongation (Crognale et al., 2021; Fortney et al., 2021). Besides, *Candidatus* Pseudoramibacter fermentans is an uncultured species identified by multi-omics analysis suspected to produce *n*-caproate from lactate (Scarborough et al., 2020). Our correlation analysis showed no connection between the *Caproiciproducens* relatives and *n*-caproate formation, while both *Pseudoramibacter* relatives showed significant correlations ([Figure 31b](#)). Inhibition of *n*-caproate formation by *Caproiciproducens* spp. due to CO was observed previously ([Section 3.3.3](#)), but no studies with *Pseudoramibacter* and CO were found.

Oscillibacter (ASVs 003 and 018), *Colidextribacter* (ASV 009), and *Sporanaerobacter* (ASV 025) are genera often found to be abundant in communities producing medium-chain carboxylates (Liu et al., 2017; Zagrodnik et al., 2020; Joshi et al., 2021). Only few isolates of these genera have been characterized. *Oscillibacter valericigenes*, *Colidextribacter massiliensis*, and *Sporanaerobacter acetigenes* are heterotrophs that produce short-chain carboxylates via sugar fermentation (Hernandez-Eugenio, 2002; Katano et al., 2012; Ricaboni et al., 2017), with *O. valericigenes* being described additionally as an *n*-valerate producer. *Oscillibacter* isolates growing autotrophically on H_2/CO_2 or CO and producing *i*-valerate have been reported (Park et al., 2013a; Park et al., 2013b). Here, *Oscillibacter* and *Colidextribacter* correlated to *n*-caproate formation and not to gas consumption ([Figure 31b](#)), suggesting a heterotrophic chain elongation metabolism. On the other hand, the *Sporanaerobacter* ASV correlated significantly (p<0.01) with homoacetogenic activity.

Other clostridial ASVs had either low similarity to their closest cultured relatives (i.e. ASVs 014 and 023, related to *Anaerococcus provenciensis* 9402080 and *Absiella* sp. 1XD42-72, respectively) or limited literature information on their metabolism (concerning ASVs 019 and 021, related to *Tissierellia* sp. JN-28 and *Frisingicoccus caecimuris* PG-426-CC-1, respectively). Their roles in the community remained elusive as they presented few significant correlations (Figure 31b).

Expectedly, *Acidipropionibacterium* spp. correlated with propionate formation. What was less expected, however, was the correlation of propionate formation with *Caproiciproducens* spp. (Figure 31b). The *Caproiciproducens* spp. isolated so far were not found to produce propionate (Flaiz et al., 2020). *Caproiciproducens* spp. and *Acidipropionibacterium* spp. often co-occur (as seen in Section 5.3.2 and in Kim et al. (2022)) since they compete for similar ecological niches in lactate consumption. Here, the abundances of both genera peaked at about the same time in different experiments (see Figure E5 and Reactor 2 in Figure 29). Therefore, the correlation between *Caproiciproducens* and propionate formation was probably indirect due to the frequent co-occurrence of *Caproiciproducens* and *Acidipropionibacterium*. Another likely indirect correlation seen in Figure 31b is between *Acidipropionibacterium* spp. and *n*-valerate production. *n*-Valerate is a common chain elongation product from propionate and its production is, hence, enhanced by increased propionate production.

6.3.5. Clostridial community dynamics

Figure 32 illustrates the community composition over the whole experimental time by grouping the most abundant clostridial ASVs according to their closest relative species. The composition of *Clostridium* sensu stricto 12 below the genus level was fundamentally different in the two reactors during the start-up period (until 61 d). *Cl. luticellarii* relatives were abundant in the diverse community of Reactor 1, whereas relatives of *Cl. tyrobutyricum* predominated in the enriched community of Reactor 2. This difference helps explain the absence of autotrophic and chain elongation activities in Reactor 2 during this period (Figure 29). After the diverse community was distributed to both reactors on day 61, *Cl. tyrobutyricum*, *P. alactolyticus*, and *Ca. fermentans* were outcompeted by *Cl. luticellarii*.
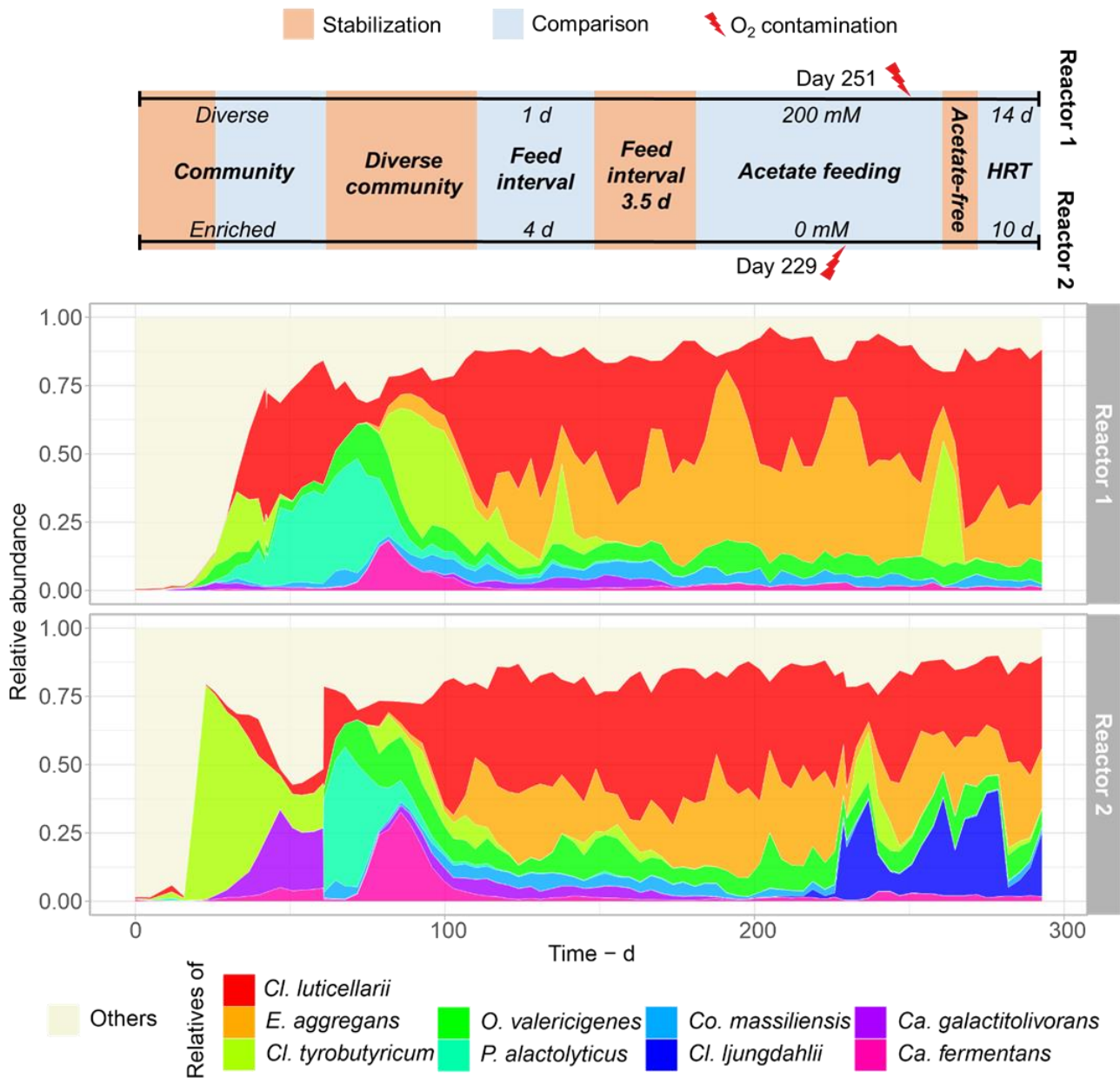
Figure 32. Dynamics of the ten most abundant clostridial species over the whole reactor experiment. "Others" groups all ASVs not assigned to any of these species. The timeline represents the experimental phases in both reactors.

Different dynamics were observed after we changed the operating conditions. After day 181, acetate supply in Reactor 2 was stopped, causing acetate to be washed out of the broth from a concentration of 10.5 to 3.2 g L^{-1} (Figure E6). Initially, the lower acetate concentration did not have a strong effect on the community composition in Reactor 2, but an unintentional air contamination on day 229 triggered an abrupt increase in the abundances of *Cl. tyrobutyricum* and *Cl. ljungdahlii* at the cost of *Cl. luticellarii* and *E. aggregans* (Figure 32). *Clostridium* species not related to *n*-caproate production, such as *Cl. ljungdahlii* and *Cl. tyrobutyricum*, were shown to be resistant to low levels of oxygen contamination (Section 5.4.4). Moreover, *Cl. ljungdahlii* is known for some degree of oxygen tolerance (Whitham et al., 2015). The presence of *Cl. tyrobutyricum* was transient but *Cl. ljungdahlii* remained in Reactor 2 after day 229 until the end

of the experiment, coinciding with acetate accumulation again up to 9.4 g L^{-1} on day 272 (Figure E6). The lower acetate concentration in Reactor 2 may have given *Cl. ljungdahlii* the opportunity to establish in the community by occupying the niche of acetate production from H$_2$, CO$_2$, and CO. Coincidently, Reactor 1 suffered from a similar oxygen shock a few days later (day 251) while having a relatively high acetate concentration of 11.5 g L^{-1} (Figure E6). In this case, the transient abundance of *Cl. tyrobutyricum* ASVs occurred without the increase of *Cl. ljungdahlii* abundance (Figure 32), reinforcing our assumption that the low acetate concentration in Reactor 2 was the cause of the new community structure.

6.3.6. Mixotrophic efficiency
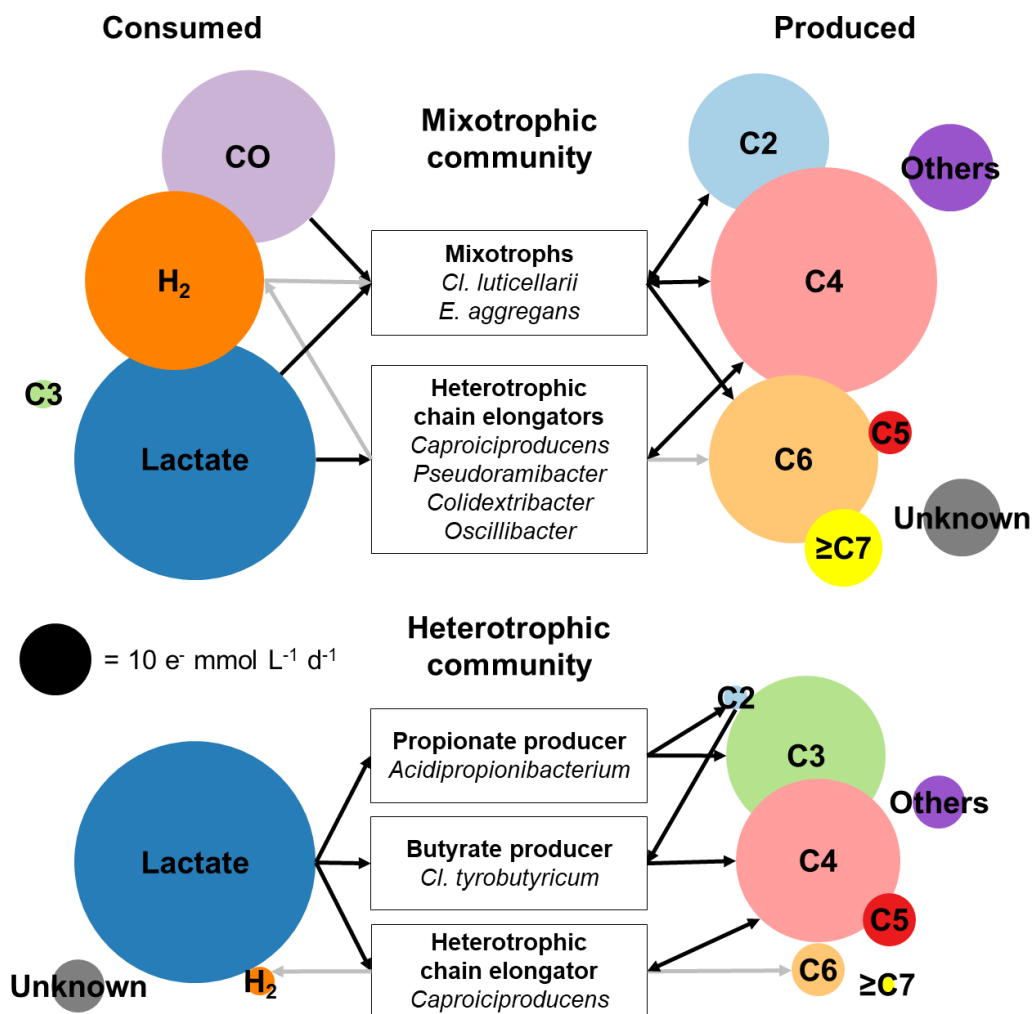
Figure 33. Electron balances in Reactor 1 with the mixotrophic community and Reactor 2 with the heterotrophic community in the period 26 - 61 d. Levels of production and consumption rates are proportional to the circular areas. Community members with their putative metabolic function are indicated. Black arrows indicate main fermentation routes while gray arrows indicate pathways that were inhibited by CO. C2: acetate and ethanol; C3: propionate and *n*-propanol; C4: *n*-butyrate, *i*-butyrate, and *n*-butanol; C5: *n*-valerate, *i*-valerate, and *n*-pentanol; C6: *n*-caproate, *i*-caproate, and *n*-hexanol; ≥C7: *n*-heptanoate and *n*-caprylate; Others: biomass, formate, CH$_4$, and electron losses due to O$_2$ contamination; "Unknown" is the difference between the electrons in the consumed and produced pools.

The time window between days 26 and 61 ([Figure 29](#)) gave an opportunity to compare a mixotrophic and a heterotrophic community since the enriched community in Reactor 2 consumed virtually no gas. [Figure 33](#) illustrates the electron balances for this period together with putative functions of the most abundant bacterial taxa based on our analyses.

Both communities consumed the same amount of lactate (112 e$^-$ mmol L^{-1} d^{-1}), however, the mixotrophic community consumed twice as much EDs since it additionally consumed 119 e$^-$ mmol L^{-1} d^{-1}, which came in approximately equal shares from H$_2$ and CO ([Figure 33](#)). The doubling of ED consumption by the mixotrophic community was reflected by 82% higher production of C2-C8 carboxylates (except lactate) and alcohols, compared to the purely heterotrophic community. The increased consumption did not only enhance the production of acetate (C2), which is a trivial product of syngas fermentation. In fact, the increase in the production of compounds with chains longer than C2 (i.e. C3-C8) due to H$_2$ and CO consumption was 50%.

The mixotrophic community produced eleven times more medium-chain carboxylates and alcohols (i.e. C6-C8 compounds) than the heterotrophic community (66.6 and 5.7 e$^-$ mmol L^{-1} d^{-1}, respectively). Still, this specific comparison should not be extrapolated to all chain elongation communities. The heterotrophic community in Reactor 2 grew in the presence of CO, which is an inhibitor of some chain elongating bacteria such as *Cl. kluyveri* (Diender et al., 2016) and *Caproiciproducens* ([Figure 16](#)).

Another atypical aspect of the fermentation in Reactor 2 was that the production of *n*-butyrate and *n*-caproate was not accompanied by H$_2$ evolution. This was likely due to the presence of CO, which inhibits hydrogenases used by acetogens for H$_2$ formation (Menon and Ragsdale, 1996). The heterotrophic community even showed a minor H$_2$ consumption (2 e$^-$ mmol L^{-1} d^{-1}), which might have been caused by scarcely abundant *Cl. luticellarii* relatives ([Figure 33](#)). When not inhibited by CO, heterotrophic lactate-based chain elongation communities route a considerable share of electrons to H$_2$ (Brodowski et al., 2021) yielding less carboxylates. In principle, H$_2$ can be an interesting by-product of anaerobic fermentation. In practice, however, H$_2$ is readily consumed by methanogens in open cultures (Cabrol et al., 2017) and its separation is challenging at typical concentrations in the headspace of a fermenter (Levin and Chahine, 2010).

We did not observe strong solventogenic activity and the concentration of alcohols remained below 1 g L^{-1} throughout the study. Nevertheless, some *n*-butanol and *n*-hexanol was produced by the mixotrophic community (9.4 and 5.2 e$^-$ mmol L^{-1} d^{-1}, respectively) accounting for ca. 10% of the electron pools of C4 and C6 compounds, respectively. Conversely, alcohol production by the heterotrophic community was negligible. Yet, when alcohol production is the main goal, other bioreactor operation strategies should be taken into account (He et al., 2021) or a chemical conversion route from carboxylates should be considered (Holtzapple et al., 2022).

6.4. Conclusion

The use of microbial communities capable of simultaneously consuming organic substrates, H_2, CO_2, and CO is a promising way to make anaerobic fermentation more feasible. By producing more MCCs from a fixed amount of organic substrate, mixotrophic chain elongation alleviates one of the main limitations of fermentation technology, namely the dependence on the cost, quality, and availability of the organic feedstock. Relatives of *Cl. luticellarii* and *E. aggregans* composed the core of the mixotrophic community and competed for lactate while producing *n*-caproate. The relative abundances of these bacteria were influenced by the CO partial pressure: *Cl. luticellarii* consumed CO, whereas *E. aggregans* did not. Bacteria with pure heterotrophic metabolism (*Pseudoramibacter*, *Caproiciproducens*, *Colidextribacter*, *Oscillibacter*, *Cl. tyrobutyricum*, and *Acidipropionibacterium*) had either a transient dominance or low abundances in the reactor. High acetate concentrations (ca. 11 g L^{-1}) were important to maintain the dominance of mixotrophs but also slowed down carbon fixation. When acetate supply stopped, the production of elongated carboxylates (C≥4) deteriorated and a relative of *Cl. ljungdahlii* seized the opportunity left by lower acetate concentrations and grew autotrophically on syngas, thereby replenishing acetate. To better assess the potential of mixotrophic chain elongation, we recommend applying the concept with real organic feedstocks. Future experiments using additional high-resolution community analyses such as metagenomics or proteomics could unravel the intricate microbial interactions and explain other phenomena we observed, such as the transient dominance of *Pseudoramibacter* or the roles of less abundant community members.

7. Final conclusions and outlook

In this work, simultaneous fermentation of organic and inorganic substrates was used to produce a spectrum of monocarboxylates with two to eight carbon atoms. This one-pot strategy uses microbial communities as self-regenerating biocatalysts to merge two chemical platforms, each possessing complementary limitations and strengths. The community structure under simultaneous availability of organic substrates and H_2, CO_2, and CO (syngas) was analyzed in parallel to chemical balances. The lessons learned from the closed-system experiments were used to iteratively design and operate a reactor system that enriches mixotrophic communities with a stable output of carboxylates.

The basic aspects of co-fermenting H_2/CO_2 and $H_2/CO_2/CO$ were firstly explored in closed systems under several conditions. The highest *n*-caproate production was achieved using a diverse community as inoculum with both H_2, lactate, and ethanol being used as electron donors. Higher electron acceptor availability (acetate), slightly acidic pH, and a constant high H_2 partial pressure proved to be favorable conditions for MCC production. Hydrogenotrophic methanogenesis was identified as a major competing pathway. Due to the need of keeping high partial pressures of H_2 and CO_2, conventional measures to inhibit methanogenesis were not sufficient. Misrouting of H_2 to CH_4 could only be tackled by using chemical inhibitors such as 2-BES or ethylene. CO partial pressure was a decisive factor defining the performance of the fermentation as a whole. Higher CO partial pressures sustained acetogenic activity, carbon fixation, and carboxylate production at the cost of lower selectivity to MCCs. In closed systems, CE and methanogenesis were inhibited by CO despite the use of a community pre-adapted to syngas. In comparison to the communities enriched with a feedstock model, fermentation of complex biomass meant that hydrolytic bacteria (e.g., *Bacteroides* and LAB) were very abundant. Except for a slight slowdown in biomass degradation rates caused by H_2 and CO, hydrolytic bacteria remained largely unaffected by the gas mixture used.

The observation that formate presence could help bypass the inhibiting effects of CO on elongated (C≥4) carboxylate production was a novel one. When co-fermenting plant biomass and syngas, addition of 5 g L^{-1} formate to cultures fed with CO was enough to achieve *n*-butyrate and *n*-caproate concentrations similar to a H_2/CO_2 headspace. Natural formate accumulation (by LAB and acetogens) was erratic and often did not achieve the concentrations necessary to overcome CO inhibition. Procuring lab-grade formic acid to a fermenter makes little economic sense but formate-induced CO tolerance might be a useful tool when formate and CO occur together, such as in C1-based bioprocesses and bioelectrochemical systems.

The first pair of semi-continuous reactors with gas recirculation was assembled and operated with H_2/CO_2 and lactate/acetate for 84 days. In one reactor, partial pressures of H_2 were kept constantly high by using ethylene to inhibit methanogenesis. As a result, H_2 accounted for 17% of the whole electron donor consumption and was used for the production of short- and

medium-chain carboxylates in this reactor. The operating costs of continuously recirculating H_2/CO_2/ethylene per m^3 of broth were estimated to be about two orders of magnitude lower than the value of the carboxylates present in the broth. This is the first sign that gas recirculation can be an economically feasible strategy to inhibit methanogens and increase carboxylate production of anaerobic fermentation. On the other hand, use of the most popular methanogenic inhibitor (2-BES) is too expensive at the necessary concentrations.

The gas recirculation systems allowed to indirectly track O_2 intrusion. This offered novel insights on the effect of small air contaminations since it is impractical to directly measure O_2 in anaerobic fermenters. By running stirred-tank and bubble column reactors with H_2/CO_2/ethylene recirculation for over 110 days, two new long-term operational challenges could be identified: the detrimental effect of air intrusion on *n*-caproate production and the acclimatization of methanogens to ethylene. While O_2 was counterproductive to the carboxylate CE, it favored propionic acid bacteria opening a window of opportunity to steer product pool from even- to odd-numbered carboxylates. Ethylene lost most of its inhibiting power when certain methanogens – assumingly using nickel-free hydrogenases – were selected. Activity of ethylene-tolerant methanogens was slower than normal methanogens but still sufficiently fast to limit H_2 availability to acetogens. Therefore, a solution to avoid ethylene-tolerant methanogens is to use ethylene in conjunction with CO. This is not expected to be a technical challenge as these two gases often co-occur in real syngas mixtures.

The last pair of gas recirculation reactors was operated with a complete syngas mixture ($H_2/CO_2/CO$/ethylene) and an organic feedstock model for almost 300 days with no electron losses to methane. In this experiment, a mixotrophic community acclimatized to CO and was shown to be more efficient than a purely heterotrophic one while producing MCCs. Due to H_2/CO consumption, the mixotrophic community consumed 106% more electron equivalents than the heterotrophic community. Syngas consumption increased not only the production of acetate but also that of the more valuable carboxylates such as *n*-butyrate and *n*-caproate. The mixotrophic reactor also showed potential for carbon fixation, presenting average rates up to 1.4 g CO_2 eq. L^{-1} d^{-1}, comparable to the fixation rates of state-of-the-art photoautotrophic microalgal reactors.

Community analysis showed that acetogens from the two most frequently enriched genera, *Clostridium* sensu stricto 12 and *Eubacterium*, correlated to syngas consumption and MCC production. Their behavior in the community was coherent to the description of their closest relatives, which are mixotrophic chain-elongating bacteria. This finding is contrary to the common assumption that the syngas boost of MCC production is an intrinsically slow process that occurs via ethanol transfer between community members. Additionally, bacteria related to *Megasphaera*, *Oscillibacter*, *Colidextribacter*, and *Caproiciproducens* should be seen as candidate mixotrophs as they performed well in H_2-rich environments while correlating with high MCC selectivity. So far, bacteria of these genera are assumingly heterotrophic. One exploratory line for microbiologists is to use the gas recirculation reactor as a tool to enrich similar

microorganisms, hence, helping isolating and characterizing novel strains with industrially useful mixotrophic metabolism.

From an engineering perspective, this thesis establishes foundational knowledge for the future endeavors of upscaling co-fermentation of syngas with sustainable feedstocks into an economic and sustainable bioprocess. If done adequately, the boosting effect of mixotrophy on elongated carboxylate production is in the order of 50% and could define the success of the carboxylate platform to substitute our current fossil-based chemical platforms. Besides, merging the syngas and carboxylate platforms can convert anaerobic fermentation into a carbon-fixing process. Depending on how syngas is supplied and on the applications of the produced carboxylates, the merged platforms have potential to contribute in much-needed climate change mitigation.

List of references

Abbassi-Guendouz, A., Brockmann, D., Trably, E., Dumas, C., Delgenès, J.-P., Steyer, J.-P., et al. (2012). Total solids content drives high solid anaerobic digestion via mass transfer limitation. *Bioresource technology* 111, 55-61.

Abdoulmoumine, N., Kulkarni, A., and Adhikari, S. (2014). Effects of Temperature and Equivalence Ratio on Pine Syngas Primary Gases and Contaminants in a Bench-Scale Fluidized Bed Gasifier. *Industrial & Engineering Chemistry Research* 53(14), 5767-5777. DOI: 10.1021/ie404401n.

Agler, M.T., Spirito, C.M., Usack, J.G., Werner, J.J., and Angenent, L.T. (2014). Development of a highly specific and productive process for *n*-caproic acid production: applying lessons from methanogenic microbiomes. *Water Sci Technol* 69(1), 62-68. DOI: 10.2166/wst.2013.549.

Agler, M.T., Werner, J.J., Iten, L.B., Dekker, A., Cotta, M.A., Dien, B.S., et al. (2012). Shaping reactor microbiomes to produce the fuel precursor n-butyrate from pretreated cellulosic hydrolysates. *Environ Sci Technol* 46(18), 10229-10238. DOI: 10.1021/es302352c.

Andersen, S.J., Candry, P., Basadre, T., Khor, W.C., Roume, H., Hernandez-Sanabria, E., et al. (2015). Electrolytic extraction drives volatile fatty acid chain elongation through lactic acid and replaces chemical pH control in thin stillage fermentation. *Biotechnol Biofuels* 8, 221. DOI: 10.1186/s13068-015-0396-7.

Angelidaki, I., and Ahring, B.K. (1995). Isomerization of n- and i-butyrate in anaerobic methanogenic systems. *Antonie Van Leeuwenhoek* 68(4), 285-291. DOI: 10.1007/BF00874138.

Angenent, L.T., Richter, H., Buckel, W., Spirito, C.M., Steinbusch, K.J., Plugge, C.M., et al. (2016). Chain Elongation with Reactor Microbiomes: Open-Culture Biotechnology To Produce Biochemicals. *Environ Sci Technol* 50(6), 2796-2810. DOI: 10.1021/acs.est.5b04847.

Apelt, M. (2020). "Examination of samples of solids (substrates) and digestates with HPLC for aliphatic and aromatic acids, alcohols and aldehydes," in *Series "Biomass Energy Use": Collection of Methods for Biogas: Methods to determine parameters for analysis purposes and parameters that describe processes in the biogas sector,* eds. J. Liebetrau, D. Pfeiffer & D. Thrän. 2nd ed (Leipzig: DBFZ), 75 - 80.

Arslan, D., Steinbusch, K.J., Diels, L., De Wever, H., Buisman, C.J., and Hamelers, H.V. (2012). Effect of hydrogen and carbon dioxide on carboxylic acids patterns in mixed culture fermentation. *Bioresour Technol* 118, 227-234. DOI: 10.1016/j.biortech.2012.05.003.

Arslan, D., Steinbusch, K.J.J., Diels, L., Hamelers, H.V.M., Strik, D.P.B.T.B., Buisman, C.J.N., et al. (2016). Selective short-chain carboxylates production: A review of control mechanisms to direct mixed culture fermentations. *Critical Reviews in Environmental Science and Technology* 46(6), 592-634. DOI: 10.1080/10643389.2016.1145959.

Asimakopoulos, K., Gavala, H.N., and Skiadas, I.V. (2018). Reactor systems for syngas fermentation processes: A review. *Chemical Engineering Journal* 348, 732-744. DOI: 10.1016/j.cej.2018.05.003.

Azman, S., Khadem, A.F., van Lier, J.B., Zeeman, G., and Plugge, C.M. (2015). Presence and Role of Anaerobic Hydrolytic Microbes in Conversion of Lignocellulosic Biomass for Biogas Production. *Critical Reviews in Environmental Science and Technology* 45(23), 2523-2564. DOI: 10.1080/10643389.2015.1053727.

Baleeiro, F.C.F., Ardila, M.S., Kleinsteuber, S., and Sträuber, H. (2021a). Effect of Oxygen Contamination on Propionate and Caproate Formation in Anaerobic Fermentation. *Front Bioeng Biotechnol* 9, 725443. DOI: 10.3389/fbioe.2021.725443.

Benevenuti, C., Amaral, P., Ferreira, T., and Seidl, P. (2021). Impacts of Syngas Composition on Anaerobic Fermentation. *Reactions* 2(4), 391-407. DOI: 10.3390/reactions2040025.

Bengelsdorf, F.R., Beck, M.H., Erz, C., Hoffmeister, S., Karl, M.M., Riegler, P., et al. (2018). Bacterial Anaerobic Synthesis Gas (Syngas) and CO_2+H_2 Fermentation. *Adv Appl Microbiol* 103, 143-221. DOI: 10.1016/bs.aambs.2018.01.002.

Bertsch, J., and Müller, V. (2015). CO Metabolism in the Acetogen *Acetobacterium woodii*. *Appl Environ Microbiol* 81(17), 5949-5956. DOI: 10.1128/AEM.01772-15.

Biddy, M.J., Scarlata, C., and Kinchin, C. (2016). "Chemicals from biomass: a market assessment of bioproducts with near-term potential". National Renewable Energy Lab.(NREL), Golden, CO (United States)).

Bjornsson, L., Murto, M., and Mattiasson, B. (2000). Evaluation of parameters for monitoring an anaerobic co-digestion process. *Appl Microbiol Biotechnol* 54(6), 844-849. DOI: 10.1007/s002530000471.

Boga, H.I., Ji, R., Ludwig, W., and Brune, A. (2007). *Sporotalea propionica* gen. nov. sp. nov., a hydrogen-oxidizing, oxygen-reducing, propionigenic firmicute from the intestinal tract of a soil-feeding termite. *Arch Microbiol* 187(1), 15-27. DOI: 10.1007/s00203-006-0168-7.

Bonk, F., Popp, D., Weinrich, S., Sträuber, H., Kleinsteuber, S., Harms, H., et al. (2018). Intermittent fasting for microbes: how discontinuous feeding increases functional stability in anaerobic digestion. *Biotechnol Biofuels* 11, 274. DOI: 10.1186/s13068-018-1279-5.

Braune, M., Yuan, B., Sträuber, H., McDowall, S.C., Nitzsche, R., and Gröngroft, A. (2021). A Downstream Processing Cascade for Separation of Caproic and Caprylic Acid from Maize Silage-Based Fermentation Broth. *Front Bioeng Biotechnol* 9, 725578. DOI: 10.3389/fbioe.2021.725578.

Brodowski, F., Lezyk, M., Gutowska, N., and Oleskowicz-Popiel, P. (2021). Effect of external acetate on lactate-based carboxylate platform: Shifted lactate overloading limit and hydrogen co-production. *Sci Total Environ* 802, 149885. DOI: 10.1016/j.scitotenv.2021.149885.

Brouzes, R., and Knowles, R. (1971). Inhibition of growth of Clostridium pasteurianum by acetylene: implication for nitrogen fixation assay. *Can J Microbiol* 17(12), 1483-1489. DOI: 10.1139/m71-238.

Cabrol, L., Marone, A., Tapia-Venegas, E., Steyer, J.P., Ruiz-Filippi, G., and Trably, E. (2017). Microbial ecology of fermentative hydrogen producing bioprocesses: useful insights for driving the ecosystem function. *FEMS Microbiol Rev* 41(2), 158-181. DOI: 10.1093/femsre/fuw043.

Callahan, B.J., McMurdie, P.J., Rosen, M.J., Han, A.W., Johnson, A.J., and Holmes, S.P. (2016). DADA2: High-resolution sample inference from Illumina amplicon data. *Nat Methods* 13(7), 581-583. DOI: 10.1038/nmeth.3869.

Calvo, D.C., Ontiveros-Valencia, A., Krajmalnik-Brown, R., Torres, C.I., and Rittmann, B.E. (2021). Carboxylates and alcohols production in an autotrophic hydrogen-based membrane biofilm reactor. *Biotechnol Bioeng*. DOI: 10.1002/bit.27745.

Cavalcante, W.A., Gehring, T.A., Santaella, S.T., Freitas, I.B.F., Angenent, L.T., van Haandel, A.C., et al. (2020). Upgrading sugarcane biorefineries: Acetate addition allows for conversion of fermented sugarcane molasses into high-value medium chain carboxylic acids. *Journal of Environmental Chemical Engineering* 8(2). DOI: 10.1016/j.jece.2019.103649.

Cavalcante, W.D., Leitao, R.C., Gehring, T.A., Angenent, L.T., and Santaella, S.T. (2017). Anaerobic fermentation for n-caproic acid production: A review. *Process Biochemistry* 54, 106-119. DOI: 10.1016/j.procbio.2016.12.024.

Chahal, S.P., and Starr, J. (2006). "Lactic Acid, Ullmann's Encyclopedia of Industrial Chemistry". Wiley-VCH, GmbH & Co. KGaA: Weinheim, Germany).

Chapleur, O., Madigou, C., Civade, R., Rodolphe, Y., Mazeas, L., and Bouchez, T. (2016). Increasing concentrations of phenol progressively affect anaerobic digestion of cellulose and associated microbial communities. *Biodegradation* 27(1), 15-27. DOI: 10.1007/s10532-015-9751-4.

ChemAnalyst (2021). *Ethylene Prices Overview* [Online]. Available: https://www.chemanalyst.com/Pricing-data/ethylene-40 [Accessed May 5, 2021 2021].

Chen, L., Liu, M.-Y., Legall, J., Fareleira, P., Santos, H., and Xavier, A.V. (1993). Rubredoxin oxidase, a new flavo-hemo-protein, is the site of oxygen reduction to water by the "strict anaerobe" *Desulfovibrio gigas*. *Biochemical and biophysical research communications* 193(1), 100-105. DOI: 10.1006/bbrc.1993.1595.

Chen, W.S., Strik, D., Buisman, C.J.N., and Kroeze, C. (2017). Production of Caproic Acid from Mixed Organic Waste: An Environmental Life Cycle Perspective. *Environ Sci Technol* 51(12), 7159-7168. DOI: 10.1021/acs.est.6b06220.

Chen, W.S., Ye, Y., Steinbusch, K.J.J., Strik, D.P.B.T.B., and Buisman, C.J.N. (2016). Methanol as an alternative electron donor in chain elongation for butyrate and caproate formation. *Biomass & Bioenergy* 93, 201-208. DOI: 10.1016/j.biombioe.2016.07.008.

Contreras-Dávila, C.A., Ali, A., Buisman, C.J.N., and Strik, D.P.B.T.B. (2021). Lactate Metabolism and Microbiome Composition Are Affected by Nitrogen Gas Supply in Continuous Lactate-Based Chain Elongation. *Fermentation* 7(1). DOI: 10.3390/fermentation7010041.

Crognale, S., Braguglia, C.M., Gallipoli, A., Gianico, A., Rossetti, S., and Montecchio, D. (2021). Direct Conversion of Food Waste Extract into Caproate: Metagenomics Assessment of Chain Elongation Process. *Microorganisms* 9(2). DOI: 10.3390/microorganisms9020327.

Cueto-Rojas, H.F., van Maris, A.J., Wahl, S.A., and Heijnen, J.J. (2015). Thermodynamics-based design of microbial cell factories for anaerobic product formation. *Trends Biotechnol* 33(9), 534-546. DOI: 10.1016/j.tibtech.2015.06.010.

Dannenberg, S., Kroder, M., Dilling, W., and Cypionka, H. (1992). Oxidation of H_2, organic compounds and inorganic sulfur compounds coupled to reduction of O_2 or nitrate by sulfate-reducing bacteria. *Archives of Microbiology* 158(2), 93-99. DOI: 10.1007/BF00245211.

De Groof, V., Coma, M., Arnot, T., Leak, D.J., and Lanham, A.B. (2019). Medium Chain Carboxylic Acids from Complex Organic Feedstocks by Mixed Culture Fermentation. *Molecules* 24(3), 398. DOI: 10.3390/molecules24030398.

de Leeuw, K.D., Buisman, C.J.N., and Strik, D. (2019). Branched Medium Chain Fatty Acids: Iso-Caproate Formation from Iso-Butyrate Broadens the Product Spectrum for Microbial Chain Elongation. *Environ Sci Technol* 53(13), 7704-7713. DOI: 10.1021/acs.est.8b07256.

de Leeuw, K.D., de Smit, S.M., van Oossanen, S., Moerland, M.J., Buisman, C.J.N., and Strik, D.P.B.T.B. (2020). Methanol-Based Chain Elongation with Acetate to *n*-Butyrate and Isobutyrate at Varying Selectivities Dependent on pH. *ACS Sustainable Chemistry & Engineering* 8(22), 8184-8194. DOI: 10.1021/acssuschemeng.0c00907.

de Medeiros, E.M., Posada, J.A., Noorman, H., Osseweijer, P., and Filho, R.M. (2017). Hydrous bioethanol production from sugarcane bagasse via energy self-sufficient gasification-fermentation hybrid route: Simulation and financial analysis. *Journal of Cleaner Production* 168, 1625-1635. DOI: 10.1016/j.jclepro.2017.01.165.

de Smit, S.M., de Leeuw, K.D., Buisman, C.J.N., and Strik, D. (2019). Continuous *n*-valerate formation from propionate and methanol in an anaerobic chain elongation open-culture bioreactor. *Biotechnol Biofuels* 12, 132. DOI: 10.1186/s13068-019-1468-x.

De Vrieze, J., Coma, M., Debeuckelaere, M., Van der Meeren, P., and Rabaey, K. (2016). High salinity in molasses wastewaters shifts anaerobic digestion to carboxylate production. *Water Res* 98, 293-301. DOI: 10.1016/j.watres.2016.04.035.

Detman, A., Laubitz, D., Chojnacka, A., Kiela, P.R., Salamon, A., Barberán, A., et al. (2021). Dynamics of dark fermentation microbial communities in the light of lactate and butyrate production. *Microbiome* 9(1). DOI: 10.1186/s40168-021-01105-x.

Diamond, L.W., and Akinfiev, N.N. (2003). Solubility of CO_2 in water from -1.5 to 100 degrees C and from 0.1 to 100 MPa: evaluation of literature data and thermodynamic modelling. *Fluid Phase Equilibria* 208(1-2), 265-290. DOI: 10.1016/S0378-3812(03)00041-4.

Dias, M.O.D., Maciel, R., Mantelatto, P.E., Cavalett, O., Rossell, C.E.V., Bonomi, A., et al. (2015). Sugarcane processing for ethanol and sugar in Brazil. *Environmental Development* 15, 35-51. DOI: 10.1016/j.envdev.2015.03.004.

Diender, M., Parera Olm, I., Gelderloos, M., Koehorst, J.J., Schaap, P.J., Stams, A.J.M., et al. (2019). Metabolic shift induced by synthetic co-cultivation promotes high yield of chain elongated acids from syngas. *Sci Rep* 9(1), 18081. DOI: 10.1038/s41598-019-54445-y.

Diender, M., Stams, A.J., and Sousa, D.Z. (2015). Pathways and Bioenergetics of Anaerobic Carbon Monoxide Fermentation. *Front Microbiol* 6, 1275. DOI: 10.3389/fmicb.2015.01275.

Diender, M., Stams, A.J., and Sousa, D.Z. (2016). Production of medium-chain fatty acids and higher alcohols by a synthetic co-culture grown on carbon monoxide or syngas. *Biotechnol Biofuels* 9, 82. DOI: 10.1186/s13068-016-0495-0.

Ding, H.B., Tan, G.Y., and Wang, J.Y. (2010). Caproate formation in mixed-culture fermentative hydrogen production. *Bioresour Technol* 101(24), 9550-9559. DOI: 10.1016/j.biortech.2010.07.056.

DOE, U.D.o.E.-. (2016). *Biomass For Electricity Generation* [Online]. Washington, DC: US Department of Energy. Available: https://www.wbdg.org/resources/biomass-electricity-generation [Accessed].

Doud, D.F.R., Holmes, E.C., Richter, H., Molitor, B., Jander, G., and Angenent, L.T. (2017). Metabolic engineering of Rhodopseudomonas palustris for the obligate reduction of n-butyrate to n-butanol. *Biotechnol Biofuels* 10, 178. DOI: 10.1186/s13068-017-0864-3.

Dröge, S., Fröhlich, J., Radek, R., and König, H. (2006). *Spirochaeta coccoides* sp. nov., a novel coccoid spirochete from the hindgut of the termite *Neotermes castaneus*. *Appl Environ Microbiol* 72(1), 392-397. DOI: 10.1128/AEM.72.1.392-397.2006.

Duber, A., Jaroszynski, L., Zagrodnik, R., Chwialkowska, J., Juzwa, W., Ciesielski, S., et al. (2018). Exploiting the real wastewater potential for resource recovery - n-caproate production from acid whey. *Green Chemistry* 20(16), 3790-3803. DOI: 10.1039/c8gc01759j.

Duber, A., Zagrodnik, R., Chwialkowska, J., Juzwa, W., and Oleskowicz-Popiel, P. (2020). Evaluation of the feed composition for an effective medium chain carboxylic acid production in an open culture fermentation. *Sci Total Environ* 728, 138814. DOI: 10.1016/j.scitotenv.2020.138814.

Elsden, S., and Lewis, D. (1953). The production of fatty acids by a gram-negative coccus. *Biochemical Journal* 55(1), 183.

Endres, H.-J., and Siebert-Raths, A. (2009). Technische Biopolymere. *Rahmenbedingungen, Marktsituation, Herstellung, Aufbau und Eigenschaften. 1st ed. München: Hanser*.

Esquivel-Elizondo, S., Bagci, C., Temovska, M., Jeon, B.S., Bessarab, I., Williams, R.B.H., et al. (2020). The Isolate *Caproiciproducens* sp. 7D4C2 Produces *n*-Caproate at Mildly Acidic Conditions From Hexoses: Genome and rBOX Comparison With Related Strains and Chain-Elongating Bacteria. *Front Microbiol* 11, 594524. DOI: 10.3389/fmicb.2020.594524.

Esquivel-Elizondo, S., Delgado, A.G., and Krajmalnik-Brown, R. (2017a). Evolution of microbial communities growing with carbon monoxide, hydrogen, and carbon dioxide. *FEMS Microbiol Ecol* 93(6). DOI: 10.1093/femsec/fix076.

Esquivel-Elizondo, S., Delgado, A.G., Rittmann, B.E., and Krajmalnik-Brown, R. (2017b). The effects of CO_2 and H_2 on CO metabolism by pure and mixed microbial cultures. *Biotechnol Biofuels* 10, 220. DOI: 10.1186/s13068-017-0910-1.

Esquivel-Elizondo, S., Miceli, J., 3rd, Torres, C.I., and Krajmalnik-Brown, R. (2018). Impact of carbon monoxide partial pressures on methanogenesis and medium chain fatty acids production during ethanol fermentation. *Biotechnol Bioeng* 115(2), 341-350. DOI: 10.1002/bit.26471.

Fernandez-Naveira, A., Abubackar, H.N., Veiga, M.C., and Kennes, C. (2016). Efficient butanol-ethanol (B-E) production from carbon monoxide fermentation by Clostridium carboxidivorans. *Appl Microbiol Biotechnol* 100(7), 3361-3370. DOI: 10.1007/s00253-015-7238-1.

Fernandez-Naveira, A., Veiga, M.C., and Kennes, C. (2019). Selective anaerobic fermentation of syngas into either C2-C6 organic acids or ethanol and higher alcohols. *Bioresour Technol* 280, 387-395. DOI: 10.1016/j.biortech.2019.02.018.

Fernández-Naveira, Á., Veiga, M.C., and Kennes, C. (2017). H-B-E (hexanol-butanol-ethanol) fermentation for the production of higher alcohols from syngas/waste gas. *Journal of Chemical Technology & Biotechnology* 92(4), 712-731. DOI: 10.1002/jctb.5194.

Flaiz, M., Baur, T., Brahner, S., Poehlein, A., Daniel, R., and Bengelsdorf, F.R. (2020). *Caproicibacter fermentans* gen. nov., sp. nov., a new caproate-producing bacterium and emended description of the genus *Caproiciproducens. Int J Syst Evol Microbiol* 70(7), 4269-4279. DOI: 10.1099/ijsem.0.004283.

Flaiz, M., Baur, T., Stibitsky, S., Brahner, S., Poehlin, A., Daniel, R., et al. (2019). "Caprobacter fermentans gen. nov., sp. nov., a new caproic acid producing bacterium", in: *Annual Conference of the Association for General and Applied Microbiology.* (Mainz, Germany).

Fortney, N.W., Hanson, N.J., Rosa, P.R.F., Donohue, T.J., and Noguera, D.R. (2021). Diverse Profile of Fermentation Byproducts From Thin Stillage. *Front Bioeng Biotechnol* 9, 695306. DOI: 10.3389/fbioe.2021.695306.

Friedman, E.S., Bittinger, K., Esipova, T.V., Hou, L., Chau, L., Jiang, J., et al. (2018). Microbes vs. chemistry in the origin of the anaerobic gut lumen. *Proc Natl Acad Sci U S A* 115(16), 4170-4175. DOI: 10.1073/pnas.1718635115.

Fu, H., Lin, M., Tang, I.C., Wang, J., and Yang, S.T. (2021). Effects of benzyl viologen on increasing NADH availability, acetate assimilation, and butyric acid production by *Clostridium tyrobutyricum. Biotechnol Bioeng* 118(2), 770-783. DOI: 10.1002/bit.27602.

Ganigue, R., Ramio-Pujol, S., Sanchez, P., Baneras, L., and Colprim, J. (2015). Conversion of sewage sludge to commodity chemicals via syngas fermentation. *Water Sci Technol* 72(3), 415-420. DOI: 10.2166/wst.2015.222.

Ganigue, R., Sanchez-Paredes, P., Baneras, L., and Colprim, J. (2016). Low Fermentation pH Is a Trigger to Alcohol Production, but a Killer to Chain Elongation. *Front Microbiol* 7, 702. DOI: 10.3389/fmicb.2016.00702.

Gänzle, M.G. (2015). Lactic metabolism revisited: metabolism of lactic acid bacteria in food fermentations and food spoilage. *Current Opinion in Food Science* 2, 106-117. DOI: 10.1016/j.cofs.2015.03.001.

Ge, S., Usack, J.G., Spirito, C.M., and Angenent, L.T. (2015). Long-Term *n*-Caproic Acid Production from Yeast-Fermentation Beer in an Anaerobic Bioreactor with Continuous Product Extraction. *Environ Sci Technol* 49(13), 8012-8021. DOI: 10.1021/acs.est.5b00238.

Gildemyn, S., Molitor, B., Usack, J.G., Nguyen, M., Rabaey, K., and Angenent, L.T. (2017). Upgrading syngas fermentation effluent using Clostridium kluyveri in a continuous fermentation. *Biotechnol Biofuels* 10, 83. DOI: 10.1186/s13068-017-0764-6.

Godwin, S., Kang, A., Gulino, L.M., Manefield, M., Gutierrez-Zamora, M.L., Kienzle, M., et al. (2014). Investigation of the microbial metabolism of carbon dioxide and hydrogen in the kangaroo foregut by stable isotope probing. *ISME J* 8(9), 1855-1865. DOI: 10.1038/ismej.2014.25.

Gonzalez-Cabaleiro, R., Lema, J.M., and Rodriguez, J. (2015). Metabolic energy-based modelling explains product yielding in anaerobic mixed culture fermentations. *PLoS One* 10(5), e0126739. DOI: 10.1371/journal.pone.0126739.

González-Cabaleiro, R., Lema, J.M., Rodríguez, J., and Kleerebezem, R. (2013). Linking thermodynamics and kinetics to assess pathway reversibility in anaerobic bioprocesses. *Energy & Environmental Science* 6(12). DOI: 10.1039/c3ee42754d.

Gonzalez-Garcia, R., McCubbin, T., Navone, L., Stowers, C., Nielsen, L., and Marcellin, E. (2017). Microbial Propionic Acid Production. *Fermentation* 3(2). DOI: 10.3390/fermentation3020021.

González-Tenorio, D., Muñoz-Páez, K.M., Buitrón, G., and Valdez-Vazquez, I. (2020). Fermentation of organic wastes and $CO_2 + H_2$ off-gas by microbiotas provides short-chain fatty acids and ethanol for n-caproate production. *Journal of CO2 Utilization* 42. DOI: 10.1016/j.jcou.2020.101314.

Granda, C.B. (Year). "Production of Highly Pure Fatty Acids from Anaerobic Digestion", in: *World Congress on Industrial Biotechnology*, (Montréal).

Greenwood, N.N., and Earnshaw, A. (2012). *Chemistry of the Elements*. Elsevier.

Grimalt-Alemany, A., Lezyk, M., Lange, L., Skiadas, I.V., and Gavala, H.N. (2018). Enrichment of syngas-converting mixed microbial consortia for ethanol production and thermodynamics-based design of enrichment strategies. *Biotechnol Biofuels* 11, 198. DOI: 10.1186/s13068-018-1189-6.

Groher, A., and Weuster-Botz, D. (2016). Comparative reaction engineering analysis of different acetogenic bacteria for gas fermentation. *J Biotechnol* 228, 82-94. DOI: 10.1016/j.jbiotec.2016.04.032.

Grootscholten, T.I., Steinbusch, K.J., Hamelers, H.V., and Buisman, C.J. (2013). Improving medium chain fatty acid productivity using chain elongation by reducing the hydraulic retention time in an upflow anaerobic filter. *Bioresour Technol* 136, 735-738. DOI: 10.1016/j.biortech.2013.02.114.

Grootscholten, T.I.M., Strik, D.P.B.T.B., Steinbusch, K.J.J., Buisman, C.J.N., and Hamelers, H.V.M. (2014). Two-stage medium chain fatty acid (MCFA) production from municipal solid waste and ethanol. *Applied Energy* 116, 223-229. DOI: 10.1016/j.apenergy.2013.11.061.

Guiot, S.R., Cimpoia, R., and Carayon, G. (2011). Potential of wastewater-treating anaerobic granules for biomethanation of synthesis gas. *Environ Sci Technol* 45(5), 2006-2012. DOI: 10.1021/es102728m.

Gupta, R.S., Chen, W.J., Adeolu, M., and Chai, Y. (2013). Molecular signatures for the class Coriobacteriia and its different clades; proposal for division of the class Coriobacteriia into the emended order Coriobacteriales, containing the emended family *Coriobacteriaceae* and *Atopobiaceae* fam. nov., and Eggerthellales ord. nov., containing the family *Eggerthellaceae* fam. nov. *Int J Syst Evol Microbiol* 63(Pt 9), 3379-3397. DOI: 10.1099/ijs.0.048371-0.

He, S.H., Woo, S.B., DerVartanian, D.V., Le Gall, J., and Peck, H.D., Jr. (1989). Effects of acetylene on hydrogenases from the sulfate reducing and methanogenic bacteria. *Biochem Biophys Res Commun* 161(1), 127-133. DOI: 10.1016/0006-291x(89)91570-2.

He, Y., Lens, P.N.L., Veiga, M.C., and Kennes, C. (2021). Selective butanol production from carbon monoxide by an enriched anaerobic culture. *Sci Total Environ* 806(Pt 2), 150579. DOI: 10.1016/j.scitotenv.2021.150579.

Heimann, A., Jakobsen, R., and Blodau, C. (2010). Energetic constraints on H_2-dependent terminal electron accepting processes in anoxic environments: a review of observations and model approaches. *Environ Sci Technol* 44(1), 24-33. DOI: 10.1021/es9018207.

Her, J., and Kim, J. (2013). *Rummeliibacillus suwonensis* sp. nov., isolated from soil collected in a mountain area of South Korea. *J Microbiol* 51(2), 268-272. DOI: 10.1007/s12275-013-3126-5.

Hermann, M., Teleki, A., Weitz, S., Niess, A., Freund, A., Bengelsdorf, F.R., et al. (2020). Electron availability in CO_2, CO and H_2 mixtures constrains flux distribution, energy management and product formation in *Clostridium ljungdahlii*. *Microb Biotechnol* 13(6), 1831-1846. DOI: 10.1111/1751-7915.13625.

Hernandez-Eugenio, G. (2002). *Sporanaerobacter acetigenes* gen. nov., sp. nov., a novel acetogenic, facultatively sulfur-reducing bacterium. *International Journal of Systematic and Evolutionary Microbiology* 52(4), 1217-1223. DOI: 10.1099/ijs.0.01992-0.

Holtzapple, M.T., Wu, H., Weimer, P.J., Dalke, R., Granda, C.B., Mai, J., et al. (2022). Microbial communities for valorizing biomass using the carboxylate platform to produce volatile fatty acids: A review. *Bioresour Technol* 344(Pt B), 126253. DOI: 10.1016/j.biortech.2021.126253.

Horn, M.A., Matthies, C., Küsel, K., Schramm, A., and Drake, H.L. (2003). Hydrogenotrophic methanogenesis by moderately acid-tolerant methanogens of a methane-emitting acidic peat. *Applied and Environmental Microbiology* 69(1), 74-83.

Hu, Y., Jing, Z., Sudo, Y., Niu, Q., Du, J., Wu, J., et al. (2015). Effect of influent $COD/SO_4(2-)$ ratios on UASB treatment of a synthetic sulfate-containing wastewater. *Chemosphere* 130, 24-33. DOI: 10.1016/j.chemosphere.2015.02.019.

Huang, S., Kleerebezem, R., Rabaey, K., and Ganigue, R. (2020). Open microbiome dominated by *Clostridium* and *Eubacterium* converts methanol into *i*-butyrate and *n*-butyrate. *Appl Microbiol Biotechnol* 104(11), 5119-5131. DOI: 10.1007/s00253-020-10551-w.

Hyman, M.R., and Arp, D.J. (1988). Acetylene inhibition of metalloenzymes. *Anal Biochem* 173(2), 207-220. DOI: 10.1016/0003-2697(88)90181-9.

Infantes-López, A. (2020). *Advancing towards biomass-derived syngas fermentation - Evaluation of process parameters and gas composition effects.* Ph.D. thesis.

Jankowska, E., Duber, A., Chwialkowska, J., Stodolny, M., and Oleskowicz-Popiel, P. (2018). Conversion of organic waste into volatile fatty acids - The influence of process operating parameters. *Chemical Engineering Journal* 345, 395-403. DOI: 10.1016/j.cej.2018.03.180.

Jaros, A., Rova, U., and Berglund, K.A. (2012). Effect of Acetate on Fermentation Production of Butyrate. *Cellulose Chemistry and Technology* 46(5-6), 341-347.

Jeon, B.S., Choi, O., Um, Y., and Sang, B.I. (2016). Production of medium-chain carboxylic acids by *Megasphaera* sp. MH with supplemental electron acceptors. *Biotechnol Biofuels* 9, 129. DOI: 10.1186/s13068-016-0549-3.

Jeong, J., Bertsch, J., Hess, V., Choi, S., Choi, I.G., Chang, I.S., et al. (2015). Energy Conservation Model Based on Genomic and Experimental Analyses of a Carbon Monoxide-Utilizing, Butyrate-Forming Acetogen, *Eubacterium limosum* KIST612. *Appl Environ Microbiol* 81(14), 4782-4790. DOI: 10.1128/AEM.00675-15.

Johnson, L.A., and Hug, L.A. (2019). Distribution of reactive oxygen species defense mechanisms across domain bacteria. *Free Radic Biol Med* 140, 93-102. DOI: 10.1016/j.freeradbiomed.2019.03.032.

Joshi, S., Robles, A., Aguiar, S., and Delgado, A.G. (2021). The occurrence and ecology of microbial chain elongation of carboxylates in soils. *ISME J* 15(7), 1907-1918. DOI: 10.1038/s41396-021-00893-2.

Jourdin, L., Raes, S.M.T., Buisman, C.J.N., and Strik, D.P.B.T.B. (2018). Critical Biofilm Growth throughout Unmodified Carbon Felts Allows Continuous Bioelectrochemical Chain Elongation from CO_2 up to Caproate at High Current Density. *Frontiers in Energy Research* 6. DOI: 10.3389/fenrg.2018.00007.

Kalia, V.C., Mukherjee, T., Bhushan, A., Joshi, J., Shankar, P., and Huma, N. (2011). Analysis of the unexplored features of rrs (16S rDNA) of the Genus Clostridium. *BMC Genomics* 12, 18. DOI: 10.1186/1471-2164-12-18.

Kaneko, T., Mori, H., Iwata, M., and Meguro, S. (1994). Growth Stimulator for Bifidobacteria Produced by *Propionibacterium freudenreichii* and Several Intestinal Bacteria. *Journal of Dairy Science* 77(2), 393-404. DOI: 10.3168/jds.S0022-0302(94)76965-4.

Kang, S., Song, Y., Jin, S., Shin, J., Bae, J., Kim, D.R., et al. (2020). Adaptive Laboratory Evolution of *Eubacterium limosum* ATCC 8486 on Carbon Monoxide. *Front Microbiol* 11, 402. DOI: 10.3389/fmicb.2020.00402.

Karthikeyan, D.R., Dimple, K.K., Ashokkumar, M.S., Ajay, K., Hasan, K.A., Raymond, L.H., et al. (2016). Critical factors affecting the integration of biomass gasification and syngas fermentation technology. *AIMS Bioengineering* 3(2), 188-210. DOI: 10.3934/bioeng.2016.2.188.

Katano, Y., Fujinami, S., Kawakoshi, A., Nakazawa, H., Oji, S., Iino, T., et al. (2012). Complete genome sequence of *Oscillibacter valericigenes* Sjm18-20(T) (=NBRC 101213(T)). *Stand Genomic Sci* 6(3), 406-414. DOI: 10.4056/sigs.2826118.

Kato, M.T., Field, J.A., and Lettinga, G. (1997). Anaerobe Tolerance to Oxygen and the Potentials of Anaerobic and Aerobic Cocultures for Wastewater Treatment. *Brazilian Journal of Chemical Engineering* 14(4), 395-407. DOI: 10.1590/s0104-66321997000400015.

Kaur, G., Garcia-Gonzalez, L., Elst, K., Truzzi, F., Bertin, L., Kaushik, A., et al. (2020). Reactive extraction for in-situ carboxylate recovery from mixed culture fermentation. *Biochemical Engineering Journal* 160. DOI: 10.1016/j.bej.2020.107641.

Kenealy, W.R., and Waselefsky, D.M. (1985). Studies on the Substrate Range of *Clostridium kluyveri* - the Use of Propanol and Succinate. *Archives of Microbiology* 141(3), 187-194. DOI: Doi 10.1007/Bf00408056.

Kim, B.-C., Moon, C., Choi, Y., and Nam, K. (2022). Long-Term Stability of High-*n*-Caproate Specificity-Ensuring Anaerobic Membrane Bioreactors: Controlling Microbial Competitions through Feeding Strategies. *ACS Sustainable Chemistry & Engineering*. DOI: 10.1021/acssuschemeng.1c07259.

Kim, B.C., Seung Jeon, B., Kim, S., Kim, H., Um, Y., and Sang, B.I. (2015). *Caproiciproducens galactitolivorans* gen. nov., sp. nov., a bacterium capable of producing caproic acid from galactitol, isolated from a wastewater treatment plant. *Int J Syst Evol Microbiol* 65(12), 4902-4908. DOI: 10.1099/ijsem.0.000665.

Kleerebezem, R., and Stams, A.J. (2000). Kinetics of syntrophic cultures: a theoretical treatise on butyrate fermentation. *Biotechnol Bioeng* 67(5), 529-543. DOI: 10.1002/(sici)1097-0290(20000305)67:5<529::aid-bit4>3.0.co;2-q.

Kleerebezem, R., and van Loosdrecht, M.C. (2007). Mixed culture biotechnology for bioenergy production. *Curr Opin Biotechnol* 18(3), 207-212. DOI: 10.1016/j.copbio.2007.05.001.

Kleerebezem, R., and Van Loosdrecht, M.C.M. (2010). A Generalized Method for Thermodynamic State Analysis of Environmental Systems. *Critical Reviews in Environmental Science and Technology* 40(1), 1-54. DOI: 10.1080/10643380802000974.

Klindworth, A., Pruesse, E., Schweer, T., Peplies, J., Quast, C., Horn, M., et al. (2013). Evaluation of general 16S ribosomal RNA gene PCR primers for classical and next-generation sequencing-based diversity studies. *Nucleic Acids Res* 41(1), e1. DOI: 10.1093/nar/gks808.

Kosaric, N., Duvnjak, Z., Farkas, A., Sahm, H., Bringer-Meyer, S., Goebel, O., et al. (2000). Ethanol. *Ullmann's encyclopedia of industrial chemistry*, 1-72.

Koster, I.W., and Koomen, E. (1988). Ammonia inhibition of the maximum growth rate (μ m) of hydrogenotrophic methanogens at various pH-levels and temperatures. *Applied microbiology and biotechnology* 28(4-5), 500-505.

Krab, K., Oltmann, L., and Stouthamer, A. (1982). Linkage of formate hydrogenlyase with anaerobic respiration in *Proteus mirabilis*. *Biochimica et Biophysica Acta (BBA)-Bioenergetics* 679(1), 51-59.

Krayzelova, L., Bartacek, J., Diaz, I., Jeison, D., Volcke, E.I.P., and Jenicek, P. (2015). Microaeration for hydrogen sulfide removal during anaerobic treatment: a review. *Reviews in Environmental Science and Bio-Technology* 14(4), 703-725. DOI: 10.1007/s11157-015-9386-2.

Kucek, L.A., Nguyen, M., and Angenent, L.T. (2016a). Conversion of L-lactate into *n*-caproate by a continuously fed reactor microbiome. *Water Res* 93, 163-171. DOI: 10.1016/j.watres.2016.02.018.

Kucek, L.A., Spirito, C.M., and Angenent, L.T. (2016b). High *n*-caprylate productivities and specificities from dilute ethanol and acetate: chain elongation with microbiomes to upgrade products from syngas fermentation. *Energy & Environmental Science* 9(11), 3482-3494. DOI: 10.1039/c6ee01487a.

Kucek, L.A., Xu, J., Nguyen, M., and Angenent, L.T. (2016c). Waste Conversion into *n*-Caprylate and *n*-Caproate: Resource Recovery from Wine Lees Using Anaerobic Reactor Microbiomes and In-line Extraction. *Front Microbiol* 7, 1892. DOI: 10.3389/fmicb.2016.01892.

Lambrecht, J., Cichocki, N., Schattenberg, F., Kleinsteuber, S., Harms, H., Muller, S., et al. (2019). Key sub-community dynamics of medium-chain carboxylate production. *Microb Cell Fact* 18(1), 92. DOI: 10.1186/s12934-019-1143-8.

Lee, N.-R., Lee, C.H., Lee, D.-Y., and Park, J.-B. (2020). Genome-Scale Metabolic Network Reconstruction and In Silico Analysis of Hexanoic acid Producing Megasphaera elsdenii. *Microorganisms* 8(4). DOI: 10.3390/microorganisms8040539.

Levin, D.B., and Chahine, R. (2010). Challenges for renewable hydrogen production from biomass. *International Journal of Hydrogen Energy* 35(10), 4962-4969. DOI: 10.1016/j.ijhydene.2009.08.067.

Liebetrau, J., Weinrich, S., Sträuber, H., and Kretzschmar, J. (2019). "Anaerobic Fermentation of Organic Material: Biological Processes and Their Control Parameters," in *Energy from Organic Materials (Biomass)*, ed. M. Kaltschmitt. (New York, NY: Springer New York), 779-807.

Liew, F., Martin, M.E., Tappel, R.C., Heijstra, B.D., Mihalcea, C., and Kopke, M. (2016). Gas Fermentation-A Flexible Platform for Commercial Scale Production of Low-Carbon-Fuels and Chemicals from Waste and Renewable Feedstocks. *Front Microbiol* 7, 694. DOI: 10.3389/fmicb.2016.00694.

Liou, J.S., Balkwill, D.L., Drake, G.R., and Tanner, R.S. (2005). *Clostridium carboxidivorans* sp. nov., a solvent-producing clostridium isolated from an agricultural settling lagoon, and reclassification of the acetogen *Clostridium scatologenes* strain SL1 as *Clostridium drakei* sp. nov. *Int J Syst Evol Microbiol* 55(Pt 5), 2085-2091. DOI: 10.1099/ijs.0.63482-0.

Litty, D., and Müller, V. (2021). Butyrate production in the acetogen *Eubacterium limosum* is dependent on the carbon and energy source. *Microb Biotechnol* 14(6), 2686-2692. DOI: 10.1111/1751-7915.13779.

Liu, B., Kleinsteuber, S., Centler, F., Harms, H., and Sträuber, H. (2020a). Competition Between Butyrate Fermenters and Chain-Elongating Bacteria Limits the Efficiency of Medium-Chain Carboxylate Production. *Front Microbiol* 11, 336. DOI: 10.3389/fmicb.2020.00336.

Liu, B., Popp, D., Muller, N., Sträuber, H., Harms, H., and Kleinsteuber, S. (2020b). Three Novel Clostridia Isolates Produce *n*-Caproate and iso-Butyrate from Lactate: Comparative Genomics of Chain-Elongating Bacteria. *Microorganisms* 8(12). DOI: 10.3390/microorganisms8121970.

Liu, B., Popp, D., Sträuber, H., Harms, H., and Kleinsteuber, S. (2020c). Draft Genome Sequences of Three Clostridia Isolates Involved in Lactate-Based Chain Elongation. *Microbiol Resour Announc* 9(32). DOI: 10.1128/MRA.00679-20.

Liu, C., Luo, G., Wang, W., He, Y.F., Zhang, R.H., and Liu, G.Q. (2018). The effects of pH and temperature on the acetate production and microbial community compositions by syngas fermentation. *Fuel* 224, 537-544. DOI: 10.1016/j.fuel.2018.03.125.

Liu, C., Wang, W., S, O.T., Yang, Z., Zhang, S., Liu, G., et al. (2020d). Microbial insights of enhanced anaerobic conversion of syngas into volatile fatty acids by co-fermentation with carbohydrate-rich synthetic wastewater. *Biotechnol Biofuels* 13, 53. DOI: 10.1186/s13068-020-01694-z.

Liu, H., Wang, J., Wang, A., and Chen, J. (2011). Chemical inhibitors of methanogenesis and putative applications. *Appl Microbiol Biotechnol* 89(5), 1333-1340. DOI: 10.1007/s00253-010-3066-5.

Liu, Y., He, P., Shao, L., Zhang, H., and Lu, F. (2017). Significant enhancement by biochar of caproate production via chain elongation. *Water Res* 119, 150-159. DOI: 10.1016/j.watres.2017.04.050.

Logroño, W., Popp, D., Kleinsteuber, S., Sträuber, H., Harms, H., and Nikolausz, M. (2020). Microbial Resource Management for Ex Situ Biomethanation of Hydrogen at Alkaline pH. *Microorganisms* 8(4), 614. DOI: 10.3390/microorganisms8040614.

Marounek, M., Fliegrova, K., and Bartos, S. (1989). Metabolism and Some Characteristics of Ruminal Strains of Megasphaera-Elsdenii. *Applied and Environmental Microbiology* 55(6), 1570-1573. DOI: Doi 10.1128/Aem.55.6.1570-1573.1989.

Martin, M. (2011). Cutadapt removes adapter sequences from high-throughput sequencing reads. *EMBnet.journal* 17(1), 3. DOI: 10.14806/ej.17.1.200.

Martin, W.F., and Sousa, F.L. (2015). Early Microbial Evolution: The Age of Anaerobes. *Cold Spring Harb Perspect Biol* 8(2), a018127. DOI: 10.1101/cshperspect.a018127.

Matassa, S., Verstraete, W., Pikaar, I., and Boon, N. (2016). Autotrophic nitrogen assimilation and carbon capture for microbial protein production by a novel enrichment of hydrogen-oxidizing bacteria. *Water Res* 101, 137-146. DOI: 10.1016/j.watres.2016.05.077.

McCubbin, T., Gonzalez-Garcia, R.A., Palfreyman, R.W., Stowers, C., Nielsen, L.K., and Marcellin, E. (2020). A Pan-Genome Guided Metabolic Network Reconstruction of Five *Propionibacterium* Species Reveals Extensive Metabolic Diversity. *Genes (Basel)* 11(10). DOI: 10.3390/genes11101115.

McDougall, T.J., and Barker, P.M. (2011). Getting started with TEOS-10 and the Gibbs Seawater (GSW) oceanographic toolbox. *SCOR/IAPSO WG* 127, 1-28.

[Dataset] McLaren, M.R. (2020). *Silva SSU taxonomic training data formatted for DADA2 (Silva version 138).* Zenodo. DOI: 10.5281/zenodo.3731176. Available: https://doi.org/10.5281/zenodo.3731176.

McMurdie, P.J., and Holmes, S. (2013). phyloseq: an R package for reproducible interactive analysis and graphics of microbiome census data. *PLoS One* 8(4), e61217. DOI: 10.1371/journal.pone.0061217.

Mechichi, T., Labat, M., Woo, T.H., Thomas, P., Garcia, J.L., and Patel, B.K. (1998). *Eubacterium aggregans* sp. nov., a new homoacetogenic bacterium from olive mill wastewater treatment digestor. *Anaerobe* 4(6), 283-291. DOI: 10.1006/anae.1998.0179.

Menon, A., and Lyng, J.G. (2021). Circular bioeconomy solutions: driving anaerobic digestion of waste streams towards production of high value medium chain fatty acids. *Reviews in Environmental Science and Bio-Technology* 20(1), 189-208. DOI: 10.1007/s11157-020-09559-5.

Menon, S., and Ragsdale, S.W. (1996). Unleashing hydrogenase activity in carbon monoxide dehydrogenase/acetyl-CoA synthase and pyruvate:ferredoxin oxidoreductase. *Biochemistry* 35(49), 15814-15821. DOI: 10.1021/bi9615598.

Misra, H.P., and Fridovich, I. (1971). The Generation of Superoxide Radical during the Autoxidation of Ferredoxins. *Journal of Biological Chemistry* 246(22), 6886-6890. DOI: 10.1016/s0021-9258(19)45929-2.

Mock, J., Zheng, Y., Mueller, A.P., Ly, S., Tran, L., Segovia, S., et al. (2015). Energy Conservation Associated with Ethanol Formation from H_2 and CO_2 in *Clostridium autoethanogenum* Involving Electron Bifurcation. *J Bacteriol* 197(18), 2965-2980. DOI: 10.1128/JB.00399-15.

Mohr, T., Aliyu, H., Kuchlin, R., Polliack, S., Zwick, M., Neumann, A., et al. (2018). CO-dependent hydrogen production by the facultative anaerobe *Parageobacillus thermoglucosidasius*. *Microb Cell Fact* 17(1), 108. DOI: 10.1186/s12934-018-0954-3.

Molitor, B., Marcellin, E., and Angenent, L.T. (2017). Overcoming the energetic limitations of syngas fermentation. *Curr Opin Chem Biol* 41, 84-92. DOI: 10.1016/j.cbpa.2017.10.003.

Moreira, J.P.C., Diender, M., Arantes, A.L., Boeren, S., Stams, A.J.M., Alves, M.M., et al. (2021). Propionate production from carbon monoxide by synthetic co-cultures of *Acetobacterium wieringae* spp. and propionigenic bacteria. *Appl Environ Microbiol*. DOI: 10.1128/AEM.02839-20.

Morgulis, A., Coulouris, G., Raytselis, Y., Madden, T.L., Agarwala, R., and Schaffer, A.A. (2008). Database indexing for production MegaBLAST searches. *Bioinformatics* 24(16), 1757-1764. DOI: 10.1093/bioinformatics/btn322.

Myers, J.A., Curtis, B.S., and Curtis, W.R. (2013). Improving accuracy of cell and chromophore concentration measurements using optical density. *BMC Biophys* 6(1), 4. DOI: 10.1186/2046-1682-6-4.

NCBI (2018). "Database resources of the National Center for Biotechnology Information", in: *Nucleic Acids Res.* 2017/11/16 ed.).

Nguyen, D., and Khanal, S.K. (2018). A little breath of fresh air into an anaerobic system: How microaeration facilitates anaerobic digestion process. *Biotechnology Advances* 36(7), 1971-1983. DOI: 10.1016/j.biotechadv.2018.08.007.

Ntagia, E., Chatzigiannidou, I., Carvajal-Arroyo, J.M., Arends, J.B.A., and Rabaey, K. (2021). Continuous H_2/CO_2 fermentation for acetic acid production under transient and continuous sulfide inhibition. *Chemosphere* 285, 131536. DOI: 10.1016/j.chemosphere.2021.131536.

Nzeteu, C.O., Trego, A.C., Abram, F., and O'Flaherty, V. (2018). Reproducible, high-yielding, biological caproate production from food waste using a single-phase anaerobic reactor system. *Biotechnol Biofuels* 11, 108. DOI: 10.1186/s13068-018-1101-4.

Oswald, F., Stoll, I.K., Zwick, M., Herbig, S., Sauer, J., Boukis, N., et al. (2018a). Formic Acid Formation by *Clostridium ljungdahlii* at Elevated Pressures of Carbon Dioxide and Hydrogen. *Front Bioeng Biotechnol* 6, 6. DOI: 10.3389/fbioe.2018.00006.

Oswald, F., Zwick, M., Omar, O., Hotz, E.N., and Neumann, A. (2018b). Growth and Product Formation of *Clostridium ljungdahlii* in Presence of Cyanide. *Front Microbiol* 9, 1213. DOI: 10.3389/fmicb.2018.01213.

Paradis, E., Claude, J., and Strimmer, K. (2004). APE: Analyses of Phylogenetics and Evolution in R language. *Bioinformatics* 20(2), 289-290. DOI: 10.1093/bioinformatics/btg412.

Park, S., Yasin, M., Kim, D., Park, H.D., Kang, C.M., Kim, D.J., et al. (2013a). Rapid enrichment of (homo)acetogenic consortia from animal feces using a high mass-transfer gas-lift reactor fed with syngas. *J Ind Microbiol Biotechnol* 40(9), 995-1003. DOI: 10.1007/s10295-013-1292-4.

Park, S., Yasin, M., Kim, D., Roh, H., Choi, I.-G., and Chang, I.S. (Year). "Characterization of CO-Utilizing and Isovalerate Producing Acetogen; *Oscillibacter* sp. C5 Isolated from Cow Feces", in: *KSBB Spring Meeting*), 264-264.

Parks, D.H., Chuvochina, M., Waite, D.W., Rinke, C., Skarshewski, A., Chaumeil, P.A., et al. (2018). A standardized bacterial taxonomy based on genome phylogeny substantially revises the tree of life. *Nat Biotechnol* 36(10), 996-1004. DOI: 10.1038/nbt.4229.

Peters, J.W., Schut, G.J., Boyd, E.S., Mulder, D.W., Shepard, E.M., Broderick, J.B., et al. (2015). [FeFe]- and [NiFe]-hydrogenase diversity, mechanism, and maturation. *Biochim Biophys Acta* 1853(6), 1350-1369. DOI: 10.1016/j.bbamcr.2014.11.021.

Petrognani, C., Boon, N., and Ganigué, R. (2020). Production of isobutyric acid from methanol by *Clostridium luticellarii*. *Green Chemistry* 22(23), 8389-8402. DOI: 10.1039/d0gc02700f.

Pham, V., Holtzapple, M., and El-Halwagi, M. (2010). Techno-economic analysis of biomass to fuel conversion via the MixAlco process. *J Ind Microbiol Biotechnol* 37(11), 1157-1168. DOI: 10.1007/s10295-010-0763-0.

Phillips, J.R., Atiyeh, H.K., Tanner, R.S., Torres, J.R., Saxena, J., Wilkins, M.R., et al. (2015). Butanol and hexanol production in *Clostridium carboxidivorans* syngas fermentation: Medium development and culture techniques. *Bioresour Technol* 190, 114-121. DOI: 10.1016/j.biortech.2015.04.043.

Piwowarek, K., Lipinska, E., Hac-Szymanczuk, E., Kieliszek, M., and Scibisz, I. (2018). *Propionibacterium* spp.-source of propionic acid, vitamin B12, and other metabolites important for the industry. *Appl Microbiol Biotechnol* 102(2), 515-538. DOI: 10.1007/s00253-017-8616-7.

Plugge, C.M., Zhang, W., Scholten, J.C., and Stams, A.J. (2011). Metabolic flexibility of sulfate-reducing bacteria. *Front Microbiol* 2, 81. DOI: 10.3389/fmicb.2011.00081.

Poehlein, A., Bremekamp, R., Lutz, V.T., Schulz, L.M., and Daniel, R. (2018). Draft Genome Sequence of the Butanoic Acid-Producing Bacterium *Clostridium luticellarii* DSM 29923, Used for Strong Aromatic Chinese Liquor Production. *Genome Announc* 6(18). DOI: 10.1128/genomeA.00377-18.

Popp, D., Harms, H., and Sträuber, H. (2016). The alkaloid gramine in the anaerobic digestion process-inhibition and adaptation of the methanogenic community. *Appl Microbiol Biotechnol* 100(16), 7311-7322. DOI: 10.1007/s00253-016-7571-z.

Quast, C., Pruesse, E., Yilmaz, P., Gerken, J., Schweer, T., Yarza, P., et al. (2013). The SILVA ribosomal RNA gene database project: improved data processing and web-based tools. *Nucleic Acids Res* 41(Database issue), D590-596. DOI: 10.1093/nar/gks1219.

Rabaey, K., and Rozendal, R.A. (2010). Microbial electrosynthesis - revisiting the electrical route for microbial production. *Nat Rev Microbiol* 8(10), 706-716. DOI: 10.1038/nrmicro2422.

Ragsdale, S.W. (2004). Life with carbon monoxide. *Crit Rev Biochem Mol Biol* 39(3), 165-195. DOI: 10.1080/10409230490496577.

Ramachandriya, K.D., Kundiyana, D.K., Wilkins, M.R., Terrill, J.B., Atiyeh, H.K., and Huhnke, R.L. (2013). Carbon dioxide conversion to fuels and chemicals using a hybrid green process. *Applied Energy* 112, 289-299. DOI: 10.1016/j.apenergy.2013.06.017.

Ramio-Pujol, S., Ganigue, R., Baneras, L., and Colprim, J. (2014). Impact of formate on the growth and productivity of *Clostridium ljungdahlii* PETC and *Clostridium carboxidivorans* P7 grown on syngas. *Int Microbiol* 17(4), 195-204. DOI: 10.2436/20.1501.01.222.

Ramio-Pujol, S., Ganigue, R., Baneras, L., and Colprim, J. (2015). Incubation at 25 degrees C prevents acid crash and enhances alcohol production in *Clostridium carboxidivorans* P7. *Bioresour Technol* 192, 296-303. DOI: 10.1016/j.biortech.2015.05.077.

Rao, J.U., Rash, B.A., Nobre, M.F., da Costa, M.S., Rainey, F.A., and Moe, W.M. (2012). *Actinomyces naturae* sp. nov., the first *Actinomyces* sp. isolated from a non-human or animal source. *Antonie Van Leeuwenhoek* 101(1), 155-168. DOI: 10.1007/s10482-011-9644-4.

Reddy, M.V., ElMekawy, A., and Pant, D. (2018). Bioelectrochemical synthesis of caproate through chain elongation as a complementary technology to anaerobic digestion. *Biofuels Bioproducts & Biorefining-Biofpr* 12(6), 966-977. DOI: 10.1002/bbb.1924.

Ricaboni, D., Mailhe, M., Cadoret, F., Vitton, V., Fournier, P.E., and Raoult, D. (2017). 'Colidextribacter massiliensis' gen. nov., sp. nov., isolated from human right colon. *New Microbes New Infect* 17, 27-29. DOI: 10.1016/j.nmni.2016.11.023.

Richter, H., Loftus, S.E., and Angenent, L.T. (2013). Integrating syngas fermentation with the carboxylate platform and yeast fermentation to reduce medium cost and improve biofuel productivity. *Environ Technol* 34(13-16), 1983-1994. DOI: 10.1080/09593330.2013.826255.

Richter, H., Molitor, B., Diender, M., Sousa, D.Z., and Angenent, L.T. (2016a). A Narrow pH Range Supports Butanol, Hexanol, and Octanol Production from Syngas in a Continuous Co-culture of Clostridium ljungdahlii and Clostridium kluyveri with In-Line Product Extraction. *Front Microbiol* 7, 1773. DOI: 10.3389/fmicb.2016.01773.

Richter, H., Molitor, B., Wei, H., Chen, W., Aristilde, L., and Angenent, L.T. (2016b). Ethanol production in syngas-fermenting *Clostridium ljungdahlii* is controlled by thermodynamics rather than by enzyme expression. *Energy & Environmental Science* 9(7), 2392-2399. DOI: 10.1039/c6ee01108j.

Roghair, M., Hoogstad, T., Strik, D., Plugge, C.M., Timmers, P.H.A., Weusthuis, R.A., et al. (2018a). Controlling Ethanol Use in Chain Elongation by CO_2 Loading Rate. *Environ Sci Technol* 52(3), 1496-1505. DOI: 10.1021/acs.est.7b04904.

Roghair, M., Liu, Y., Adiatma, J.C., Weusthuis, R.A., Bruins, M.E., Buisman, C.J.N., et al. (2018b). Effect of *n*-Caproate Concentration on Chain Elongation and Competing Processes. *ACS Sustain Chem Eng* 6(6), 7499-7506. DOI: 10.1021/acssuschemeng.8b00200.

Rosenberg, E., DeLong, E.F., Lory, S., Stackebrandt, E., and Thompson, F. (2014). *The prokaryotes: Firmicutes and tenericutes.* Springer.

Sakamoto, M., Ikeyama, N., Toyoda, A., Murakami, T., Mori, H., Iino, T., et al. (2020). *Dialister hominis* sp. nov., isolated from human faeces. *Int J Syst Evol Microbiol* 70(1), 589-595. DOI: 10.1099/ijsem.0.003797.

Sander, R. (2015). Compilation of Henry's law constants (version 4.0) for water as solvent. *Atmospheric Chemistry and Physics* 15(8), 4399-4981. DOI: 10.5194/acp-15-4399-2015.

Savant, D.V., Shouche, Y.S., Prakash, S., and Ranade, D.R. (2002). *Methanobrevibacter acididurans* sp. nov., a novel methanogen from a sour anaerobic digester. *Int J Syst Evol Microbiol* 52(Pt 4), 1081-1087. DOI: 10.1099/00207713-52-4-1081.

Scarborough, M.J., Lawson, C.E., Hamilton, J.J., Donohue, T.J., and Noguera, D.R. (2018a). Metatranscriptomic and Thermodynamic Insights into Medium-Chain Fatty Acid Production Using an Anaerobic Microbiome. *Msystems* 3(6), e00221-00218. DOI: 10.1128/mSystems.00221-18.

Scarborough, M.J., Lynch, G., Dickson, M., McGee, M., Donohue, T.J., and Noguera, D.R. (2018b). Increasing the economic value of lignocellulosic stillage through medium-chain fatty acid production. *Biotechnol Biofuels* 11, 200. DOI: 10.1186/s13068-018-1193-x.

Scarborough, M.J., Myers, K.S., Donohue, T.J., and Noguera, D.R. (2020). Medium-Chain Fatty Acid Synthesis by "*Candidatus* Weimeria bifida" gen. nov., sp. nov., and "*Candidatus* Pseudoramibacter fermentans" sp. nov. *Appl Environ Microbiol* 86(3). DOI: 10.1128/AEM.02242-19.

Schink, B. (1985a). Fermentation of Acetylene by an Obligate Anaerobe, *Pelobacter acetylenicus* sp. nov. *Archives of Microbiology* 142(3), 295-301. DOI: Doi 10.1007/Bf00693407.

Schink, B. (1985b). Inhibition of Methanogenesis by Ethylene and Other Unsaturated-Hydrocarbons. *Fems Microbiology Ecology* 31(2), 63-68. DOI: Doi 10.1016/0378-1097(85)90001-1.

Schink, B. (1997). Energetics of syntrophic cooperation in methanogenic degradation. *Microbiol Mol Biol Rev* 61(2), 262-280. DOI: 10.1128/mmbr.61.2.262-280.1997.

Schliep, K., Potts, A.J., Morrison, D.A., Grimm, G.W., and Fitzjohn, R. (2017). Intertwining phylogenetic trees and networks. *Methods in Ecology and Evolution* 8(10), 1212-1220. DOI: 10.1111/2041-210x.12760.

Scholz, C.F.P., and Kilian, M. (2016). The natural history of cutaneous propionibacteria, and reclassification of selected species within the genus *Propionibacterium* to the proposed novel genera *Acidipropionibacterium* gen. nov., *Cutibacterium* gen. nov. and *Pseudopropionibacterium* gen. nov. *Int J Syst Evol Microbiol* 66(11), 4422-4432. DOI: 10.1099/ijsem.0.001367.

Schuchmann, K., and Muller, V. (2016). Energetics and Application of Heterotrophy in Acetogenic Bacteria. *Appl Environ Microbiol* 82(14), 4056-4069. DOI: 10.1128/AEM.00882-16.

Schuchmann, K., and Müller, V. (2014). Autotrophy at the thermodynamic limit of life: a model for energy conservation in acetogenic bacteria. *Nat Rev Microbiol* 12(12), 809-821. DOI: 10.1038/nrmicro3365.

Seeliger, S., Janssen, P.H., and Schink, B. (2002). Energetics and kinetics of lactate fermentation to acetate and propionate via methylmalonyl-CoA or acrylyl-CoA. *FEMS Microbiology Letters* 211(1), 65-70. DOI: 10.1111/j.1574-6968.2002.tb11204.x.

Seinfeld, J.H., and Pandis, S.N. (2016). *Atmospheric chemistry and physics: from air pollution to climate change.* John Wiley & Sons.

Shen, N., Dai, K., Xia, X.-Y., Zeng, R.J., and Zhang, F. (2018). Conversion of syngas (CO and H_2) to biochemicals by mixed culture fermentation in mesophilic and thermophilic hollow-fiber membrane biofilm reactors. *Journal of Cleaner Production* 202, 536-542. DOI: 10.1016/j.jclepro.2018.08.162.

Sikarwar, V.S., Zhao, M., Clough, P., Yao, J., Zhong, X., Memon, M.Z., et al. (2016). An overview of advances in biomass gasification. *Energy & Environmental Science* 9(10), 2939-2977. DOI: 10.1039/c6ee00935b.

Skidmore, B.E., Baker, R.A., Banjade, D.R., Bray, J.M., Tree, D.R., and Lewis, R.S. (2013). Syngas fermentation to biofuels: effects of hydrogen partial pressure on hydrogenase efficiency. *Biomass and Bioenergy* 55, 156-162.

Smet, A., Cools, P., Krizova, L., Maixnerova, M., Sedo, O., Haesebrouck, F., et al. (2014). *Acinetobacter gandensis* sp. nov. isolated from horse and cattle. *Int J Syst Evol Microbiol* 64(Pt 12), 4007-4015. DOI: 10.1099/ijs.0.068791-0.

Spirito, C.M., Richter, H., Rabaey, K., Stams, A.J., and Angenent, L.T. (2014). Chain elongation in anaerobic reactor microbiomes to recover resources from waste. *Curr Opin Biotechnol* 27, 115-122. DOI: 10.1016/j.copbio.2014.01.003.

Sprott, G.D., Jarrell, K.F., Shaw, K.M., and Knowles, R. (1982). Acetylene as an Inhibitor of Methanogenic Bacteria. *Journal of General Microbiology* 128(Oct), 2453-2462.

Stadtman, E.R., Stadtman, T.C., Pastan, I., and Smith, L.D. (1972). *Clostridium barkeri* sp. n. *J Bacteriol* 110(2), 758-760. DOI: 10.1128/jb.110.2.758-760.1972.

Stamatopoulou, P., Malkowski, J., Conrado, L., Brown, K., and Scarborough, M. (2020). Fermentation of Organic Residues to Beneficial Chemicals: A Review of Medium-Chain Fatty Acid Production. *Processes* 8(12), 1571. DOI: 10.3390/pr8121571.

Stams, A.J., de Bok, F.A., Plugge, C.M., van Eekert, M.H., Dolfing, J., and Schraa, G. (2006). Exocellular electron transfer in anaerobic microbial communities. *Environ Microbiol* 8(3), 371-382. DOI: 10.1111/j.1462-2920.2006.00989.x.

Steinbusch, K.J., Hamelers, H.V., and Buisman, C.J. (2008). Alcohol production through volatile fatty acids reduction with hydrogen as electron donor by mixed cultures. *Water Res* 42(15), 4059-4066. DOI: 10.1016/j.watres.2008.05.032.

Steinbusch, K.J.J., Hamelers, H.V.M., Plugge, C.M., and Buisman, C.J.N. (2011). Biological formation of caproate and caprylate from acetate: fuel and chemical production from low grade biomass. *Energy & Environmental Science* 4(1), 216-224. DOI: 10.1039/c0ee00282h.

Stiebritz, M.T., and Reiher, M. (2012). Hydrogenases and oxygen. *Chemical Science* 3(6). DOI: 10.1039/c2sc01112c.

Strach, K. (2020). "Determination of total solids (dry matter) and volatile solids (organic dry matter)," in *Series "Biomass Energy Use": Collection of Methods for Biogas: Methods to determine parameters for analysis purposes and parameters that describe processes in the biogas sector,* eds. J. Liebetrau, D. Pfeiffer & D. Thrän. 2nd ed (Leipzig: DBFZ).

Sträuber, H., Buhligen, F., Kleinsteuber, S., and Dittrich-Zechendorf, M. (2018). Carboxylic acid production from ensiled crops in anaerobic solid-state fermentation - trace elements as pH controlling agents support microbial chain elongation with lactic acid. *Eng Life Sci* 18(7), 447-458. DOI: 10.1002/elsc.201700186.

Sträuber, H., Lucas, R., and Kleinsteuber, S. (2016). Metabolic and microbial community dynamics during the anaerobic digestion of maize silage in a two-phase process. *Appl Microbiol Biotechnol* 100(1), 479-491. DOI: 10.1007/s00253-015-6996-0.

Strazzera, G., Battista, F., Tonanzi, B., Rossetti, S., and Bolzonella, D. (2021). Optimization of short chain volatile fatty acids production from household food waste for biorefinery applications. *Environmental Technology & Innovation* 23. DOI: 10.1016/j.eti.2021.101562.

Sutton, J.M., Baesman, S.M., Fierst, J.L., Poret-Peterson, A.T., Oremland, R.S., Dunlap, D.S., et al. (2017). Complete Genome Sequences of Two Acetylene-Fermenting *Pelobacter acetylenicus* Strains. *Genome Announc* 5(6), e01572-01516. DOI: 10.1128/genomeA.01572-16.

Takahashi, N., Kalfas, S., and Yamada, T. (1994). The role of the succinate pathway in sorbitol fermentation by oral *Actinomyces viscosus* and *Actinomyces naeslundii*. *Oral microbiology and immunology* 9(4), 218-223. DOI: 10.1111/j.1399-302X.1994.tb00061.x.

Takahashi, N., and Yamada, T. (1999). Effects of pH on the glucose and lactate metabolisms by the washed cells of *Actinomyces naeslundii* under anaerobic and aerobic conditions. *Oral microbiology and immunology* 14(1), 60-65. DOI: 10.1034/j.1399-302X.1999.140108.x.

Takors, R., Kopf, M., Mampel, J., Bluemke, W., Blombach, B., Eikmanns, B., et al. (2018). Using gas mixtures of CO, CO$_2$ and H$_2$ as microbial substrates: the do's and don'ts of successful

technology transfer from laboratory to production scale. *Microb Biotechnol* 11(4), 606-625. DOI: 10.1111/1751-7915.13270.

Thauer, R.K., Kaster, A.K., Goenrich, M., Schick, M., Hiromoto, T., and Shima, S. (2010). Hydrogenases from methanogenic archaea, nickel, a novel cofactor, and H_2 storage. *Annu Rev Biochem* 79, 507-536. DOI: 10.1146/annurev.biochem.030508.152103.

Tholozan, J.-L., Samain, E., and Grivet, J.-P. (1988). Isomerization between *n*-butyrate and isobutyrate in enrichment cultures. *FEMS Microbiology Letters* 53(3-4), 187-191. DOI: 10.1111/j.1574-6968.1988.tb02663.x.

Thompson, T., Conrad, R., and Zeikus, J. (1984). Regulation of carbon and electron flow in *Propionispira arboris*: physiological function of hydrogenase and its role in homopropionate formation. *FEMS microbiology letters* 22(3), 265-271. DOI: 10.1111/j.1574-6968.1984.tb00739.x.

Tomazetto, G., Hahnke, S., Wibberg, D., Puhler, A., Klocke, M., and Schluter, A. (2018). *Proteiniphilum saccharofermentans* str. M3/6(T) isolated from a laboratory biogas reactor is versatile in polysaccharide and oligopeptide utilization as deduced from genome-based metabolic reconstructions. *Biotechnol Rep (Amst)* 18, e00254. DOI: 10.1016/j.btre.2018.e00254.

UniProt-Consortium (2021). UniProt: the universal protein knowledgebase in 2021. *Nucleic Acids Res* 49(D1), D480-D489. DOI: 10.1093/nar/gkaa1100.

Urban, C., Xu, J.J., Sträuber, H., Dantas, T.R.D., Muhlenberg, J., Hartig, C., et al. (2017). Production of drop-in fuels from biomass at high selectivity by combined microbial and electrochemical conversion. *Energy & Environmental Science* 10(10), 2231-2244. DOI: 10.1039/c7ee01303e.

Vaishampayan, P., Miyashita, M., Ohnishi, A., Satomi, M., Rooney, A., La Duc, M.T., et al. (2009). Description of *Rummeliibacillus stabekisii* gen. nov., sp. nov. and reclassification of *Bacillus pycnus* Nakamura et al. 2002 as *Rummeliibacillus pycnus* comb. nov. *Int J Syst Evol Microbiol* 59(Pt 5), 1094-1099. DOI: 10.1099/ijs.0.006098-0.

Valgepea, K., de Souza Pinto Lemgruber, R., Abdalla, T., Binos, S., Takemori, N., Takemori, A., et al. (2018). H_2 drives metabolic rearrangements in gas-fermenting *Clostridium autoethanogenum*. *Biotechnol Biofuels* 11, 55. DOI: 10.1186/s13068-018-1052-9.

Vassilev, I., Hernandez, P.A., Batlle-Vilanova, P., Freguia, S., Kromer, J.O., Keller, J., et al. (2018). Microbial Electrosynthesis of Isobutyric, Butyric, Caproic Acids, and Corresponding Alcohols from Carbon Dioxide. *Acs Sustainable Chemistry & Engineering* 6(7), 8485-8493. DOI: 10.1021/acssuschemeng.8b00739.

Vassilev, I., Kracke, F., Freguia, S., Keller, J., Kromer, J.O., Ledezma, P., et al. (2019). Microbial electrosynthesis system with dual biocathode arrangement for simultaneous acetogenesis, solventogenesis and carbon chain elongation. *Chem Commun (Camb)* 55(30), 4351-4354. DOI: 10.1039/c9cc00208a.

Vasudevan, D., Richter, H., and Angenent, L.T. (2014). Upgrading dilute ethanol from syngas fermentation to *n*-caproate with reactor microbiomes. *Bioresour Technol* 151, 378-382. DOI: 10.1016/j.biortech.2013.09.105.

Wade, W.G. (2015). "*Eubacterium*," in *Bergey's Manual of Systematics of Archaea and Bacteria*.), 1-36.

Wallace, R.J., Chaudhary, L.C., Miyagawa, E., McKain, N., and Walker, N.D. (2004). Metabolic properties of *Eubacterium pyruvativorans*, a ruminal 'hyper-ammonia-producing' anaerobe with metabolic properties analogous to those of *Clostridium kluyveri*. *Microbiology (Reading)* 150(Pt 9), 2921-2930. DOI: 10.1099/mic.0.27190-0.

Wang, H., Li, X., Wang, Y., Tao, Y., Lu, S., Zhu, X., et al. (2018). Improvement of *n*-caproic acid production with Ruminococcaceae bacterium CPB6: selection of electron acceptors and

carbon sources and optimization of the culture medium. *Microb Cell Fact* 17(1), 99. DOI: 10.1186/s12934-018-0946-3.

Wang, J., and Yin, Y. (2022). Biological production of medium-chain carboxylates through chain elongation: An overview. *Biotechnol Adv* 55, 107882. DOI: 10.1016/j.biotechadv.2021.107882.

Wang, Q., Wang, C.D., Li, C.H., Li, J.G., Chen, Q., and Li, Y.Z. (2015). *Clostridium luticellarii* sp. nov., isolated from a mud cellar used for producing strong aromatic liquors. *Int J Syst Evol Microbiol* 65(12), 4730-4733. DOI: 10.1099/ijsem.0.000641.

Wang, S., Huang, H., Kahnt, J., Mueller, A.P., Köpke, M., and Thauer, R.K. (2013). NADP-specific electron-bifurcating [FeFe]-hydrogenase in a functional complex with formate dehydrogenase in *Clostridium autoethanogenum* grown on CO. *J Bacteriol* 195(19), 4373-4386. DOI: 10.1128/JB.00678-13.

Weghoff, M.C., Bertsch, J., and Muller, V. (2015). A novel mode of lactate metabolism in strictly anaerobic bacteria. *Environ Microbiol* 17(3), 670-677. DOI: 10.1111/1462-2920.12493.

Weimer, P.J., and Moen, G.N. (2013). Quantitative analysis of growth and volatile fatty acid production by the anaerobic ruminal bacterium *Megasphaera elsdenii* T81. *Appl Microbiol Biotechnol* 97(9), 4075-4081. DOI: 10.1007/s00253-012-4645-4.

Weimer, P.J., Nerdahl, M., and Brandl, D.J. (2015). Production of medium-chain volatile fatty acids by mixed ruminal microorganisms is enhanced by ethanol in co-culture with Clostridium kluyveri. *Bioresource technology* 175, 97-101.

Werner, J.J., Knights, D., Garcia, M.L., Scalfone, N.B., Smith, S., Yarasheski, K., et al. (2011). Bacterial community structures are unique and resilient in full-scale bioenergy systems. *Proc Natl Acad Sci U S A* 108(10), 4158-4163. DOI: 10.1073/pnas.1015676108.

Whitham, J.M., Tirado-Acevedo, O., Chinn, M.S., Pawlak, J.J., and Grunden, A.M. (2015). Metabolic response of *Clostridium ljungdahlii* to oxygen exposure. *Appl Environ Microbiol* 81(24), 8379-8391. DOI: 10.1128/AEM.02491-15.

Willems, A., and Collins, M.D. (2015). "*Pseudoramibacter*," in *Bergey's Manual of Systematics of Archaea and Bacteria*.), 1-8.

Wright, E.S. (2015). DECIPHER: harnessing local sequence context to improve protein multiple sequence alignment. *BMC Bioinformatics* 16, 322. DOI: 10.1186/s12859-015-0749-z.

Wu, Q., Guo, W., You, S., Bao, X., Luo, H., Wang, H., et al. (2019). Concentrating lactate-carbon flow on medium chain carboxylic acids production by hydrogen supply. *Bioresour Technol* 291, 121573. DOI: 10.1016/j.biortech.2019.121573.

Xu, J., Sun, L., Xing, X., Sun, Z., Gu, H., Lu, X., et al. (2020). Culturing Bacteria From Fermentation Pit Muds of Baijiu With Culturomics and Amplicon-Based Metagenomic Approaches. *Front Microbiol* 11, 1223. DOI: 10.3389/fmicb.2020.01223.

Yahya, L., Harun, R., and Abdullah, L.C. (2020). Screening of native microalgae species for carbon fixation at the vicinity of Malaysian coal-fired power plant. *Sci Rep* 10(1), 22355. DOI: 10.1038/s41598-020-79316-9.

Yang, G., and Wang, J. (2018). Pretreatment of grass waste using combined ionizing radiation-acid treatment for enhancing fermentative hydrogen production. *Bioresour Technol* 255, 7-15. DOI: 10.1016/j.biortech.2018.01.105.

Yasin, M., Jeong, Y., Park, S., Jeong, J., Lee, E.Y., Lovitt, R.W., et al. (2015). Microbial synthesis gas utilization and ways to resolve kinetic and mass-transfer limitations. *Bioresour Technol* 177, 361-374. DOI: 10.1016/j.biortech.2014.11.022.

Yilmaz, P., Parfrey, L.W., Yarza, P., Gerken, J., Pruesse, E., Quast, C., et al. (2014). The SILVA and "All-species Living Tree Project (LTP)" taxonomic frameworks. *Nucleic Acids Res* 42(Database issue), D643-648. DOI: 10.1093/nar/gkt1209.

Yutin, N., and Galperin, M.Y. (2013). A genomic update on clostridial phylogeny: Gram-negative spore formers and other misplaced clostridia. *Environ Microbiol* 15(10), 2631-2641. DOI: 10.1111/1462-2920.12173.

Zagrodnik, R., Duber, A., Lezyk, M., and Oleskowicz-Popiel, P. (2020). Enrichment Versus Bioaugmentation-Microbiological Production of Caproate from Mixed Carbon Sources by Mixed Bacterial Culture and *Clostridium kluyveri*. *Environ Sci Technol* 54(9), 5864-5873. DOI: 10.1021/acs.est.9b07651.

Zhang, F., Ding, J., Zhang, Y., Chen, M., Ding, Z.W., van Loosdrecht, M.C., et al. (2013). Fatty acids production from hydrogen and carbon dioxide by mixed culture in the membrane biofilm reactor. *Water Res* 47(16), 6122-6129. DOI: 10.1016/j.watres.2013.07.033.

Zhang, W., Dai, K., Xia, X.Y., Wang, H.J., Chen, Y., Lu, Y.Z., et al. (2018). Free acetic acid as the key factor for the inhibition of hydrogenotrophic methanogenesis in mesophilic mixed culture fermentation. *Bioresour Technol* 264, 17-23. DOI: 10.1016/j.biortech.2018.05.049.

Zheng, J., Wittouck, S., Salvetti, E., Franz, C., Harris, H.M.B., Mattarelli, P., et al. (2020). A taxonomic note on the genus Lactobacillus: Description of 23 novel genera, emended description of the genus *Lactobacillus* Beijerinck 1901, and union of *Lactobacillaceae* and *Leuconostocaceae*. *Int J Syst Evol Microbiol* 70(4), 2782-2858. DOI: 10.1099/ijsem.0.004107.

Zhu, X., Feng, X., Liang, C., Li, J., Jia, J., Feng, L., et al. (2021). Microbial Ecological Mechanism for Long-Term Production of High Concentrations of *n*-Caproate via Lactate-Driven Chain Elongation. *Appl Environ Microbiol* 87(11). DOI: 10.1128/AEM.03075-20.

Zhu, X., Tao, Y., Liang, C., Li, X., Wei, N., Zhang, W., et al. (2015). The synthesis of *n*-caproate from lactate: a new efficient process for medium-chain carboxylates production. *Sci Rep* 5, 14360. DOI: 10.1038/srep14360.

Zhu, X., Zhou, Y., Wang, Y., Wu, T., Li, X., Li, D., et al. (2017). Production of high-concentration *n*-caproic acid from lactate through fermentation using a newly isolated Ruminococcaceae bacterium CPB6. *Biotechnol Biofuels* 10, 102. DOI: 10.1186/s13068-017-0788-y.

Zhu, Y., and Yang, S.T. (2004). Effect of pH on metabolic pathway shift in fermentation of xylose by *Clostridium tyrobutyricum*. *J Biotechnol* 110(2), 143-157. DOI: 10.1016/j.jbiotec.2004.02.006.

Zinder, S.H., Anguish, T., and Cardwell, S.C. (1984). Selective inhibition by 2-bromoethanesulfonate of methanogenesis from acetate in a thermophilic anaerobic digestor. *Appl Environ Microbiol* 47(6), 1343-1345. DOI: 10.1128/AEM.47.6.1343-1345.1984.

List of figures

List of tables

List of abbreviations

2-BES: 2-Bromoethanosulfonate.

A.: *Acidipropionibacterium*.

AM: Acetotrophic (acetoclastic) methanogenesis.

ASV: Amplicon sequence variant.

BCR: Bubble column reactor.

C2: Acetate and ethanol.

C3: Propionate and propanol (lactate not included).

C4: *n*-Butyrate, *i*-butyrate, and *n*-butanol.

C6: *n*-Caproate, *i*-caproate, and *n*-hexanol.

C7: *n*-Heptanoate (enanthate).

C8: *n*-Caprylate.

Ca.: *Caproiciproducens*.

CE: Chain elongation.

Cl.: *Clostridium*.

CO: Carbon monoxide.

Co.: *Colidextribacter*.

DSP: Downstream processing.

E.: *Eubacterium*.

e^-: Electron equivalent.

ED: Electron donor.

ENA: European Nucleotide Archive

GC: Gas chromatography.

HM: Hydrogenotrophic methanogenesis.

HPLC: High performance liquid chromatography.

HRT: Hydraulic retention time.

LAB: Lactic acid bacteria.

M.: *Megasphaera*.

MCA: Medium-chain alcohol.

MCC: Medium-chain carboxylate.

ORP: Oxidation-reduction potential.

PBS: Phosphate-buffered saline (solution).

PCR: Polymerase chain reaction.

p.p: Percentage point.

RBO: Reverse β-oxidation.

RID: Refractive index detector.

ROS: Reactive oxygen species.

SCC: Short-chain carboxylate.

SF: Syngas fermentation.

SRB: Sulfate-reducing bacteria.

s.s.: Sensu stricto.

STR: Stirred-tank reactor.

TCD: Temperature conductivity detector.

TS: Total solids.

VS: Volatile solids.

WLP: Wood-Ljungdahl pathway (also known as reductive acetyl-CoA pathway).

Appendix A

Table A1. Duration of the experiments in Chapter 2 in days.

Experiment	Community A	Community B	Community C
Acidic pH values	51	-	21
Acetate concentration	63	92	63
Acidic/neutral pH or methanogenesis inhibition	77	48	77
Lactate and ethanol addition	26	40	26

Table A2. Components and conversion factors for carbon and electron balances.

Compound (formula)	Molar mass g mol^{-1}	mol C mol^{-1}	mol e$^-$ mol^{-1}
Biomass and yeast extract ($C_1H_{1.8}O_{0.5}N_{0.2}$)	24.6	1.0	4.2
Formic acid/formate ($C_1H_2O_2$)	46.0	1.0	2.0
Acetic acid/acetate ($C_2H_4O_2$)	60.0	2.0	8.0
Ethanol (C_2H_6O)	46.0	2.0	12.0
Propionic acid/propionate ($C_3H_6O_2$)	74.0	3.0	14.0
n-Propanol (C_3H_8O)	60.0	3.0	18.0
Lactic acid/lactate ($C_3H_6O_3$)	90.0	3.0	12.0
n-Butyric acid/n-butyrate ($C_4H_8O_2$)	88.0	4.0	20.0
i-Butyric acid/i-butyrate ($C_4H_8O_2$)	88.0	4.0	20.0
n-Butanol ($C_4H_{10}O$)	74.0	4.0	24.0
n-Valeric acid/n-valerate ($C_5H_{10}O_2$)	102.1	5.0	26.0
i-Valeric acid/i-valerate ($C_5H_{10}O_2$)	102.1	5.0	26.0
n-Pentanol ($C_5H_{12}O$)	88.1	5.0	30.0
n-Caproic acid/n-caproate ($C_6H_{12}O_2$)	116.1	6.0	32.0
i-Caproic acid/i-caproate ($C_6H_{12}O_2$)	116.1	6.0	32.0
n-Hexanol ($C_6H_{14}O$)	102.1	6.0	36.0
n-Heptanoic acid/n-heptanoate ($C_7H_{14}O_2$)	129.1	7.0	38.0
n-Caprylic acid/n-caprylate ($C_8H_{16}O_2$)	143.1	8.0	44.0
H_2	2.0	0.0	2.0
CO_2	44.0	1.0	0.0
CO	28.0	1.0	2.0
CH_4	16.0	1.0	8.0

Table A3. Production rates of *n*-butyrate and *n*-caproate for the experiments in Chapter 2 in mg L^{-1} d^{-1}. Errors are standard errors.

Experiment	Condition	Community A				Community B				Community C			
		n-Butyrate		*n*-Caproate		*n*-Butyrate		*n*-Caproate		*n*-Butyrate		*n*-Caproate	
		H_2-free	w/ H_2	H_2-free	w/ H_2	H_2-free	w/ H_2	H_2-free	w/ H_2	H_2-free	w/ H_2	H_2-free	w/ H_2
Acidic pH values	pH 4.8	9.7 ± 0.5	11 ± 2	11 ± 1	9.5 ± 0.6	-	-	-	-	5.0 ± 0.2	13.5 ± 0.2	1.2 ± 0.8	5 ± 1
	pH 5.5	46 ± 3	57 ± 2	11 ± 2	12.8 ± 0.1	-	-	-	-	3 ± 2	1.1 ± 0.2	3.3 ± 0.9	4 ± 1
Acetate concentration	Acetate 100 mM	0.2 ± 0.9	16 ± 5	-0.8 ± 0.1	-0.4 ± 0.1	1.0 ± 0.4	5 ± 2	5.6 ± 0.7	6.2 ± 0.4	1.9 ± 0.3	8 ± 2	0.1 ± 0.2	2 ± 1
	Acetate 200 mM	0 ± 1	12 ± 2	-0.1 ± 0.4	-0.4 ± 0.1	3.0 ± 0.1	12.0 ± 0.2	4.6 ± 0.1	5.8 ± 0.7	2.7 ± 0.2	14 ± 4	0.3 ± 0.4	3.9 ± 0.8
Acidic/neutral pH or methanogenesis inhibition	pH 5.5 or uninhibited	0.3 ± 0.2	19 ± 9	0.0 ± 0.0	0.0 ± 0.0	4.5 ± 0.0	23 ± 1	4.2 ± 0.1	25.7 ± 0.7	1.2 ± 0.4	12 ± 8	0.7 ± 0.3	4 ± 2
	pH 7.0 or inhibited	0.3 ± 0.1	-0.5 ± 0.1	0.0 ± 0.0	0.0 ± 0.0	4.3 ± 0.2	32 ± 3	4 ± 1	14 ± 6	2 ± 1	30 ± 17	2 ± 1	10 ± 3
Lactate and ethanol addition	pH 5.5 or uninhibited	181 ± 8	317 ± 107	0.0 ± 0.0	8 ± 10	44.4 ± 0.7	49 ± 22	34 ± 1	86 ± 17	116.2 ± 0.6	190 ± 12	76.2 ± 0.4	72 ± 2
	pH 7.0 or inhibited	35	172.9 ± 0.7	0	0.0 ± 0.0	49 ± 8	32 ± 39	33 ± 4	61.0 ± 0.5	116.1 ± 0.3	167	43 ± 10	107

Table A4. Taxonomy table with the 30 most abundant ASVs in the experiments of Chapter 2. The closest cultured species are shown together with their BLAST similarity and the NCBI accession number. *ASV_0017 also has 100% similarity with an isolate from reactor A (Liu et al., 2020b; Liu et al., 2020c), i.e. Clostridiales bacterium isolate BL-6 (LR778135.1).

	Family	Genus	Most similar cultured species (BLAST similarity, accession number)
ASV_0001	Clostridiaceae	*Clostridium* sensu stricto 12	*Clostridium tyrobutyricum* (100%, NR_044718.2)
ASV_0002	Methanobacteriaceae	*Methanobacterium*	*Methanobacterium congolense* (98.7%, NR_028175.1)
ASV_0003	Clostridiaceae	*Clostridium* sensu stricto 12	*Clostridium luticellarii* (98.3%, NR_145907.1)
ASV_0004	Methanobacteriaceae	*Methanobacterium*	*Methanobacterium congolense* (98.2%, NR_028175.1)
ASV_0005	Clostridiaceae	*Clostridium* sensu stricto 12	*Clostridium luticellarii* (99.0%, NR_145907.1)
ASV_0006	Anaerovoracaceae	-	*Eubacterium pyruvativorans* (92.0%, NR_042074.1)
ASV_0007	Anaerovoracaceae	-	*Eubacterium pyruvativorans* (91.8%, NR_042074.1)
ASV_0008	Anaerovoracaceae	-	*Eubacterium pyruvativorans* (92.1%, NR_042074.1)
ASV_0009	Clostridiaceae	*Clostridium* sensu stricto 12	*Clostridium luticellarii* (99.8%, NR_145907.1)
ASV_0010	Ruminococcaceae	*Caproiciproducens*	*Caprobacter fermentans* (95.0%, MN851263.1)
ASV_0011	Methanobacteriaceae	*Methanobrevibacter*	*Methanobrevibacter boviskoreani* (100%, NR_118565.1)
ASV_0012	Atopobiaceae	*Olsenella*	*Olsenella scatoligenes* (100%, NR_134781.1)
ASV_0016	Lactobacillaceae	*Lactobacillus*	*Lactobacillus mucosae* (100%, MT613566.1)
ASV_0017*	Ruminococcaceae	*Caproiciproducens*	*[Clostridium] sporosphaeroides* (96.8%, NR_044835.2)
ASV_0018	Peptostreptococcales-Tissierellales	-	*Soehngenia saccharolytica* (92.8%, NR_117382.1)
ASV_0020	Oscillospiraceae	*Oscillibacter*	*Oscillibacter ruminantium* (92.1%, NR_118156.1)
ASV_0021	Clostridiaceae	*Clostridium* sensu stricto 12	*Clostridium luticellarii* (97.8%, NR_145907.1)
ASV_0022	Limnochordia class	-	*Natranaerobaculum magadiense* (88.8%, NR_135713.1)
ASV_0029	Ruminococcaceae	*Caproiciproducens*	*Caprobacter fermentans* (95.0%, MN851263.1)
ASV_0033	Veillonellaceae	*Megasphaera*	*Megasphaera hexanoica* (100%, NR_157635.1)
ASV_0035	Actinomycetaceae	*Actinomyces*	*Actinomyces polynesiensis* (100%, NR_144691.1)
ASV_0036	Lactobacillaceae	*Lactobacillus*	*Lactobacillus mucosae* (100%, MT539050.1)
ASV_0038	Erysipelotrichaceae	*Solobacterium*	*Anaerorhabdus furcosa* (90.8%, NR_117779.1)
ASV_0039	Acidaminococcaceae	*Acidaminococcus*	*Acidaminococcus fermentans* (96.3%, NR_037018.1)
ASV_0042	Lachnospiraceae	*Syntrophococcus*	*[Eubacterium] cellulosolvens* (95.2%, NR_026106.1)
ASV_0043	Limnochordia class	-	*Sporanaerobacter acetigenes* (87.8%, NR_117381.1)
ASV_0048	Veillonellaceae	*Megasphaera*	*Megasphaera elsdenii* (99.8%, NR_113306.1)
ASV_0051	Peptostreptococcales-Tissierellales	-	*Soehngenia saccharolytica* (93.0%, NR_117382.1)
ASV_0054	Propionibacteriaceae	*Cutibacterium*	*Cutibacterium avidum* (99.5%, NR_118647.1)
ASV_0073	Coriobacteriales Incertae Sedis	-	*Gordonibacter pamelaeae* (91.1%, MK544834.1)

(A)

(B)

(C)
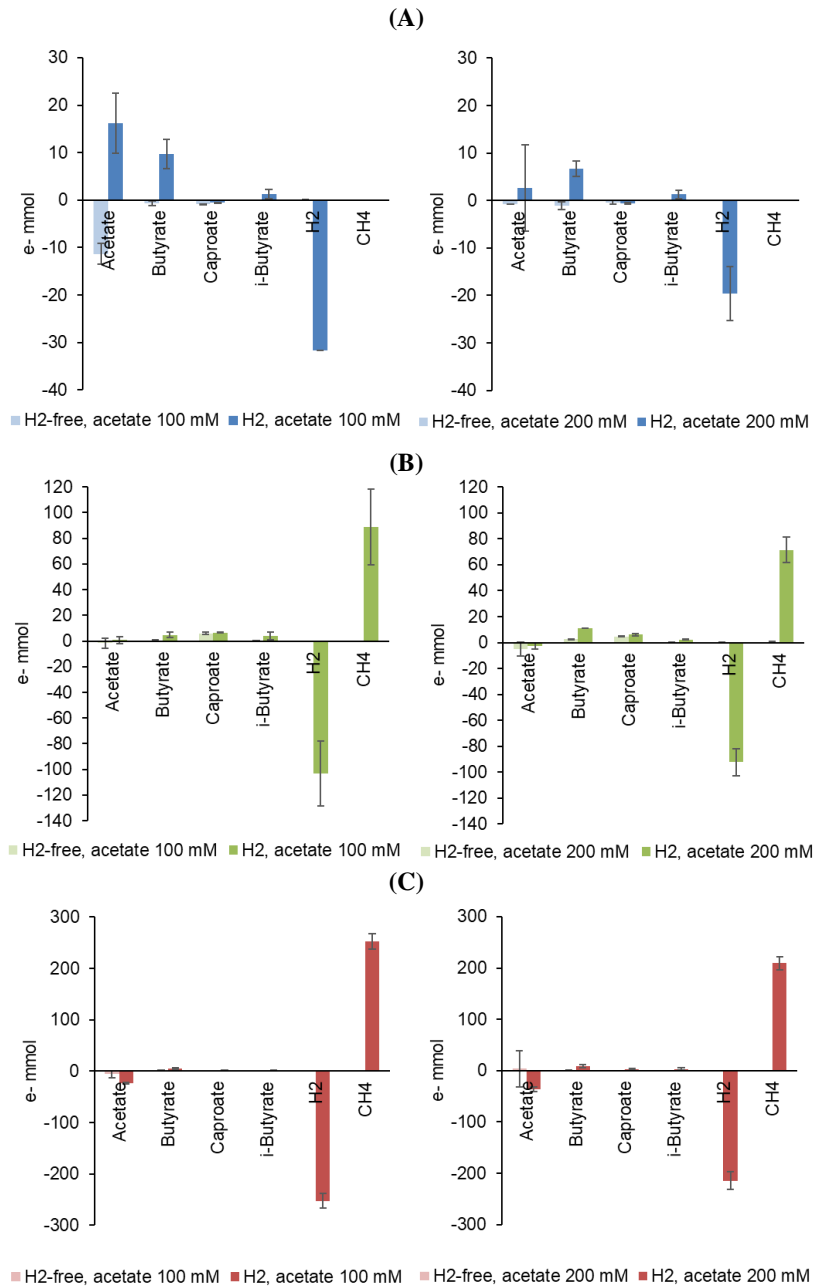
Figure A1. Electron balances for the acetate concentration experiment with communities A (**a**), B (**b**), and C (**c**) in equivalent mmol of electrons. Biomass, lactate, propionate, and *n*-valerate are not shown due to negligible variations for these components. Error bars indicate standard errors.

(A)　　　　　　**(B)**
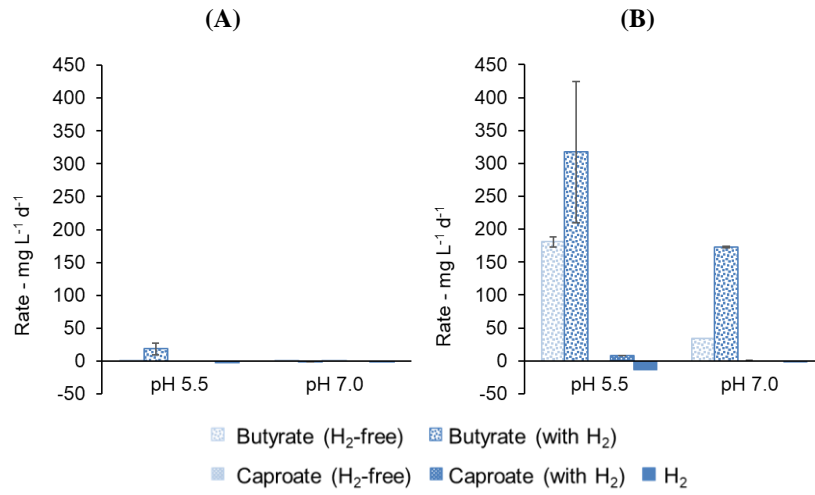
Figure A2. Effects of pH and H_2 before (**a**) and after (**b**) ethanol and lactate addition on rates of *n*-caproate, *n*-butyrate, and H_2 by community A. One of the duplicates of community A without H_2 at pH 7.0 in **b** was lost and no standard error bar is shown for this condition. Error bars are standard errors.
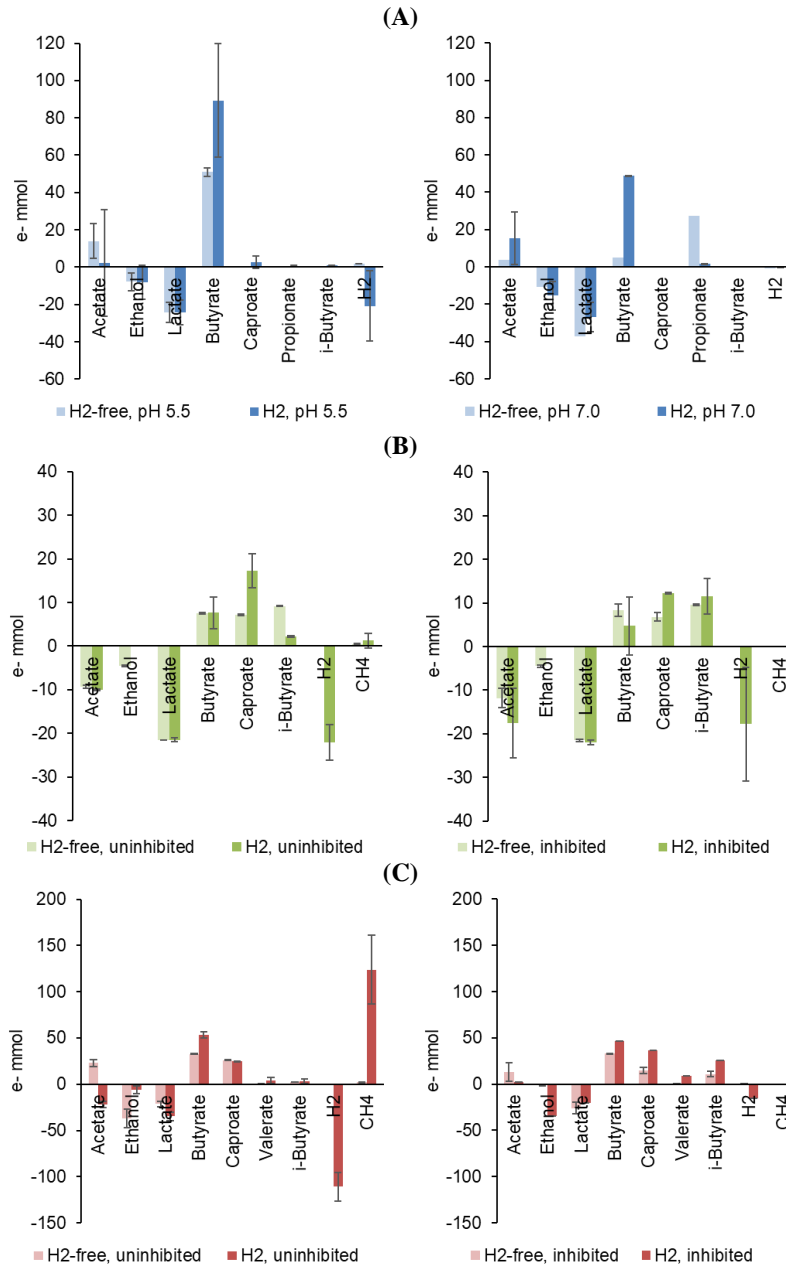
Figure A3. Electron balances for the lactate and ethanol addition experiment of Chapter 2 for communities A (**a**), B (**b**), and C (**c**) in equivalent mmol of electrons. Components that had negligible variation throughout the experiment are omitted. Error bars indicate standard errors.

(A) **(B)**
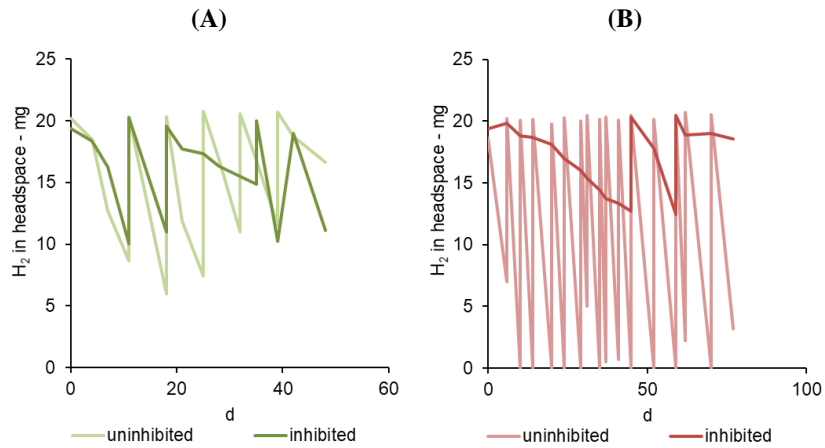
Figure A4. Amount of H₂ in the headspace for communities B (**a**) and C (**b**) in the methanogenesis inhibition experiment of Chapter 2. In community B neither inhibited nor uninhibited bottles had complete H₂ depletion. On the other hand, uninhibited culture bottles with community C faced H₂ depletion often.

(A) **(B)**
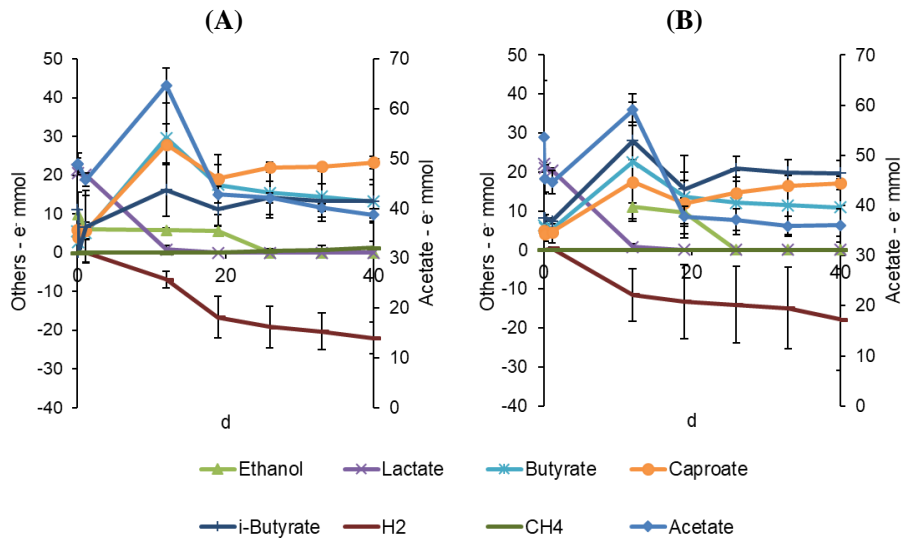
Figure A5. Kinetics profiles for community B of Chapter 2 after lactate and ethanol addition to the bottles without (**a**) and with (**b**) methanogenesis inhibitor. Error bars indicate standard errors.
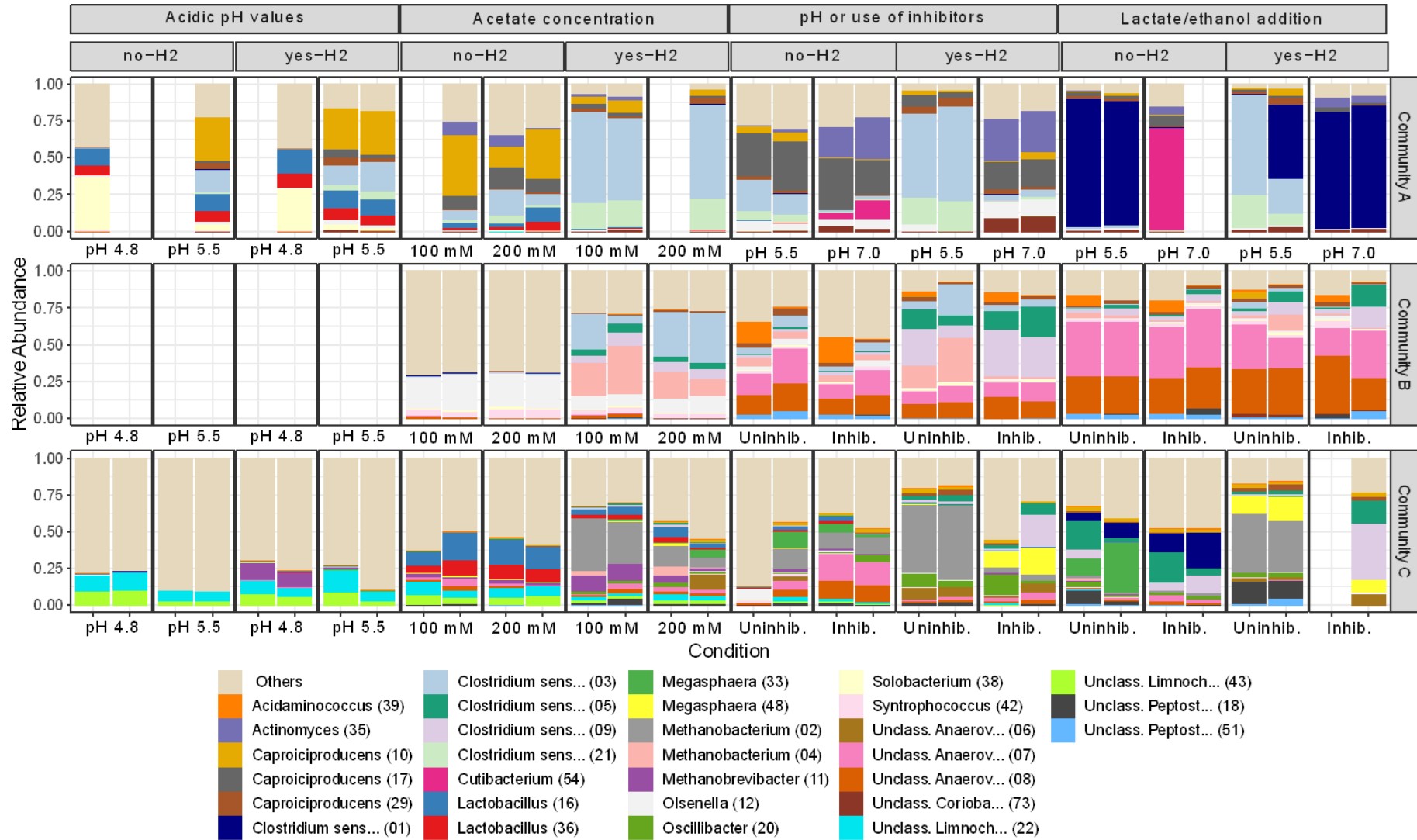
Figure A6. Community profiles at each condition tested in the study resolved to the ASV level for the 30 most abundant ASVs in the dataset (ASV number in parenthesis). Duplicates are shown. Slots left blank represent samples that could not be sequenced.
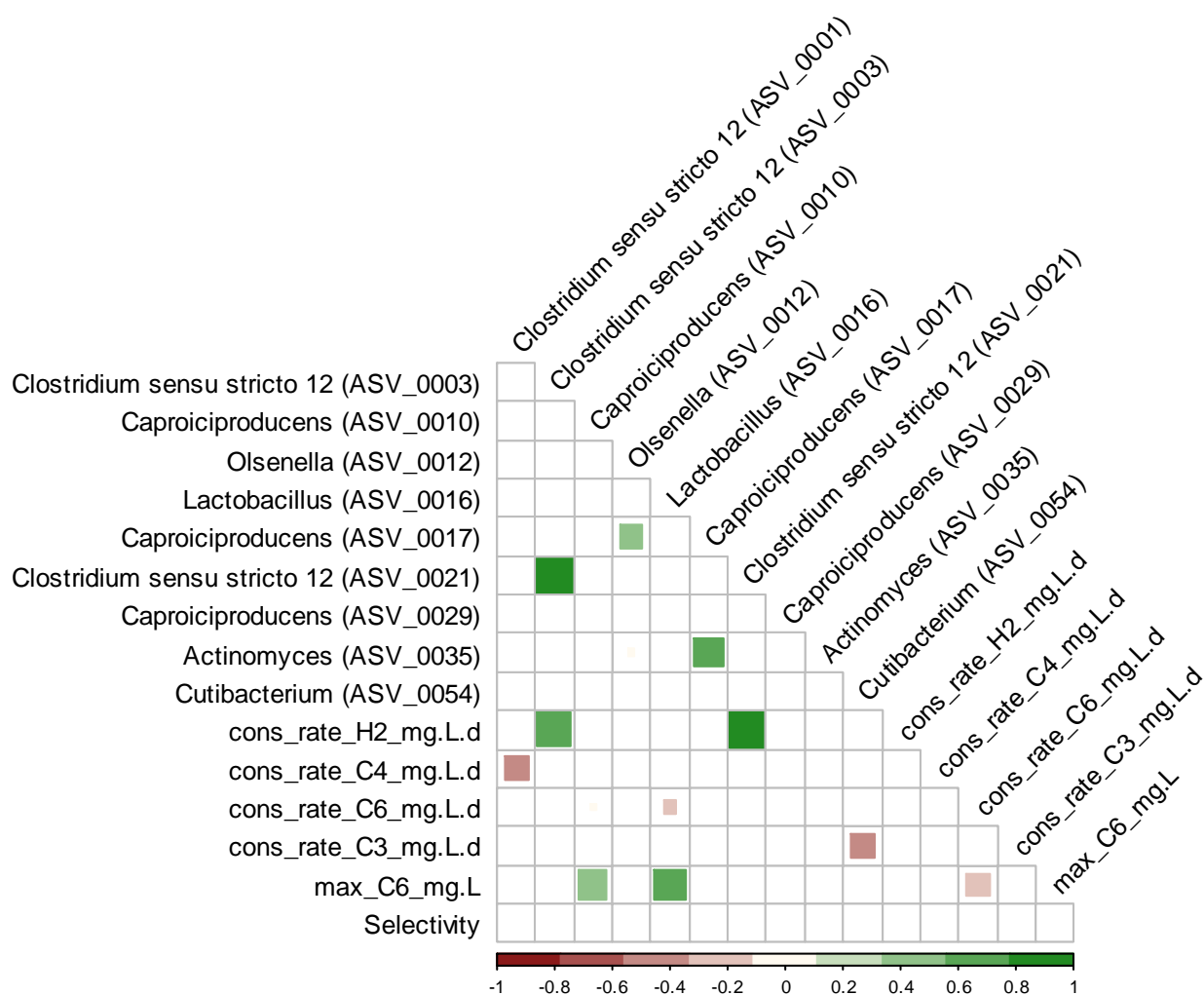
Figure A7. Spearman correlations (p<0.01) between the 10 most abundant ASVs of community A and abiotic parameters (rates of H₂, *n*-butyrate, *n*-caproate, and propionate, as well as maximum *n*-caproate concentration, and selectivity of EDs to *n*-caproate). As a convention, all rates are presented as consumption rates. Thus, a negative correlation to *n*-caproate consumption rate is equivalent to a positive correlation to *n*-caproate formation rate and vice-versa.
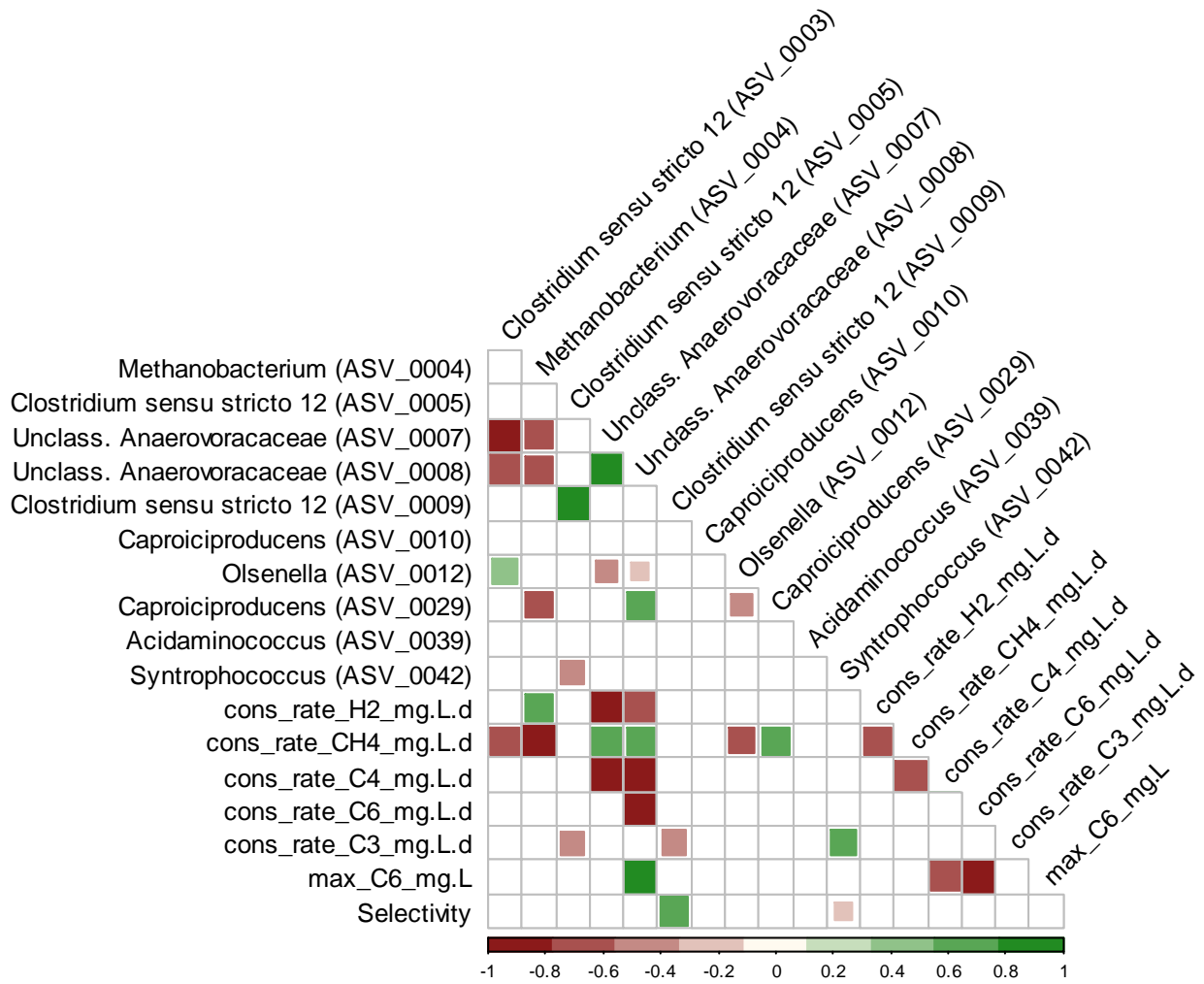
Figure A8. Spearman correlations (p<0.01) between the 10 most abundant ASVs of community B, ASV 10, and abiotic parameters (rates of H_2, CH_4, *n*-butyrate, *n*-caproate, and propionate, as well as maximum *n*-caproate concentration, and selectivity of EDs to *n*-caproate). As a convention, all rates are presented as consumption rates. Thus, a negative correlation to *n*-caproate consumption rate is equivalent to a positive correlation to *n*-caproate formation rate.
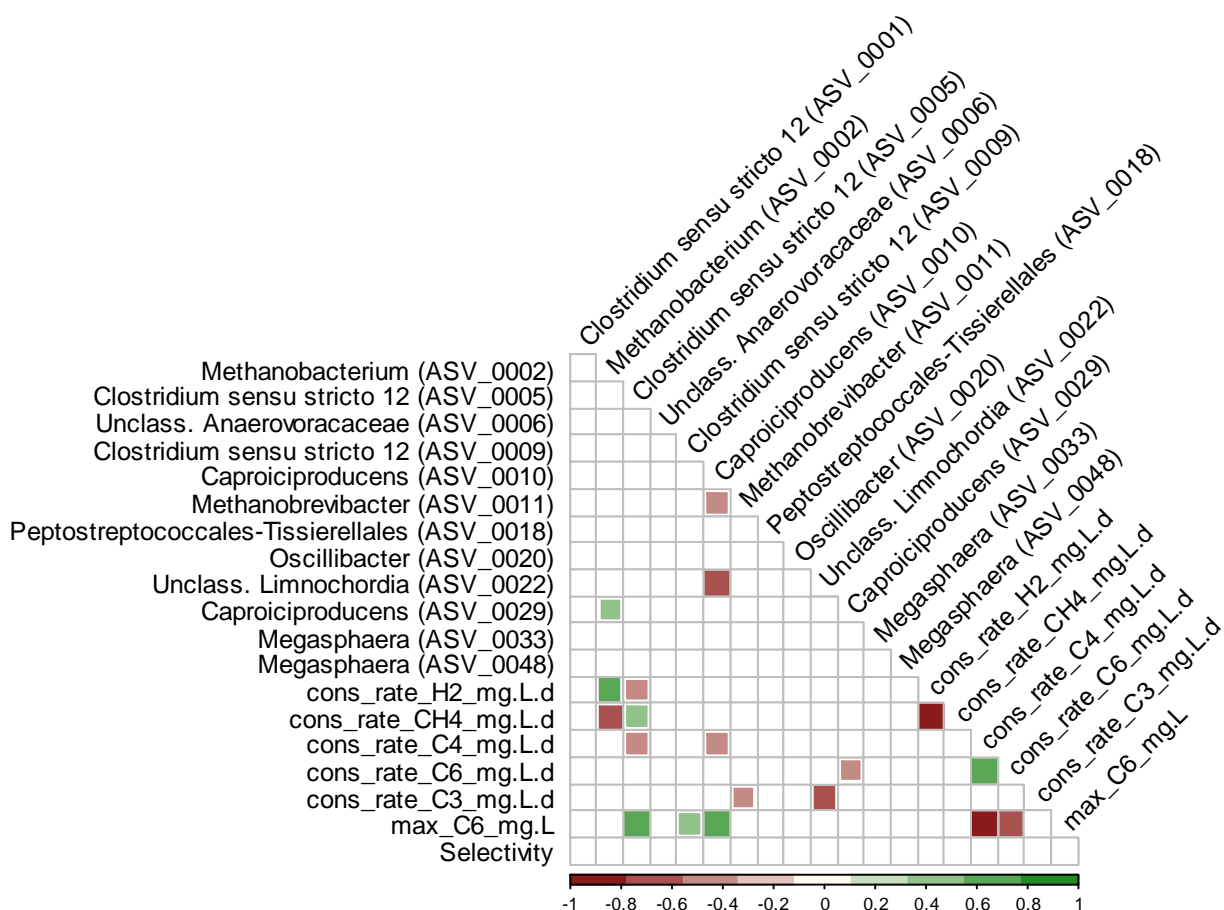
Figure A9. Spearman correlations (p<0.01) between the 10 most abundant ASVs of community C, ASV 6, ASV 10, ASV 29 and abiotic parameters (rates of H_2, CH_4, *n*-butyrate, *n*-caproate, and propionate, as well as maximum *n*-caproate concentration, and selectivity of EDs to *n*-caproate). As a convention, all rates are presented as consumption rates. Thus, a negative correlation to *n*-caproate consumption rate is equivalent to a positive correlation to *n*-caproate formation rate.

Appendix B

B.1. Mineral medium preparation

All medium ingredients (Table B1), except vitamins and cysteine, were mixed under oxic conditions. After adjusting the pH to 6.0 with 4 M NaOH, the mixture was stirred (700 rpm) in an anaerobic chamber (1-5% H_2 with the rest as N_2) for at least 3 hours to be make it anoxic. The anoxic solution was transferred to a glass bottle and capped and autoclaved at 121°C for 20 minutes. Stock solutions with vitamins and with cysteine were prepared separately and were only mixed with the rest of the ingredients on the day of the start of the batch experiment inside the anaerobic chamber. The vitamin and cysteine stock solutions were stored in serum bottles sealed with butyl rubber stoppers and aluminum crimps. The concentrated 30 g L^{-1} cysteine hydrochloride solution was prepared with anoxic, deionized water inside an anaerobic chamber and was made sterile by autoclaving at 121°C for 20 minutes. The 1000-fold concentrated vitamin stock solution was sterilized with a nylon 0.22 μm syringe filter and then made anoxic with at least 15 pressurization-depressurization cycles with pure N_2 lasting 2 min each.

B.2. Further details on the experimental setup

The experiments described in Figure 14 were divided into three batches lasting between 31 and 38 d depending on the carboxylate production. The first batch lasted 31 d and compared different starting communities (the autochthonous and the syngas-adapted communities) as well as the way of inoculating the adapted community (with washed cells, 10 vol % reactor broth, or 100 vol % reactor broth). This batch was realized under a syngas atmosphere with 49 kPa H_2, 49 kPa CO, and 24 kPa CO_2. The second batch lasted 35 d and compared the effects of the presence or absence of H_2 and CO on the autochthonous community and on the adapted community. The third batch lasted 38 d and tested the adapted community under intermediate partial pressures of CO (from 0 to 30 kPa). During this batch, the effect of 1.5 kPa ethylene (at 0 and 5 kPa CO) and the effect of the addition of 5 g L^{-1} formate (at 9 kPa CO) were also tested.

Table B1. Mineral medium composition.

Major components - g L^{-1}	
NH$_4$Cl	1.61
KH$_2$PO$_4$	13.6
NaCl	2.0
NaOH (approx.)	>1.0 (correction to pH 6.0)
Minor components - mg L^{-1}	
MgCl$_2$ × 6 H$_2$O	54
CaCl$_2$ × 2 H$_2$O	65
Resazurin	0.5
Cysteine hydrochloride	30
Transition metals, selenium, and boron - µg L^{-1}	
FeCl$_2$ × 4 H$_2$O	1500
CuCl$_2$ × 2 H$_2$O	2.0
CoCl$_2$ × 6 H$_2$O	190
MnCl$_2$	100
Na$_2$MoO$_4$ × 2 H$_2$O	36
NiCl$_2$ × 6 H$_2$O	24
Na$_2$WO$_4$ × 2 H$_2$O	20
Na$_2$SeO$_3$ × 5 H$_2$O	3.0
ZnCl$_2$	70
H$_3$BO$_3$	6.0
Vitamins - µg L^{-1}	
Biotin	20
Folic acid	20
Pyridoxine	100
Thiamine	50
Riboflavin	50
Niacin	50
Calcium pantothenate	50
Cobalamin	20
p-Aminobenzoic acid	80
Lipoic acid	50

Figure B1. Concentration of organic acids and electron balances in the abiotic controls. Mean values of duplicate bottles are shown. Error bars indicate standard errors.
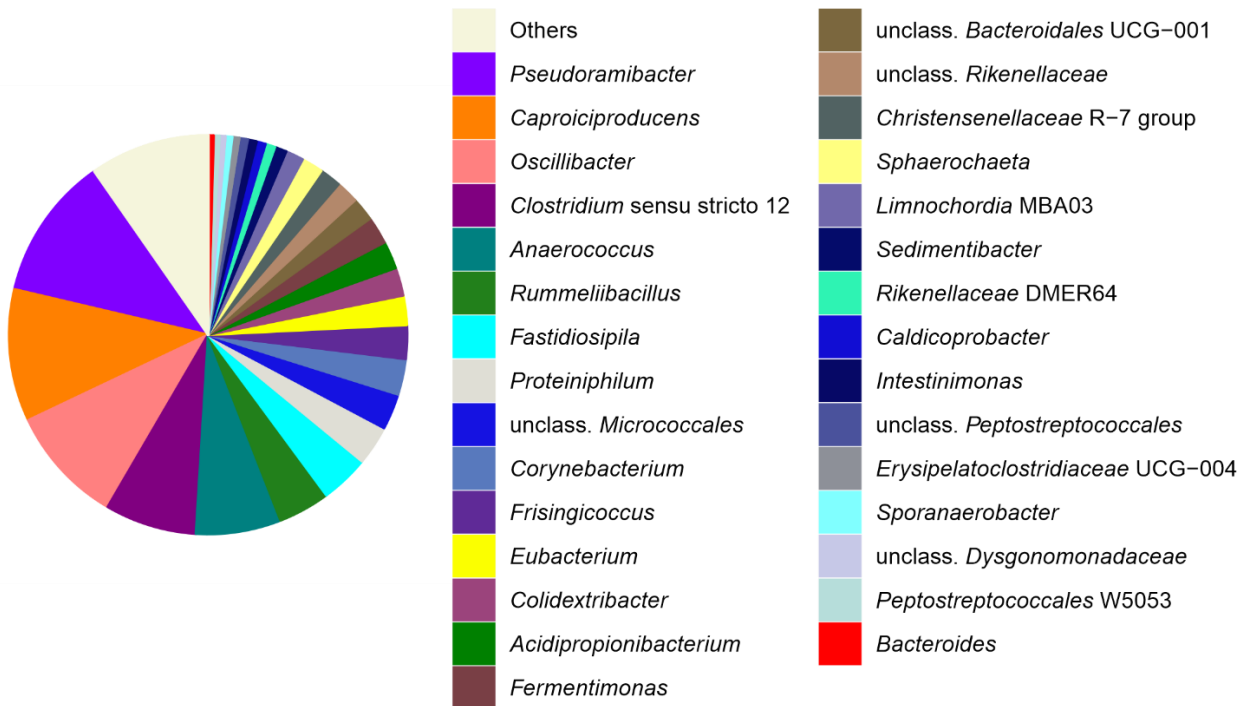
Figure B2. Composition of the syngas-adapted community used as inoculum. The 30 most abundant genera are shown.
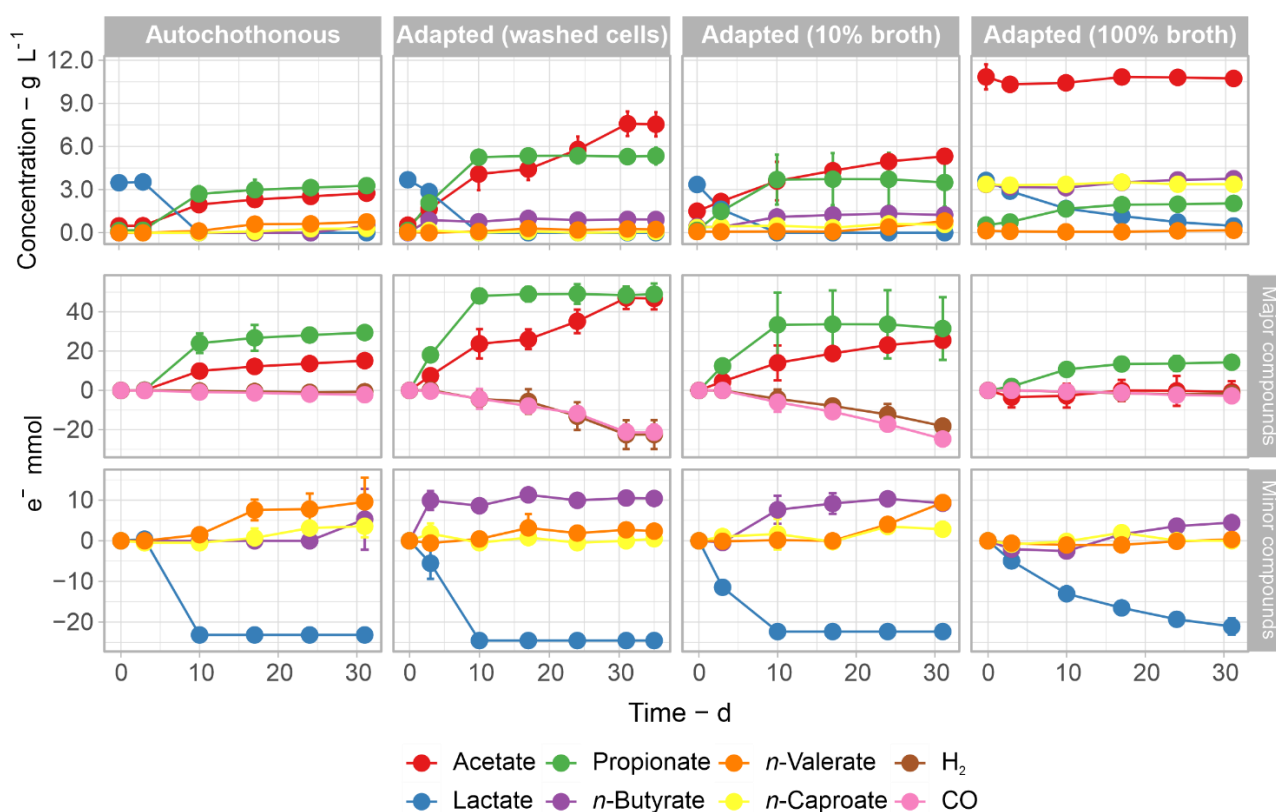
Figure B3. Concentration of organic acids and electron balances during the fermentation of corn silage + syngas ($H_2/CO/CO_2$ ratio of 49:49:24 kPa) depending on the inoculation with the syngas-adapted community (see Figure B2). From left to right: autochthonous community (corn silage community only), inoculation with the adapted community (washed cells), inoculation with 10 vol% reactor broth, and inoculation with 100 vol% reactor broth. Mean values of duplicate bottles are shown. Error bars indicate standard errors.

B.3. Inoculation with a syngas-adapted community

Regardless of the initial microbial community, production of carboxylates with more than three carbon atoms (i.e. n-butyrate, n-valerate, and n-caproate) remained less than 1.5 g L^{-1} (Figure B3). Besides, no methane formation was observed. Cultures that contained only the autochthonous community of corn silage presented a longer lag phase than bottles inoculated with the adapted community, as evidenced by the late start of lactate consumption. Still, the autochthonous community started to slowly consume CO in the middle of the batch.

In comparison to the fermentations with the corn silage community alone, inoculation with the adapted community via washed cells or via the addition of 10 vol% reactor broth caused higher production of acetate and propionate. In addition, the highest H_2 and CO consumption was also observed in these two sets. Originally, the reactor broth used for the inoculation contained a high concentration of carboxylates (ca. 11 g L^{-1} acetate, 4.5 g L^{-1} C4 carboxylates, and 2.6 g L^{-1} n-caproate). Therefore, when 100 vol% of the enrichment reactor broth was used as inoculum, the carboxylates present in the broth strongly inhibited the fermentation of corn silage and syngas, and only a slow conversion of the lactate from corn silage into propionate was

observed. The carboxylates from the broth that entered the bottles via inoculation were neither consumed nor converted into alcohols.
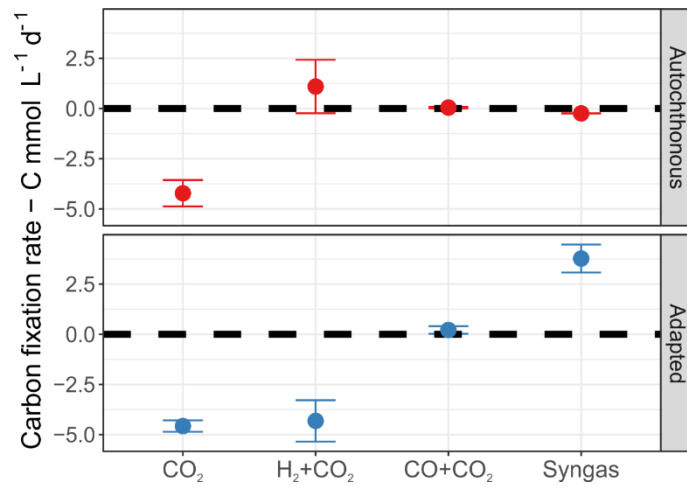
Figure B4. Carbon fixation rates achieved with the autochthonous corn silage community and with the inoculated (adapted) community at different components of syngas. Mean values of duplicate bottles are shown. Error bars indicate standard errors.
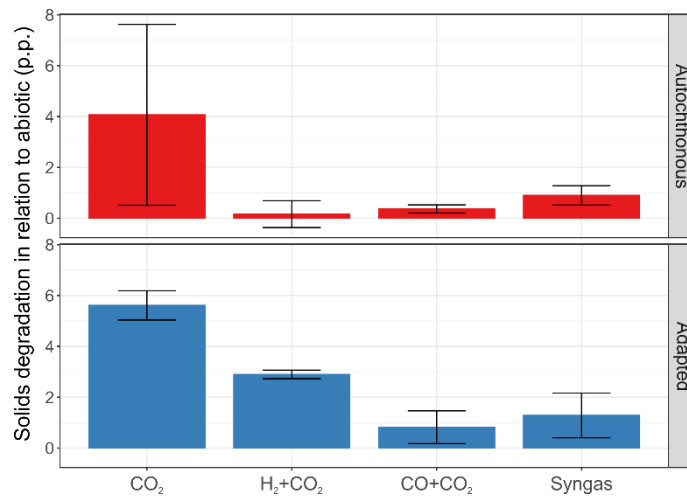
Figure B5. Solids degradation relative to the abiotic controls (in percentage points, p.p.) during the fermentation of corn silage in the presence of different gases and with different inocula. Mean values of duplicate bottles are shown. Error bars indicate standard errors.
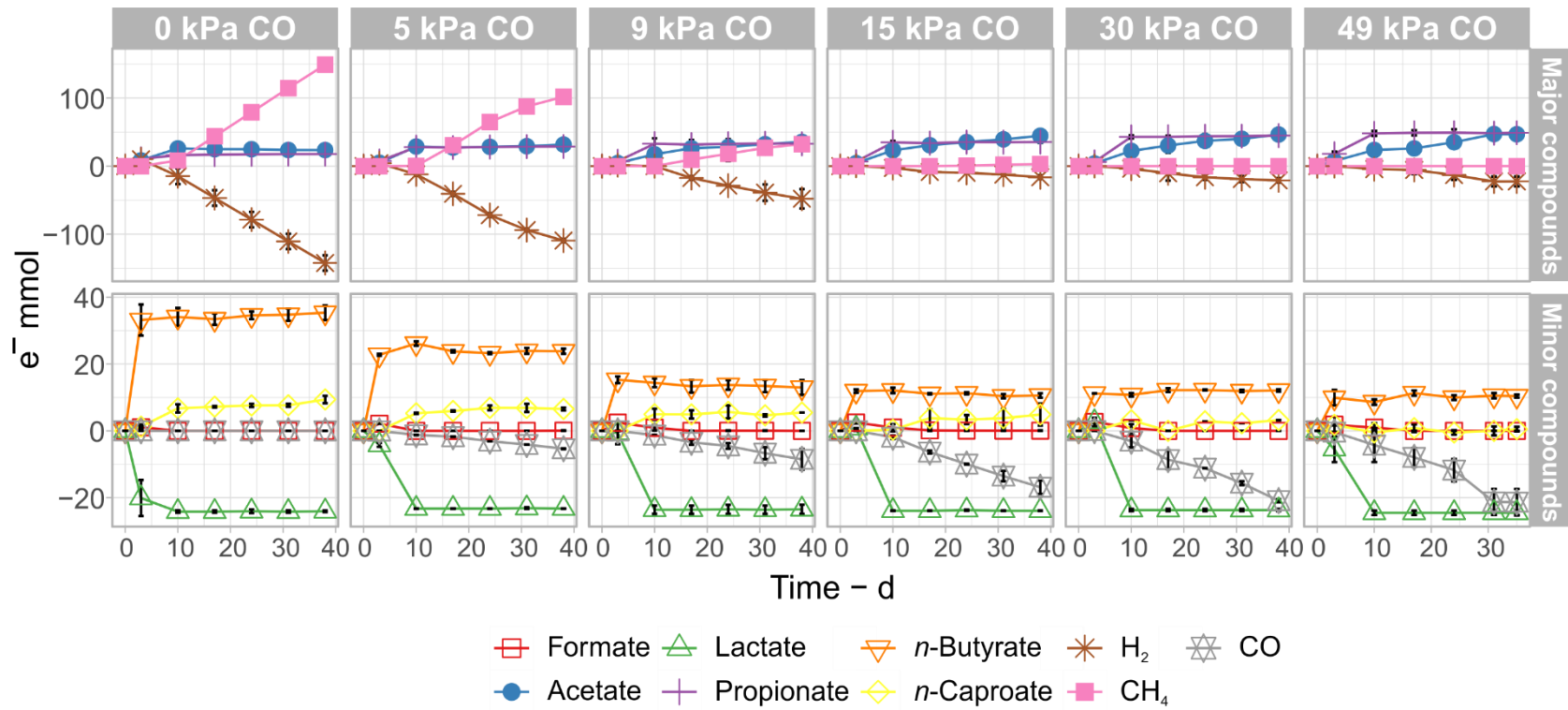
Figure B6. Electron balance kinetics for fermentations of corn silage in the presence of different partial pressures of CO. Cultures inoculated with the adapted community were used for this experiment. Mean values of duplicate bottles are shown. Error bars indicate standard errors.
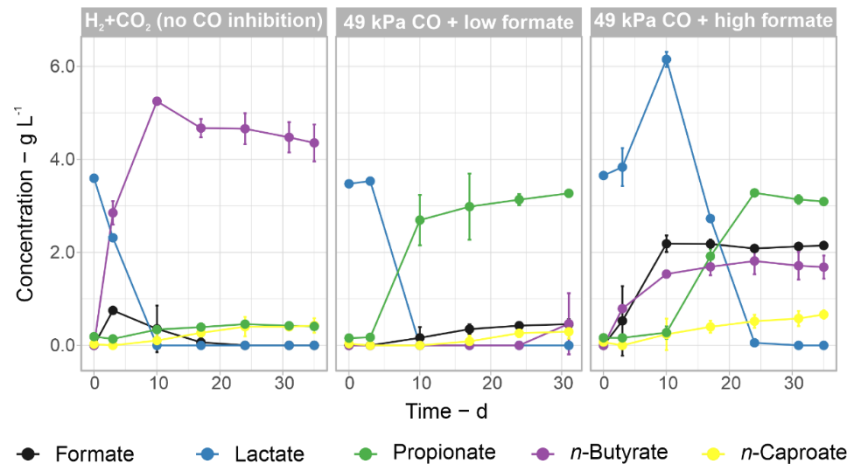
Figure B7. Fermentation profiles of the autochthonous community under a H_2+CO_2 headspace (uninhibited reference) and under a syngas headspace (49 kPa CO) with low and high formate accumulation. Mean values of duplicate bottles are shown. Error bars indicate standard errors.
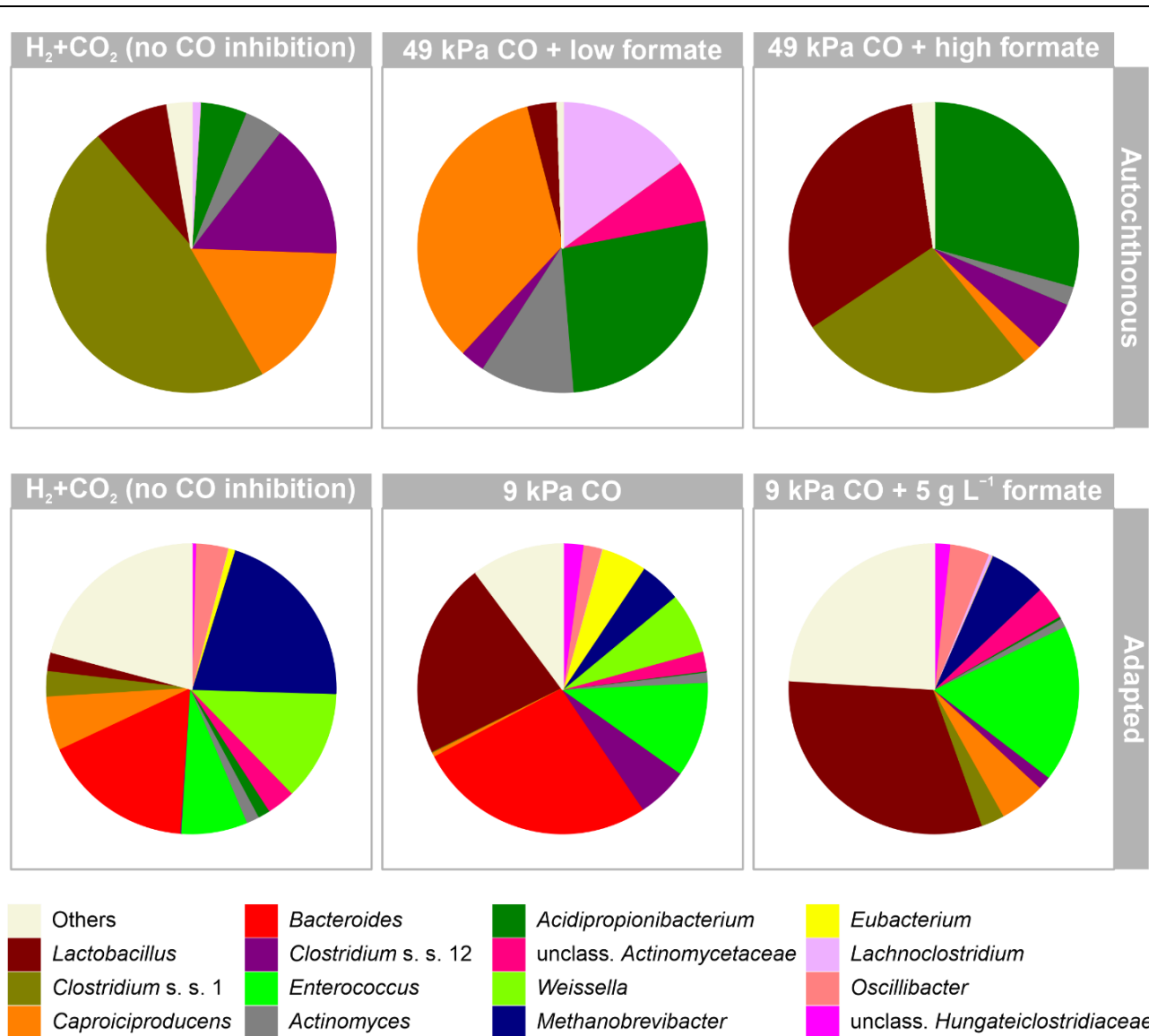
Figure B8. Composition of the autochthonous community and the syngas-adapted community depending on CO inhibition and formate availability. The 15 most abundant genera in the set are shown.

Appendix C

Table C1. Fermentation conditions tested in the batch experiments of Chapter 4.

Experiment	$H_2:CO_2$ (Effect of ethylene and stability)			$H_2:CO_2$ + 1.7 g L^{-1} ethanol (Ethylene vs. 2-BES)		
Condition / **Inhibitor**	$H_2:CO_2$	$N_2:CO_2$	Abiotic	$H_2:CO_2$	$N_2:CO_2$	Abiotic
Uninhibited	2 bottles	2 bottles	1 bottle	2 bottles	2 bottles	-
With ethylene	2 bottles	2 bottles	1 bottle	2 bottles	-	-
With 2-BES	-	-	-	2 bottles	-	-
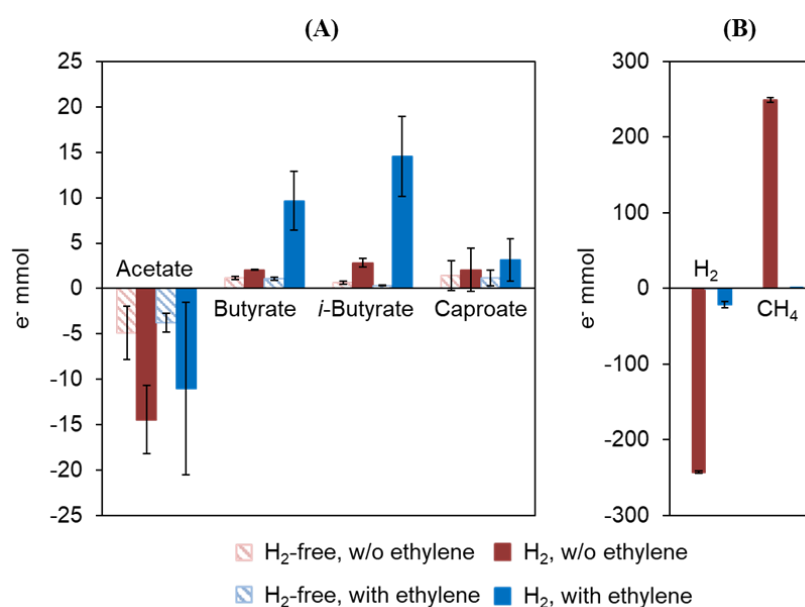
Figure C1. Effect of ethylene as inhibitor in enrichment cultures growing on H_2 and CO_2 in the first batch test of Chapter 4. Consumption and production of chemicals in the aqueous phase (**a**) and in the gas phase (**b**) after 48 days of fermentation in terms of electron equivalents is shown. H_2-free cultures and cultures without ethylene served as controls. Error bars are standard errors.
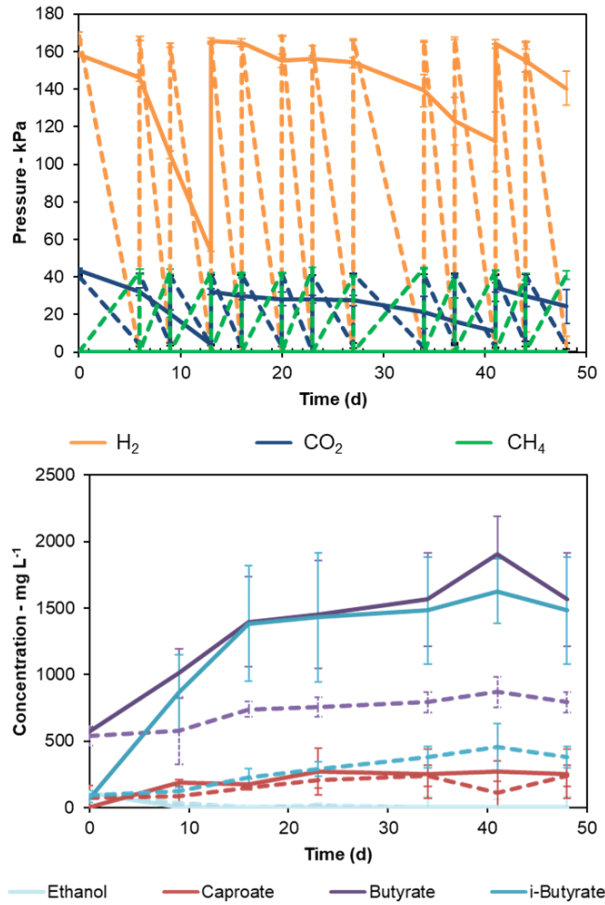
Figure C2. Partial pressure of gases and concentration of key chemicals in the enrichment cultures growing on H_2 and CO_2 in the first batch test of Chapter 4. Continuous lines are for cultures with ethylene and dashed lines are for cultures without ethylene. Error bars are standard errors.
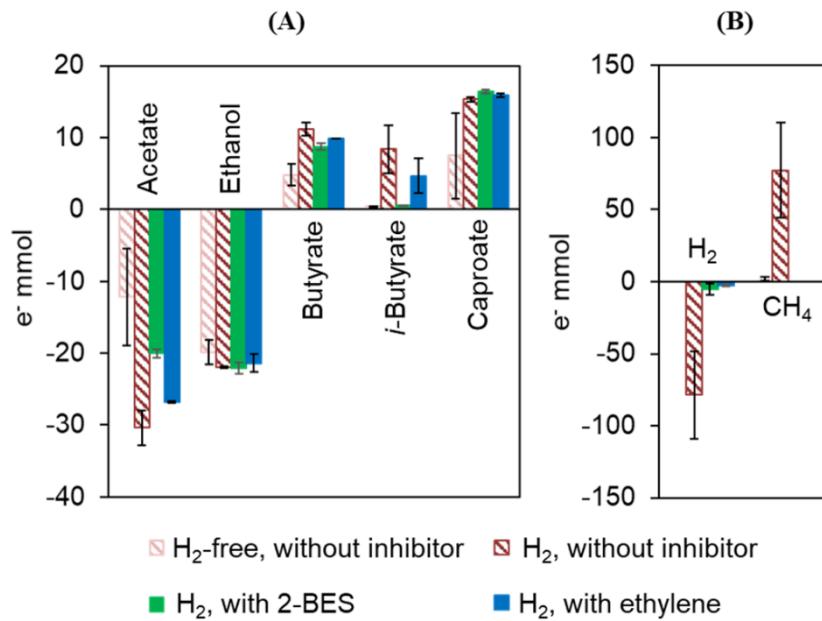
Figure C3. Effects of ethylene and 2-BES on cultures fed with H_2, CO_2, and ethanol in the second batch test of Chapter 4. Consumption and production of chemicals in the liquid phase (**a**) and in the gas phase (**b**) after 63 days of fermentation in terms of electron equivalents. Error bars are standard errors.
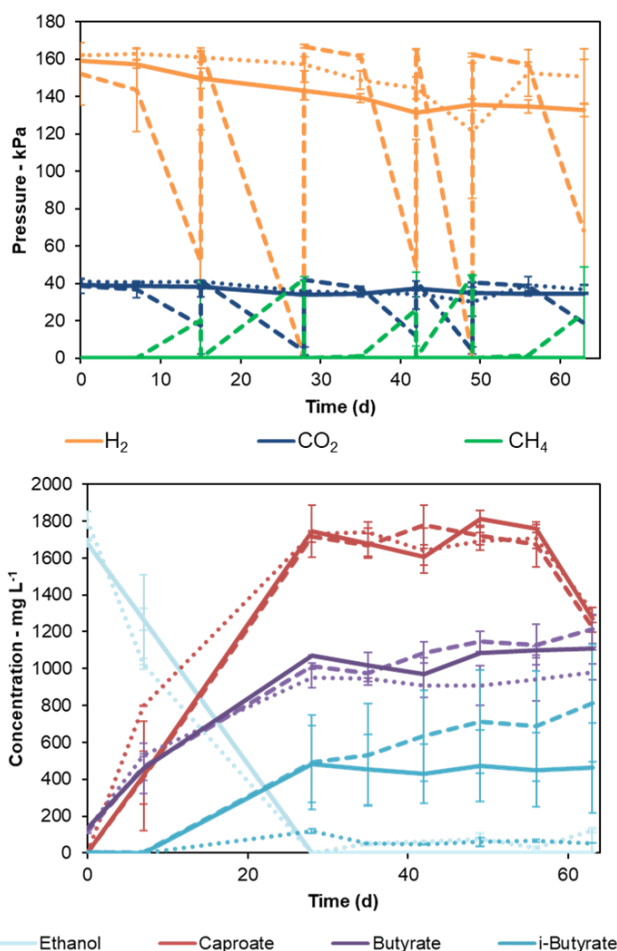
Figure C4. Partial pressure of gases and concentration of key chemicals in the enrichment cultures growing on H_2 and CO_2 in the second batch test of Chapter 4. Continuous lines are cultures with ethylene, dotted lines are cultures with 2-BES, and dashed lines are cultures without a methanogenesis inhibitor. Error bars are standard errors.
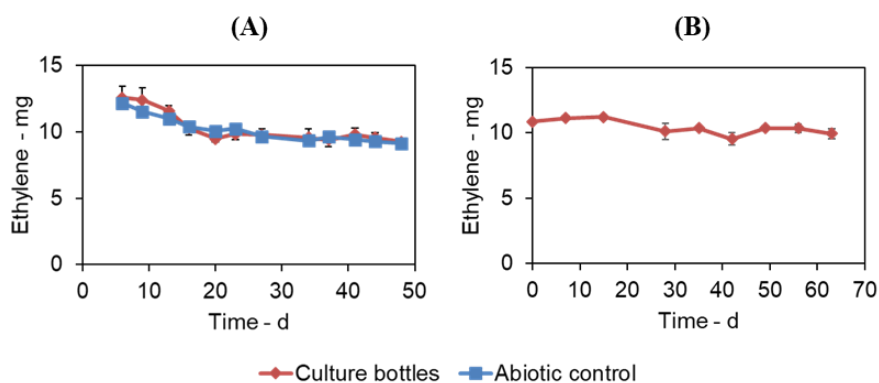
Figure C5. Monitoring of the amount of ethylene in the headspace of the culture bottles in the batch experiments of Chapter 4. No signs of ethylene degradation were detected. The monitoring was done in the presence of H_2 and CO_2 with abiotic controls (**a**) and in the presence of H_2, CO_2, and ethanol without abiotic controls (**b**).

Figure C6. Effect of ethylene inhibition on the microbial community composition in the first (**a**) and second (**b**) batch experiments of Chapter 4. Duplicates are shown and indicated as -1 and -2. The 20 most abundant genera are shown. Abiotic cultures did not show growth and were not analyzed.
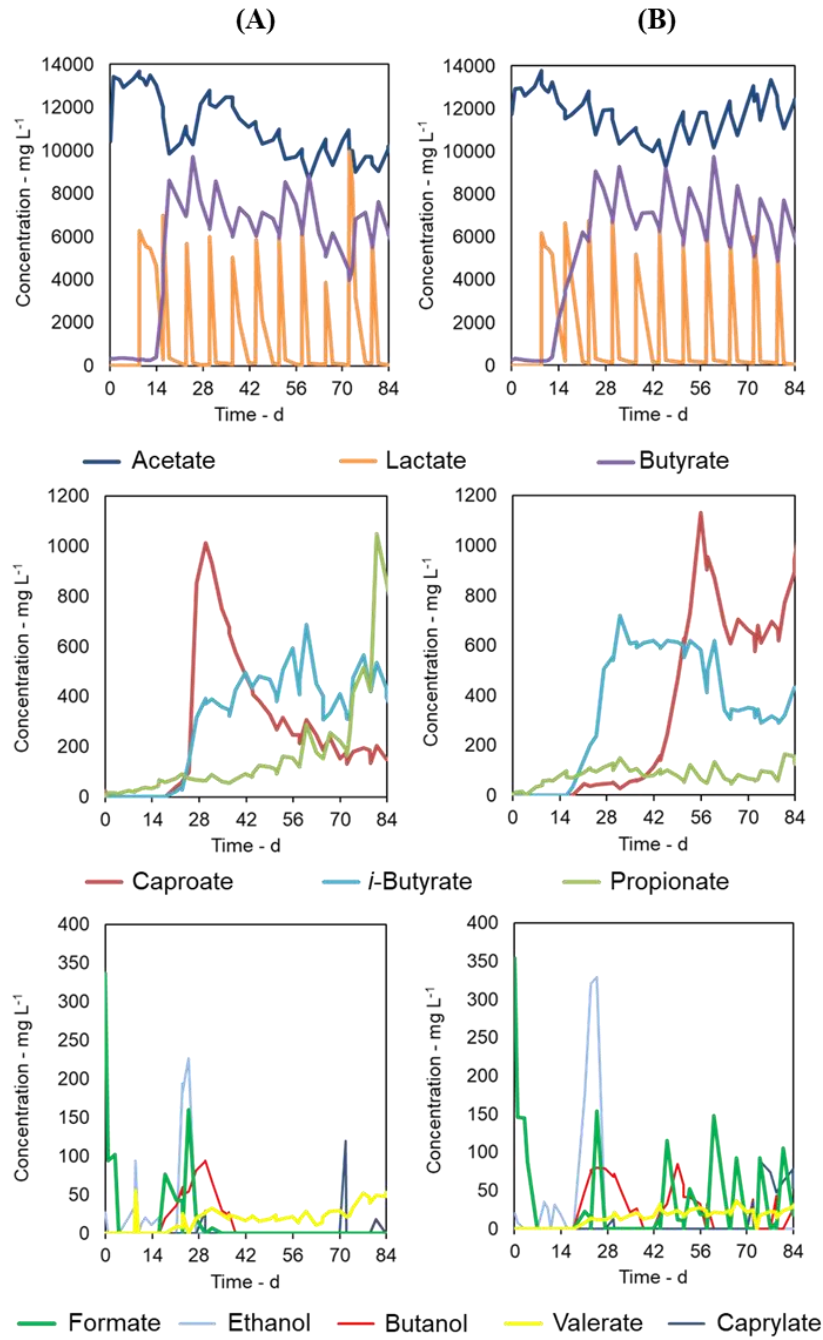
Figure C7. Concentration profiles of substrates and metabolites in the control reactor (**a**) and in the test reactor (**b**), the latter with ethylene addition after day 42.
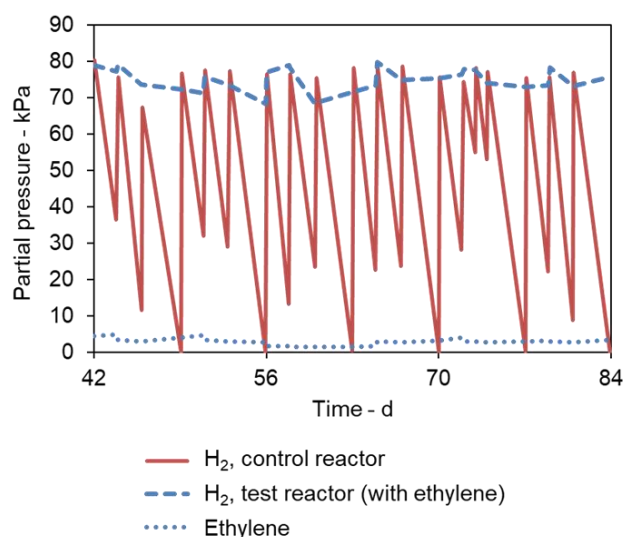
Figure C8. Partial pressures of H_2 and ethylene in the gas recirculation reactors in the period between operation days 42 and 84. Variations of the partial pressure of ethylene were caused by manual gas purging and refilling procedures. No consumption of ethylene was observed.
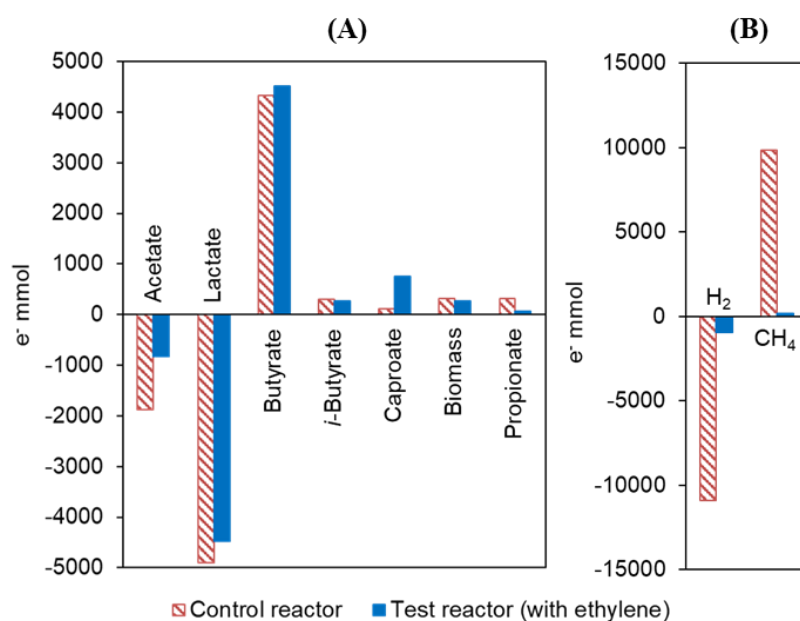
Figure C9. Component balances for the gas recirculation reactors in the period when ethylene was used in the test reactor (day 42 to 84) shown as electron equivalents. Production (positive) and consumption (negative) of components in the aqueous phase (**a**) and in the gas phase (**b**).
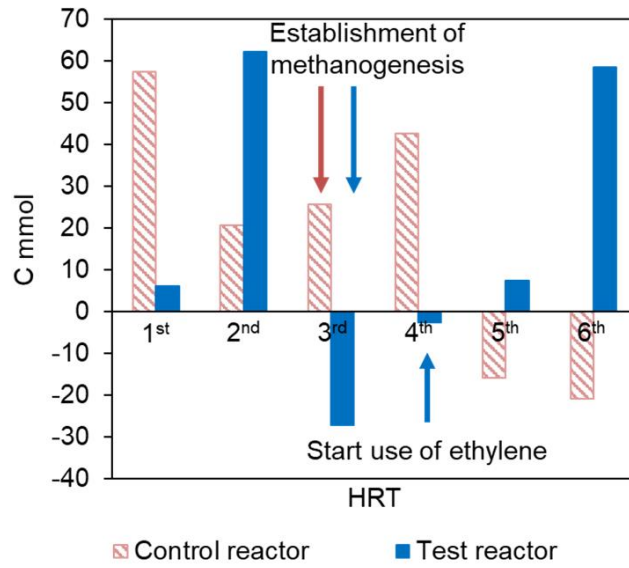
Figure C10. Net carbon fixation during each HRT period. One HRT period equals 14 days. The time points of starting methanogenesis in both reactors and of ethylene use in the test reactor are indicated. Assuming a CO_2 partial pressure of 21 kPa, a temperature of 25°C, a basal growth medium originally free of carbonates, and an equilibrium pH of 6.0, no more than 10.5 mmol C per HRT period can be explained by dissolution of CO_2 in water.
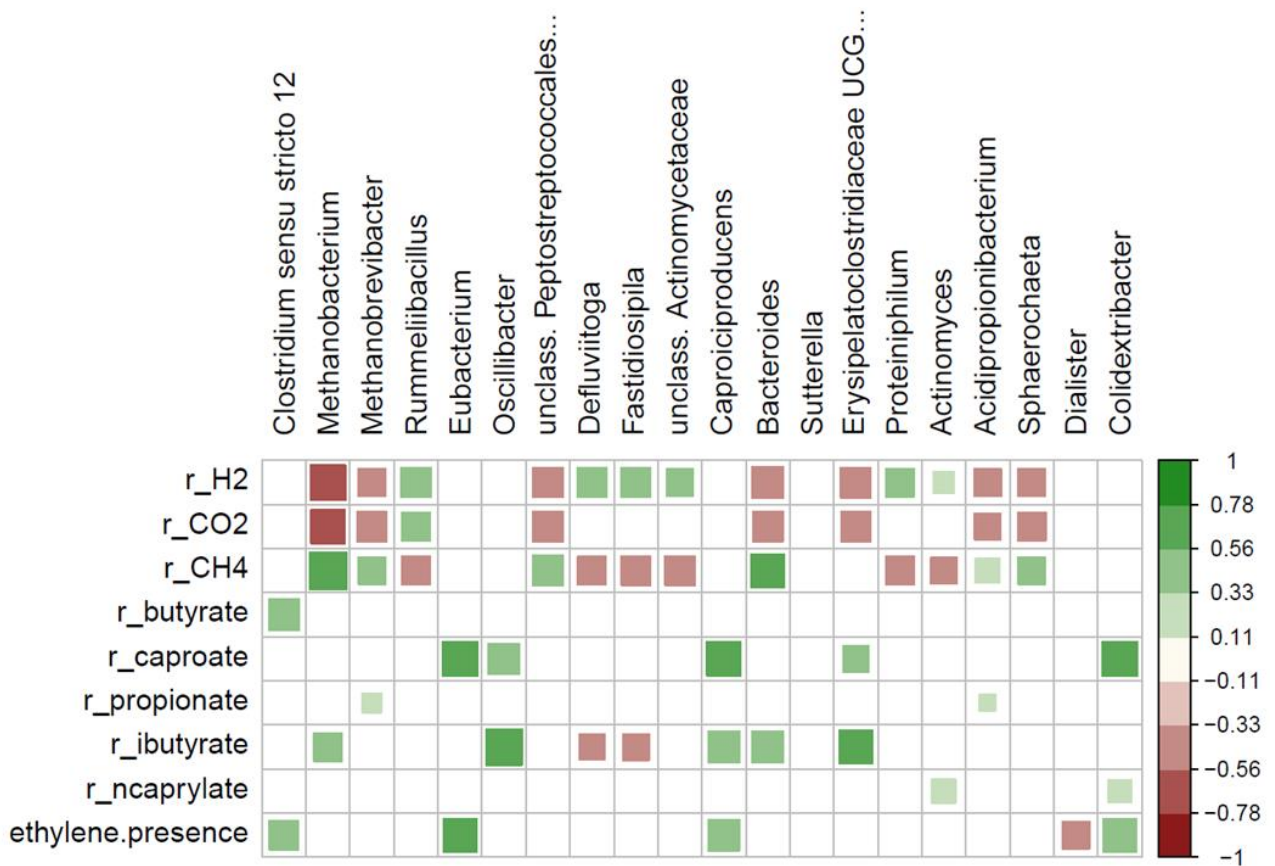
Figure C11. Correlation plot with the top 20 most abundant ASVs production rates of H_2, CO_2, CH_4, *n*-butyrate, *n*-caproate, propionate, *i*-butyrate, *n*-caprylate, and presence of ethylene. Spearman correlation is shown with p<0.01.
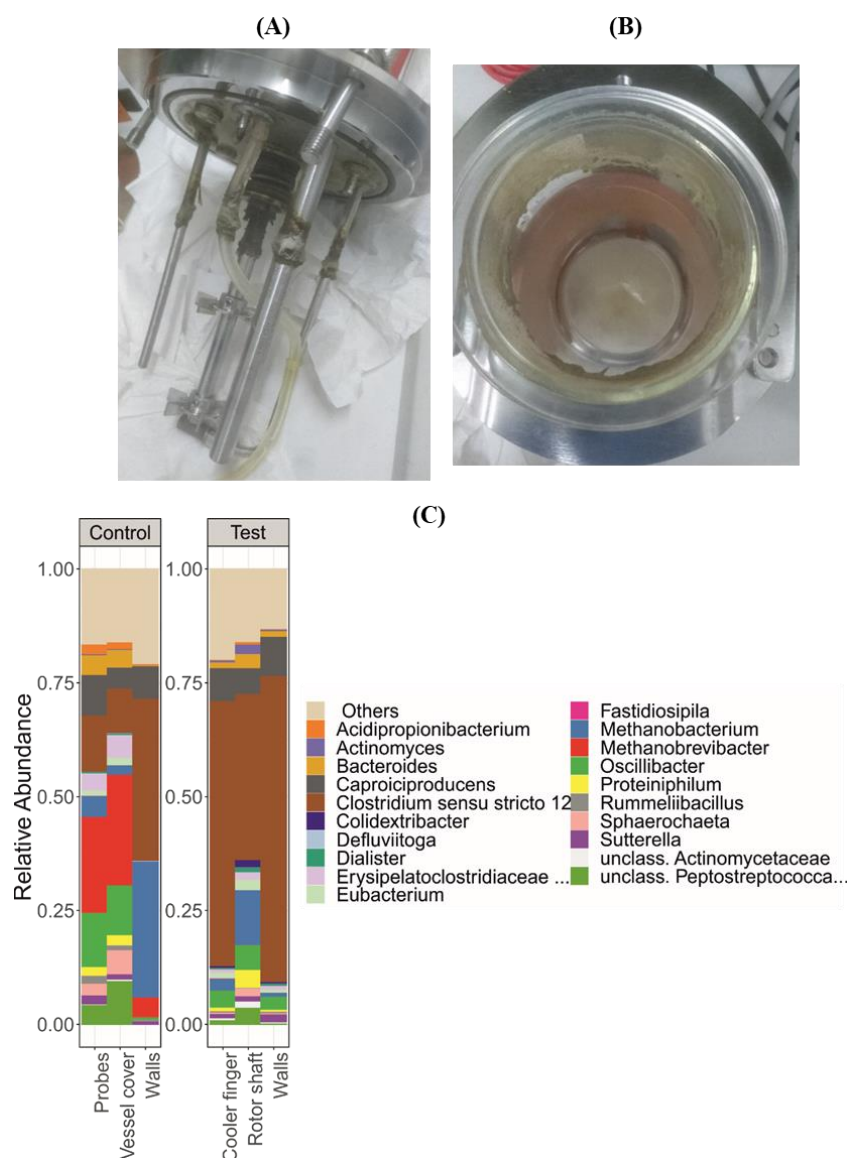
Figure C12. In biofilms attached to vessel cover, reactor probes, rotor shaft (**a**), and vessel walls (**b**), methanogens were detected regardless the use of ethylene (**c**). Methanogens were present in the planktonic community before ethylene addition but were washed out in the test reactor.

C.1. Basal medium composition

The basal medium used in the batch experiments contained 5.47 g L^{-1} KH_2PO_4, 10.42 g L^{-1} K_2HPO_4, 13.24 g L^{-1} sodium acetate, 2.31 g L^{-1} acetic acid, 500 mg L^{-1} yeast extract, 474 mg L^{-1} NH_4Cl, 54 mg L^{-1} $MgCl_2 \times 6\ H_2O$, 65 mg L^{-1} $CaCl_2 \times 2\ H_2O$, 30 mg L^{-1} cysteine-HCl, 1.5 mg L^{-1} $FeCl_2 \times 4\ H_2O$, 20 µg L^{-1} biotin, 20 µg L^{-1} folic acid, 100 µg L^{-1} pyridoxine, 50 µg L^{-1} thiamine, 50 µg L^{-1} riboflavin, 50 µg L^{-1} nicotinic acid, 50 µg L^{-1} calcium pantothenate, 20 µg L^{-1} cobalamin, 80 µg L^{-1} *p*-amino benzoic acid, 50 µg L^{-1} lipoic acid, 2 µg L^{-1} $CuCl_2 \times 2\ H_2O$, 190 µg L^{-1} $CoCl_2 \times 6\ H_2O$, 100 µg L^{-1} $MnCl_2$, 36 µg L^{-1} $Na_2MoO_4 \times 2H_2O$, 24 µg L^{-1} $NiCl_2 \times 6\ H_2O$, 20 µg L^{-1} $Na_2WO_4 \times 2\ H_2O$, 3 µg L^{-1} $Na_2SeO_3 \times 5\ H_2O$, 70 µg L^{-1} $ZnCl_2$, and 6 µg L^{-1} H_3BO_3. When applicable, the medium also contained 1.70 g L^{-1} ethanol and 10.55 g L^{-1} sodium 2-bromoethanosulfonate (or 2.92 g L^{-1} NaCl) were added.

The basal medium used in the gas recirculation reactor experiment was similar to the medium used in the culture bottle experiments, with the following changes: it contained 12.0 g L^{-1} acetic acid and 1.61 g L^{-1} NH$_4$Cl, it was free of yeast extract, sodium acetate, ethanol, and sodium 2-bromosulfonate, and it contained no added NaCl.

C.2. Calculations for component balances

To enable component balances in the gas recirculation system, a set of calculation steps was done. For the gaseous phase during a sampling procedure, N:

$$V_{Total_N} = \frac{y_{He_{N-1}}}{y_{He_N}} V_{Total_{N-1}} \qquad \text{(C1)}$$

$$V_{Gas\ Bag_N} = V_{Gas\ Bag_{N-1}} + \left(V_{Total_N} - V_{Total_{N-1}} \right) \qquad \text{(C2)}$$

where V_{Total} is the total gaseous volume of the system; y_{He} is the molar or volume fraction of the tracer gas, helium; and $V_{Gas\ Bag}$ is the volume of gas in the gas reservoir.

The accumulated gas production for a gaseous compound i, M_i, on a molar or mass basis was calculated as follows:

$$M_{i_N} = M_{i_{N-1}} + \left(m_{i_N} - m_{i_{N-1}} \right) \qquad \text{(C3)}$$

where m_i is the total amount of compound i in the system on a molar or mass basis.

If the sampling happens just after the gas replenishment, the volume of the gaseous phase is calculated as follows:

$$V_{Gas\ Bag_N} = V_{H2} + V_{CO2} + V_{CO} + V_{He} + V_{C2H4} \qquad \text{(C4)}$$

$$V_{Total_N} = V_{Gas\ Bag_N} + V_{rigid} \qquad \text{(C5)}$$

where V_{H2}, V_{CO2}, V_{CO}, V_{He}, V_{C2H4} are the volumes of newly injected H$_2$, CO$_2$, CO (when applicable), He, and C$_2$H$_4$, respectively; and V_{rigid} is the volume of the gas phase of the system outside the gas reservoir.

There is a discontinuity in the amount and composition of the gas in the system after gas replenishment. To account for it, the gas phase was sampled just before and immediately after the replenished gas mixture is homogenized. Since the gas replenishment and mixing lasts only a short period of time in comparison to the whole duration of the fermentation, it was assumed that

$$t_N \approx t_{N-1} \quad \therefore \quad M_{i_N} \approx M_{i_{N-1}} \qquad \text{(C6)}$$

where t_N, in days, is the fermentation time related to the sampling point N, just after gas replenishment and homogenization.

For the accumulated balances of compounds in the aqueous phase, both feeding and washing out of chemicals were considered. The washout of chemicals in the broth was estimated using

the average of the concentration values at sampling points N and $N-1$. Accumulated amounts for the compound j at sampling N was calculated as follows:

$$M_{j_N} = M_{j_{N-1}} + \left(\frac{c_{j_N} - c_{j_{N-1}}}{2} - c_{j_{feed}}\right) V_{broth} \frac{(t_N - t_{N-1})}{HRT} \tag{C7}$$

where M_j is the accumulated amount of the aqueous-phase compound j on a molar or mass basis; c_j and $c_{j\,feed}$ are the concentrations of compound j in the broth and in the feed medium, respectively; V_{broth} is the working volume of the reactor; and HRT is the hydraulic retention time, in days.

The amount of carbon fixed by the system during a certain period, n_{fixed}, in mmol C, was calculated as follows:

$$n_{fixed} = -(\Delta n_{CH4} + \Delta n_{CO2} + \Delta n_{CO}) \tag{C8}$$

where Δn_{CH4}, Δn_{CO2}, and Δn_{CO} are the variations of CH_4, CO_2, and CO (when applicable) in the system, respectively, in mmol C.

C.3. Assumptions for economic analysis

To estimate operating costs of using 2-BES, a price of 41 US$ per kilogram of sodium 2-BES (cost insurance & freight (CIF) Hamburg) was assumed. The price is based on a quote from a chemicals provider (Changzhou, China) for a purchase of at least 1,000 kg sodium 2-BES with ≥98% purity (CAS Registry Number: 4263-52-9). To estimate costs for acquiring ethylene, an approximate price of 1 US$ kg^{-1} was considered (ChemAnalyst, 2021) and a continuous loss of 1% of the flow of ethylene was assumed (to account for leakages and washing out of ethylene that is dissolved in the broth). For electricity consumption by gas recirculation, an efficiency of 90% of an isentropic compressor with an inlet gas pressure of 1.0 bar$_a$ and an electricity price of 0.12 US$ kWh^{-1} was assumed (Figure 7). For the mixture of H_2/CO_2/ethylene, a gas mixture with 78.5% H_2, 20% CO_2, and 1.5% ethylene was considered. An HRT of 14 days was considered. For the range of values of the carboxylate broth, an average price of carboxylates of 2 US$ kg^{-1} and an extractable amount of carboxylates between 4 g L^{-1} (lowest broth value) and 20 g L^{-1} (highest broth value) was assumed.

C.4. Further discussion of the results from batch experiments

Communities in the two batch experiments (Figure C6) differed due to slightly different inocula origins. The first batch was inoculated from cultures of the experiment "use of inhibitors" and the second batch was inoculated from the cultures of the experiment "acetate concentration" described in Chapter 2. Both cultures belonged to "community C" and the community of the "use of inhibitors" experiment represented a further enrichment of the community of the "acetate concentration" experiment.

In the first batch experiment of Chapter 4, H_2 was the only electron donor given as substrate and little growth was observed when methanogenesis was inhibited (OD600 0.35 ± 0.02 in

comparison to 1.2 ± 0.1 when no inhibitor was used). Combined with the fact that the culture bottle was a closed system, the low growth explains why relative abundance of methanogens was still relatively low by the end of the batch in the presence of H_2/CO_2 and ethylene (<u>Figure C6a</u>). When ethanol was co-fed with H_2 in the second batch (<u>Figure C6b</u>), stronger growth was observed when methanogenesis inhibitors were present (OD600 0.59 ± 0.03 with ethylene and 0.59 ± 0.02 with 2-BES) and a lower relative abundance of methanogens was observed by the end of the experiment.

C.5. Possible metabolic intermediates

Formate, ethanol, and *n*-butanol were detected in low concentrations (<350 mg L^{-1}) in appearance/disappearance cycles. Disappearance of these compounds could not be explained solely by washing-out, pointing to the possible role of these compounds as intermediates (<u>Figure C7</u>). After day 42, cycles of *n*-butanol and formate continued to occur in the test reactor (<u>Figure C7b</u>) whereas no more cycles were seen in the control reactor in the same period (<u>Figure C7a</u>). Interestingly, the concentration profile of *n*-caproate was not synchronized with the weekly feeding of lactate suggesting that *n*-caproate production could have counted on another electron donor than lactate. Formate is an intermediate of homoacetogenesis and, together with H_2, can be used as a substrate by some chain-elongating bacteria(Stamatopoulou et al., 2020; Litty and Müller, 2021). Short-chain alcohols (methanol, ethanol, and *n*-propanol) are electron donors for CE. *n*-Butanol, however, has not yet been shown to be an electron donor for chain elongation. *n*-Valerate and *n*-caprylate concentrations remained below 50 mg L^{-1} and 120 mg L^{-1} during the fermentation, respectively.

C.6. ASV similarities to species level

ASVs assigned to *Acidipropionibacterium* were related to *Acidipropionibacterium microaerophilum* (98.3% similarity of the V3-V4 regions of the 16S rRNA gene). Within the *Clostridium* sensu stricto 12 genus, ASVs were related to four different species. The most abundant clostridial species in both reactors were *Cl. tyrobutyricum* (99.8% similarity) followed by *Cl. luticellarii* (>99% similarity), a relative of *Cl. algifaecis* (>96.8% similarity), and *Cl. autoethanogenum* (100% similarity, with ambiguity to other species with identical V3-V4 16S rRNA gene: *Cl. ljungdahlii*, *Cl. ragsdalei*, and *Cl. coskatii*). The *Eubacterium* ASV had 98.3% similarity to *E. limosum* and the *Colidextribacter* ASV had 97.5% similarity to *Co. massiliensis*. *Caproiciproducens galactitolivorans* was the most similar species to the *Caproiciproducens* ASV present in the system (94.1% similarity).

Appendix D

Table D1. Average specific rates for each reactor and period. Values in bold correspond to periods with the highest O_2 contamination. Positive values are production rates and negative values are consumption rates. Formate, ethanol, n-butanol, i-caproate, and n-heptanoate were also monitored but had negligible rates. "non-CH_4 H_2" stands for hydrogen after discounting methane formation. Shorter O_2 contamination periods occurred in STR-test during 104 - 111 d and 125 - 128 d but are not shown separately. *During this period, O_2 concentrations of up to 18% were detected in the gas phase, since O_2 concentrations below detection level are assumed in the estimation of the O_2 contamination rate, the value shown may not be accurate.

Reactor	Period (days)	Specific O_2 contamination rate (mL L^{-1} d^{-1})	Average specific rate (mmol L^{-1} d^{-1})													
			O_2	H_2	CO_2	CH_4	non-CH_4 H_2	Biomass	Acetate	Lactate	Propionate	n-Butyrate	i-Butyrate	n-Valerate	n-Caproate	n-Caprylate
STR-test	**27 – 59**	**220 ± 33**	**-8.86**	**-50.5**	**-0.2**	**6.05**	**-26.3**	**1.48**	**-1.80**	**-7.52**	**0.76**	**1.78**	**0.36**	**0.10**	**0.56**	**0.02**
	59 - 111	21 ± 33	-0.87	-71.2	-10.2	19.5	7.07	1.72	-2.18	-8.92	0.67	1.51	0.23	0.21	1.78	0.02
	115 - 119	**474 ± 33**	**-19.1**	**-86.1**	**-3.4**	**5.33**	**-64.7**	**2.03**	**-2.65**	**-9.88**	**0.61**	**2.76**	**-0.19**	**0.29**	**1.06**	**-0.02**
	119 - 139	39 ± 33	-1.56	-76.8	-12.7	18.7	-1.95	1.74	-4.38	-9.85	0.36	4.77	-0.01	-0.07	0.97	0.11
STR-control	27 - 139	7 ± 33	-0.21	-62.3	-10.7	16.5	3.73	1.37	-2.91	-8.63	0.13	1.71	0.06	0.07	2.12	0.11
BCR-test	4 – 11	0 ± 28	-0.01	-31.2	-5.51	8.73	3.72	1.30	0.42	-7.58	1.10	2.18	-0.04	0.06	0.06	0.00
	11 – 36 *	**97 ± 28 ***	**-3.9 ***	**-15.9**	**1.2**	**0.42**	**-14.2**	**1.21**	**-1.39**	**-6.39**	**1.37**	**1.98**	**0.27**	**0.13**	**0.04**	**0.00**
	39 – 50	**129 ± 28**	**-5.2**	**-11.5**	**9.3**	**1.41**	**-5.86**	**0.54**	**-1.63**	**-7.13**	**1.78**	**1.22**	**1.08**	**0.29**	**0.03**	**0.00**
	50 - 116	3 ± 28	-0.12	-47.2	-8.5	11.9	0.27	1.24	-2.32	-8.02	0.34	1.84	0.37	0.15	1.40	0.00
BCR-control	4 – 116	0 ± 28	-0.01	-63.9	-12.71	15.9	-0.50	1.13	-1.98	-7.54	0.75	2.25	0.60	0.25	0.66	0.00

Table D2. Spearman correlation coefficients and their p-values (in parentheses).

	Caproici-producens	*Methano-brevibacter*	*Cl. sensu stricto 12*	*Oscillibacter*	*Unclassif. Micro-coccales*	*Unclassif. Egger-thellaceae*	*Acidipropioni-bacterium*	*Eubacterium*	*Unclassif. Peptostrepto-coccaceae*	*Acidaminococcus*	*Actinomyces*
O$_2$ contamination	-0.071 (0.61)	-0.368 (0.002)	-0.121 (0.675)	-0.237 (0.488)	0.315 (0.032)	0.183 (9.63E-6)	0.115 (0.882)	-0.246 (0.145)	-0.215 (0.703)	-0.188 (0.021)	0.389 (1.45E-5)
H$_2$ consumption	0.233 (1.95E-3)	0.411 (1.36E-7)	-0.014 (0.73)	0.152 (0.371)	-0.29 (4.73E-4)	0.14 (0.582)	-0.392 (5.10E-5)	-0.082 (0.456)	0.504 (3.88-08)	0.108 (0.902)	-0.291 (2.15E-3)
CO$_2$ consumption	0.17 (1.55E-3)	0.434 (5.7E-11)	0.04 (0.875)	0.218 (0.086)	-0.339 (2.02E-6)	-0.068 (0.001)	-0.266 (4.33E-3)	0.101 (0.476)	0.369 (1.05E-4)	0.258 (0.169)	-0.423 (1.75E-9)
CH$_4$ production	0.263 (6.50E-4)	0.539 (4.8E-12)	-0.038 (0.585)	0.212 (0.241)	-0.353 (2.14E-8)	0.12 (0.762)	-0.461 (3.01E-7)	-0.021 (0.905)	0.601 (8.5E-11)	0.189 (0.398)	-0.35 (1.77E-5)
non-CH$_4$ H$_2$ consumption	-0.134 (0.163)	-0.33 (7.34E-5)	0.047 (0.63)	-0.175 (0.438)	0.119 (2.72E-6)	-0.082 (0.13)	0.287 (3.66E-3)	0.028 (0.294)	-0.453 (3.18E-3)	-0.211 (0.063)	0.237 (2.43E-3)
Acetate consumption	0.072 (0.2)	0.202 (0.037)	-0.053 (0.651)	0.116 (0.11)	-0.152 (0.865)	0.001 (0.798)	-0.228 (0.067)	0.062 (0.813)	0.153 (0.159)	-0.104 (0.725)	-0.137 (0.076)
Lactate consumption	0.18 (0.107)	0.501 (1.20E-6)	-0.018 (0.341)	0.4 (0)	-0.302 (5.42E-3)	-0.151 (6.9E-3)	-0.395 (1.80E-4)	0.109 (0.21)	0.408 (5.08E-5)	0.167 (0.17)	-0.454 (2.30E-7)
Propionate production	-0.404 (6.71E-7)	-0.107 (0.019)	0.271 (0.015)	0.074 (0.721)	0.162 (0.159)	-0.15 (0.604)	0.286 (9.34E-5)	0.218 (0.162)	-0.069 (0.077)	0.115 (0.539)	0.055 (0.073)
***n*-Butyrate production**	-0.04 (0.471)	0.149 (0.357)	0.112 (0.234)	0.192 (0.257)	-0.077 (0.509)	-0.2 (0.413)	-0.172 (0.57)	0.17 (0.504)	0.215 (0.078)	0.059 (0.796)	-0.179 (0.084)
***i*-Butyrate production**	-0.375 (4.63E-3)	-0.304 (3.84E-3)	0.436 (1.45E-8)	-0.099 (0.591)	0.384 (0.0172)	-0.133 (0.189)	0.532 (8.72E-5)	0.161 (0.915)	-0.334 (3.66E-4)	0.343 (0.001)	0.161 (0.956)
***n*-Valerate production**	-0.046 (0.212)	-0.084 (0.059)	0.21 (6.42E-5)	0.053 (0.616)	-0.001 (0.285)	-0.211 (0.138)	0.254 (4.86E-3)	0.2 (0.717)	-0.186 (0.057)	0.344 (0.001)	-0.006 (0.729)
***n*-Caproate production**	0.498 (2.01E-8)	0.391 (1.38E-5)	-0.327 (1.10E-4)	0.101 (0.474)	-0.366 (1.79E-5)	0.25 (0.848)	-0.461 (1.06E-6)	-0.179 (0.573)	0.343 (1.88E-3)	-0.08 (0.439)	-0.151 (0.069)
***n*-Caprylate production**	0.162 (0.061)	0.064 (0.769)	-0.181 (0.205)	-0.027 (0.568)	-0.109 (0.299)	0.155 (0.755)	-0.141 (0.936)	-0.137 (0.346)	0.076 (0.997)	-0.19 (0.101)	0.038 (0.477)

Table D2 (continued).

	Bacteroides	*Unclassif. Actino-mycetaceae*	*Prevotella*	*Burkholderia*	*Rummeliibacillus*	*Dialister*	*Proteiniphilum*	*Sphaerochaeta*	*Sutterella*
O_2 contamination	-0.201 (0.075)	0.215 (2.23E-7)	0.016 (0.131)	0.099 (0.94)	0.09 (0.955)	-0.17 (0.422)	0.131 (0.006)	-0.104 (0.245)	-0.147 (0.166)
H_2 consumption	-0.153 (0.035)	0.195 (0.604)	0.177 (0.329)	-0.317 (4.27E-6)	-0.231 (1.53E-7)	-0.015 (0.326)	0.024 (0.253)	0.21 (0.018)	-0.268 (5.07E-4)
CO_2 consumption	0.079 (0.675)	-0.038 (2.07E-5)	0.068 (0.676)	-0.215 (2.17E-5)	-0.254 (9.10E-6)	0.105 (0.724)	-0.078 (0)	0.185 (0.016)	-0.075 (0.156)
CH_4 production	-0.121 (0.065)	0.157 (0.078)	0.213 (0.732)	-0.303 (2.01E-5)	-0.266 (5.96E-8)	-0.028 (0.297)	0.069 (0.311)	0.294 (0.002)	-0.191 (0.010)
non-CH_4 H_2 consumption	0.066 (0.968)	-0.115 (0.011)	-0.089 (0.327)	0.223 (0.548)	0.069 (0.099)	0.133 (0.694)	-0.152 (0.938)	-0.292 (0.052)	0.059 (0.466)
Acetate consumption	-0.03 (0.621)	0.004 (0.491)	0.165 (0.323)	-0.092 (5.71E-4)	-0.031 (0.0793)	-0.003 (0.731)	-0.114 (0.204)	-0.084 (0.669)	-0.11 (0.509)
Lactate consumption	0.041 (0.642)	-0.126 (8.76E-3)	0.214 (0.082)	-0.154 (0.014)	-0.177 (0.091)	-0.05 (0.029)	-0.08 (0.01)	0.042 (0.652)	-0.076 (0.596)
Propionate production	0.216 (0.133)	-0.229 (0.517)	-0.166 (0.204)	0.253 (1.5E-10)	0.065 (0.019)	0.158 (0.016)	0.227 (0.002)	-0.248 (0.06)	0.223 (0.039)
n-Butyrate production	0.114 (0.693)	-0.193 (0.224)	0.139 (0.416)	0.12 (0.877)	0.028 (0.94)	0.041 (0.455)	0.03 (0.874)	-0.071 (0.653)	0.108 (0.683)
i-Butyrate production	0.314 (0.003)	-0.17 (0.927)	-0.376 (0.08)	0.349 (0.115)	0.026 (0.343)	0.305 (4.41E-6)	0.067 (0.708)	-0.194 (0.852)	0.399 (5.53E-6)
n-Valerate production	0.224 (0.223)	-0.208 (0.638)	-0.274 (0.048)	0.206 (0.353)	-0.196 (0.128)	0.307 (1.03E-4)	-0.088 (0.476)	-0.161 (0.225)	0.268 (0.013)
n-Caproate production	-0.306 (0.029)	0.33 (0.252)	0.284 (0.12)	-0.423 (4.14E-4)	-0.305 (6.19E-4)	-0.234 (1.06E-3)	-0.149 (0.017)	0.362 (0.029)	-0.322 (7.02E-4)
n-Caprylate production	-0.137 (0.653)	0.096 (0.396)	0.216 (0.897)	-0.09 (0.562)	-0.101 (0.571)	0.144 (0.73)	-0.003 (0.382)	0.077 (0.838)	-0.112 (0.441)
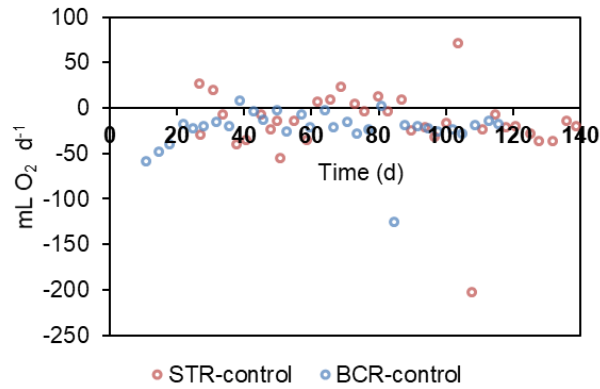
Figure D1. Distribution of estimated oxygen contamination rates in the reactors STR-test and BCR-test. These reactors remained anoxic. Thus, the distribution was used to determine the standard error of the procedure for quantifying oxygen contamination rates in STR-test and BCR-test.
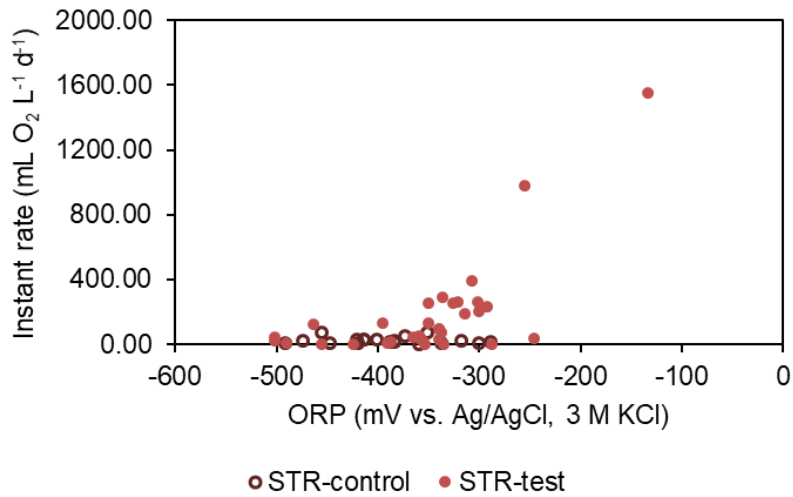
Figure D2. Instant O_2 contamination rate versus oxidation-reduction potential (ORP) measurement. No clear relation between O_2 contamination rates and ORP measurements was found at lower contamination rates.
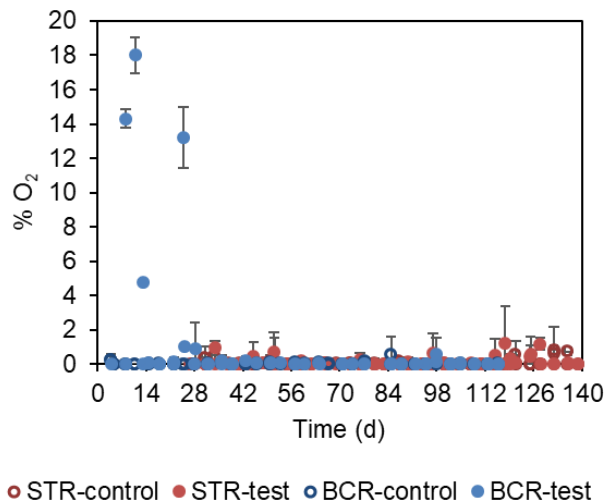
Figure D3. O_2 concentrations in the recirculating gas.
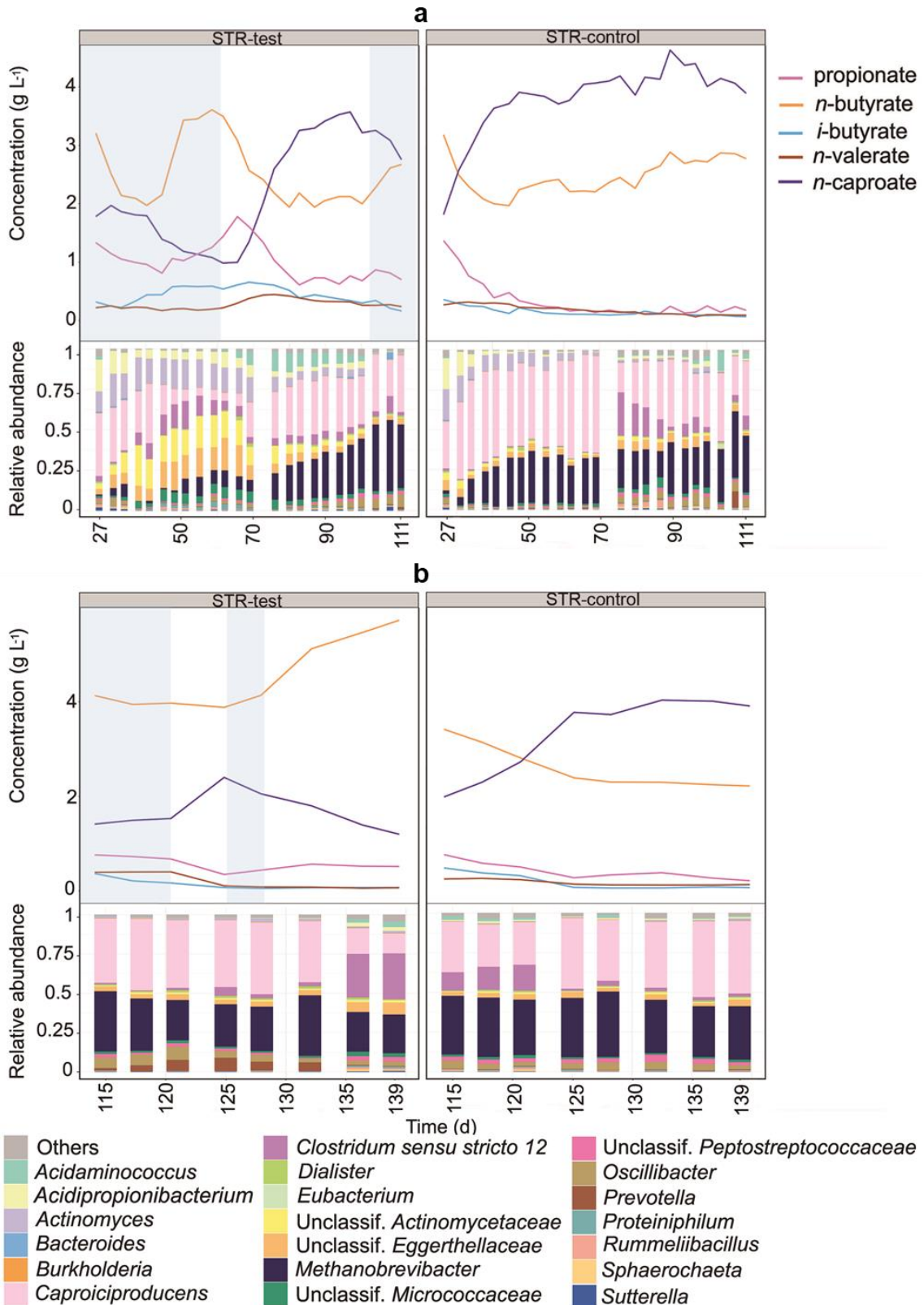
Figure D4. Concentrations of the main carboxylates produced and community composition at genus level between days 27 and 111 (**a**) and days 115 and 139 (**b**) for STR-test and STR-control. Blue shading indicates the O_2 contamination period.
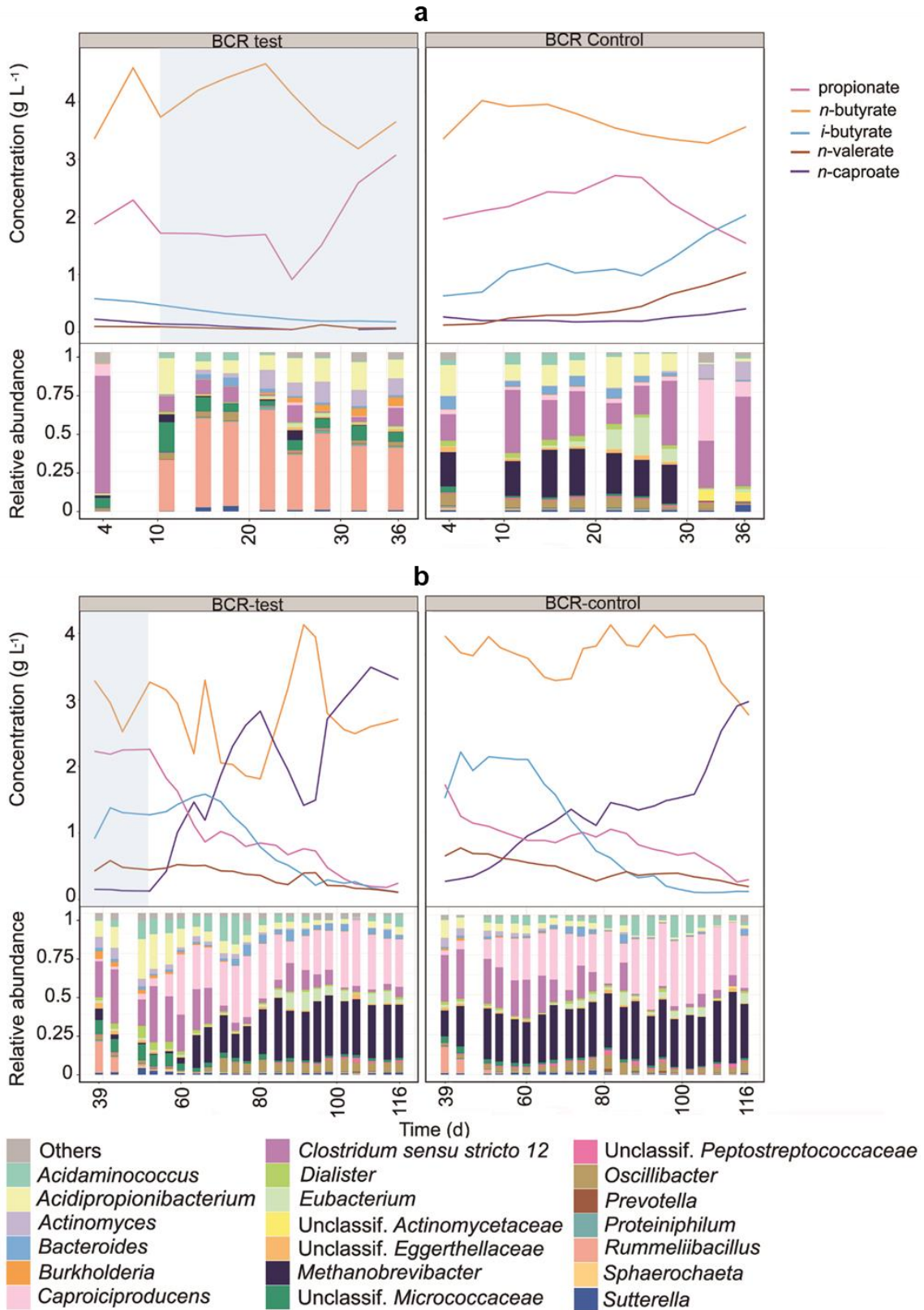
Figure D5. Concentrations of the main carboxylates produced and community composition at genus level between days 4 and 36 (**a**) and days 39 and 116 (**b**) for BCR-test and BCR-control. Blue shading indicates the O_2 contamination period.

Appendix E

E.1. Reactor operation

Neoprene tubes were used for the peristaltic pump heads that worked with liquids, except for the lines that were in contact with the base solution, for which silicon tubes were used. PVC tubing (Tygon® LMT-55, Saint-Gobain Performance Plastics Nagano, Japan) was used for all gas and the remaining liquid lines.

The flexible gas reservoir had a maximum volume of 22 L and the rigid headspace volume of the system was 2.3 L. The gaseous substrate was replenished when one of the following conditions was met: all CO was consumed, the gas reservoir volume was less than 10 L, or the gas bag volume was bigger than 20 L due to net gas production. During replenishment, the empty gas reservoir was filled with 17 L syngas mixture (32% H_2, 32% CO, 16% CO_2, 20% N_2) with 480 mL He injected as a tracer gas and, when applicable, ethylene. Ethylene was used as a methanogenesis inhibitor auxiliary to CO. Since we had previously observed acclimatization of methanogens to ethylene after long exposure (Section 5.4.1), 2 kPa ethylene (ca. 420 mL) was only used when deemed necessary (between days 47 and 92). This way, methanogenic activity was kept low, with a maximum of 4.4% CH_4 accumulating in the gas phase and an average CH_4 production rate of 11 mL L^{-1} d^{-1}, corresponding to less than 1% of the total organic carbon fed. Air contamination of the systems was monitored by measuring the N_2 content of the gas phase. The details and calculations for monitoring air contamination have been described in Section 5.2.4. Except for two unintended air contamination events during overnight operation on days 229 (Reactor 2) and 251 (Reactor 1), the reactors were kept largely anoxic with an average ORP of -386 ± 73 mV and an average O_2 intrusion rate of 13 mL L^{-1} d^{-1}.

The rate of carbon fixation r_{fixed} (in C mmol L^{-1} d^{-1}) was calculated as described in Equation E1.

$$r_{fixed} = -(r_{CH4} + r_{CO2} + r_{CO}) \tag{E1}$$

where r_{CH4}, r_{CO2}, and r_{CO} are the production (+) or consumption (-) rates of CH_4, CO_2, and CO, respectively, in C mmol L^{-1} d^{-1}.

Table E1. Growth medium composition. Adapted from <u>Appendix C.1</u>.

Concentration of major components - g L^{-1}	
NH$_4$Cl	1.61
KH$_2$PO$_4$	13.6
DL-Lactic acid	12.0
Acetic acid	12.0 (with acetate) 0.0 (acetate-free)
NaOH (approx.)	11.4 (with acetate) 7.0 (acetate-free)
Concentration of minor components - mg L^{-1}	
MgCl$_2$ × 6 H$_2$O	54
CaCl$_2$ × 2 H$_2$O	65
Resazurin	0.5
Cysteine hydrochloride	30
Transition metals, selenium, and boron - µg L^{-1}	
FeCl$_2$ × 4 H$_2$O	1500
CuCl$_2$ × 2 H$_2$O	2.0
CoCl$_2$ × 6 H$_2$O	190
MnCl$_2$	100
Na$_2$MoO$_4$ × 2 H$_2$O	36
NiCl$_2$ × 6 H$_2$O	24
Na$_2$WO$_4$ × 2 H$_2$O	20
Na$_2$SeO$_3$ × 5 H$_2$O	3.0
ZnCl$_2$	70
H$_3$BO$_3$	6.0
Vitamins - µg L^{-1}	
Biotin	20
Folic acid	20
Pyridoxine	100
Thiamine	50
Riboflavin	50
Niacin	50
Calcium pantothenate	50
Cobalamin	20
p-Aminobenzoic acid	80
Lipoic acid	50

E.2. Growth medium preparation

Firstly, the medium components, except vitamins, cysteine, and NaOH, were dissolved in deionized water under aerobic conditions. The resulting solution was then made anoxic by stirring for at least three hours in an anaerobic chamber. Then, the anoxic solution was transferred into a 2-L borosilicate glass bottle with a two-port cap. The ports of the bottle were kept sealed by crimped silicon tubes during transportation and storage in the anaerobic chamber. Afterwards, the glass bottle with the solution was sterilized by autoclaving (121°C for 20 minutes) and stored inside the anaerobic chamber. Vitamins and cysteine hydrochloride

were added to the medium in the anaerobic chamber just before connecting the bottle to the reactor system's feed pump. These solutions stemmed from concentrated solutions of vitamins (previously sterilized with a 0.2 μm syringe filter) and cysteine hydrochloride (previously sterilized by autoclaving). Originally, the medium had a pH value of 2.6 (with acetate) or 3.9 (acetate-free). The pH was automatically adjusted to 6.0 by adding 4 M NaOH after being pumped into the reactor. During operation, the salinity of the broth depended on the amount of NaOH added to keep a stable pH value. Therefore, the salinity depended on the total amount of carboxylates in the broth and was estimated to be between 13 and 28 g NaCl eq. L^{-1}.

E.3. Inocula

The reactor from which the diverse community stemmed was a pilot-scale anaerobic digester of the Deutsches Biomasseforschungszentrum (DBFZ, Germany) fed with corn silage and cow manure and operated at 37°C. The inoculum of the enriched community consisted of broth harvested from the reactor designated as "STR-control" (Section 5.2.1) until operation day 87. STR-control was operated anoxically at 32°C and pH 6.0 with an HRT of 14 d and fed with a growth medium similar to the one used here (200 mM acetate, 133 mM lactate). The inocula were stored in closed screw cap plastic bottles at 4°C in the dark for about 3 months before being used. On the sampling day of the inoculum, the sludge of the pilot-scale digester had a low carboxylate concentration (343 mg L^{-1} acetate, 58 mg L^{-1} propionate, and 69 mg L^{-1} *n*-butyrate), whereas the broth of the enrichment culture was rich in various carboxylates (9.13 g L^{-1} acetate, 2.53 g L^{-1} *n*-butyrate, 4.62 g L^{-1} *n*-caproate, and 1.21 g L^{-1} *n*-caprylate).

E.4. ASV clustering

Among the 25 most abundant ASVs found in this dataset, the ones assigned to Clostridia (i.e. 22 ASVs) were aligned *de novo* using the library Decipher for R (Wright, 2015). The aligned sequences were clustered using the Neighbor Joining model with help of the libraries Phangorn (Schliep et al., 2017) and Ape (Paradis et al., 2004) for R. To identify poor alignment due to short sequences (ASVs were ~400 base pairs long), the sequences were additionally aligned with a reference *E. coli* sequence using the web-based tool SILVA Alignment, Classification and Tree Service (Quast et al., 2013). All alignments had a score of 98 or more.
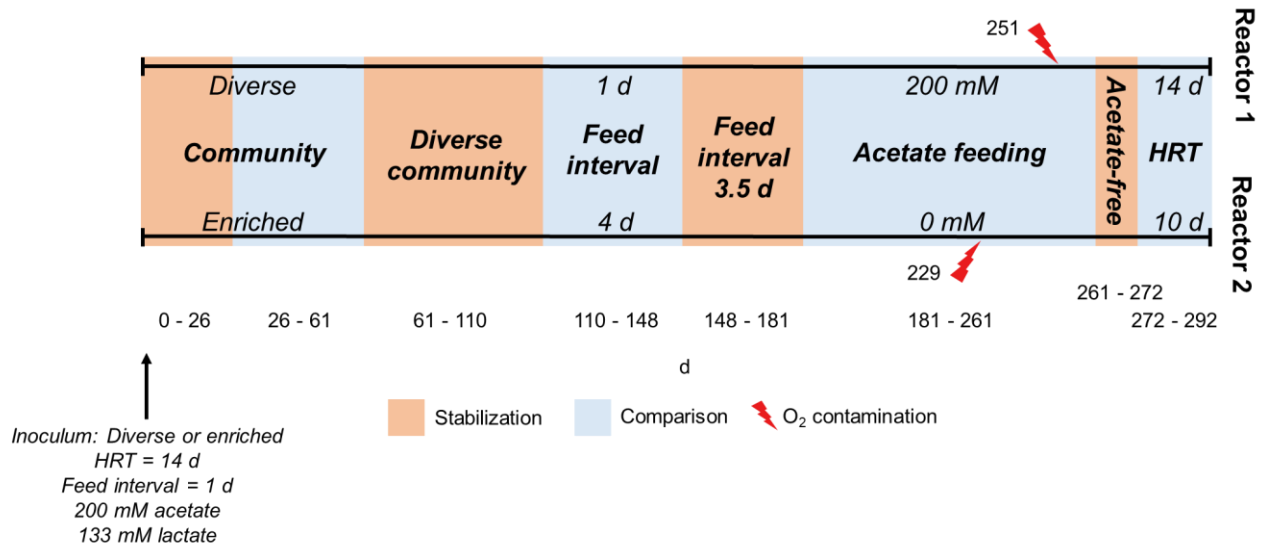
Figure E1. Summary of the operating conditions in Reactors 1 and 2.
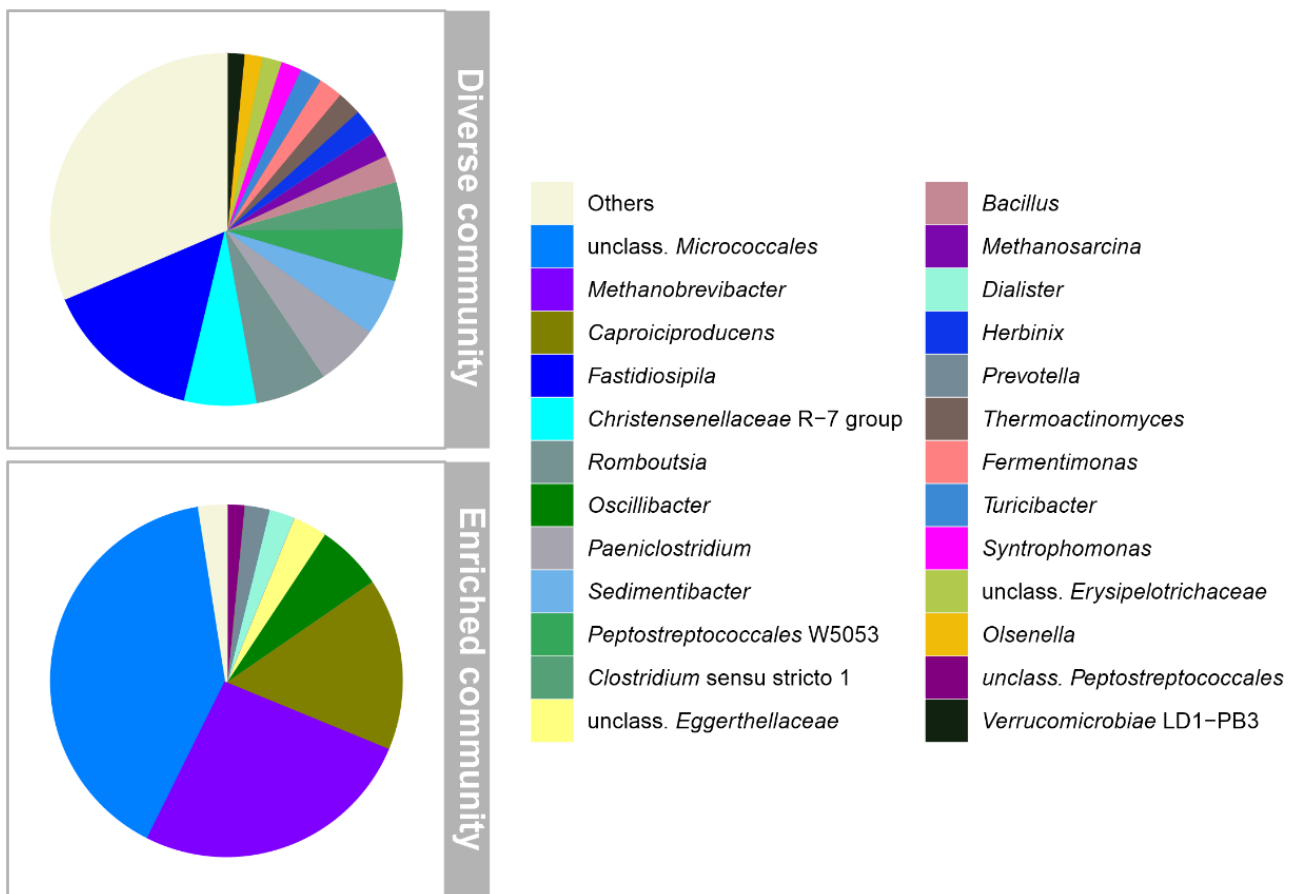
Figure E2. Microbial community composition of the two inocula used in the study. The 25 most abundant genera in the inocula are shown with the remaining grouped in "Others".
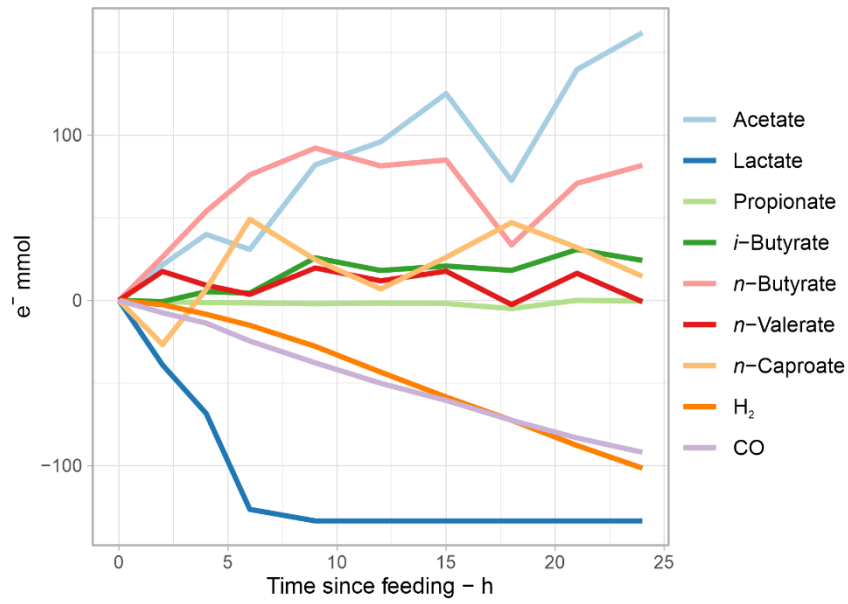
Figure E3. Cumulative electron profiles of chemicals over the feeding cycle of day 42 in Reactor 1.
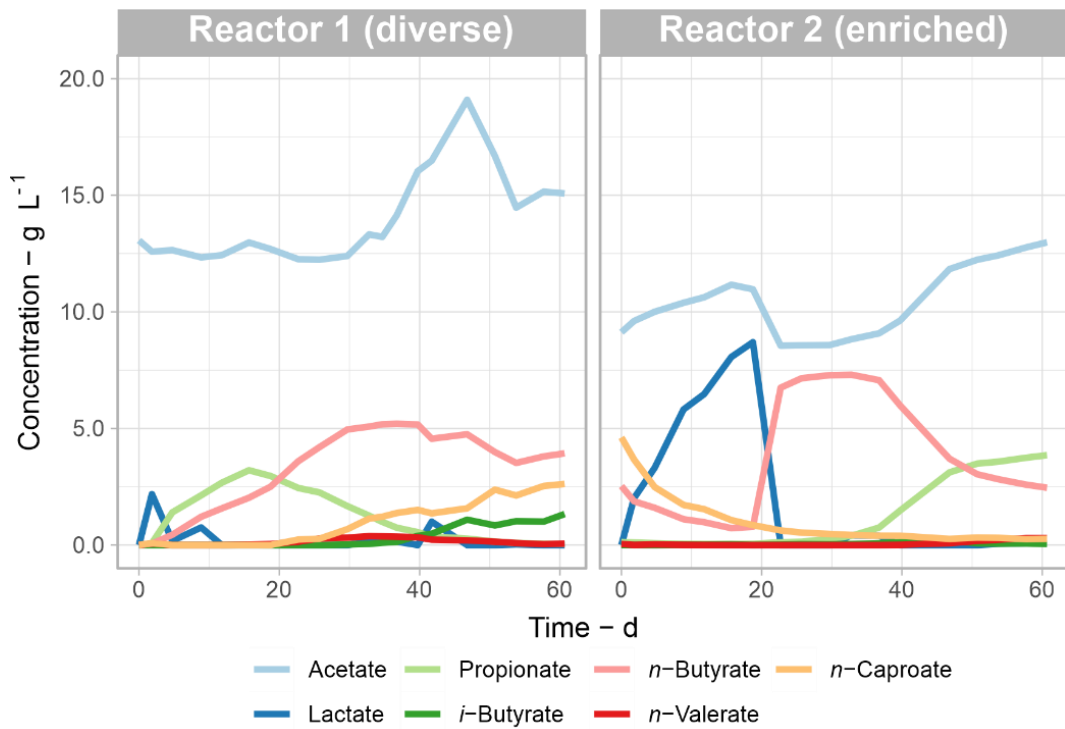
Figure E4. Concentration profiles of carboxylates during the first 61 days of fermentation in Reactor 1 inoculated with a diverse community and Reactor 2 inoculated with an enriched culture.
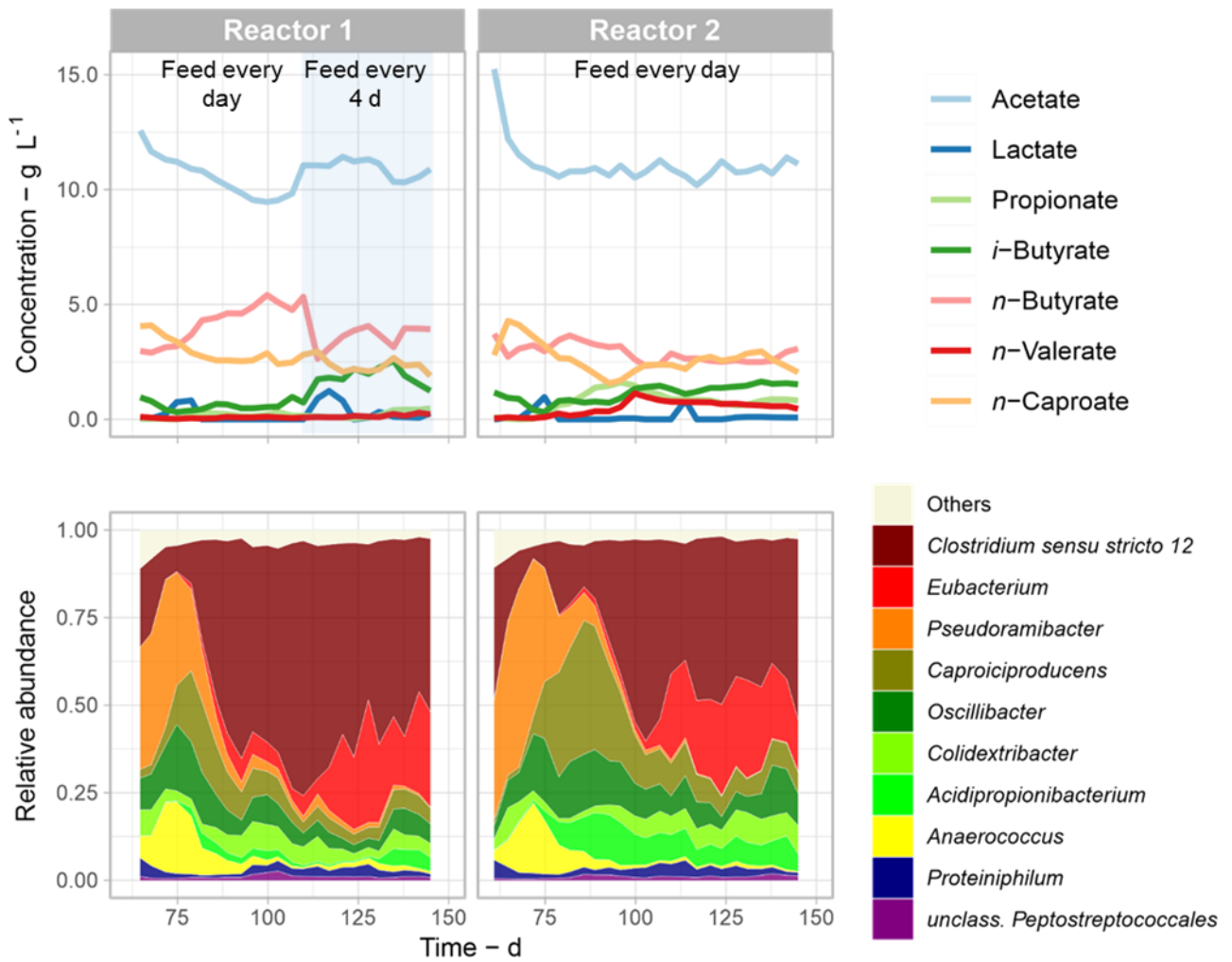
Figure E5. Concentration of chemicals and community composition at the genus level between days 61 and 148. Between days 61 and 110, both reactors were fed once a day. Afterwards, Reactor 1 was fed once every four days, whereas the feeding regime of Reactor 2 remained unchanged. No clear effect of longer feeding intervals was seen.
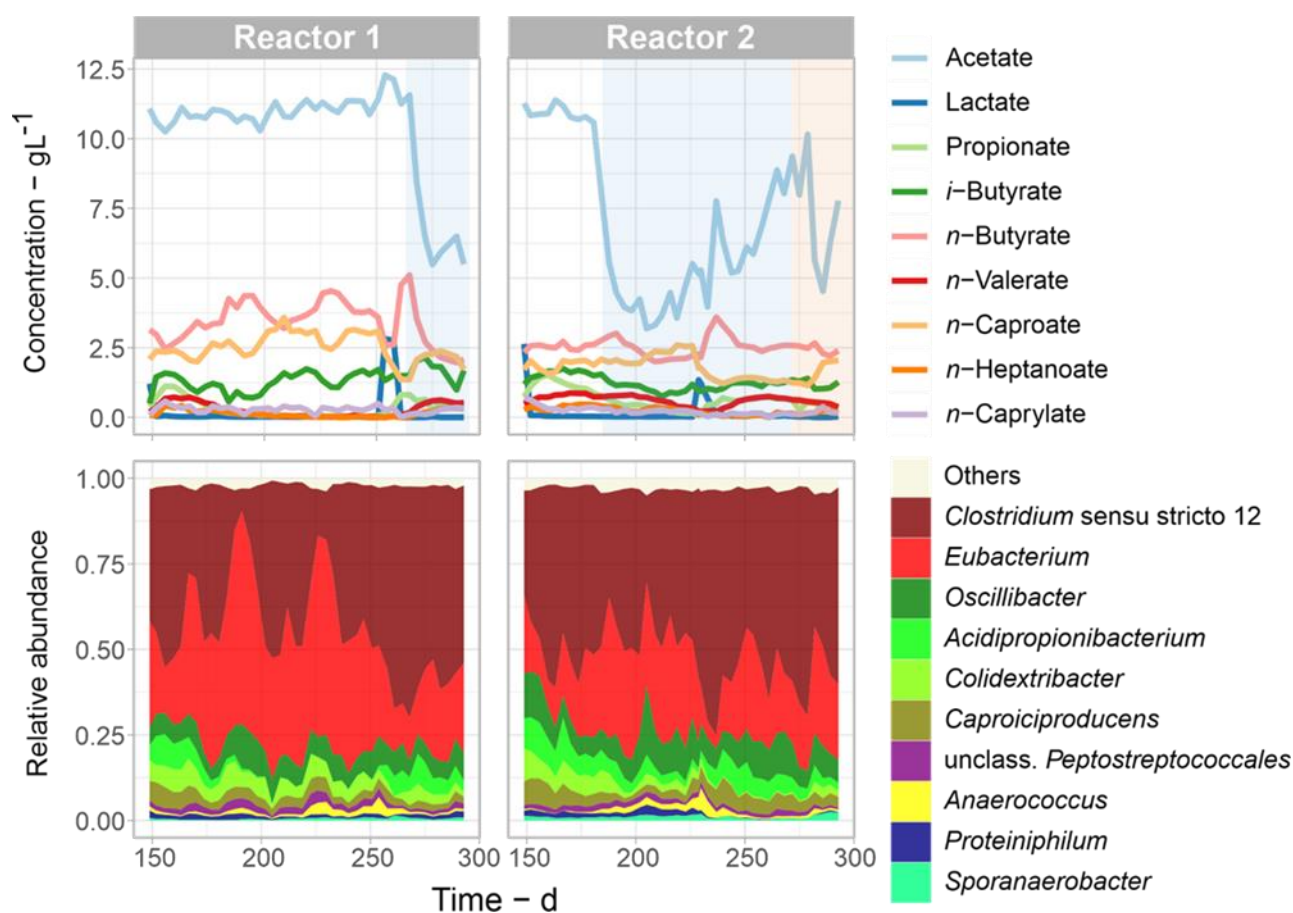
Figure E6. Concentration of chemicals and community composition between days 148 and 292. The blue shading represents the period when acetate-free medium was fed. The period with a decrease of HRT to 10 d is shown with orange shading.

E.5. Effects of changing operating conditions

During the period of 61 – 148 d, both reactors showed similar community dynamics, even when the feeding interval was changed from 1 to 4 days in Reactor 1 on day 110 (Figure E5). Excess acetate from the previous operation period (Reactor 1, Figure E4) was washed out until it reached a relatively stable concentration of about 11 g L^{-1}. The highest concentration of n-caproate in the study (4.1 and 4.3 g L^{-1} n-caproate in Reactors 1 and 2, respectively) was observed in the period succeeding the acetate peak (Figure E4 and Figure E5). The n-caproate peak coincided with a steep increase in the relative abundances of *Pseudoramibacter* and *Anaerococcus* in both reactors. However, these two genera were only transiently detected in the community, as *Caproiciproducens*, *Clostridium* sensu stricto 12, *Oscillibacter*, and *Eubacterium* became more abundant from day 75. Between days 75 and 110, the n-caproate concentrations settled at around 2.5 g L^{-1} and the most distinctive feature between the two reactors was a higher propionate concentration coinciding with higher abundance of *Acidipropionibacterium*, the putative propionate producer.

In comparison to the first 61 days of fermentation with the diverse community (Reactor 1, Figure 29), the period between days 110 and 148 in Reactor 1 (feeding interval 4 d) showed net

acetate consumption (13.6 e⁻ mmol L⁻¹ d⁻¹), a decrease in gas consumption by 40% (to 45.2 e⁻ mmol L⁻¹ d⁻¹ or 554 mL L⁻¹ d⁻¹ of H_2 + CO), and an increase in elongation to *n*-caproate by about 47% (to 45 e⁻ mmol L⁻¹ d⁻¹) (Reactor 1, Figure E7a). For the following experiments, both reactors were operated with a feeding interval of 3.5 days (feeding twice per week) for ease of operation.

Reactor 2 received an acetate-free medium after day 181 (Figure E6) causing higher gas consumption rates (84.0 e⁻ mmol H_2+CO L⁻¹ d⁻¹) than Reactor 1 for the same period (34.2 e⁻ mmol H_2+CO L⁻¹ d⁻¹) as seen in Figure E7a (Acetate-free feed and 200 mM acetate, respectively). Ceasing acetate supply in Reactor 2 caused 42 e⁻ mmol L⁻¹ d⁻¹ to be routed from substrates to acetate in contrast to Reactor 1 that kept consuming 10 e⁻ mmol acetate L⁻¹ d⁻¹. Consequently, the productivity of C≥4 carboxylates (i.e. *n*-butyrate, *i*-butyrate, *n*-valerate, *n*-caproate, *n*-heptanoate, and *n*-caprylate) in Reactor 2 decreased by 25% (from 132 to 98.9 e⁻ mmol L⁻¹ d⁻¹) after acetate feeding had been stopped (Figure E7a).

Interrupting acetate supply greatly increased carbon fixation rates in both reactors but decreasing HRT did not show a clear effect on fixation rates. Once both reactors were operating without acetate supply, a carbon fixation rate of 31.0 C mmol L⁻¹ d⁻¹ was seen in Reactor 1 with an HRT of 14 d and 28.0 C mmol L⁻¹ d⁻¹ was seen in Reactor 2 with an HRT of 10 d during the same period (Figure E7b). Net carbon fixation was majorly due to CO consumption since CO_2 was a net product under all conditions. Net consumption of CO_2 can likely be achieved, if a syngas mixture with less CO is to be used.

The decrease of HRT from 14 to 10 d (i.e. a 40% dilution rate increase) corresponded to a 41% increase in the production rates of C≥4 carboxylates (from 111 to 156 e⁻ mmol L⁻¹ d⁻¹, Figure E7a) pointing out that the system could be optimized for higher rates without loss of selectivity to longer-chain carboxylates.
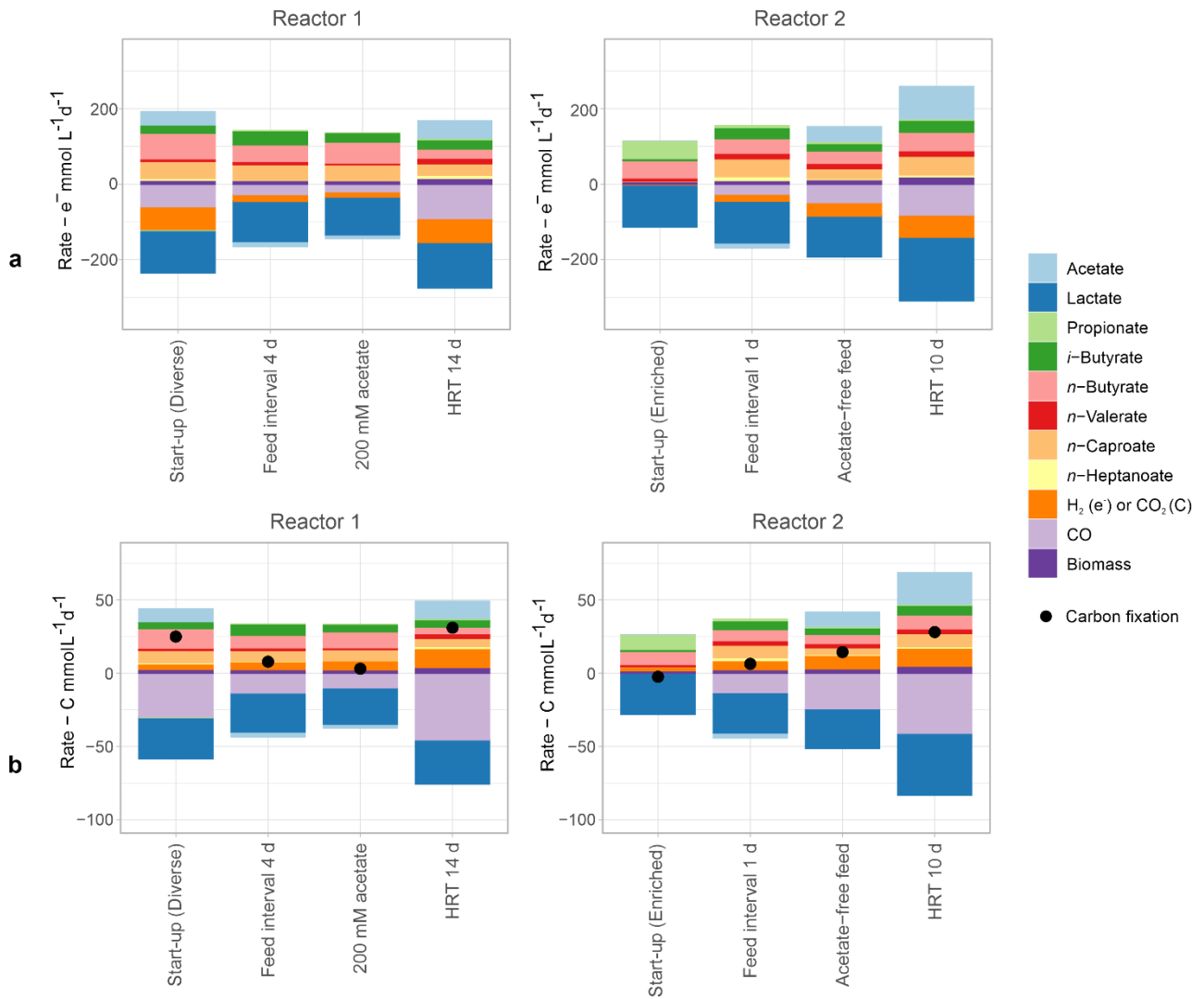
Figure E7. Production (positive) and consumption (negative) rates in terms of **a** electron equivalents and **b** carbon equivalents for the different conditions tested in the study. Except for the start-up of Reactor 2, the diverse community was used in all tests.